Discovery of catechol-O-methyltransferase inhibitors through virtual screening

M Smit

23111518

Dissertation submitted in fulfilment of the requirements for the degree *Magister Scientiae* in Pharmaceutical Chemistry at the Potchefstroom Campus of the North-West University

Supervisor:	Dr ACU Lourens
Co-Supervisor:	Prof A Petzer
Assistant Supervisor:	Prof JP Petzer

November 2016

The financial assistance of the National Research Foundation (NRF) towards this research is hereby acknowledged. Opinions expressed and conclusions arrived at, are those of the author and are not necessarily to be attributed to the NRF.

ABSTRACT

KEYWORDS

Parkinson's disease, catechol-*O*-methyltransferase, monoamine oxidase, virtual screening, enzyme inhibition.

BACKGROUND AND RATIONALE

Parkinson's disease (PD) is a progressive neurodegenerative disease that is caused by the death of dopaminergic neurons in the substantia nigra resulting in a loss of dopamine in the striatum. Neurodegeneration in PD is typified by symptoms such as rigidity, tremor at rest, slowness (bradykinesia) and impairment of postural balance.

Currently, there is no cure for PD and current therapies only provide symptomatic relief. In spite of several side effects, levodopa is still used in most cases, while several enzymes and receptors serve as drug targets. One of these targets is the monoamine oxidase (MAO) enzyme, in particular the MAO-B isoform. The MAO enzymes are responsible for the metabolism of amine neurotransmitters, such as dopamine. The inhibition of MAO-B has proven to be an effective strategy to increase dopamine levels in the brain.

Since MAO-A is responsible for the breakdown of noradrenalin, adrenalin, serotonin and tyramine, non-selective and selective MAO-A inhibitors have therapeutic applications in other neurological and psychiatric disorders such as depression. MAO-A inhibitors, particularly irreversible inhibitors, are also notable from a toxicological point of view. Irreversible MAO-A inhibitors may lead to potentially dangerous effects when combined with serotonergic drugs and certain foods containing tyramine, such as cheeses and processed meats. Selective MAO-B inhibitors and reversible MAO-A inhibitors appear to be free of these interactions.

The catechol-*O*-methyltransferase (COMT) enzyme is another enzymatic target. The inhibition of COMT results in a decrease of the clearance of L-dopa and dopamine, thus leading to a maintained level of dopamine in the brain and increased L-dopa efficacy. Currently used COMT inhibitors include tolcapone and entacapone.

However, due to the side effects, which may include severe dopaminergic, gastro-intestinal and other adverse reactions, their use is rather limited.

Based on the considerations above, this study aimed to identify compounds with COMT inhibitory activity by virtual screening. The secondary aim of this study was to screen the same set of compounds for MAO inhibitory activity as the identification of a dual targeted compound would be an added advantage.

METHODS:

The following methods were used: *Virtual screening:* Firstly, three pharmacophore models were constructed using a crystal structure (PDB: 3BWM) of COMT. The Discovery Studio® software package (Accelrys) was used for this purpose. A virtual library of drugs approved by the United States Food and Drug Administration (FDA) were then screened. Secondly, in order to maximise the potential hits in this study, several other methods for identifying hits were used. These included the use of ligand fingerprinting, the use of molecular docking, the identification of catechol bio-isosteres and compounds structurally related to known inhibitors such as kaempferol.

In vitro screening: COMT inhibition was determined using a fluorometric assay and norepinephrine as substrate, while MAO inhibition was determined using a fluorometric assay and kynuramine as substrate.

RESULTS

COMT inhibition studies: A list of twenty-six compounds were selected based on results from the pharmacophore mapping, screening of a library by fingerprinting, molecular docking, the bio-isostere approach, chemical similarity, cost and availability. These compounds were to be subjected to *in vitro* bio-assays (using porcine COMT) in order to determine their potencies (IC_{50} values) as inhibitors of COMT. Unfortunately, the Department of Fishery and Forestry placed a moratorium on the import of porcine products, which meant that the porcine COMT enzyme could no longer be obtained. The possibility of using the human enzyme was also investigated, but due to cost contraints its use was deemed unfeasible. Only eleven

of the test compounds were thus evaluated as *in vitro* inhibitors of COMT. Among the compounds that were tested, only kaempferol (IC_{50} = 2.799 µM) exhibited inhibitory activity towards the COMT enzyme, most likely due to its structural similarity to quercetin.

MAO inhibition studies: The IC_{50} values and selectivity index (SI) of eighteen compounds from the original COMT hit-list were also determined to investigate the inhibitory activity of these compounds towards an alternative target. Three of the eighteen test compounds exhibited promising IC_{50} values, and may thus be considered as MAO-A and MAO-B inhibitors. Kaempferol was the most potent MAO-A inhibitor with an IC_{50} value of 0.589 µM and oxybenzone was the most potent MAO-B inhibitor with IC_{50} values of 24.967 µM and 2.872 µM for MAO-A and MAO-B, respectively. Nitrendipine (16.353 µM) and (-)-riboflavin (13.119 µM) also showed some inhibition activity towards MAO-B.

Docking studies: To complete this study and rationalise the results of the MAO inhibition studies, molecular modelling was carried out and the eighteen compounds screened for MAO-inhibitory activity were docked into the active sites of MAO-A and MAO-B by using the CDOCKER module of Discovery Studio®. Some insights were obtained regarding the binding of kaempferol, oxybenzone, nitrendipine and (-)-riboflavin. Both kaempferol and oxybenzone had hydrogen bond interactions with Cys 323, present in the active site of MAO-A. Thus, it may be concluded that a hydrogen bond interaction with Cys 323 may be an important feature for MAO-A inhibitory activity since clorgyline (a known MAO-A inhibitor) also undergoes this interaction. Furthermore, oxybenzone, the most potent MAO-B test inhibitor, successfully docked into the active site of MAO-B, although it did not illustrate hydrogen bond interactions with any of the nearby amino acid residues. Thus, it may be postulated that the binding of oxybenzone to the active site may be due to Van der Waals interactions with the amino acid residues. Furthermore, oxybenzone also share structural similarities with chalcones which has MAO inhibitory activity. The docking results for MAO-B also showed that most of the test compounds interacted with Tyr 326 or Tyr 398, while interactions with Cys 172, Gln 206, Ile 199 and Tyr 435 also occurred.

Reversibility studies: To determine the reversibility of binding to MAO-B, the recovery of enzymatic activity after dialysis of enzyme-inhibitor complexes were determined

for oxybenzone. The results indicated that the most potent MAO-B inhibitor, oxybenzone, had a reversible mode of binding to the MAO-B isoform, since the enzyme activity was completely recovered by dialysis.

Mode of inhibition: To determine the mode of inhibition of oxybenzone**,** Lineweaver-Burk plots were constructed for the inhibition of MAO-B. The lines of the Lineweaver-Burk plots intersected at a single point at the y-axis, indicating that oxybenzone had a competitive mode of binding to the MAO-B isoform.

The results of this study showed that virtual screening may be useful in identifying existing compounds with potential dual COMT and MAO inhibitory effects. In this study, for example, the dual inhibitory of both COMT and MAO by kaempferol was illustrated for the first time. Such an approach may also be more cost effective than the *de novo* design of COMT and MAO inhibitors.

UITTREKSEL

SLEUTELWOORDE

Parkinson se siekte, katesjol-*O*-metieltransferase, monoamienoksidase, virtuele sifting, ensiem-inhibisie.

AGTERGROND EN RASIONAAL

Parkinson se siekte (PD) is 'n progressiewe, neurodegeneratiewe siekte wat patologies gekenmerk word deur die afsterwing van neurone in die substantia nigra pars compacta (SNpc) en lei tot ‘n tekort aan dopamien in die striatum. Die simptome sluit rigiditeit, tremor tydens rus, bradikinesie en posturale onstabiliteit in.

Parkinson se siekte is ‘n ongeneeslike siekte en huidige behandeling is slegs simptomaties van aard. Ten spyte van verskeie newe-effekte, word levodopa steeds in die meeste gevalle gebruik, terwyl ‘n verskeidenheid van ensieme en reseptore as geneesmiddelteikens dien. Een van hierdie teikens is die monoamienoksidase ensiem (MAO), veral die MAO-B-isoform. MAO ensieme is verantwoordelik vir die regulering en metabolisme van monoamien neuro-oordragstowwe, soos dopamien. Die inhibisie van MAO-B is ’n effektiewe strategie om die dopamienvlakke in die brein te verhoog.

Aangesien MAO-A verantwoordelik is vir die afbraak van noradrenalien, adrenalien, serotonien en tiramien, speel beide nie-selektiewe en selektiewe MAO-A-inhibeerders 'n terapeutiese rol in ander neurologiese en sielkundige afwykings soos depressie. Onomkeerbare MAO-A-inhibeerders is ook belangrik vanuit ’n toksikologiese oogpunt. Hierdie MAO-A-inhibeerders kan gevaarlike interaksies hê indien dit met serotonergiese geneesmiddels en kossoorte wat tiramien bevat, soos kase en verwerkte vleis, gekombineer word. Selektiewe MAO-B-inhibeerders en omkeerbare MAO-A-inhibeerders toon nie hierdie interaksies nie.

Die katesjol-*O*-metieltransferse (KOMT) ensiem is nog 'n ensiematiese teiken. Die inhibisie van KOMT veroorsaak 'n afname in die opruiming van L-dopa en dopamien, en sodoende word optimale vlakke van dopamien in die brein gehandhaaf wat gevolglik die geneesmiddeleffektiwiteit van L-dopa verhoog. KOMT inhibeerders wat

tans gebruik word sluit tolkapoon en entakapoon in, maar as gevolg van newe-effekte wat ernstige dopaminergiese, gastro-intestinale en ander ongunstige reaksies insluit, is die gebruik van KOMT inhibeerders redelik beperk.

In die lig van die bogenoemde, is daar met hierdie studie gepoog om, deur gebruik te maak van virtuele sifiting, verbindings met KOMT inhiberende aktiwiteit te identifiseer. ‘n Sekondêre doelwit van die studie was om dieselfde stel verbindings vir MAO inhiberende aktiwiteit te toets, aangesien die identifikasie van ‘n dubbelteikengeneesmiddel ‘n addisionele voordeel sou wees.

METODES:

Die volgende metodes is tydens die studie gebruik: *Virtuele sifting:* Eerstens is drie farmakofoormodelle geskep deur gebruik te maak van ‘n kristalstruktuur (PDB: 3BWM) van KOMT. Die Discovery Studio® sagtewarepakket van Accelrys is vir hierdie doel gebruik. Vir hierdie studie is die virtuele biblioteek van geneesmiddels geregistreer deur die Verenigde State van Amerika se Voedsel en Geneesmiddel Administrasie (FDA) gesif met die farmakofoormodelle. Tweedens, om die potensiaal vir sukses in hierdie studie te verhoog, is verskeie ander metodes gebruik. Hierdie metodes het die gebruik van ligand “vingerafdrukke”, molekulêre modellering, die identifisering van katesjol bio-isostere en verbindings wat struktureel verwant is aan reeds bestaande inhibeerders soos kaempferol, ingesluit.

In vitro sifting: Inhibisie van beide KOMT en MAO is bepaal deur gebruik te maak van fluorometriese toetse. Norepinefrien is as substraat gebruik tydens KOMT studies en kinuramien het as substraat gedien tydens MAO toetse.

RESULTATE:

KOMT inhibisie studies: 'n Lys van ses-en-twintig verbindings is geselekteer op grond van die resultate wat verkry is uit die farmakofoor kartering, sifting van 'n biblioteek deur “vingerafdrukke”, molekulêre modellering, die bio-isosteer benadering, chemiese verwantskap, koste and beskikbaarheid. Hierdie verbindings was veronderstel om *in vitro* toetse te ondergaan (deur vark KOMT te gebruik) om hulle potensie (IC_{50} waardes) as inhibeerders van KOMT te bepaal. Ongelukkig het

die Departement van Visserye en Bosbou 'n moratorium op die invoer van varkprodukte geplaas wat beteken het dat die vark KOMT ensiem toe onverkrygbaar was. Die moontlikheid om die menslike ensiem te gebruik is ook ondersoek, maar as gevolg van kostebeperkings was hierdie opsie ook nie haalbaar nie. Slegs elf van die toetsverbindings is dus geëvalueer as *in vitro* inhibeerders van KOMT. Onder die verbindings wat geëvalueer is, het slegs kaempferol (IC_{50} = 2.799 µM) inhiberende aktiwiteit teenoor die KOMT ensiem getoon. Hierdie inhiberende aktiwiteit is heel waarskynlik as gevolg van die strukturele verwantskappe met kwersetien.

MAO inhibisie studies: Die IC_{50} waardes en die selektiwiteitsindeks (SI) van agtien van die oorspronklike verbindings geselekteer vir KOMT sifting, is ondersoek vir inhiberende aktiwiteit teenoor 'n alternatiewe teiken, die MAO ensiem. Drie van die agtien toetsverbindings het belowende IC_{50} waardes getoon en kan dus oorweeg word as MAO-A- en MAO-B-inhibeerders. Kaempferol was die mees potente MAO-A-inhibeerder met 'n IC_{50} waarde van 0.589 µM en oksibensoon was die mees potente MAO-B-inhibeerder met IC_{50} waardes van 24.967 µM en 2.872 µM vir MAO-A en MAO-B, onderskeidelik. Nitrendipien (16.353 µM) en (-)-riboflavien (13.119 µM) het ook inhibisie aktiwiteit teenoor MAO-B getoon.

Molekulêre modelleringstudies: Om die resultate van die MAO-inhibisiestudies te rasionaliseer, is molekulêre modellering gedoen en die agtien verbindings waarop die *in vitro* studies gedoen is, is gepas in die aktiewe setels van MAO-A en MAO-B deur gebruik te maak van die CDOCKER-module van Discovery Studio®. Kennis rakende die binding van kaempferol, oksibensoon, nitrendipine en (-)-riboflavin was verkry. Beide kaempferol en oksibensoon het 'n waterstofbindingsinteraksie ondergaan met Cys 323 wat teenwoordig is in die aktiewe setel van MAO-A. Daar kan dus afgelei word dat 'n waterstofbindingsinteraksie met Cys 323 waarskynlik 'n belangrike vereiste mag wees vir MAO-A inhiberende aktiwiteit aangesien klorgilien ('n bestaande MAO-A-inhibeerder) ook hierdie interaksie toon. Oksibensoon, die mees potente MAO-B-inhibeerder, is suksesvol gepas in die aktiewe setel van MAO-B, alhoewel geen waterstofbindingsinteraksies met enige naasliggende aminosuurresidue geïdentifiseer is nie. Daar word dus gepostuleer dat oksibensoon bind deur van der Waals interaksies met die aminosure in die aktiewe setel te ondergaan. Verder is daar strukturele verwantskappe tussen oksibensoon en chalkone wat MAO inhiberende aktiwiteit toon. Die modelleringsresultate van MAO-B

het ook getoon dat die meeste van die toetsverbindings interaksies ondergaan met Tyr 326 of Tyr 398, terwyl interaksies met Cys 172, Gln 206, Ille 199 en Tyr 435 ook waargeneem is.

Omkeerbaarheidstudies: Om te bepaal of MAO-binding omkeerbaar was, is die herstel van ensiematiese aktiwiteit na dialise van die ensiem-inhibeerder-komplekse bepaal vir oksibensoon. Die resultate het aangedui dat die mees potente MAO-B-inhibeerder, oksibensoon, omkeerbaar bind aan die MAO-B-isoform en die ensiemaktiwiteit het dus heeltemal herstel na dialise.

Meganisme van inhibisie: Om die meganisme van inhibisie van oksibensoon te bepaal, is Lineweaver-Burk grafieke opgestel vir die inhibisie van MAO-B. Die lyne van die Lineweaver-Burk grafieke het gekruis by ‘n enkele punt op die y-as, wat aandui dat oksibensoon kompeterend aan die MAO-B-isoform bind.

Die resultate van die studie het gewys dat virtuele sifting nuttig mag wees vir die identifisering van reeds bestaande verbindings met potensiaal as beide KOMT en MAO inhibeerders. In hierdie studie, byvoorbeeld, is daar vir die eerste keer gewys dat kaempferol as 'n inhibeerder vir beide KOMT en MAO optree. Hierdie benadering kan meer koste-effektief wees as die *de novo* ontwerp van KOMT en MAO inhibeerders.

TABLE OF CONTENTS

LIST OF ABBREVIATIONS

3D	Three dimensional
3-OMD	3-O-methyldopa
[ ]	Concentration of
A	
A	Active compounds
Acc	Accuracy
ADH	Aldehyde dehydrogenase
AdoHcy	*S*-Adenosyl-homocysteine
AdoMet	*S*-Adenosyl-*L*-methionine
Arg	Arginine
Asn	Asparagine
Asp	Aspartic acid
AUC	Area under curve
B	
BBB	Blood brain barrier
BDNF	Brain-derived neurotrophic factor
C	
COMT	Catechol-*O*-methyltransferase
CSF	Cerebrospinal fluid
Cys	Cysteine
D	
D	Dopamine receptor
DA	Dopamine
DJ-1	Parkinson disease protein 7

DMSO	Dimethyl sulphoxide
DNA	Deoxyribonucleic acid
DNC	3,5-Dinitrocatechol
E	
E	Enzyme
ES	Enzyme-substrate complex
ESR	Electron spin resonance
EWG	Electron withdrawing group
F	
FAD	Flavin adenine dinucleotide
FDA	United States Food and Drug Administration
FN	False negative compounds
FP	False positive compounds
G	
GDNF	Glial-derived neurotrophic factor
Gln	Glutamine
Glu	Glutamate
Gly	Glycine
GSH	Glutathione
H	
HIV	Human immunodeficiency virus
hMAO	Human monoamine oxidase
hMAO-A	Human monoamine oxidase type A
hMAO-B	Human monoamine oxidase type B
HPLC	High performance liquid chromatography
HT-22	Hippocampal cell line

HVA	Homovanillic acid
I	
I	Inhibitor
Ibal	Balanced labelling performance
IC_{50}	Inhibitor concentration that produces 50% inhibition of an enzyme
Ile	Isoleucine
INF-y	Interferon gamma
IL	Interleukin
K	
K_i	The equilibrium constant used to indicate the reversibility of an enzyme-inhibitor complex.
K_m	Michaelis-Menten constant: substrate concentration that produces half maximal velocity.
L	
L-dopa	Levodopa
Leu	Leucine
LID	L-dopa induced dyskinesia
LNAA	Large neutral amino-acid
LRRK2	Leucine-rich repeat kinase 2
Lys	Lysine
M	
MAO	Monoamine oxidase
MAO	Monoamine oxidase type A
MAO	Monoamine oxidase type B
MB-COMT	Membrane-bound isoform of COMT
Met	Methionine

MPTP	1-Methyl-4-phenyl-1,2,3,6-tetrahydropyridine
N	
n	Number of selected hits
N	Total number of hits
NE	(-)-Norepinephrine
NGF	Nerve growth factor
NI	Non immune
NMDA	N-methyl-D-aspartate
NMN	*DL*-Normetanephrine
P	
P	Product
PCP	Phencyclidine
PD	Parkinson’s disease
PDB	Protein data bank
PDI	Peripheral decarboxylase inhibitors
Phe	Phenylalanine
PMT	Photomultiplier
Pro	Proline
R	
ROC curve	Receiver operating characteristics curve
ROS	Reactive oxygen species
S	
S	Substrate concentration
SAM	*S*-Adenosyl-*L*-methionine
SAMe	*S*-Adenosyl-*L*-methionine enzyme
S-COMT	Soluble isoform of COMT

SD	Standard deviation
Se	Sensitivity
Ser	Serine
SI	Selectivity Index
SN2	Nucleophilic substitution 2
SNpc	Substantia nigra pars compacta
Sp	Specificity
T	
Thr	Threonine
TN	True negative compounds
TNF-α	Tumor necrosis factor-alpha
TP	True positive compounds
Trp	Tryptophan
Tyr	Tyrosine
U	
U-0521	3’,4’-Dihydroxy-2-methyl-propiophenone
UDP	Uridine diphosphate
V	
V	Reaction velocity
Val	Valine
V_i	The measured initial velocity
V_{max}	Maximum velocity
Y	
Ya	Yield of actives

LIST OF FIGURES

LIST OF TABLES

LIST OF EQUATIONS

CHAPTER 1

INTRODUCTION:

1.1 GENERAL BACKGROUND AND JUSTIFICATION

1.1.1 PARKINSON'S DISEASE

Parkinson's disease (PD) is the second most common age-related neurodegenerative disease after Alzheimer's disease (Müller, 2015). PD occurs globally in all ethnic groups and affects both sexes approximately equally with a slightly higher incidence in men (Dauer & Przedborski, 2003; Kakkar & Dahiya, 2015). The classic triad of major signs of PD is made up of tremor at rest, rigidity and bradykinesia (Müller, 2015). Currently there is uncertainty about the etiology and pathogenesis of PD, but it has been suggested that a complex interaction between aging, environmental factors and genetic mutations may result in the development of the disease (Dorsey *et al.*, 2007).

The central pathophysiological event in PD is the progressive damage to the dopaminergic neurons located in the substantia nigra pars compacta (SNpc) which leads to a loss of dopamine in the striatum (Hunn *et al.*, 2014). Several theories exist regarding the pathogenesis of PD. One theory proposes that the misfolding and aggregation of proteins are instrumental in the death of SNpc dopaminergic neurons (Hsieh & Chiang, 2014). Another theory suggests that the dysfunction of the mitochondria and oxidative stress caused by reactive oxygen species (ROS) contribute to neuronal death (Segura-Aguilar *et al.*, 2010). However, neurodegeneration can also be the result of neuroinflammation (Hirsch *et al.*, 2012), apoptosis (Koppenhöfer *et al.*, 2014) and excitotoxicity (Doble, 1999).

Drugs currently used to provide symptomatic relief include levodopa, dopamine agonists, MAO inhibitors and COMT inhibitors (Müller, 2015). The introduction of levodopa (L-dopa) heralded a therapeutic breakthrough, and it is still the most efficacious drug for the treatment of PD. However, due to its short plasma half-life, high doses of L-dopa can lead to fluctuations in movement control - the so-called "on-off"-effect. "Off"-phenomena describe the reappearance of a reduced motor performance after an "on"-interval of good response to adequate dopaminergic

neurotransmission. Prolonged levodopa use is also associated with other side effects, such as dyskinesia (Müller, 2015), which is involuntary movements that mostly result from an over-stimulation of the dopaminergic system (Aminoff, 2009; Müller, 2015). Dyskinesia can occur during both “on” and “off”-periods. As the disease progresses, patients may develop dyskinesia throughout the whole “on”-time, spreading over the whole body. Generally, PD patients better tolerate and accept mild dyskinesia than “off”-periods (Müller, 2015). Although L-dopa is responsible for many motor adverse effects, it is still the most potent drug currently available (Lipski *et al.*, 2011).

Dopamine receptor agonists serve as a good alternative for levodopa since no enzyme activation is required and the duration of action is longer. Unlike L-dopa these drugs offer receptor selectivity, limiting the adverse effects (Kakkar & Dahiya, 2015). These drugs delay the need for L-dopa therapy, thus lowering the incidence of motor fluctuations and dyskinesia associated with L-dopa use (Aminoff, 2009; Müller, 2015).

None of the drugs currently in use are registered as neuroprotective or disease modifying, and present research is aimed in particular at the reversal of neurodegeneration or the prevention of further dopaminergic neuron degeneration (Dauer & Przedborski, 2003). It is thus clear that current therapies suffer from limitations with regards to both symptomatic and neuroprotective qualities, validating research in this area (Dauer & Przedborski, 2003).

1.1.2 MONOAMINE OXIDASE INHIBITORS

The monoamine oxidase (MAO) enzyme exists as two isoforms, namely MAO-A and MAO-B. MAO-B is the isoform which is predominantly responsible for the breakdown of dopamine and its selective inhibition reduces the symptoms of PD, while also being potentially neuroprotective (Youdim & Bakhle, 2006).

Currently there are two selective MAO-B inhibitors available: selegiline (**Figure 1.1 A**) and rasagiline (**Figure 1.1 B**). Selegiline, which is a propargyl amphetamine derivative undergoes hepatic metabolism to amphetamine-like metabolites. The

adverse effects associated with these metabolites may include neurotoxicity, cardiovascular and psychiatric effects (Fernandez & Chen, 2007).

Conversely, rasagiline, a second-generation MAO-B inhibitor, is a non-amphetamine derivative that undergoes first-pass metabolism resulting in an inactive aminoindan metabolite. Rasagiline can be administered as monotherapy or as an adjunct to L-dopa (Fernandez & Chen, 2007).

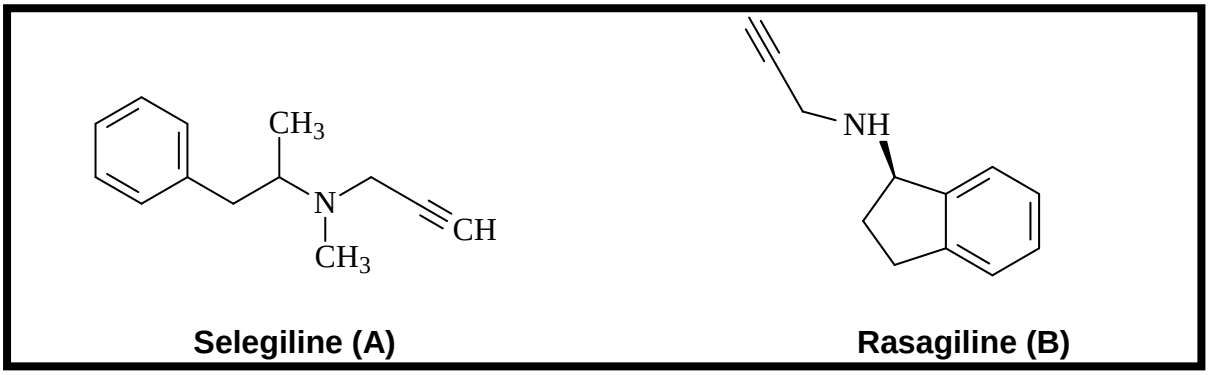

Figure 1.1: Structures of selective MAO-B inhibitors used as treatment in PD.

1.1.3 CATECHOL-O-METHYLTRANSFERASE AND ITS INHIBITORS

The catechol-O-methyltransferase (COMT) enzyme also exists as two isoforms. The soluble (S-COMT) isoform is present at high levels in the majority of tissues while the membrane-bound (MB-COMT) isoform is prevalent in the brain (Jatana *et al.*, 2013).

The enzyme can be defined as a major catabolic regulator of synaptic catecholamine neurotransmitters such as dopamine, norepinephrine and epinephrine (Ma *et al.*, 2013; Männistö & Kaakkola, 1999; Williams *et al.*, 2007). Inhibition of COMT results in a decrease of the clearance of L-dopa and dopamine (Männistö & Kaakkola, 1999), thus leading to a maintained level of dopamine in the brain and increased L-dopa efficacy (Ma *et al.*, 2013; Männistö & Kaakkola, 1990).

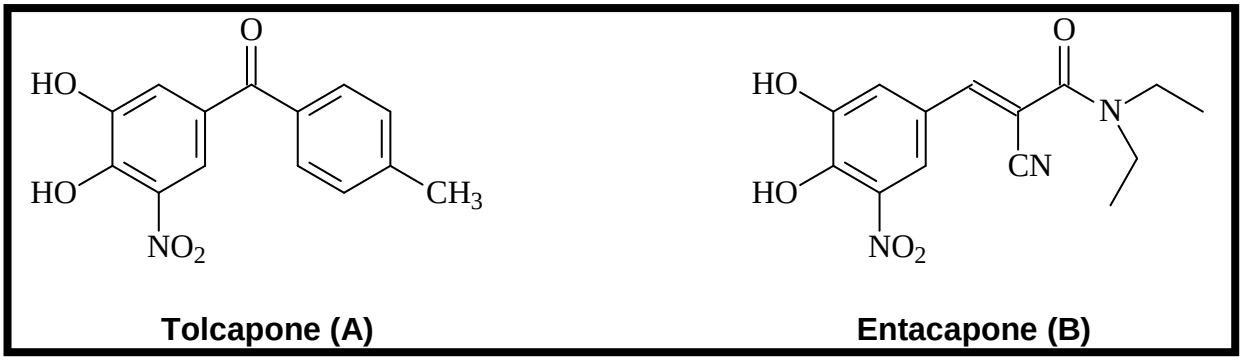

Figure 1.2: Structures of nitrocatechols used in the treatment of PD.

Currently, tolcapone (**Figure 1.2 A**) and entacapone (**Figure 1.2 B**) are the only available COMT inhibitors used clinically as treatment for PD. However, the side effects of these drugs, which may include severe dopaminergic, gastro-intestinal and other adverse reactions are of concern (Jatana *et al.*, 2013). The use of tolcapone is further limited due to its association with hepatotoxicity (Korlipara *et al.*, 2004).

1.1.4 THE ROLE OF QUERCETIN AND KAEMPFEROL IN NEURODEGENERATIVE DISORDERS

Naturally occurring flavonoids have attracted attention over the years as potential drugs and a broad range of effects have been reported for these ubiquitous compounds (Lee *et al.*, 2001). These effects include, antioxidant activity (La Casa *et al.*, 2000), anti-HIV activity (De Clercq, 2000), antibacterial activity (Alcaraz *et al.,* 2000), and tumor cell growth inhibitory activity (Ito *et al.*, 2000, Rafi *et al.*, 2000). These flavonoids may also potentially prove to have a preventative effect on neurodegeneration (Lee *et al.*, 2001).

The most abundant of all the flavonoids is quercetin, (**Figure 1.3 A**) a flavonol (Lakhanpal & Rai, 2007). Reported biological effects of quercetin include the protection of brain cells against oxidative stress (Heo *et al.,* 2004), a tissue damaging process associated with neurodegenerative disorders (Lakhanpal & Rai, 2007).

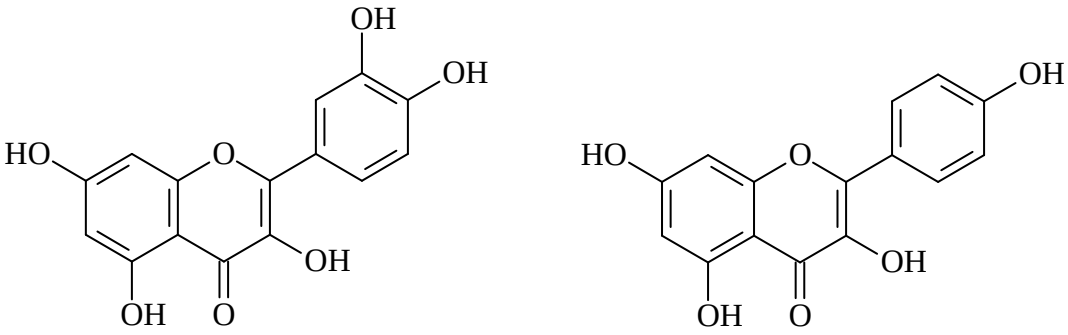

Quercetin (A) **Kaempferol (B)**

Figure 1.3: The structure of flavonoids, quercetin and kaempferol.

COMT and MAO inhibiting properties have also been reported for this compound and it could possibly serve as an effective adjunct to L-dopa therapy in Parkinson's disease (Lakhanpal & Rai, 2007; Singh & Pattipati, 2003).

Kaempferol (**Figure 1.3 B**), just like quercetin, can also be classified as a member of the flavonol subclass of flavonoids and has been reported to have strong antioxidant, anti-inflammatory and neuroprotective properties (Lakhanpal & Rai, 2007, Li & Pu, 2011, Schroeter *et al.*, 2000, Schroeter *et al.*, 2001, Ishige *et al.*, 2001). Of particular interest is the fact that a strong and prolonged protective effect against rotenone toxicity, a classical toxin used to induce parkinsonism, has been demonstrated (Filomeni *et al.,* 2010, Li & Pu, 2011).

1.1.5 MOLECULAR MODELLING IN DRUG DESIGN

During the last few years a considerable body of work, investigating the performance of three dimensional (3D) virtual screening and computational approaches in drug design, has been published. Assessments of protein-ligand docking and pharmacophore modelling in particular have created interest in the scientific community (Kirchmair *et al.*, 2008). Different molecular modelling approaches exist for the identification of novel ligands for biological protein targets. These include docking studies and pharmacophore modelling. Both docking and pharmacophore-based *in silico* screening allow for the screening of a large number of compounds for possible interaction with the binding site of biological targets, and identifies possible

non-covalent interactions between a protein and its ligand (Lee *et al.*, 2007). The advantages of these *in silico* approaches include a reduction in cost and time spent in screening, and allow for the identification of a set of chemically diverse compounds (Langer & Wolber, 2004; Wolber & Langer, 2005).

The use of a library consisting of FDA approved drugs that have already been approved for administration in human subjects is practical, since concerns such as safety and bioavailability has already been adequately addressed in humans. Clinical efficacy is the only factor that needs to be proven since preclinical and clinical development is not required. Furthermore, this approach provides the opportunity for the discovery of agents with a multi-targeted directed mode of action. This would provide several advantages over multiple-medication therapy, since the possibility of drug-drug interactions can be reduced and the adverse effect profile and pharmacokinetic considerations of the therapy can be decreased (Lee *et al.*, 2007).

1.2 RESEARCH PROBLEM

As previously mentioned, there is no cure for PD. Furthermore, the drugs currently used to treat the disease, such as levodopa, MAO and COMT inhibitors, suffer from several limitations, as discussed above. Although COMT has been identified as a promising target for the treatment of PD, the variety of scaffolds of known COMT inhibitors are rather limited. These include the nitrocatechols (**Figure 1.2**), flavonoids such as quercetin (**Figure 1.3 A**), and the pyridones (**Figure 1.4**).

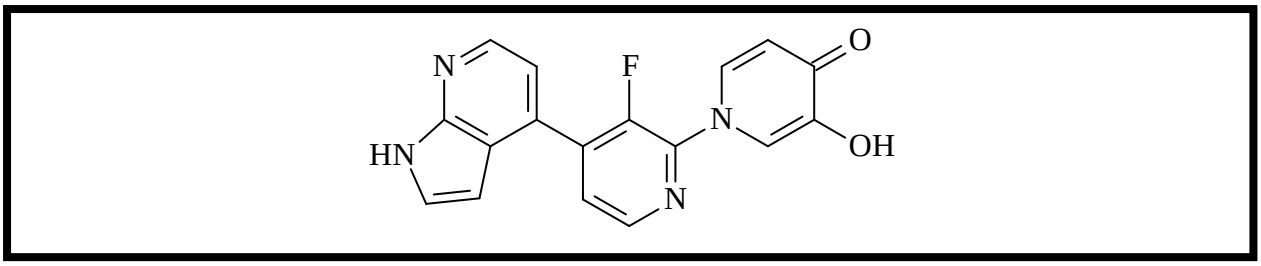

Figure 1.4: Structure of a pyridone with COMT inhibitory activity.

The nitrocatechols e.g. tolcapone and entacapone, are the only group of compounds used clinically as COMT inhibitors to treat PD. (Jatana *et al.*, 2013). Lastly, none of

the drugs currently on the market adequately address the multifactorial nature of PD (Müller, 2015).

1.3 HYPOTHESIS

Since virtual, *in silico* approaches provide a way of identifying novel scaffolds for known targets, it is postulated that active, non-nitrocatechol COMT inhibitors will be identified among a library of FDA approved drugs using a computational approach, which will include the use of pharmacophores, screening a library by fingerprinting and molecular docking. Bio-isosteric replacement is also a valuable tool for the design of highly selective enzyme inhibitors (Hübner *et al.*, 2000) and may therefore be used to identify COMT inhibitors. Furthermore, since the flavonoid quercetin shows promise as both COMT and MAO inhibitor (Lakhanpal & Rai, 2007), it is hypothesised that structurally related compounds may exhibit similar multi-targeted, biological activities.

1.4 AIMS AND OBJECTIVES

The main aim of this study is to identify non-nitrocatechol COMT inhibitors through virtual screening. Additionally, the MAO inhibitory activities of potential hits will be assessed in the hope of identifying dual-acting compounds.

The objectives of this study may therefore be summarized as follows:

The following approach will be used in the identification of potential COMT inhibitors in order to maximize potential hits:

- Discovery Studio® 3.1 modelling software will be used to construct structure-based pharmacophore models for COMT using a crystal structure of human COMT. *In silico* screening of a library of FDA approved drugs will then be performed to identify possible inhibitors.
- Secondly, selected compounds from the FDA approved drug library will also be docked into the active site of COMT. This approach will also provide information regarding possible binding orientations and establish if the inhibitor fits within the active site cavity.

- The FDA approved drug library will also be screened using a ligand fingerprint approach where the structures of known inhibitors will serve as reference library in order to identify chemically similar species.
- A literature survey will be performed to identify bio-isosteres of both phenol and catechol. After the identification of these bio-isosteres, the Sigma-Aldrich database will be searched and molecules containing these moieties identified.
- Compounds will then be selected considering the results of above mentioned methods. Since kaempferol is visually structurally similar to quercetin, it will be added to the selection. Commercial availability, price and molecular weight will also be taken into account before purchase of compounds to obtain the final hit-list.
- COMT inhibitory activity will be determined by a fluorescent assay based on the literature protocol as described by Aoyama and co-workers (2005). This assay is based on the fact that the test inhibitors would decrease the formation of normetanephrine from the COMT substrate, norepinephrine
- The MAO inhibitory activities of hits will be determined using the fluorometric method as described by Strydom *et al.* (2011). The assay is based on the measurement of the extent by which an inhibitor reduces the MAO-catalysed oxidation of kynuramine to the fluorescent product, 4-hydroxyquinoline.
- To determine possible binding orientations in the MAO-A and MAO-B active sites, screened compounds will also be docked into the active sites of both MAO-A and MAO-B using the Discovery Studio® 3.1 modelling software. Possible reasons for high or low inhibitory activity will be assessed.
- Where suitable hits are identified, the mode of inhibition (competitive or non-competitive) and type of binding (reversible or irreversible) will also be assessed for MAO.

CHAPTER 2

LITERATURE STUDY:

2.1 PARKINSON'S DISEASE

2.1.1 CLINICAL CHARACTERISTICS AND INCIDENCE

Parkinson's disease (PD) is an incurable, chronic neurodegenerative disorder that mainly affects movement (Müller, 2015). The disease is typified by symptoms such as rigidity, tremor at rest, slowness (bradykinesia) and impairment of postural balance (Müller, 2015).

Although PD is mainly considered as a movement disorder, non-motor symptoms may also occur. These symptoms include autonomic disturbances such as loss of smell, orthostatic hypotension, sensory mutations, depression, sleep disturbances, cognitive impairment and dementia (Kakkar & Dahiya, 2015).

PD is the second most common age related neurodegenerative disorder after Alzheimer's disease and occurs globally in all ethnic groups (Dauer & Przedborski, 2003). The mean age of onset is 60 years and the median duration (from diagnosis to death) of the disease is 15 years. PD affects both sexes, but men are 1.5 times more likely to develop PD compared to women. However, this may vary between different populations and countries (Lees *et al.,* 2009). In 2009 approximately 5 million PD cases were reported across the globe (Dorsey *et al.*, 2007; Kakkar & Dahiya, 2015) and it is predicted that the prevalence of PD will double by 2030 in the aging world population (Dorsey *et al.*, 2007). Therefore, improvements in anti-parkinsonian treatments are required to maintain quality of life and reduce the socio-economic burden of the disease (Dorsey *et al.*, 2007).

2.1.2 ETIOLOGY

Although the cause of PD is still unknown (Müller, 2015), it is believed to be the result of a complex interaction between aging and environmental and genetic factors (Dorsey *et al.*, 2007).

PD commonly occurs in late middle age individuals and the elderly, which indicate that aging plays an important role in the etiology of this disease (Dorsey *et al.*, 2007). During normal aging, a dopaminergic neuronal loss in the substantia nigra and the striatum occurs (Dauer & Przedborski, 2003; Dorsey *et al.*, 2007). However, although normal aging can be associated with both degeneration of dopamine and dopaminergic loss, the rate of degeneration in individuals with PD is faster (Winogrodzka *et al.*, 2001). The exact role of aging in the pathogenesis of PD is still unknown, but it is clear that an increase in age is a risk factor for PD (Dorsey *et al.*, 2007).

High risk environmental factors may include head injuries, acute and chronic exposure to pesticides such as rotenone (**Figure 2.1 A**) or paraquat (**Figure 2.1 B**), certain occupations and foods (Dorsey *et al.*, 2007).

Studies have shown that the agricultural pesticide rotenone can activate a parkinsonian condition in rodents (rats). However, constant parenteral treatment is needed. Rural environments and drinking water derived from wells are also risk factors of PD as they are indirectly linked to exposure to pesticides (Betarbet *et al.*, 2002; Sherer *et al.*, 2002).

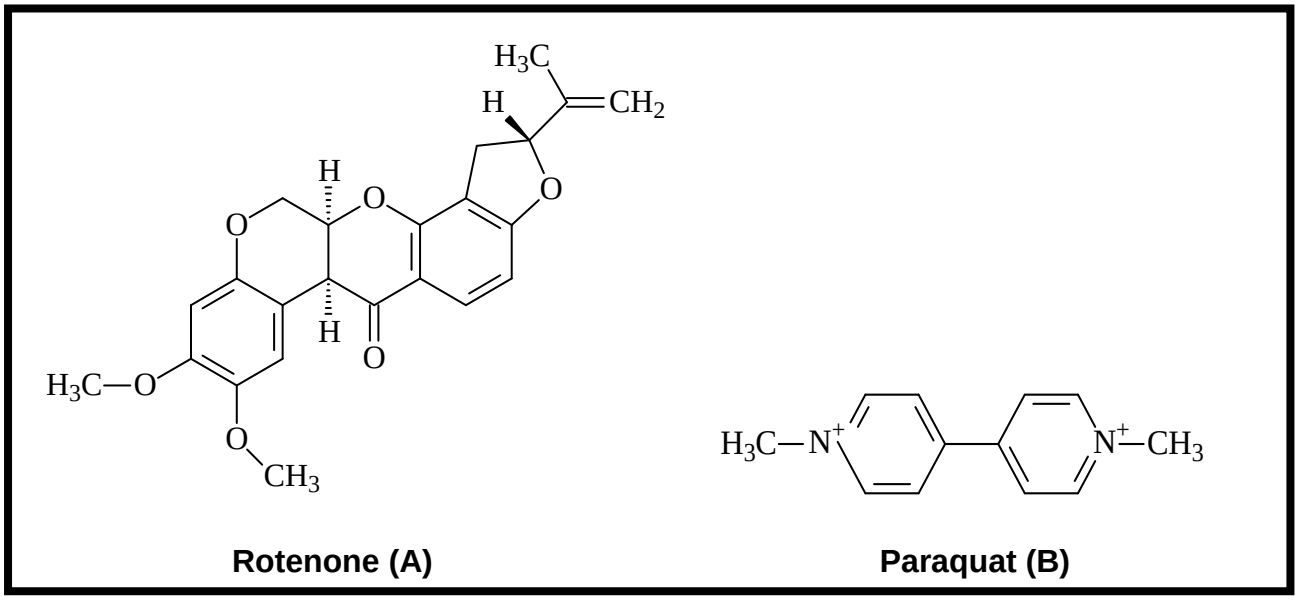

Figure 2.1: Structures of agricultural pesticides rotenone and paraquat.

The environmental toxin hypothesis gained credibility with the observation that the administration of 1-methyl-4-phenyl-1,2,3,6-tetrahydropyridine (MPTP) (**Figure 2.2**), a toxin that kills dopaminergic neurons in the brain, results in a parkinsonian syndrome strikingly similar to the idiopathic disorder in humans. (Betarbet *et al.*, 2002; Sherer *et al.*, 2002; Yu *et al.*, 2015).

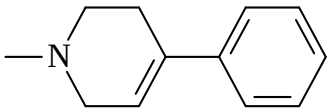

1-Methyl-4-phenyl-1,2,3,6-tetrahydropyridine

Figure 2.2: Example of a toxin used to produce animal models of PD.

Other environmental circumstances that may contribute to disease development include family difficulties, such as conflict in the household, social isolation, loss of employment, retirement at an early age and financial problems (Dorsey *et al.*, 2007).

Studies suggest that genetic defects or mutations could play a potential role in the etiology of PD. Mutations in α-synuclein, a presynaptical nerve protein, are unlikely to cause sporadic and familial PD, but it may account for those with early stage PD (Polymeropolous *et al.*, 1997). Evidence suggests that the most common cause of monogenic PD is due to mutations in the leucine-rich repeat kinase 2 (LRRK2) gene (Healy *et al.*, 2004). Six pathogenic mutations in LRRK-2 have been reported, the most common of these, the Gly2019Ser mutation, has a worldwide frequency of 1% in sporadic cases and 4% in patients with hereditary parkinsonism (Healy *et al.,* 2004; Paisán-Ruíz *et al.,* 2004). A person inheriting the Gly2019Ser mutation has a 28% risk of developing parkinsonism (if the person is younger than 60 years of age), and 74% at 79 years of age (Healy *et al*., 2004). Other genetic factors may include mutation of the genes, DJ-1 and Parkin (Dauer & Przedborski, 2003).

The main etiology of PD remains a mystery at this stage, but as more information is acquired, an improved understanding of the underlying causes resulting in the symptoms of PD will be gained (Srivatsal *et al.*, 2015).

2.1.3 PATHOGENESIS

The main pathophysiological event of PD is the progressive damage to the dopaminergic neurons located in the substantia nigra. This leads to the degeneration of dopaminergic neurons and a loss of dopamine in the striatum. The disease is further typified by the presence of Lewy bodies which are mainly composed of the α-synuclein presynaptical protein (Dorsey *et al.*, 2007; Hunn *et al.*, 2014).

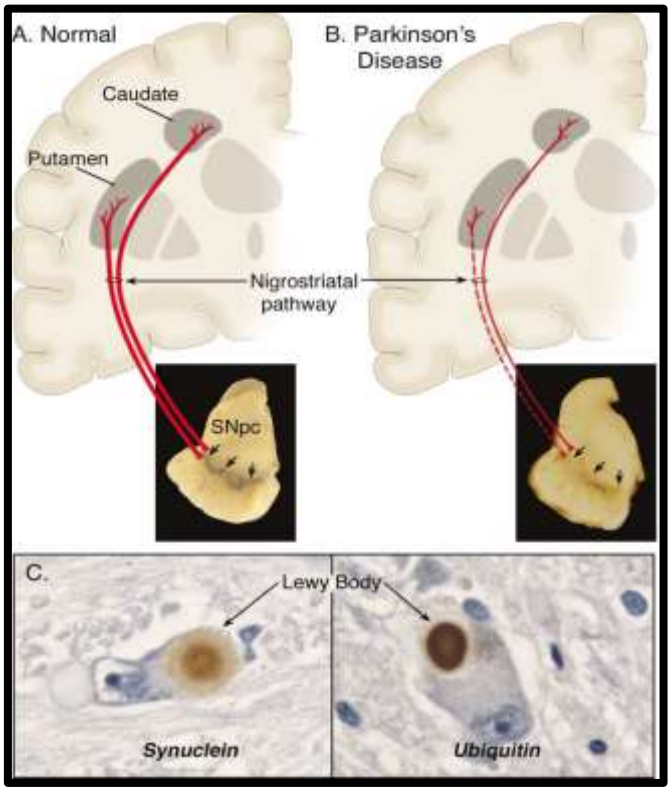

Figure 2.3: Neuropathology of PD. (A) Schematic representation of the normal dopaminergic neurons of the nigrostriatal pathway (in red) and a photograph of the normal pigmentation of the SNpc due to neuromelanin. (B) The dopaminergic neurons of the diseased nigrostriatal pathway. The dashed line indicates a marked loss and the thin red solid line indicates a more modest loss and a photograph of the depigmentation of the SNpc. (C) Immunohistochemical labelling of Lewy bodies in a SNpc dopaminergic neuron. Immunostaining with an antibody against α-synuclein reveals a Lewy body (black arrow) with an intensely immunoreactive central zone surrounded by a faintly immunoreactive peripheral zone (left photograph). Conversely, immunostaining with an antibody against ubiquitin yields more diffuse immunoreactivity within the Lewy body (right photograph) (Dauer & Przedborski, 2003).

Several theories exist regarding the molecular mechanisms which are responsible for the degeneration of dopaminergic neurons in patients who suffer from PD. For example, it has been suggested that the dysfunction of the mitochondria and oxidative stress caused by reactive oxygen species (ROS) can contribute to the pathogenesis of PD (Belluzzi *et al.*, 2012). This hypothesis is based on the fact that molecular oxygen is consumed during mitochondrial respiration leading to the formation of byproducts. These byproducts include hydrogen peroxide and superoxide radicals that can cause cellular damage via several reactions, particularly in individuals with mitochondrial dysfunction (Belluzzi *et al.*, 2012).

Several neurodegenerative disorders, including PD, is said to be a result of abnormal deposition of proteins in brain tissue. However, it is still unclear whether the abnormal proteins directly cause toxicity or if they damage cells during the formation of intercellular inclusions (such as Lewy bodies).

Inflammation of the nervous tissue (neuroinflammation) can lead to neurodegeneration as observed in PD (Hirsch *et al.*, 2012). The concentration of interleukins (IL-1β and lL-6), tumor necrosis factor-alpha gene (TNF-α) and interferon gamma (INF-γ), are high in the cerebrospinal fluid (CSF) as well as in the basal ganglia in patients with PD (Mogi *et al.*, 1994a, Mogi *et al.*, 1994b). Oxidative and nitrated forms of α-synuclein can lead to a microglial response directly and release cytotoxic factors (Hirsch *et al.*, 2012).

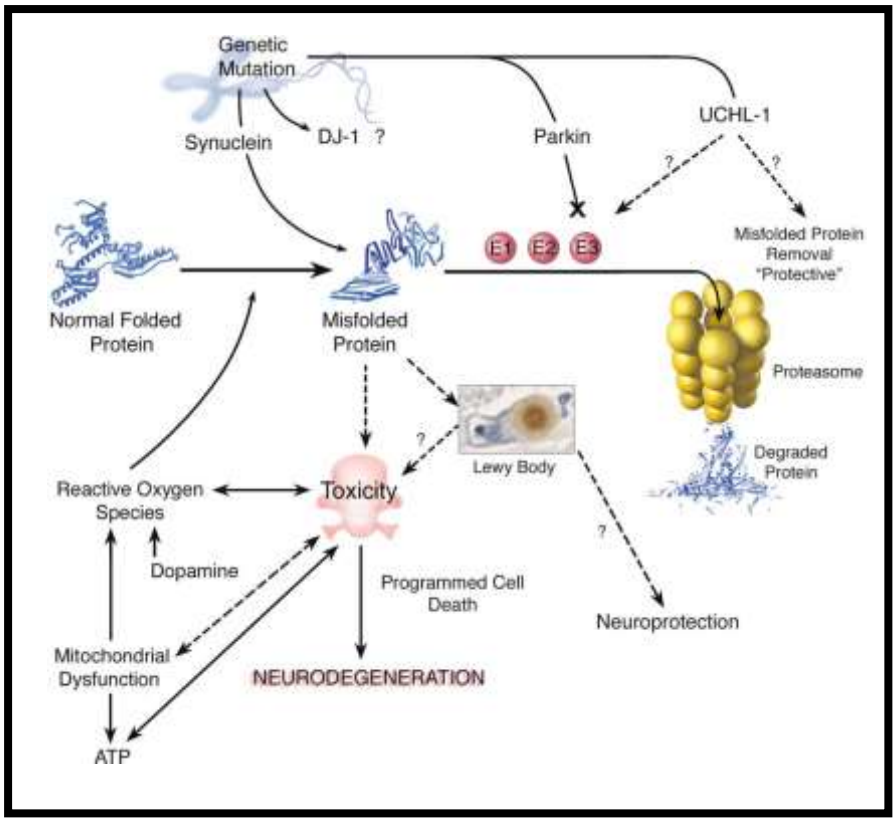

Figure 2.4: Mechanisms of neurodegeneration (Dauer & Przedborski, 2003).

Apoptosis can be described as a form of programmed cell death in which a sequence of events leads to the elimination of cells without releasing toxic substances into the target area. Evidence suggests the presence of apoptosis in neurodegenerative disorders. This is exemplified by conditions associated with increased oxidative stress (Hampton & Orrenius, 1997), e.g. hypoxic ischemic brain injuries (Li *et al.*, 2015), epilepsy (Leonard & Schapira, 2000) and Alzheimer's disease. The presence of apoptotic-like events in individuals with PD has also been suggested (Koppenhöfer *et al.*, 2014).

Excitotoxicity describes the process by which nerve cells are injured or killed by extreme stimulation by excitatory neurotransmitters such as glutamate in the brain (Doble, 1999). Although glutamate is required for regular brain function, excessive amounts can lead to severe excitotoxicity and even cell death. This increase in neurotransmitter stimulation can lead to the damage of cells in neurodegenerative diseases such as Alzheimer's and Huntington's diseases (Hynd *et al.*, 2004), but its contribution to the pathology of PD is still unknown (Van Laar *et al.*, 2015).

Neurotrophic factors are responsible for the support and survival of dopaminergic neurite outgrowth. It is has been hypothesised that a decrease in the expression of one or a combination of these factors could potentiate the degeneration of dopaminergic neurons. This is supported by the finding that brain-derived neurotrophic factor (BDNF), glial-derived neurotrophic factor (GDNF) and nerve growth factor (NGF) are decreased in the SNpc of patients with PD (Gill *et al.*, 2003; Lang & Lozano, 1998). Furthermore, in animals, GDNF and neurturin are protective against neurodegeneration (Eslamboli *et al.*, 2005). Presently, neurturin is being examined in phase II trials (Yacoubian & Standaert, 2009), while GDNF has been evaluated in human trials as antiparkinsonian agents (Lang *et al.*, 2007).

Current research aim to find the sequence in which these pathological events take place and to determine whether these events are the key to solving the pathogenesis of PD (Dauer & Przedborski, 2003)

2.2 SYMPTOMATIC TREATMENT OF PARKINSON'S DISEASE

Since the main characteristic of PD is reduced levels of dopamine (DA) (**Figure 2.5**) in the striatum, treatment is based on either increasing DA levels or effect (by administrating the DA precursor amino acid, L-dopa or by inhibiting metabolising enzymes such as the monoamine oxidase (MAO) or catechol-*O*-methyltransferase (COMT) enzymes (Brunton *et al.*, 2011).

2.2.1 DOPAMINE

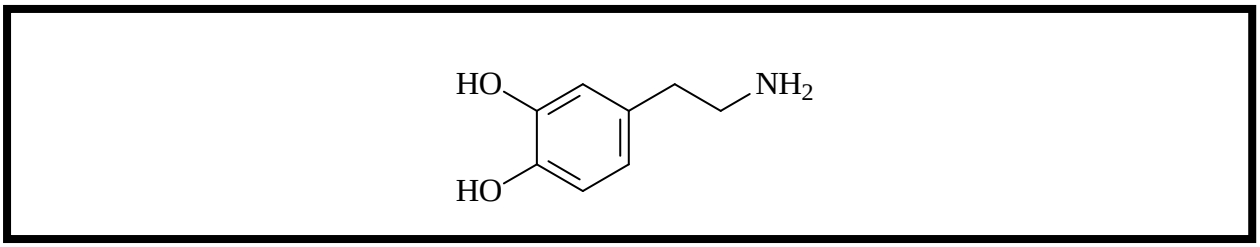

Figure 2.5: Structure of DA.

According to Eidelberg & Pourfar (2011) DA synthesis (**Figure 2.6**) begins with *L*-tyrosine. It is taken up by dopaminergic neurons where it is converted by tyrosine

hydroxylase to 3,4-dihydroxyphenylalanine (L-dopa). Dopa decarboxylase (also known as aromatic L-amino acid decarboxylase) converts L-dopa to DA in this synthetic pathway. DA is actively pumped back (by reuptake) into the nerve terminal, after release and interaction with the receptors. COMT and MAO metabolise DA resulting in the regulation of its levels in nerve terminals. DA is also a substrate for the biosynthesis of norepinephrine and epinephrine (Aminoff, 2009; Eidelberg & Pourfar, 2011).

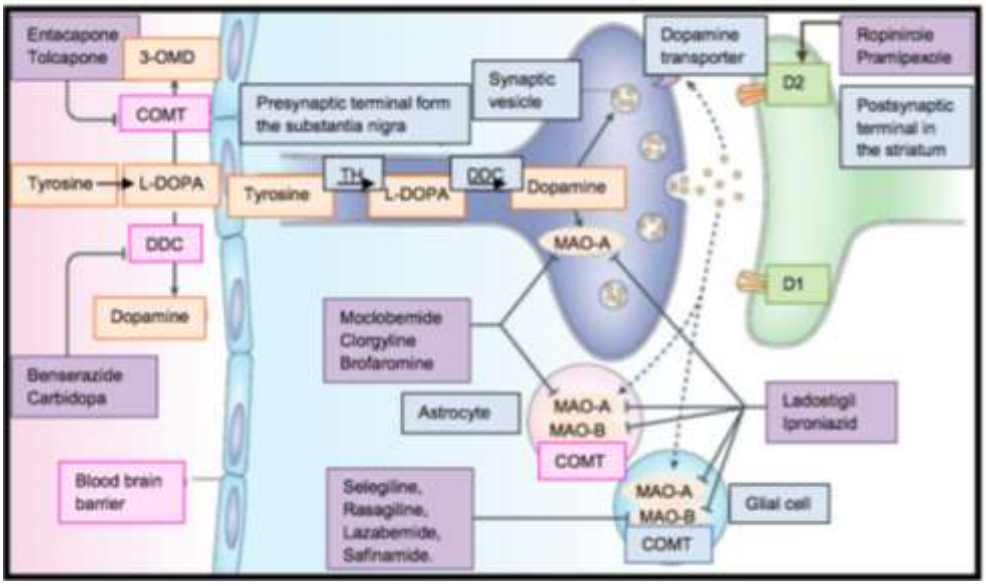

Figure 2.6: Schematic illustration of the metabolism and active transport of dopamine (Aminoff, 2009; Youdim *et al.*, 2006).

Dopaminergic receptors are classified as D1-D5. The dopamine receptors that are particularly important to movement are the D1 and D2 receptors. D1 receptors are located in the SNpc and presynaptically on striatal axons projecting from cortical neurons and from dopaminergic cells in the SNpc (Aminoff, 2009). D2 receptors on the other hand, control the extrapyramidal system (Eidelberg & Pourfar, 2011) and are located postsynaptically on striatal neurons and presynaptically on axons in the SNpc which belong to neurons in the basal ganglia. Dopaminergic antiparkinsonian therapy mainly benefit through D2 receptor stimulation, however D1 stimulation may be required for maximum benefit. Drugs which block D2 receptors can induce PD (Aminoff, 2009). Unfortunately, dopamine does not have a therapeutic effect in patients with PD, since it cannot cross the blood brain barrier (BBB).

2.2.2 L-DOPA

L-dopa or 3,4-dihydroxyphenylalanine (**Figure 2.7**) is the immediate precursor of DA. Whereas dopamine is unable to cross the BBB, L-dopa can be taken up by large neutral amino acid (LNAA) transporters and is converted to DA by the enzyme aromatic L-amino acid decarboxylase once inside the brain (Aminoff, 2009; Müller, 2015).

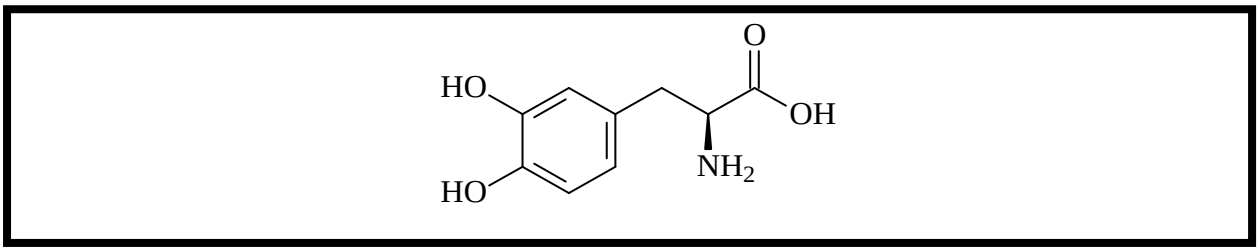

Figure 2.7: The structure of L-dopa used as treatment in PD.

L-dopa is administered in high doses when used alone, since only 1-3% enters the brain unaltered. The rest of the drug is metabolised extra-cerebrally, mainly by decarboxylation to DA, by the enzyme aromatic L-amino acid decarboxylase. However, high doses of L-dopa result in unpleasant side effects such as nausea, vomiting and even cardiovascular effects and L-dopa is therefore seldom used as monotherapy. Combination with decarboxylase inhibitors to minimise the adverse effects of high doses is therefore preferred (Aminoff, 2009; Müller, 2015).

Long-term use of L-dopa is also associated with severe side effects such as the development of the “on-off”-effect (fluctuation in movement). The “off”-effect is characterised by impaired motor functions. This reappears after the “on”-effect where patients show good response with sufficient dopaminergic neurotransmission. Dyskinesia (involuntary movements) can be present during the “on” and the “off” period (Aminoff, 2009; Müller, 2015). Administration of L-dopa with carbidopa, a decarboxylase inhibitor, has the additional benefit of reducing peak plasma levels and increasing trough plasma levels of L-dopa. As a result, the peak-trough fluctuations are diminished and the “on-off” effect is reduced (Aminoff, 2009).

2.2.3 DECARBOXYLASE INHIBITORS

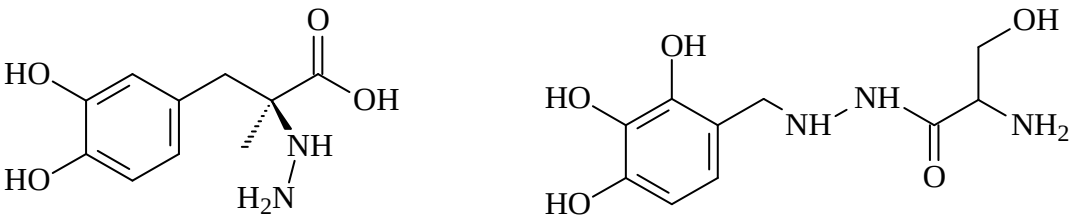

Carbidopa (A) **Benserazide (B)**

Figure 2.8: Structures of decarboxylase inhibitors used as treatment in PD.

Carbidopa (**Figure 2.8 A**) and benserazide (**Figure 2.8 B**) can be classified as peripheral decarboxylase inhibitors (PDI's). Carbidopa is administered with L-dopa to reduce the peripheral metabolism of L-dopa, thus resulting in an increase in L-dopa plasma levels, a longer plasma half-life, and an increase in available L-dopa. The daily requirements of L-dopa can thus be reduced if it is taken with a peripheral decarboxylase inhibitor leading to a reduction in the side effects associated with the use of high doses of L-dopa (Gershanik, 2015).

2.2.4 DOPAMINE AGONISTS

Dopamine receptor agonists serve as a good alternative for L-dopa since no activation by enzymes is required and the duration of action is longer. Unlike L-dopa, these drugs offer receptor selectivity, limiting the adverse effects (Kakkar & Dahiya, 2015). These drugs delay the need for L-dopa therapy, thus lowering the incidence of motor fluctuations and dyskinesia associated with L-dopa therapy. They can also be used as add-on therapy to L-dopa, especially in patients who developed motor complications. As a result the L-dopa dose may be reduced limiting the adverse effects of high doses of L-dopa (Aminoff, 2009; Müller, 2015).

Ergot derived dopaminergic agonists, such as bromocriptine (**Figure 2.9 A**) and pergolide (**Figure 2.9 B**), used in the treatment of PD, have been replaced with non-ergoline dopamineric agonists, such as ropinirole (**Figure 2.10 A**) and pramipexole (**Figure 2.10 B**). Both of these drugs have activity at D2-receptors and little or no

activity at D1 receptors, but only pramipexole has affinity for D3-receptors (Aminoff, 2009; Müller, 2015).

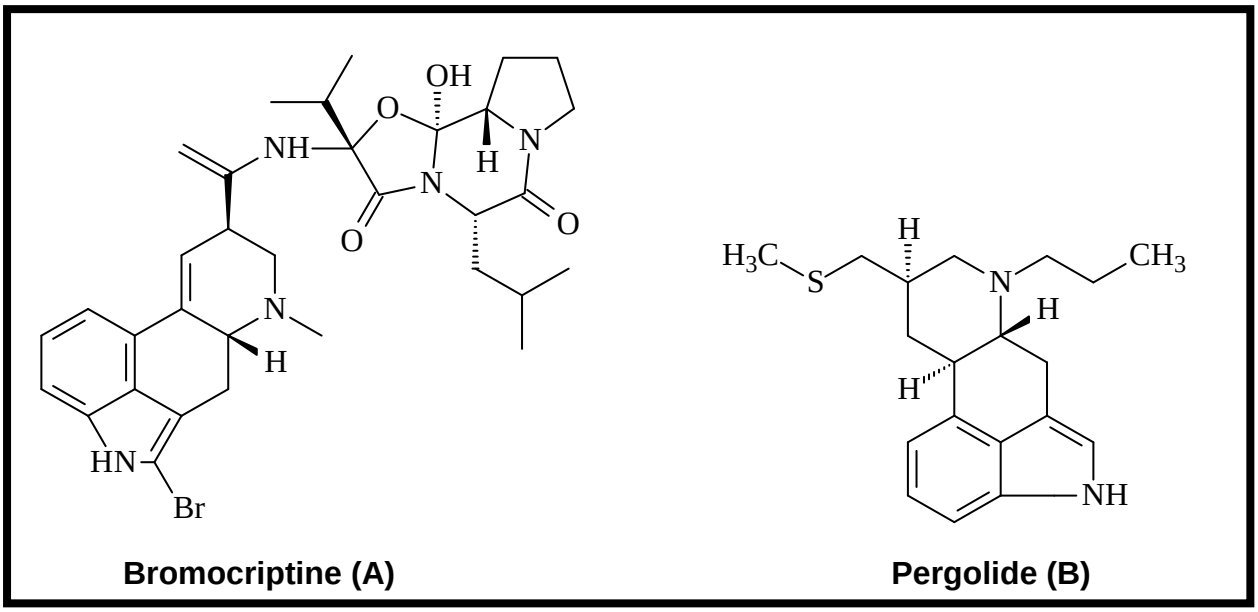

Bromocriptine (A) **Pergolide (B)**

Figure 2.9: Structures of ergoline dopaminergic agonists used as treatment in PD.

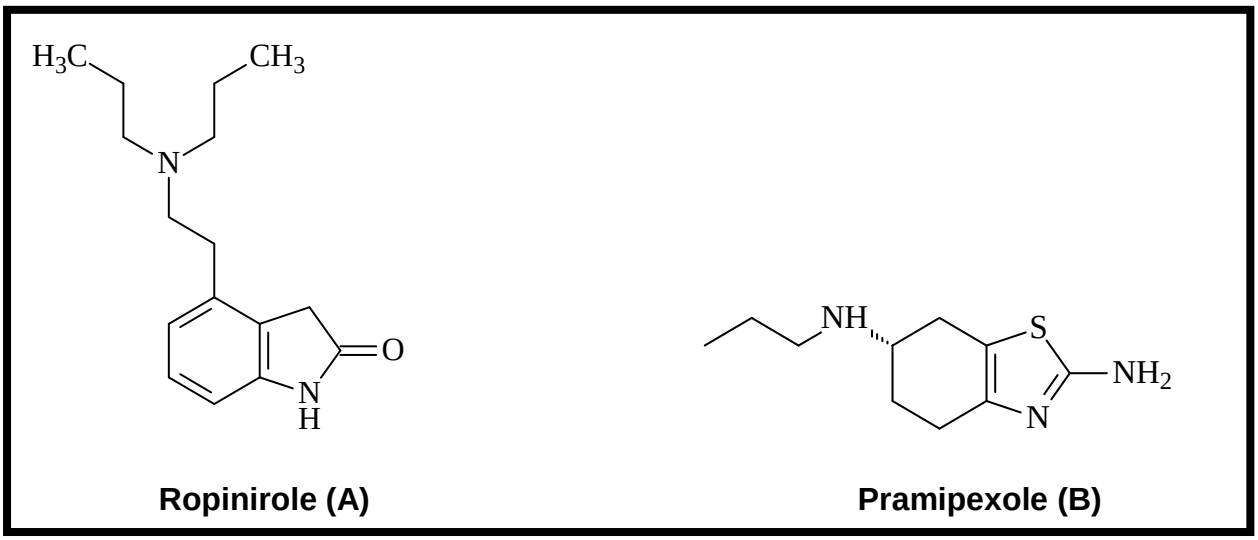

Ropinirole (A) **Pramipexole (B)**

Figure 2.10: Structures of non-ergoline dopaminergic agonists used as treatment in PD.

Adverse effects of DA agonists include hallucinations, confusion, nausea, postural hypotension, somnolence and an increase in the incidence of impulse control disorders such as pathological gambling, shopping, eating and hypersexuality (Kakkar & Dahiya, 2015). However, evidence suggests that only the use of ergolinic

DA agonists is associated with the high risk of developing cardiac valve fibrosis, therefore non-ergoline DA agonists are better tolerated (Kakkar & Dahiya, 2015).

Apomorphine (**Figure 2.11**) can be classified as a non-selective dopamine receptor agonist and has a high affinity for all five DA receptors. Apomorphine has a greater affinity for D1 receptors and resembles the profile of dopamine better when compared to other DA agonists. It also has binding affinities for adrenoreceptors (α_{1D}, α_{2B} and α_{2C}) and histamine receptors where it acts as an antagonist (Boyle & Ondo, 2015).

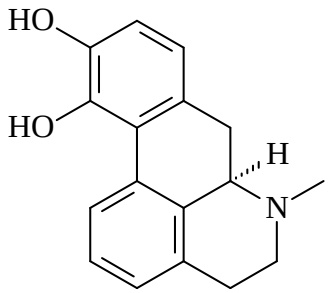

Apomorphine

Figure 2.11: Structure of apomorphine, a non-selective dopamine receptor agonist used as treatment in PD.

Apomorphine is used as an effective treatment for the symptoms of PD. Its highly lipophilic structure allows it to cross cell membranes rapidly, thus leading to the rapid onset of action for “on-off” symptoms of PD (Boyle & Ondo, 2015; Kakkar & Dahiya, 2015). Due to peripheral side effects the use of apomorphine was limited in the past, but with improved delivery systems and medications to control side effects, apomorphine is better tolerated (Boyle & Ondo, 2015).

2.2.5 AMANTADINE

Amantadine

Figure 2.12: Structure of amantadine, a NMDA glutamate receptor antagonist used as treatment in PD.

Amantadine (**Figure 2.12**), a N-methyl-D-aspartate (NMDA) glutamate receptor antagonist, is used as treatment for L-dopa induced dyskinesia (LID) in PD. Amantadine also possesses anticholinergic properties and alters DA release in the striatum (Brunton *et al.*, 2011).

2.2.6 ANTICHOLINERGIC DRUGS

Before L-dopa was discovered, muscarinic acetylcholine receptor antagonists were used as treatment in PD. Although the therapeutic effects and the mechanism of action of these drugs are not completely clear at this stage, it has been suggested that not only do these drugs block the muscarinic receptors in the striatum, but that they also inhibit the presynaptic carrier-mediated DA transport mechanism (Brunton *et al.*, 2011).

The anticholinergic drugs, trihexyphenidyl (**Figure 2.13 A**), benztropine (**Figure 2.13 B**) and diphenhydramine (**Figure 2.13 C**) are most often use as treatment for PD. These drugs have shown antagonistic activity at the NMDA receptor, resulting in the reversal of akinesia and the potentiation of L-dopa effectivity in animal models of PD. Therefore these drugs are used as treatment in early stage PD or as an adjunct to L-dopa (Brunton *et al.*, 2011).

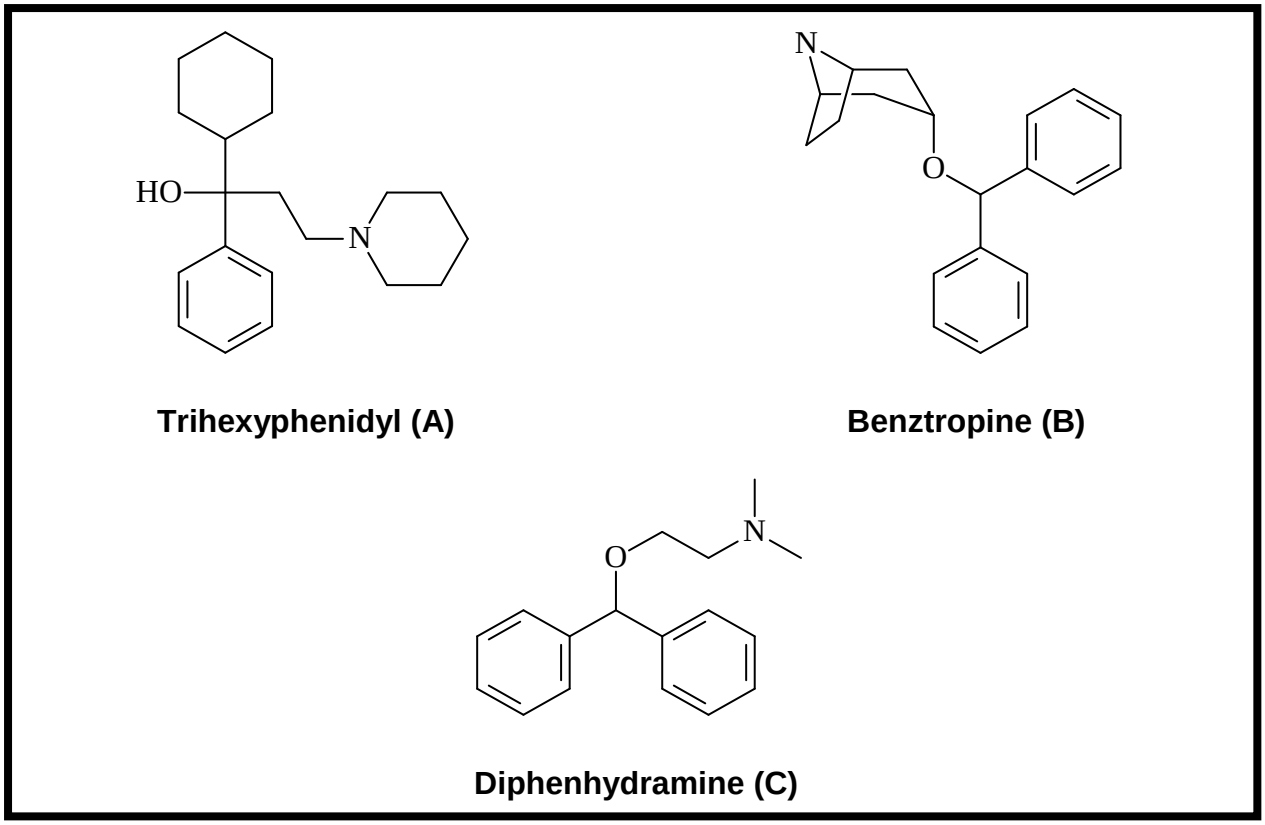

Figure 2.13: Structures of anticholinergic drugs used as treatment in PD.

Other anticholinergic options include biperiden (**Figure 2.14 A**) and orphenadrine (**Figure 2.14 B**). Biperiden is used in the management of drug-induced acute dystonic reactions, since it has anticholinergic activity both centrally and peripherally (Brown & Laiken, 2011). Orphenadrine has non-competitive NMDA receptor antagonistic properties at the PCP binding site. It also possesses atropine-like effects, which contribute to its therapeutic properties (Brunton *et al.*, 2011).

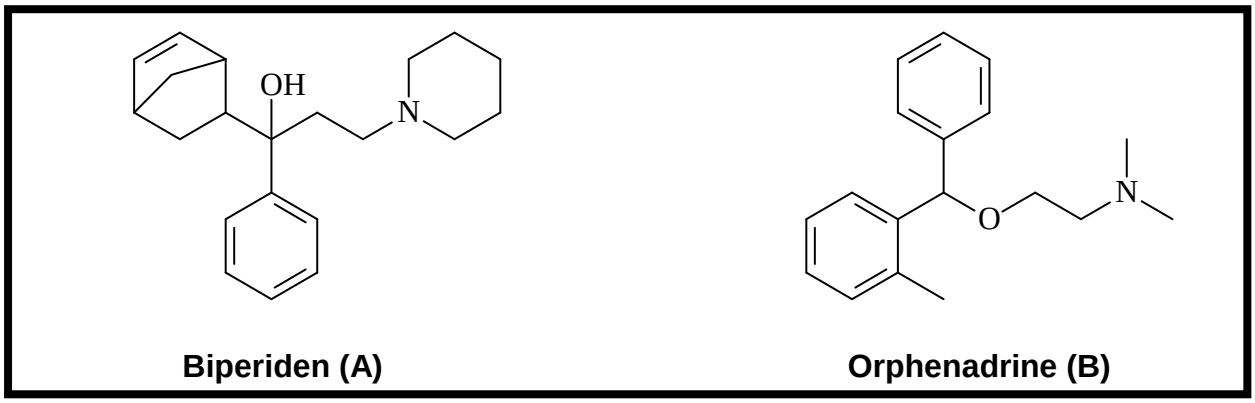

Figure 2.14: Structures of alternative anticholinergic drugs used as treatment in PD.

2.3. MONOAMINE OXIDASE (MAO) INHIBITORS

Since monoamine oxidase (MAO) inhibition is particularly relevant to this study, this enzyme, its function and inhibitors will be discussed in detail in the following sections.

2.3.1 INTRODUCTION

MAO is an enzyme responsible for the metabolism of amines such as DA, adrenaline and serotonin. The selective inhibition of the monoamine oxidase B (MAO-B) enzyme can reduce the symptoms of PD, and since several studies have shown that MAO inhibitors have neuroprotective properties, these agents may have additional advantages as antiparkinsonian agents.

2.3.2 GENERAL BACKGROUND

Mary Hare-Bernheim described the enzyme, tyramine oxidase, which catalysed the oxidative deamination of tyramine. A few years later Hugh Blaschko realized that tyramine oxidase, noradrenaline oxidase and aliphatic amine oxidase were all the same enzyme. This enzyme is capable of metabolising primary, secondary and tertiary amines, but does not metabolise diamines such as histamines. Zeller named this enzyme mitochondrial MAO (Youdim & Bakhle, 2006; Youdim & Buccafusco, 2005).

In 1960 it was discovered that the MAO enzyme consists of two isoforms, namely MAO-A and MAO-B. Although MAO-A and MAO-B are two separate enzymes, they share a 70% sequence similarity and both enzymes have the same flavin adenine dinucleotide (FAD) cofactor (Edmondson *et al.,* 2004). These isoforms further have different pH optima and sensitivity to heat inactivation. They also differ in their substrate and inhibitor specificities. MAO-B is the isoform which is predominantly responsible for the breakdown of dopamine into 3,4-dihydroxyphenylacetic acid, homovanillic acid, and also deaminates β-phenylethylamine. The selective inhibition of the MAO-B isoform reduces the symptoms of PD, and may even possess

neuroprotective qualities (Youdim & Bakhle, 2006). MAO-A inhibition on the other hand, results in anti-depressive activity.

2.3.3 THE THREE-DIMENSIONAL STRUCTURE OF MAO

2.3.3.1 THE CRYSTAL STRUCTURE OF MAO-B

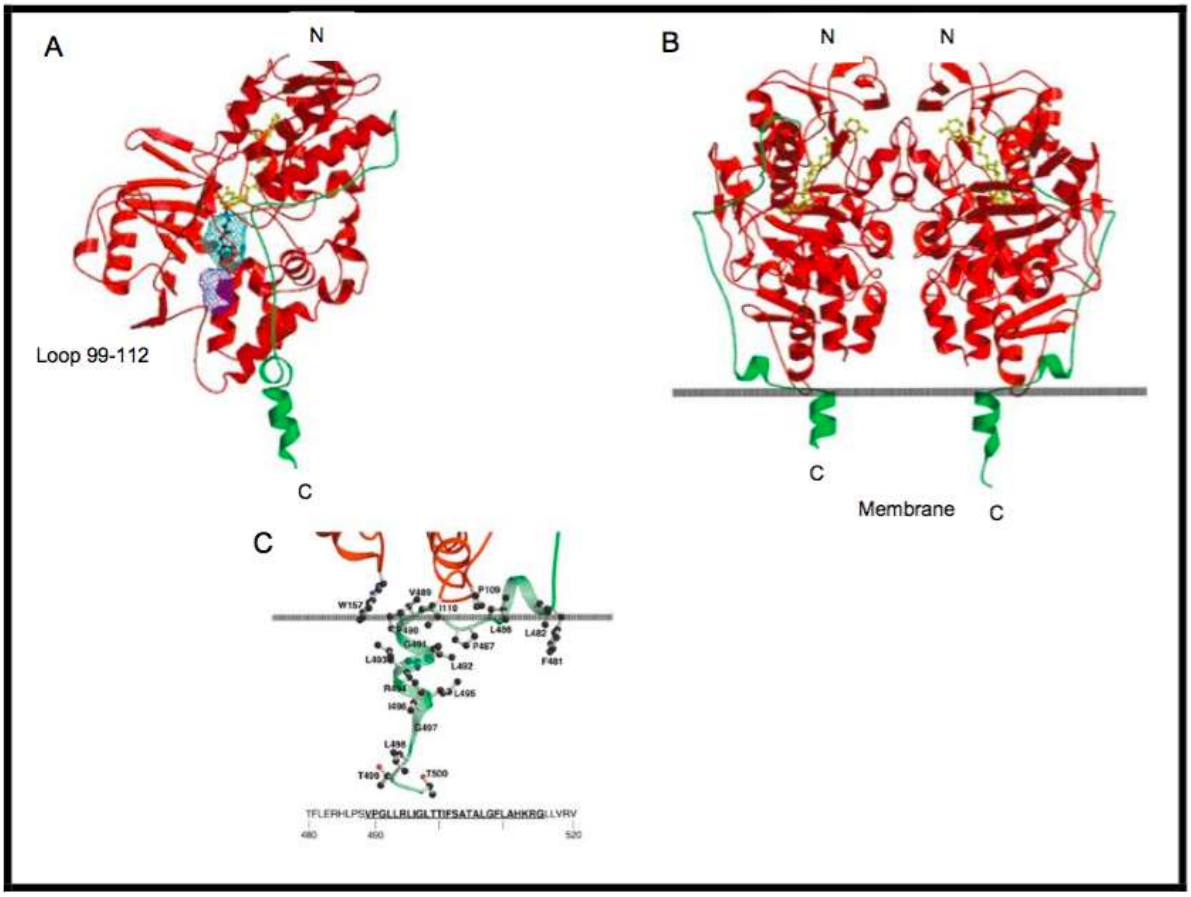

Figure 2.15: The structure of MAO-B. (A) The MAO-B monomer: Adjacent to the active site cavity (coloured in cyan) is the entrance cavity (coloured in blue). Residues 4-460 are coloured red, the C terminal tail, residues 461-500, is coloured green. The FAD cofactor is coloured in yellow. The pargyline inhibitor is shown in black. (B) Shows a ribbon diagram of the MAO-B dimer, indicating the two monomers. (C) Shows a close up view of the membrane binding region in the human MAO-B structure. The C-terminal tail is in green (Binda *et al.,* 2002).

The crystal structure of MAO-B (**Figure 2.15 A, B**) has shown that the enzyme crystallises as a dimer. Each monomeric unit contains a membrane binding domain,

a flavin-binding domain, and a substrate binding domain (**Figure 2.15 A, B**) (Edmondson *et al.*, 2004). The MAO-B active site consists of two cavities that connect the opening to the active site and the site where the flavin binds (**Figure 2.15 A**). The cavities, better known as the entrance cavity, with a volume of 290 $Å^3$, and a larger hydrophobic substrate cavity, with a volume of 420 $Å^3$, result in a total volume of 710 $Å^3$ (Binda *et al.,* 2002). The substrate cavity possesses a flat, elongated disc shape with the longer axis orientated perpendicular to the flavin ring. The amino acids lining the substrate cavity are mostly aromatic and aliphatic. They provide a hydrophobic environment for competitive inhibitors or bound substrates and it is assumed that the entry point of the substrate occurs at the surface of the outer mitochondrial membrane. A flexible loop, consisting of residues 99 -112, has to move for substrates to enter the entrance cavity (Binda *et al*., 2002).

The negatively charged membrane surface electrostatically facilitates the attraction of the positively charged amine substrates to MAO-B. However, for binding and catalysis to occur, the amine must be deprotonated (McEwen *et al.,* 1969; Miller & Edmondson, 1999). The hMAO-B active site is narrower than the hMAO-A active site. The two cavities, present in the MAO-B active site, are separated by Ile 199 and Tyr 326 (Ramsay, 2013) (**Figure 2.15 B**). Crystallographic data of MAO-B in complex with reversible and irreversible inhibitors have shown that, depending on the chemical nature and size of the bound inhibitor, the entrance and substrate cavity separation is altered (Binda *et al.,* 2002). The conformation of the side chain of Ile 199, that can exist in either an “open” or “closed” conformation, controls this separation. Thus, residue Ile 199 serves as a “gate” between the two cavities (Edmondson *et al.,* 2004; Edmondson *et al.,* 2007). Furthermore, for larger flexible inhibitors, Ile 199 would be in an “open position, the cavities would become one, and the inhibitor would bind to both the substrate and entrance cavities of the MAO-B isoform (Ramsay, 2013). For a small inhibitor, Ile 199 would remain in the “closed” position, the cavities would exist as two separate cavities, thus allowing the inhibitor to bind to only one cavity.

Modelling software can be used to visualise the crystal structures of MAO and is used to understand the binding of inhibitors to the active sites of these enzymes (Ramsay, 2013). Thus, different compounds can be evaluated in advance as

potential MAO inhibitors, making it easier to select the most promising compounds for further research.

2.3.3.2 THE CRYSTAL STRUCTURE OF MAO-A

The inhibitor selectivity between MAO-A and MAO-B is due to structural differences, including differences in the size and shape of the substrate/inhibitor cavities. For example, the hMAO-A cavity is restricted by Ile 335 and Phe 208, where as the cavities of hMAO-B is restricted by Tyr 326 and Ile 199.

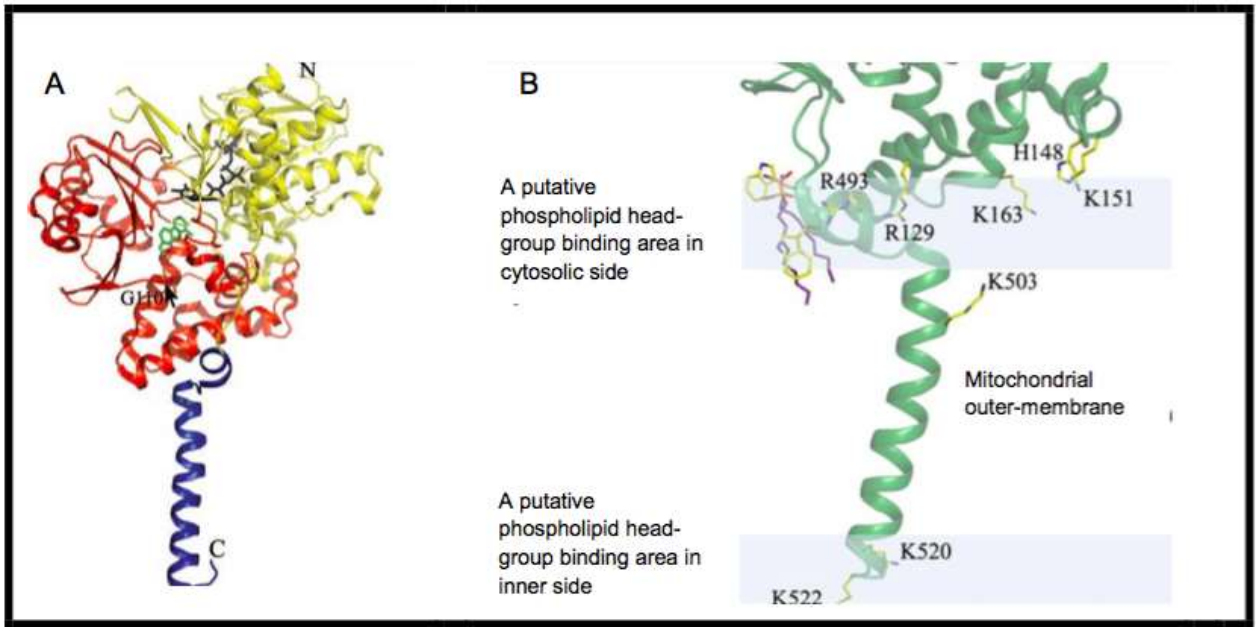

Figure 2.16: The structure of human MAO-A as well as a binding model of MAO-A to the mitochondrial outer membrane. (A) The MAO-A structure can be divided into two domains, the extra-membrane domain (yellow and red), and the membrane binding domain (blue). The FAD binding region (yellow), and the substrate/inhibitor binding region (red). The FAD cofactor (black) and harmine (green) are also shown (Son *et al.,* 2008). (B) Shows the positively charged residues Arg 129, His 148, Lys 151, Lys 163, Arg 493, Lys 503, Lys 520, and Lys 522. It is presumed that these residues interact with the phospholipid hydrophilic head group at the membrane surface, shown in the blue transparent areas. The upper area represents the cytosolic side (Son *et al*., 2008).

In contrast to hMAO-B, hMAO-A crystalises as a single monomer, and the active site only consists of a single cavity, the substrate cavity. The substrate cavity of hMAO-A

has a volume of 550 $Å^3$ and is wider than the cavity of hMAO-B (Edmondson *et al*., 2007; Ramsay, 2013). The active site cavity of hMAO-B would thus be able to accommodate larger inhibitors than that of hMAO-A.

According to Son and co-workers (2008), mutation of Gln 110 of loop 108-118, may cause a reduction in the activity of the MAO-A enzyme, unless the enzyme is anchored to the membrane. Furthermore, it has been suggested that the flexibility of loop 108-118 is very important to allow the substrate access into the hMAO-A active site (Edmondson *et al.* 2007; Son *et al.,* 2008). The C-terminal anchoring the enzyme is an important feature that is required for its biological functions (**Figure 2.16 A, B**).

2.3.4 BIOLOGICAL FUNCTION AND *IN VITRO* MEASUREMENTS OF MAO ACTIVITY

MAO-A and MAO-B are flavoproteins of the outer mitochondrial membrane and catalyse the oxidation of amines to imine (**Figure 2.17**), which is then further metabolised to aldehydes and amines. Therefore, it is assumed that in the peripheral and central nervous systems, intraneuronal MAO-A and MAO-B protect the neurons form exogenous amines, terminate the actions of neurotransmitters and regulate the contents of intracellular amine stores (Youdim *et al.,* 2006).

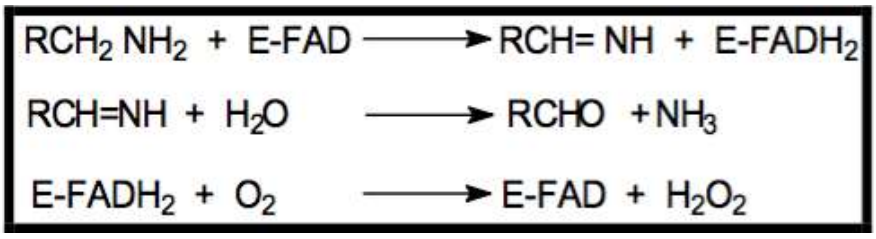

Figure 2.17: MAO-catalysed reactions (Nicotra & Parvez, 1999).

According to Nicotra & Parvez (1999) (**Figure 2.17**) the first step for a MAO substrate is the deamination to yield the corresponding imine (RCH=NH). The second step is the hydrolysis of the imineto produce an aldehyde (RCHO) and ammonia (NH_3). The aldehyde is further metabolised, forming the corresponding acid or alcohol. Molecular oxygen reoxidises the cofactor, E-$FADH_2$, to produce

hydrogen peroxide. Thus, MAO activity can be measured by monitoring the disappearance of the amine substrate, the consumption of oxygen, the formation of the aldehyde, or by monitoring ammonia and hydrogen peroxide formation (Nicotra & Parvez, 1999). The methods used may be continuous or discontinuous, and may include radiometric, fluorometric, luminometric, chromatographic, polarographic and spectrophotometric assays (Nicotra & Parvez, 1999).

Figure 2.17 is only applicable to primary monoamines, since ammonia is not generated during the metabolism of secondary and tertiary monoamines. It is also important to note that the metabolism of Parkinson-inducing MPTP does not result in the formation of ammonia or aldehydes (Nicotra & Parvez, 1999; Singer *et al.,* 1986; Singer & Ramsay, 1995).

2.3.5 THE ROLE OF MAO IN NEUROLOGICAL DISEASES

2.3.5.1 THE ROLE OF MAO-A INHIBITION IN DEPRESSION

Since both noradrenaline and serotonin (the monoamines implicated in depressive illness) are substrates of MAO-A, MAO-A inhibitors can be used to treat depression (Bonnet, 2003). Selective reversible inhibitors of MAO-A, including moclobemide, have antidepressant activity and may also improve vigilance, psychomotor speed and long-term memory (Bonnet, 2003). Furthermore, reversible MAO-A inhibitors, unlike irreversible inhibitors, do not cause liver toxicity or the “cheese reaction” (**Figure 2.18**) (Youdim *et al.,* 2006). The “cheese reaction” is due to the presence of tyramine in many fermented foods, including cheese. Tyramine is a MAO-A substrate, and with irreversible MAO-A inhibition, systemic tyramine concentrations are elevated. Tyramine increases noradrenaline release and the consequence of this can be a severe hypertensive reaction (Youdim & Weinstock, 2004).

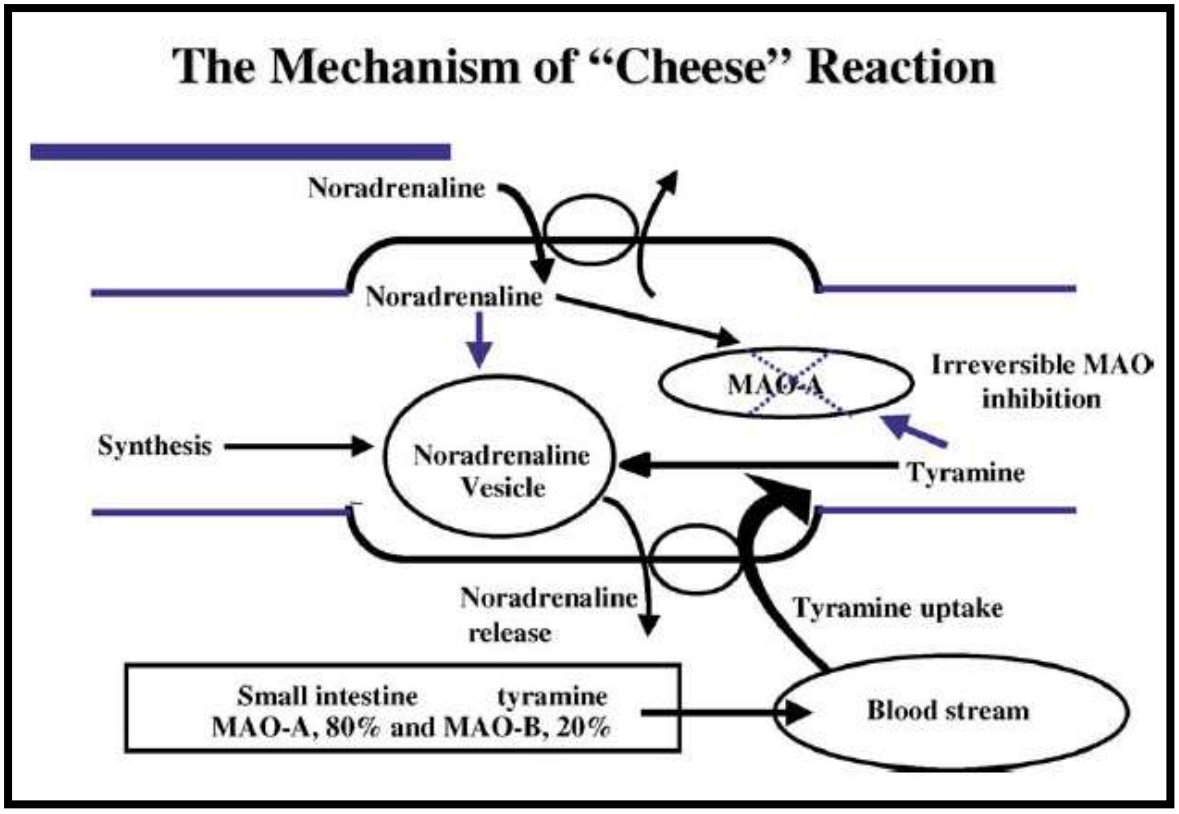

Figure 2.18: The mechanism of tyramine uptake and induced noradrenaline release from peripheral adrenergic neurons in response to irreversible inhibition of MAO-A in the small intestine, blood vessels and adrenergic neurons (Youdim & Weinstock, 2004).

Care must further be taken to not combine MAO inhibitors (especially MAO-A inhibitors) with tricyclic antidepressants or serotonin-selective reuptake inhibitors, as these combinations can cause the serotonin syndrome (Bonnet, 2003). The serotonin syndrome is the result of an excess of serotonergic agonism of the central nervous system receptors as well as the peripheral serotonergic receptors. Symptoms may include tremor, diarrhoea, delirium, neuromuscular rigidity and in life-threatening cases hyperthermia (Boyer & Shannon, 2005).

2.3.5.2 THE ROLE OF MAO-B INHIBITION IN PARKINSON'S DISEASE

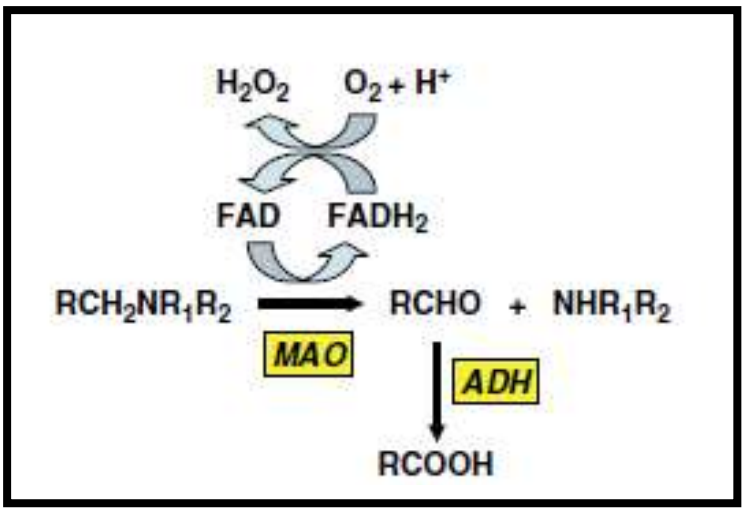

Figure 2.19: Reaction pathway of monoamine metabolism by oxidative deamination by mitochondrial MAO. The primary product of MAO acting on a monoamine is the corresponding aldehyde, usually rapidly further oxidised by aldehyde dehydrogenase (ADH) to a carboxylic acid, which is the final excreted metabolite. Note also that the FAD-$FADH_2$ cycle generates hydrogen peroxide which itself requires inactivation by catalase or, in the brain, glutathione peroxidase (Youdim & Bakhle, 2006).

MAO inhibitors inhibit the metabolism of monoamines such as dopamine, resulting in an increase in dopamine concentrations in the brain. This may providie symptomatic relief in PD. Furthermore, in PD, the sites of neuronal death in the brain are also the sites where iron accumulates (Mandel *et al.,* 2005; Zecca *et al.,* 2004). Oxidative stress appears to be the link between MAO, iron and neuronal damage. The by-product of MAO oxidation of monoamines is hydrogen peroxide (**Figure 2.19**) which is inactivated by GSH, mainly in the brain. The central GSH levels in PD are low, and the accumulated hydrogen peroxide thus becomes available for the Fenton reaction (Youdim & Bakhle, 2006). In the Fenton reaction, Fe^{2+} generates an active free radical, the hydroxyl radical, from hydrogen peroxide (Youdim & Bakhle, 2006). This radical depletes cellular antioxidants, and damages lipids, proteins and DNA. MAO inhibitors therefore not only increase the concentration of amines such as dopamine by inhibiting their metabolism, but also decrease the formation of H_2O_2, thus reducing the formation of hydroxyl radicals and oxidative stress. As a result, MAO inhibitors may prevent the neuronal damage caused by MAO-derived oxidative stress and hydroxyl radicals (Youdim & Bakhle, 2006).

Brain MAO and iron levels increase with aging, thus resulting in elevated levels of both components of the Fenton reaction. Furthermore, this potentiates the production of hydroxyl radical formation. This observation provides a further rationale for the inhibition of MAO in the aged Parkinsonian brain (Mandel *et al.,* 2005; Youdim & Bakhle, 2006).

2.3.6 INHIBITORS OF MAO-B

2.3.6.1 IRREVERSIBLE INHIBITORS OF MAO-B

Selegiline (**Figure 2.20**) and rasagiline (**Figure 2.21**) are the two MAO-B inhibitors that are currently approved for use in the treatment of PD. These drugs can be used as monotherapy or as adjunctive therapy to relieve parkinsonian symptoms (Fernandez & Chen, 2007).

SELEGILINE (*l*-DEPRENYL/(*R)*-DEPRENYL)

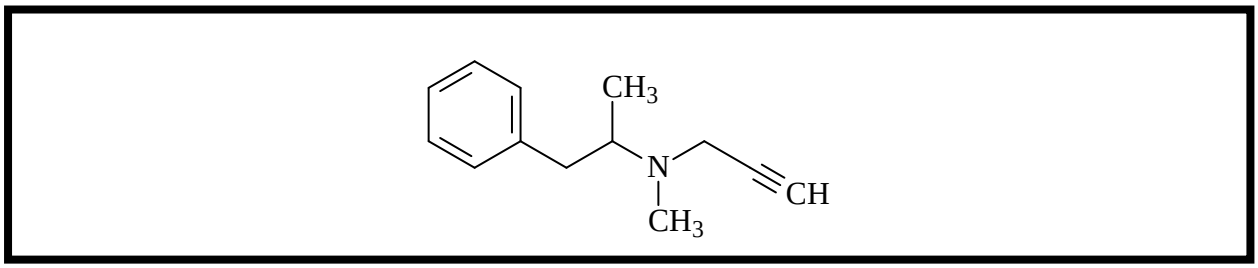

Figure 2.20: The structure of selegiline used as treatment in PD.

Patients, who have been treated with selegiline (**Figure 2.20**), show a delay in the emergence of disability and in the development of symptoms and signs associated with PD (Olanow *et al.,* 1995). Selegiline also shows neuroprotective potential and reduces oxidative stress (*in vitro*) associated with the MAO-catalysed metabolism of DA and glutamate-induced toxicity (Cohen & Spina, 1989; Mytilineou *et al.,* 1997).

During the metabolism of selegiline, neurotoxic amphetamine-derived metabolites, including L-amphetamine and L-methamphetamine, are formed. Adverse effects related to selegiline and its metabolites may include dizziness, dyskinesia, and even

cardiovascular, psychiatric and some motor adverse effects (Churchyard *et al.,* 1997; Fernandez & Chen, 2007; Montastruc *et al.,* 2000; Pålhagen, *et al.,* 2006).

RASAGILINE

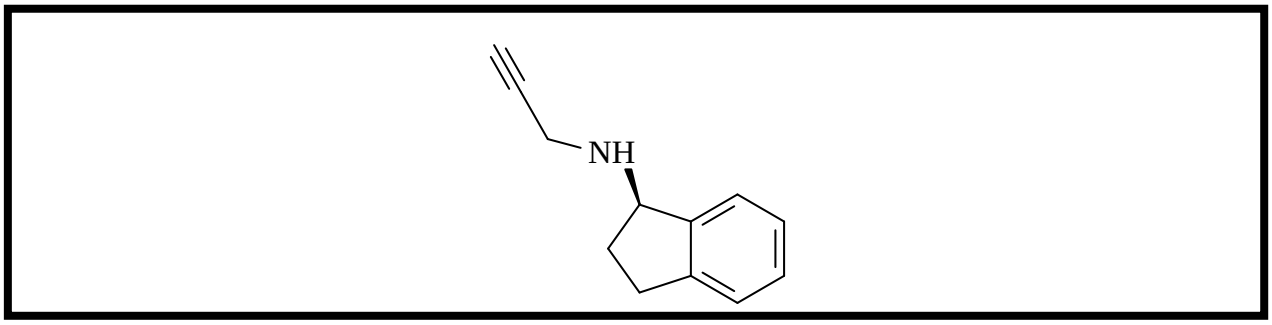

Figure 2.21: The structure of rasagiline used as treatment in PD.

Rasagiline (**Figure 2.21**) can be classified as a second generation MAO-B inhibitor. Rasagiline is recommended for adjunctive therapy to reduce the “off”-time associated with motor fluctuations in PD patients. Rasagiline inhibits degeneration of dopaminergic nigral cells of non-human primates and MPTP-treated mice, thus, indicating a neuroprotective effect in MPTP-induced parkinsonism (Chen & Swope, 2005; Kupsch *et al.,* 2001; Youdim *et al.,* 1999).

Rasagiline also has anti-apoptotic and antioxidant potential. Furthermore, it is reported that rasagiline is safer to use than selegiline, as it is not metabolised to yield toxic amphetamine-derived metabolites. In general rasagiline is well tolerated and it is not associated with vasoreactive or psychiatric adverse effects (Fernandez & Chen, 2007).

PARGYLINE

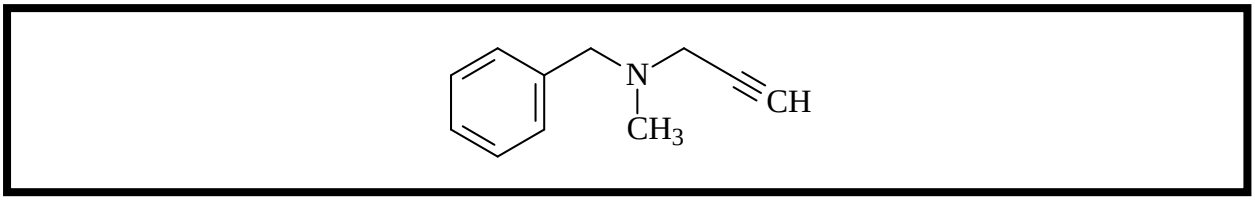

Figure 2.22: The structure of pargyline.

Pargyline (**Figure 2.22**) is a selective irreversible inhibitor of the MAO-B isoform (Yamada & Yasuharaz, 2004). Pargyline has neuroprotective activity in MPTP-treated mice (Kumagai *et al.,* 1999) as well as in 6-OHDA-treated rodents (Aristieta *et al.,* 2012). Although this drug may be used to reduce the symptoms of PD, some side effects may be expected as it is an irreversible inhibitor of the MAO-B isoform.

LADOSTIGIL

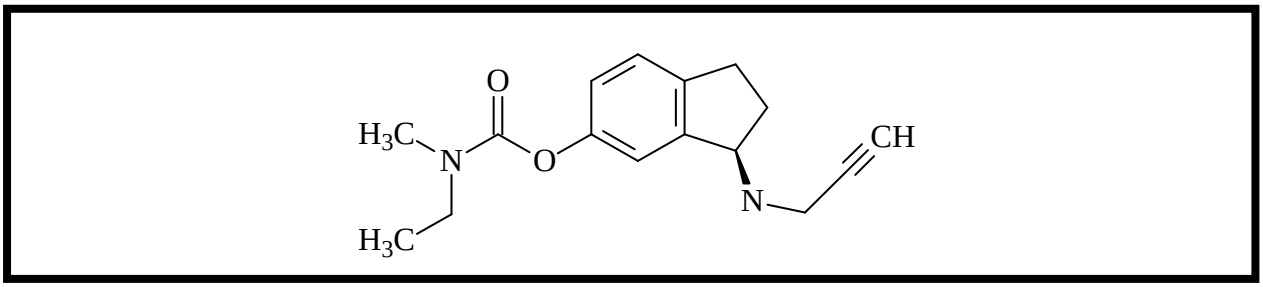

Figure 2.23: The structure of ladostigil.

Ladostigil (**Figure 2.23**) is currently in phase II clinical studies for the treatment of PD. In addition to its irreversible inhibition of MAO-A and MAO-B, ladostigil is a cholinesterase inhibitor. Studies have indicated that ladostigil selectively inhibits MAO-A and MAO-B in the brain, thus allowing tissue-selective irreversible inhibition in the brain without inhibition of MAO-A and MAO-B in the gut or liver (Mandel *et al.,* 2005; Sagi *et al.,* 2005). Ladostigil may also have antidepressant activity since it increases noradrenalin, serotonin and DA in the hippocampus and striatum of rat and mouse animal models. According to Sagi and co-workers (2005) ladostigil prevents striatal neurodegeneration and DA depletion induced by MPTP in a mouse

model. Ladostigil also has anti-apoptotic properties and it may be used to reduce the symptoms of PD (Mandel *et al.,* 2005; Youdim & Bakhle, 2006).

2.3.6.2 REVERSIBLE INHIBITORS OF MAO-B

LAZABEMIDE

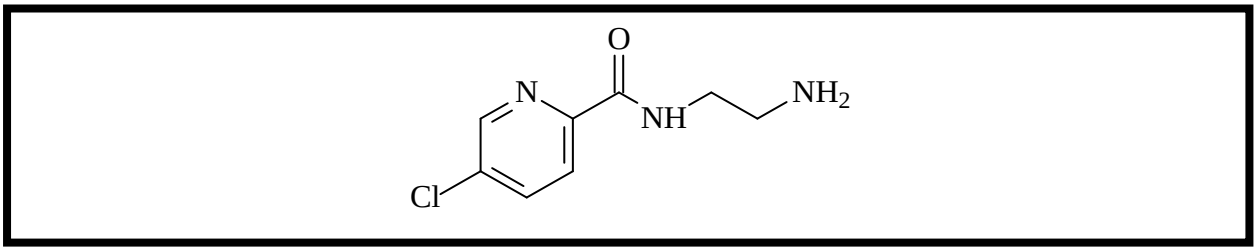

Figure 2.24: The structure of lazabemide.

According to Youdim & Bakhle (2006), lazabemide (**Figure 2.24**) is the only reversible, selective MAO-B inhibitor on the market used as treatment for PD. Lazabemide does not cause the “cheese reaction”, and should have fewer side effects than the irreversible and non-selective MAO inhibitors (Youdim & Bakhle, 2006).

Furthermore, lazabemide can be used to treat therapy resistant depression when combined with a reversible MAO-A inhibitor and it also can prevent neurodegeneration and DA depletion induced by the neurotoxin, MPTP, in mouse models of PD (Youdim & Bakhle, 2006).

SAFINAMIDE

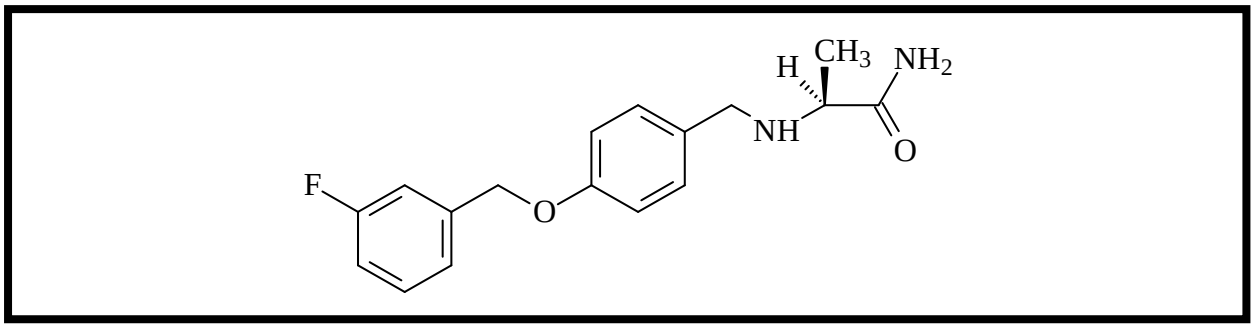

Figure 2.25: The structure of safinamide.

Safinamide (**Figure 2.25**) is an α-aminoamide derivative that shows potential as a selective, reversible MAO-B inhibitor and as well as a DA reuptake inhibitor (Binda *et al.,* 2002; Fernandez & Chen, 2007; Stocchi *et al.,* 2012). Furthermore, studies have shown that safinamide treatment can improve motor scores in PD patients. Safinamide can also be used in combination with DA replacement therapy to improve cognitive function (Binda *et al.,* 2002; Fernandez & Chen, 2007; Stocchi *et al.,* 2012).

2.3.7 INHIBITORS OF MAO-A

2.3.7.1 IRREVERSIBLE INHIBITORS OF MAO-A

Irreversible inhibitors of MAO-A include clorgyline (**Figure 2.26 A**), tranylcypromine (**Figure 2.26 B**) (also inhibits MAO-B) and phenelzine (**Figure 2.26 C**) (also inhibits MAO-B). These inhibitors are rarely used due to their ability to cause the “cheese reaction” (Youdim & Bakhle, 2006).

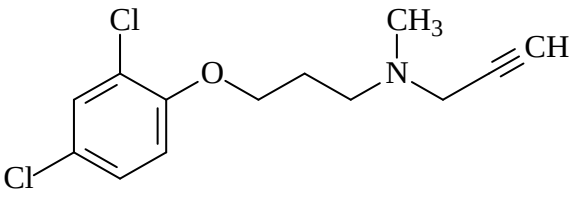

Clorgyline (A)

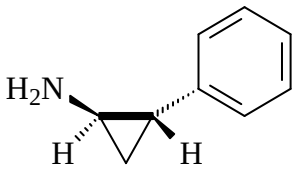

Tranylcypromine (B)

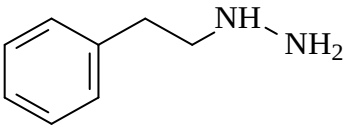

Phenelzine (C)

Figure 2.26: The structures of clorgyline, tranylcypromine and phenelzine.

Iproniazid **(Figure 2.27)** was the first MAO inhibitor used successfully to treat depressive illness. However, iproniazid may cause serious side effects including the ”cheese reaction" and liver toxicity, limiting its use (Youdim *et al*., 2006; Youdim & Bakhle, 2006).

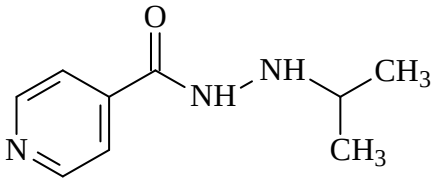

Figure 2.27: The structure of iproniazid.

2.3.7.2 REVERSIBLE INHIBITORS OF MAO-A

MOCLOBEMIDE AND BROFAROMINE

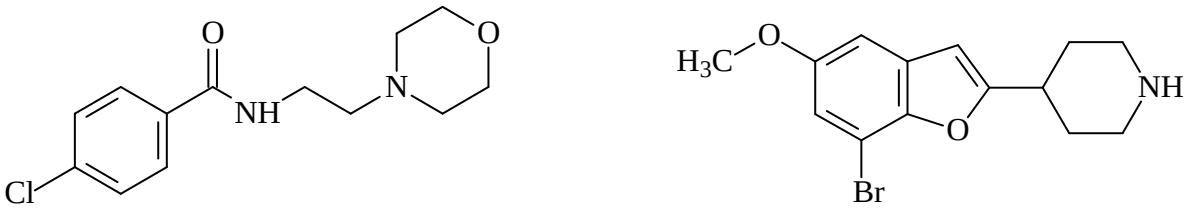

Moclobemide (A) **Brofaromine (B)**

Figure 2.28: The structures of moclobemide and brofaromine.

Moclobemide (**Figure 2.28 A**) and brofaromine (**Figure 2.28 B**) are both selective reversible MAO-A inhibitors with antidepressant activity. These drugs seem to be well-tolerated and have less side effects than the irreversible MAO-A inhibitors. Both of these inhibitors also increase DA release; however it does not alter the steady state levels of DA in the brain. Studies conducted by Youdim and Weinstock (2004) have shown that, when moclobemide was given in combination with levodopa, it had a mild symptomatic effect on motor functions in PD.

Furthermore, moclobemide also improves vigilance, psychomotor speed and long term memory (Bonnet, 2003). Moclobemide is used in therapy resistant depression and can also be used to treat depression in PD (Youdim & Bakhle, 2006; Youdim *et al.,* 2006).

2.4 CATECHOL-*O*-METHYLTRANSFERASE INHIBITORS (COMT)

2.4.1 INTRODUCTION

Since COMT inhibition is particularly relevant to this study, this enzyme, its function and inhibitors will be discussed in detail in the following sections.

The COMT enzyme can be defined as a major catabolic regulator of synaptic catecholamine neurotransmitters and catalyses the transfer of a methyl group to catecholamines, thus leading to a decrease in the concentrations of

neurotransmitters such as dopamine, norepinephrine and epinephrine (Ma *et al.*, 2013; Männistö & Kaakkola, 1999; Williams *et al.*, 2007). Inhibition of COMT results in a decrease in the clearance of L-dopa and dopamine (Männistö & Kaakkola, 1999), thus leading to a maintained level of dopamine in the brain and increased L-dopa efficacy (Ma *et al.*, 2013, Männistö & Kaakkola, 1990). The study of COMT inhibitors is important since they, in addition to their symptomatic potential, has the promise of possessing neuroprotective qualities (Cools, 2006).

2.4.2 GENERAL BACKGROUND

In 1958, the enzyme that catalyses the *O*-methylation of catechols, such as catecholamines, was first described by Axelrod and co-workers (Axelrod & Tomchick, 1958; Männistö & Kaakkola, 1999). As mentioned earlier, COMT is a major catabolic regulator of synaptic catecholamine neurotransmitters and catalyses the transfer of a methyl group to catecholamines (Ma *et al.*, 2013; Männistö & Kaakkola, 1999; Williams *et al.*, 2007). COMT exists in two forms. The soluble (S-COMT) isoform is present at high levels in the majority of tissues while the membrane-bound (MB-COMT) isoform is prevalent in the brain (Jatana *et al.*, 2013). A 50 residue long extension in the MB-form, which is the signal sequence for membrane anchoring, is the only difference between the two isoforms (Ma *et al.*, 2013). MB-COMT may be more relevant in inactivation of catecholaminergic neurotransmitters, whereas S-COMT plays a more important role in inactivation of endogenous and xenobiotic catechols in other tissues (Ma *et al.*, 2013; Männistö & Kaakkola, 1999).

The first COMT inhibitors were introduced between 1958 and 1975, and are extensively reviewed by Guldberg and Marsden (Männistö & Kaakkola, 1999). In the late 1980s, research interest in COMT inhibition was renewed with the introduction of the selective second-generation COMT inhibitors (Männistö & Kaakkola, 1990, 1999). Soon after, the structures of the two isoforms of COMT were defined, leading to the cloning of the COMT polypeptide cDNAs (Männistö & Kaakkola, 1999).

2.4.3 STRUCTURE AND CATALYTIC MECHANISM OF COMT

S-COMT of both human and rat contain 221 amino acids with a molecular mass of 24.8 and 24.4 kDa, respectively. There is an 81% similarity between the human S-COMT and the corresponding rat enzyme (Lundström *et al.,* 1995; Männistö & Kaakkola, 1999). A total of 17 amino acids in rat and 20 in human MB-COMT operate as hydrophobic membrane anchors (Lundström *et al.,* 1995; Männistö & Kaakkola, 1999). The rest of the MB-COMT molecule is suspended on the cytoplasmic side of the intracellular membranes (Lundström *et al.,* 1995; Männistö & Kaakkola, 1999).

Magnesium(II) ions and the cofactor, S-adenosyl-*L*-methionine (AdoMet/SAM), are essential requirements for the methylation of catechol substrates by the COMT enzyme. Early kinetic studies with the partially purified enzyme suggested several different catalytic mechanisms, including the ping−pong mechanism or the rapid random equilibrium mechanism (Kiss & Soares-da-Silva, 2014).

Woodard and co-workers (1980) concluded that the mechanism is sequentially ordered and that the methylation reaction proceeds in a single step via a tight S_N2-type transition state in inversion mode without the involvement of a methylated enzyme intermediate (Kiss & Soares-da-Silva, 2014; Woodard *et al.,* 1980).

The soluble form of recombinant rat COMT in complex with the methyl donor AdoMet, a magnesium(II) ion, and a simple tight-binding nitrocatechol (3,5-dinitrocatechol, 3,5-DNC) was successfully co-crystallised more-or-less three decades after Axelrod's pioneering work (Kiss & Soares-da-Silva, 2014; Vigren *et al.*, 1991). A number of other crystallographic structures of human and rat S-COMT bound to various inhibitors have also been crystallised (Kiss & Soares-da-Silva, 2014; Ma *et al.*, 2013).

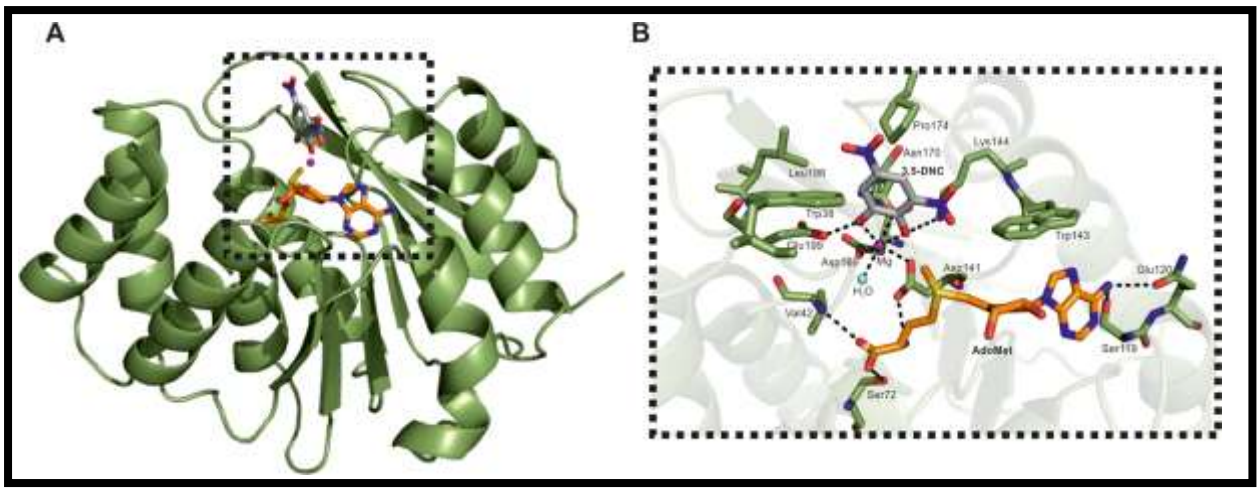

Figure 2.29: Rat S-COMT in complex with the methyl donor AdoMet, the Mg^{2+} ion and ligand 19: (A) schematic representation of the 3D structure of the protein; (B) enlarged view of the catalytic site (Kiss & Soares-da-Silva, 2014).

Analysis of the crystal structures revealed that the structural fold of human and rat S-COMT is similar. The overall structure of rat S-COMT in complex with 3,5-DNC and the enlarged view of the catalytic site are shown in **Figures 2.29 A and B**, respectively. COMT possesses a single domain, a mixed α/β-protein structure in which the eight α-helices surrounds the seven-stranded central β-sheet core (**Figure 2.29 A**). The active site of COMT consists of the catalytic region with the magnesium(II) ion and the AdoMet binding domain. The cofactor, AdoMet, can be found in a buried cleft, whereas the substrate binding site occupies a shallow groove on the outer surface of the protein (**Figure 2.30**). It has been found that AdoMet is the first ligand to bind to the enzyme, followed by the magnesium(II) ion and lastly by the substrate (Kiss & Soares-da-Silva, 2014).

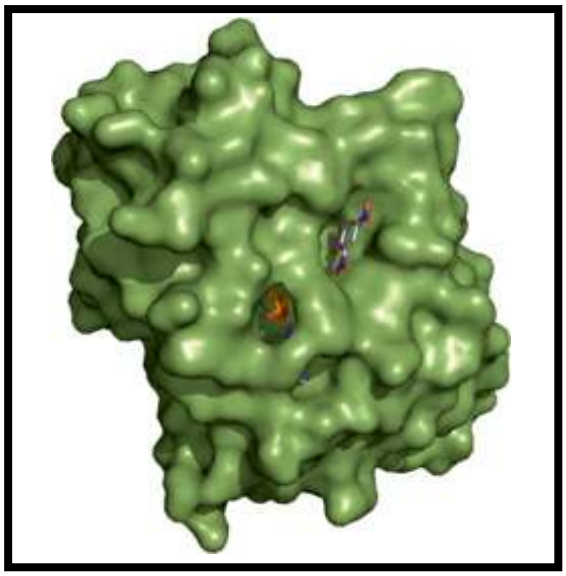

Figure 2.30: Molecular surface of COMT shown in green with the methyl donor AdoMet and 3,5-DNC represented in sticks. The Mg^{2+} ion is depicted in magenta (Kiss & Soares-da-Silva, 2014).

The major molecular interactions with the protein are shown in **Figure 2.29 B**. The adenine ring of AdoMet forms hydrogen bonds with Ser 119 and Glu 120, and van der Waals interactions with Ile 91, Ala 118 and Trp 143 are further observed (Kiss & Soares-da-Silva, 2014).

Hydrogen bonds between residues Val 42, Ser 72, and Asp 141 and the methionine fragment of AdoMet are also present. The magnesium(II) ion has no interaction with the cofactor AdoMet and is located in the centre of the catalytic site. It is octahedrally coordinated to the oxygen atoms of the side chains of aspartic acid residues Asp 141 and Asp 169 and asparagine residue Asn 170. Furthermore, another coordination site is occupied by a molecule of water (Kiss & Soares-da-Silva, 2014).

The fifth and sixth coordinating orbits of the magnesium(II) ion are chelated to each of the two hydroxyl groups belonging to the catechol substrate. The magnesium(II) ion lowers the substrate pK_a, thus, facilitating the deprotonation of the more acidic hydroxyl group of the catechol nucleus by Lys 144. AdoMet is able to methylate the resultant phenolate anion immediately (Kiss & Soares-da-Silva, 2014).

Hydrogen bonding interactions between the hydroxyls of the catechol ring and the side chains of Glu 199 and Lys 144 have also been identified. The so-called hydrophobic “gatekeeper” residues (Trp 38, Trp 143, Pro 174 and Leu 198), maintain the substrate correctly positioned for methylation by making favourable interactions

with the catechol ring. For high binding affinity, the interaction of the catechol ring with Trp 38 is essential. Furthermore, the replacement of Trp 38 with arginine in pig COMT dramatically decreases the binding affinity of the catechol substrate (Kiss & Soares-da-Silva, 2014).

Utilising these observations, several families of inhibitors have been designed and synthesised (Kiss & Soares-da-Silva, 2014; Ma *et al.,* 2013). The analysis of the crystal structures clearly suggest that COMT can interact well with various types of inhibitors incorporating the catechol pharmacophore. The catechol ring binds to the enzyme in a groove at the surface of the protein while the side chain extends out of the catalytic site cavity toward the solvent region. Furthermore, this side chain can be a target for optimization of the pharmacokinetic profile of the inhibitor (Kiss & Soares-da-Silva, 2014).

However, the design of non-catechol inhibitors are more challenging and the limited number of scaffolds identified with COMT inhibitory activity bears testament to this (Männistö & Kaakkola, 1999). According to Kiss and Soares-da-Silva (2014) the replacement of the nitro group with other electron withdrawing groups (EWGs) (e.g., cyano) can result in highly potent trisubstituted COMT inhibitors *in vitro*, but it has been reported that some exhibited shorter *in vivo* half-lives than their disubstituted nitrocatechol analogues. The fact that the active site is close to the surface of the protein is problematic in this case, as the possible interactions with available residues are limited. Another factor which makes COMT a rather difficult target is the fact that the conformation of the enzyme keeps changing as the magnesium, cofactor and substrate binds (Kiss & Soares-da-Silva, 2014; Männistö & Kaakkola, 1999).

2.4.4 THE ROLE OF COMT INHIBITION IN PARKINSON'S DISEASE

The current most effective combination for treating patients with PD involves the co-administration of COMT inhibitors with L-dopa therapy (Aminoff, 2009; Kaakkola, 2000).

COMT inhibitors are added as an adjunct to L-dopa therapy for several reasons such as a decrease in L-dopa elimination, an increase in the area under the concentration

time curve (AUC) of L-dopa, a reduction in the formation of 3-*O-methyldopa* (3-OMD), improvement in the delivery of L-dopa to the brain, a reduction in the L-dopa dose and improvement in the clinical response to L-dopa (Kaakkola, 2000; Männistö & Kaakkola, 1999).

The predominant metabolic pathway for L-dopa elimination includes O-methylation to produce 3-OMD. The formation of 3-OMD occurs mainly in the peripheral organs, such as the liver, the kidney and the gut, where the highest activity of COMT is also observed. Although 3-OMD possesses a long elimination half-life, during chronic L-dopa therapy it has no therapeutic value. 3-OMD is said to be associated with the fluctuations caused by L-dopa therapy and may even be in competition with L-dopa for the transport across the intestinal mucosa and the BBB (Kaakkola, 2000; Männistö & Kaakkola, 1999).

By inhibiting central COMT, the conversion of L-dopa to 3-OMD and the metabolism of DA to 3-methoxytyramine will be inhibited, resulting in higher levels of L-dopa response and activity (Kaakkola, 2000, Männistö & Kaakkola, 1999).

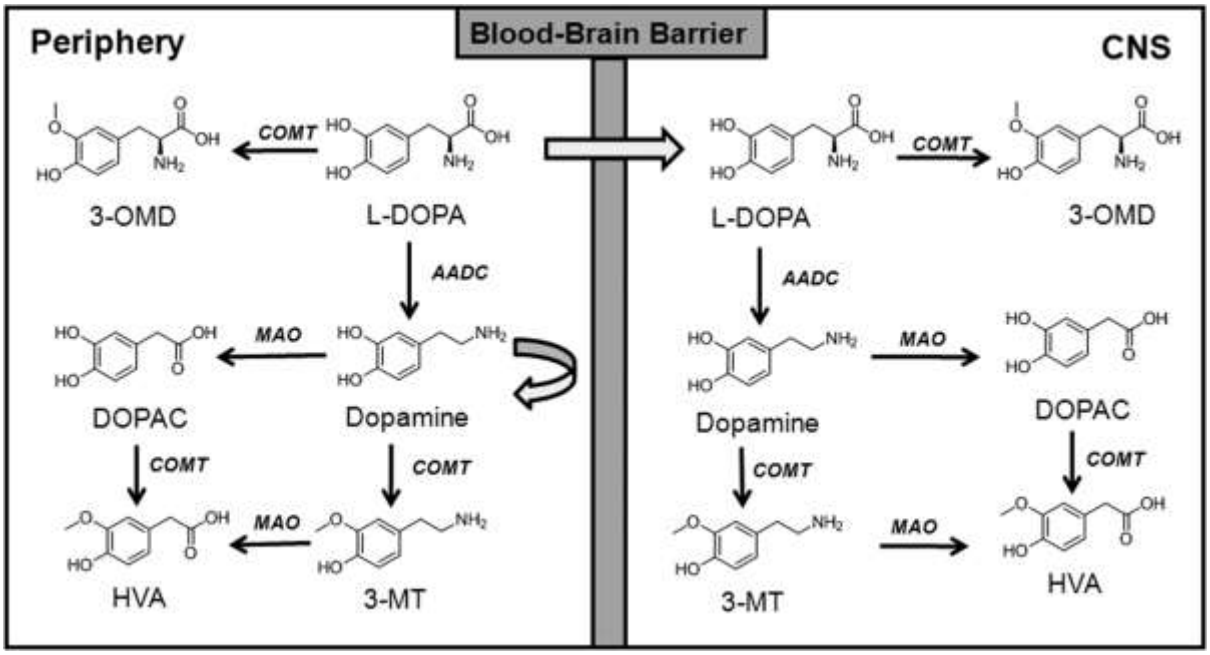

Figure 2.31: Schematic illustration of the metabolism of L-dopa via COMT and MAO pathway (Kiss & Soares-da-Silva, 2014).

The action of other compounds with a catechol structure can also be prolonged by COMT inhibition. Apomorphine is a dopaminergic agent with antiparkinsonian activity which can be defined as one of these drugs with a catechol structure that undergoes O-methylation (Kaakkola, 2000). Although Symes and co-workers (1975) indicated that COMT inhibition can increase the bioavailability and the dopaminergic effects of apomorphine, no clinical results of the combination of apomorphine and a COMT inhibitor are currently available (Kaakkola, 2000; Männistö & Kaakkola, 1999).

2.4.5 COMT INHIBITORS

2.4.5.1 FIRST-GENERATION COMT INHIBITORS

Early COMT inhibitors include pyrogallol and its derivatives, catechol derivatives, tropolones, 8-hydroxyquinolines, iodophenol derivatives, 3-mercaptotyramine, S-adenosylhomocysteine, pyridoxal-5'-phosphate, *l*-ascorbic acid, sulfhydryl binding agents, gallates and U-0521 (3',4'-dihydroxy-2-methyl-propiophenone) (Guldberg & Marsden, 1975). These compounds showed adequate *in vitro* enzyme inhibition, however, their efficacy *in vivo* is low. They are also short acting, lack selectivity and high toxicity levels are frequently observed (Guldberg & Marsden, 1975). These early COMT inhibitors have poor oral bioavailability profiles and are thus excluded from routine clinical use (Guldberg & Marsden, 1975; Männistö & Kaakkola, 1999). Furthermore, a trial with butylgallate and U-0521 was performed in combination with L-dopa therapy in PD, but results were disappointing and these compounds are thus not clinically useful (Kaakkola, 2000; Männistö & Kaakkola, 1990, 1999).

2.4.5.2 SECOND-GENERATION COMT INHIBITORS

Three laboratories independently developed very potent, highly selective, and orally active COMT inhibitors. In most of these molecules, the nitrocatechol moiety is present.

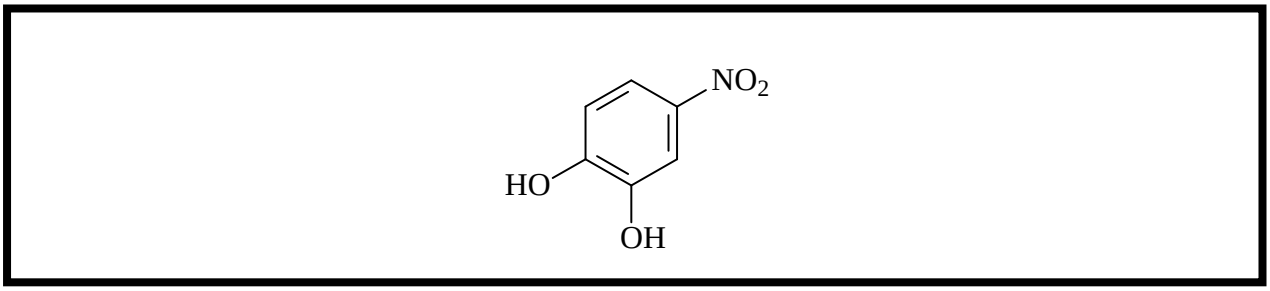

Figure 2.32: Structure of nitrocatechol.

The new COMT inhibitors can be divided into three groups:

1) The mainly peripherally acting compounds.
2) The broad-spectrum compounds working in both the periphery and the brain.
3) The atypical compounds, probably acting in the brain.

This classification was derived from comparative studies done by Männistö and co-workers (Männistö & Kaakkola, 1999), where the decrease in plasma and brain concentration of 3-OMD was used as a marker for peripheral COMT inhibition. On the other hand, the decrease in brain homovanillic acid (HVA) and 3-methoxytyramine concentrations, after pargyline treatment, were used as an indication of COMT inhibition in the brain (Männistö & Kaakkola, 1999).

Available second-generation COMT inhibitors include tolcapone (**Figure 2.33 A**) and entacapone (**Figure 2.33 B**). Both were introduced into clinical practice for PD in the late 1990's (Männistö & Kaakkola, 1999; Müller, 2015).

From a pharmacological point of view, tolcapone appears to be more efficacious than entacapone, with higher inhibition of COMT activity, central action and a longer duration of action after oral administration to rats and humans (Männistö & Kaakkola, 1999; Müller, 2015). Tolcapone was introduced before entacapone and, similar to entacapone, may induce dyskinesia to a considerable extent, depending on the design of the trial. Repeated dosing of L-dopa is known to result in an increase of maximum concentration and bioavailability in plasma (Müller, 2015). Tolcapone possesses the ability to reduce motor symptoms to a similar extent in comparison with the dopamine agonists, bromocriptine and pergolide. However, the quality of life scores are significant better with tolcapone use due to fewer dopamine agonist related side effects.

From November 1998 until April 2004 tolcapone was temporarily withdrawn after three fatal cases of hepatotoxicity occurred. Soon after it was approved again as therapy in PD, however, the administration of tolcapone is now restricted to prescription and supervision by physicians experienced in the management of advanced PD. Furthermore, liver function tests must be carried out on a regular basis (Müller, 2015). It is now known that mutations in the *UDP-glucuronosyltransferase 1A9 gene*, which leads to defective glucuronidation activity, can predispose for hepatotoxicity caused by tolcapone (Müller, 2015). Furthermore, patients with PD must fail to respond or be intolerant of other COMT inhibitors before tolcapone therapy is initiated (Müller, 2015).

Entacapone is the only peripherally acting COMT inhibitor and was initially given as an extra tablet with each L-dopa or periheral decarboxylase inhibitor (PDI) dose. It improves the efficacy of L-dopa on motor impairment, and especially reduces “off"-time in patients with fluctuating PD (Männistö & Kaakkola, 1999; Müller, 2015). Although entacapone is generally well tolerated in the treatment of PD, adverse effects may include a harmless discoloration of the urine, diarrhoea which may occur up to 2–4 months after initial treatment and dyskinesia (Männistö & Kaakkola, 1999; Müller, 2015).

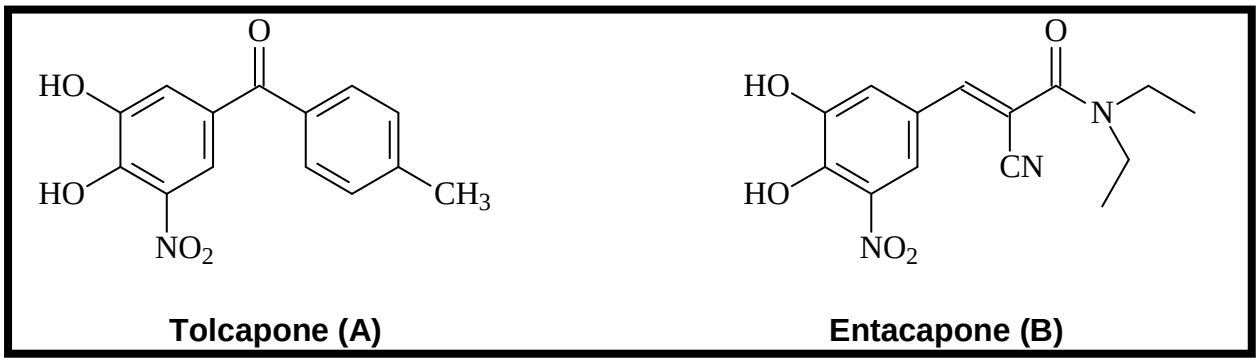

Tolcapone (A) **Entacapone (B)**

Figure 2.33: Structures of second-generation COMT inhibitors used as treatment for PD.

Striatal dopamine can be metabolised by both COMT and MAO-B. Thus, central COMT inhibition with tolcapone alone or in combination with MAO-B inhibition might

provide a symptomatic benefit for patients not receiving L-dopa (Männistö & Kaakkola, 1999; Müller, 2015).

2.5 THE ROLE OF FLAVONOIDS IN NEURODEGENERATIVE DISORDERS

2.5.1 INTRODUCTION

Flavonoids are a group of natural substances with variable phenolic structures and can be found in fruits, vegetables, grains, bark roots, stem, flowers, tea and wine (Lakhanpal & Rai, 2007; Middleton, 1998).

Flavonoids occur as aglycones, glycosides and methylated derivatives. The flavonoid aglycone (**Figure 2.34**) consists of a phenyl ring (A) condensed with a six membered ring (C), which in the 2-position carries a phenyl ring (B) as a substituent (Lakhanpal & Rai, 2007; Narayana *et al.,* 2001).

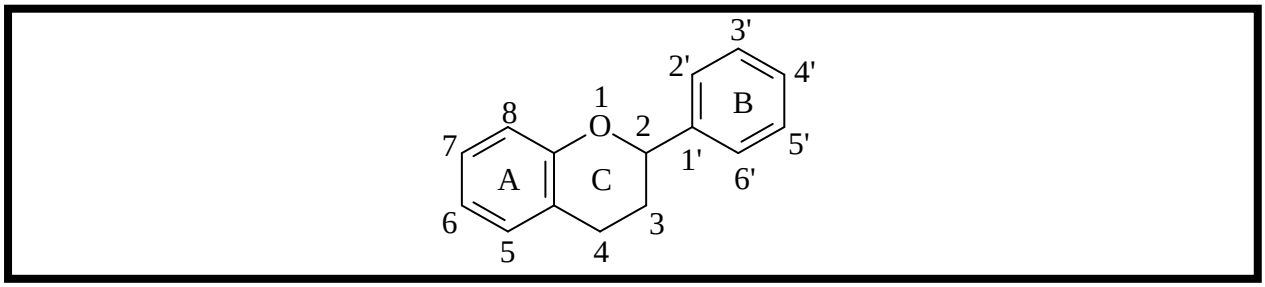

Figure 2.34: The basic structure of flavonoids (Lakhanpal & Rai, 2007).

Flavonoids can be divided into various classes based on their molecular structures (Lakhanpal & Rai, 2007). The six-member ring condensed with the phenyl ring can be either a pyrone (flavonols and flavonones) or its dihydro-derivative (flavanols and flavanones). Furthermore, the position of the benzenoid substituent divides the flavonoid class into flavonoids (2-position) and isoflavonoids (3-position). The structure of flavonols differs from flavonones with regards to the hydroxyl group on the 3-position and the C2-C3 double bond (Havsteen, 1983; Lakhanpal & Rai, 2007). Flavonoids are usually hydroxylated in position 3, 5, 7, 2', 3', 4', 5'. Flavonoids (**Figure 2.35, Table 2.1**) can be divided into seven major groups (Lakhanpal & Rai, 2007; Murphy *et al.,* 2003).

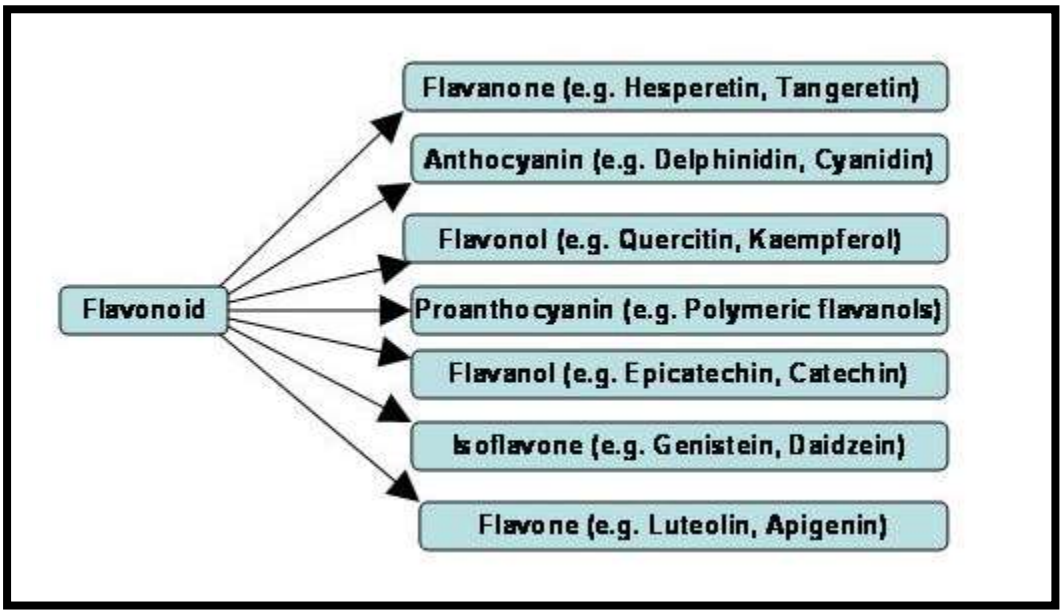

Figure 2.35: A diagram of the major classes of the flavonoids (Lakhanpal & Rai, 2007; Murphy *et al.,* 2003).

Table 2.1: The seven main groups of flavonoids, examples and structures (Lakhanpal & Rai, 2007; Murphy *et al.,* 2003).

Groups	Compounds	Structure
Flavonols	Quercetin Kaempferol Myricetin Isorhamnetin Quercetagetin	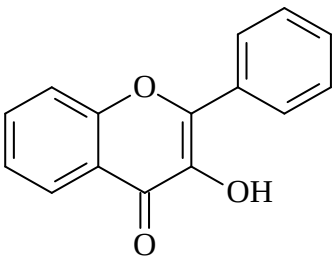
Flavones	Tangeretin Heptamethoxyflavone Nobiletin Sinensetin Quercetogetin Chrysin Apigenin	

	Luteolin Diosmetin Triacetin	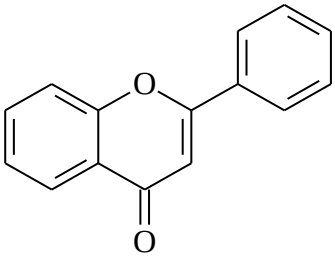
Flavanones	Naringenin Eriodictyol Hesperetin Dihydroquercetin Dihydrofisetin Dihydrobinetin	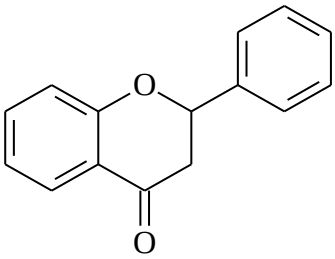
Flavanols	Silibinin Silymarin Taxifolin Pinobanksin	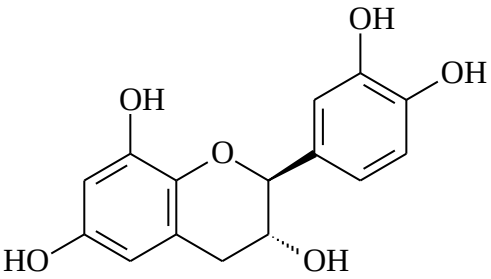
Catechins (Proanthocyanidins)	(+) Catechin Gallocatechin (-) Epicatechin Epigallocatechin Epicatechin 3-gallate Epigallocatechin 3-gallate	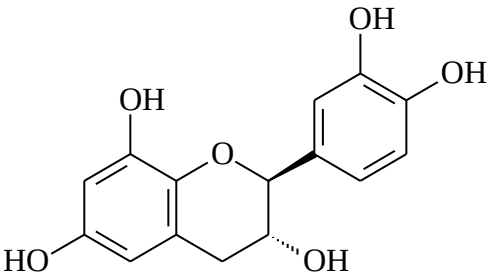
Isoflavones	Daidzein Genistein Glycitein	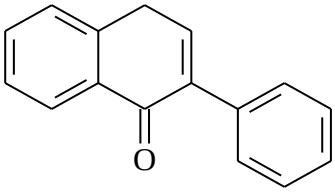

Anthocyanins	Cyanidin Delphinidin Malvidin Pelargonidin Peonidin Petunidin	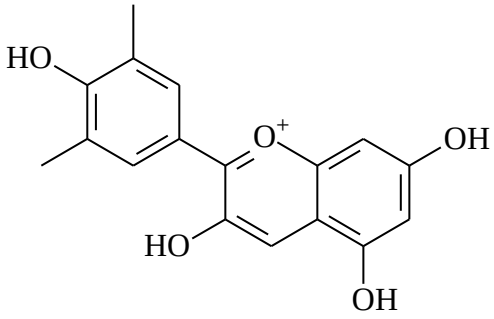

Naturally occurring flavonoids have attracted attention over the years because of a variety of beneficial effects (Lee *et al.*, 2001). These effects may include, antioxidant activity (La Casa *et al.*, 2000), MAO-B inhibitory activity (Lee *et al*., 2001), platelet aggregation, anti-HIV activity (De Clercq, 2000), antibacterial activity (Alcaraz *et al.,* 2000) and tumor cell growth inhibition (Ito *et al.*, 2000; Rafi *et al.*, 2000).

2.5.2 QUERCETIN AND ITS ROLE IN NEURODEGENERATIVE DISORDERS

The most abundant of all the flavonoids is quercetin. It is a bioflavonoid which was first discovered by Nobel Prize laureate Albert Szent Gyorgyi in the 1930's (Lakhanpal & Rai, 2007). The quercetin structure (**Figure 2.36**) consists of 3 rings and 5 hydroxyl groups and can be classified as a member of the class of flavonoids called flavonols. The quercetin scaffold is also present in many other flavonoids including the citrus flavonoids like rutin, the hesperitins, naringenin and tangeretin. In plants it can be found as a glycone or carbohydrate conjugate (Lakhanpal & Rai, 2007).

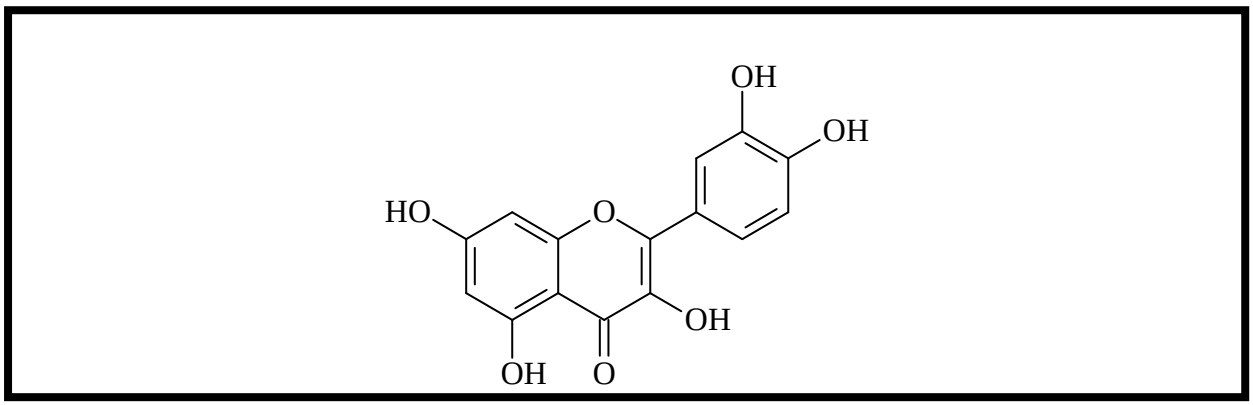

Figure 2.36: The structure of quercetin (Lakhanpal & Rai, 2007; Moskuag *et al.*, 2004).

According to Heo and co-workers (2004) quercetin appears to protect brain cells against oxidative stress, a tissue damaging process associated with Alzheimer's disease and other neurodegenerative disorders (Lakhanpal & Rai, 2007). Quercetin seems to protect the brain functions by inhibiting the formation of fibrillated beta-amyloid, the senile plaque found in Alzheimer's brain (Lakhanpal & Rai, 2007; Tzeng *et al.*, 1991). Singh and co-workers (2003) used an animal model (consisting of ethanol intoxicated mice) to demonstrate the possible cognitive effects of quercetin, where chronic quercetin treatment had shown the reversal of cognitive deficits (Lakhanpal & Rai, 2007).

Quercetin possesses COMT and MAO inhibiting properties and may even reduce the catabolism of L-dopa (Lakhanpal & Rai, 2007). According to Singh and Pattipati (2003) quercetin could possibly serve as an effective adjunct to L-dopa therapy in PD (Lakhanpal & Rai, 2007). In a study conducted by Lee and co-workers (2001), four flavonoids, namely quercitrin, isoquercitrin, rutin, and quercetin (**Figure 2.36**), were isolated from *Melastoma candidum*. MAO-B inhibitory activity and direct hydroxyl radical scavenging activity were illustrated for the four isolated flavonoids by ESR spectroscopy.

Quercetin further has the potential to improve neuroleptic-induced extrapyramidal side effects, such as those caused by haloperidol (Lakhanpal & Rai, 2007; Naidu & Kulkarni, 2004). Quercetin (a powerful antioxidant) seems to be one of the most powerful flavonoids for protecting the body against reactive oxygen species,

produced during the normal oxygen metabolism or induced by mitochondrial toxins (Lakhanpal & Rai, 2007).

2.5.3 KAEMPFEROL IN NEURODEGENERATIVE DISORDERS

Kaempferol (**Figure 2.37**), just like quercetin, can also be classified as a prototype member of the flavonol subclass of flavonoids and is said to have strong antioxidant and anti-inflammatory properties. Kaempferol can be found in tea, broccoli, grapefruit, Brussel sprouts and apples (Li & Pu, 2011; Zuk *et al.*, 2011). It is known to have efficient absorption when given orally and the bioavailability is proportional to its dose (Li & Pu, 2011; Nirmala & Ramanathan, 2011).

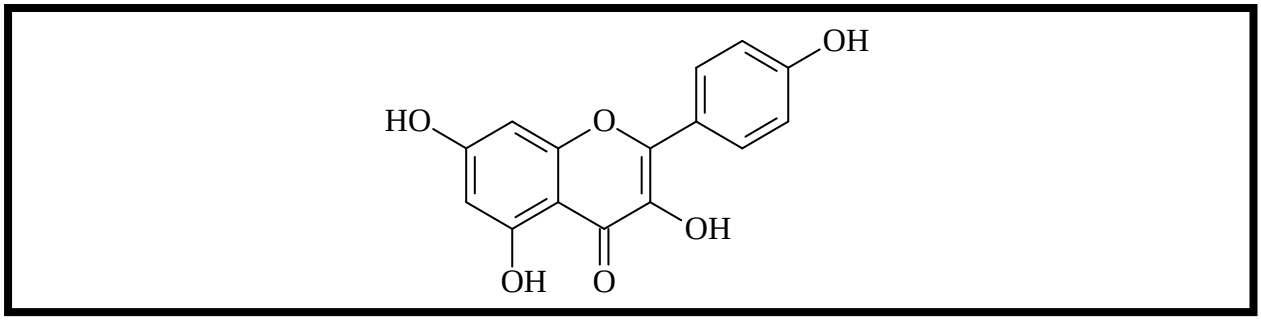

Figure 2.37: The structure of kaempferol (Li & Pu, 2011).

According to Li & Pu (2011) kaempferol has neuroprotective properties against several apoptosis and necrosis-inducing insults, including oxidised low-density lipoproteins (Schroeter *et al.*, 2000; Schroeter *et al.*, 2001) and L-glutamate (Ishige *et al.*, 2001). Ishige and co-workers (2001) have demonstrated that kaempferol effectively blocks the increase in ROS associated with oxidative stress caused by glutamate in the mouse hippocampal cell line HT-22 (Li & Pu, 2011). It has also been demonstrated that kaempferol exerts a strong and prolonged protective effect against rotenone toxicity, a classical toxin that may induce PD (Filomeni *et al.,* 2010; Li & Pu, 2011).

According to Li & Pu (2011) striatal glutamatergic response of rat brain slices was also preserved by kaempferol, posing a more general protection of kaempferol in PD. Furthermore, studies conducted by the same authors have shown that kaempferol derivatives prevent oxidative stress-induced cell death in a DJ-1-

dependent manner *in vitro*. Since DJ-1 is a causative gene product of a familial form of PD, this is also indicative of a neuroprotective effect for kaempferol in PD (Hwang, 2013). However, there has been no systematic research on this topic *in vivo* thus far (Li & Pu, 2011).

2.5.4 QUERCETIN AND KAEMPFEROL AS COMT AND MAO INHIBITORS

Table 2.2: This table contains a summary of the properties of quercetin and kaempferol.

	Quercetin	**Kaempferol**
Flavonoid Class	Flavonol	Flavonol
Structure	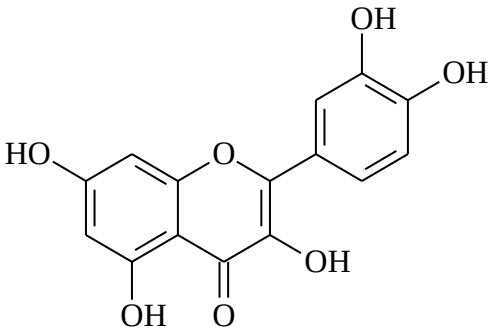	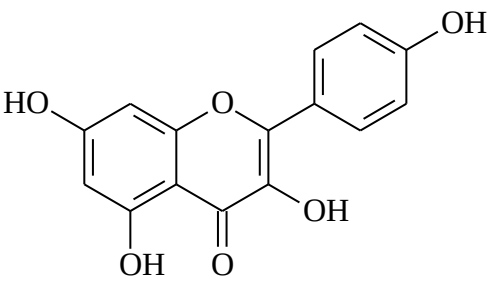
Role in PD	1. Protects brain cells against oxidative stress. 2. COMT inhibitor. 3. MAO inhibitor. 4. Symptomatic treatment for neuroleptic-induced extrapyramidal side effects.	1. Protects brain cells against oxidative stress. 2. Neuroprotective properties against apoptosis and necrosis-inducing insults. 3. Protective qualities against rotenone toxicity. 4. Possess the ability to preserve the striatal glutamatergic response

		of rat brain slices.

2.6 VIRTUAL SCREENING IN DRUG DESIGN

Computer-aided molecular design methods, which includes pharmacophore design and 3D database searches, are aimed at decreasing the overall cost associated with the discovery and development of new drugs by identifying the most promising candidates to focus the experimental efforts on (Kirchmair *et al.*, 2008; Langer & Wolber, 2004; Seidel *et al.*, 2010; Wolber & Langer, 2005). Pharmacophores are a representation of interactions of a group of compounds with a biological target and may be considered as the largest common denominator by a set of active molecules. However, it should be remembered that pharmacophores are not molecules (Langer & Wolber, 2004; Seidel *et al.*, 2010; Wolber & Langer, 2005).

The search of databases, scaffold hopping, ligand profiling, activity prediction, fragment design and pose filtering can be used during pharmacophore design. To develop a pharmacophore, different approaches, such as the structure-based approach and the ligand-based approach could be incorporated (Langer & Wolber, 2004; Wolber & Langer, 2005).

Furthermore, pharmacophore generation may be done manually or automatically. Manual construction includes the use of aligned analogues for ligand-based design and aligned receptor active sites for structure-based design. Automatic ligand-based construction can be divided into a qualitative approach and a quantitative approach. The qualitative approach finds features shared by a set of similarly active ligands, whereas quantitative approach finds features that relate to activity. Furthermore, ligand-based pharmacophore generation consists of two important steps. The first step is the analysis of the training set molecules to identify pharmacophore features whereas the second step is the alignment of the assumed bioactive conformations of the molecules to determine the best overlay of the corresponding features (Langer & Wolber, 2004; Wolber & Langer, 2005).

When a pharmacophore model is generated, molecules which map to its features may be identified by *de novo* design and 3D database search (**Figure 2.38**). The *de novo* approach seeks to generate structures that are chemically reasonable and

novel by linking the parts of the pharmacophore together with fragments (Kirchmair *et al.*, 2008; Langer & Wolber, 2004; Wolber & Langer, 2005). 3D database searches can identify compounds that may exhibit properties outside of the set of compounds used for building the pharmacophore. Furthermore, it can help in the identification of novel chemical structures and molecular features, which are termed scaffold hopping and lead hopping, respectively (Langer & Wolber, 2004; Wolber & Langer, 2005).

The quality of the match between a ligand and a pharmacophore may be given by a fit value. The fit value gives a measure of how well the ligands fit to the pharmacophore. The weights assigned to the pharmacophore features and how close the features correspond to the location constraints are two of the most important parameters. After mapping a ligand to a pharmacophore, there may be multiple mappings to the pharmacophore for one ligand. Therefore the best alignment may be achieved when less pharmacophore features are mapped. For example, best mapping is defined as the ligand that fits the most features or has the highest fit, which does not necessarily match all the features (Kirchmair *et al.*, 2008; Langer & Wolber, 2004; Seidel *et al.*, 2010; Wolber & Langer, 2005).

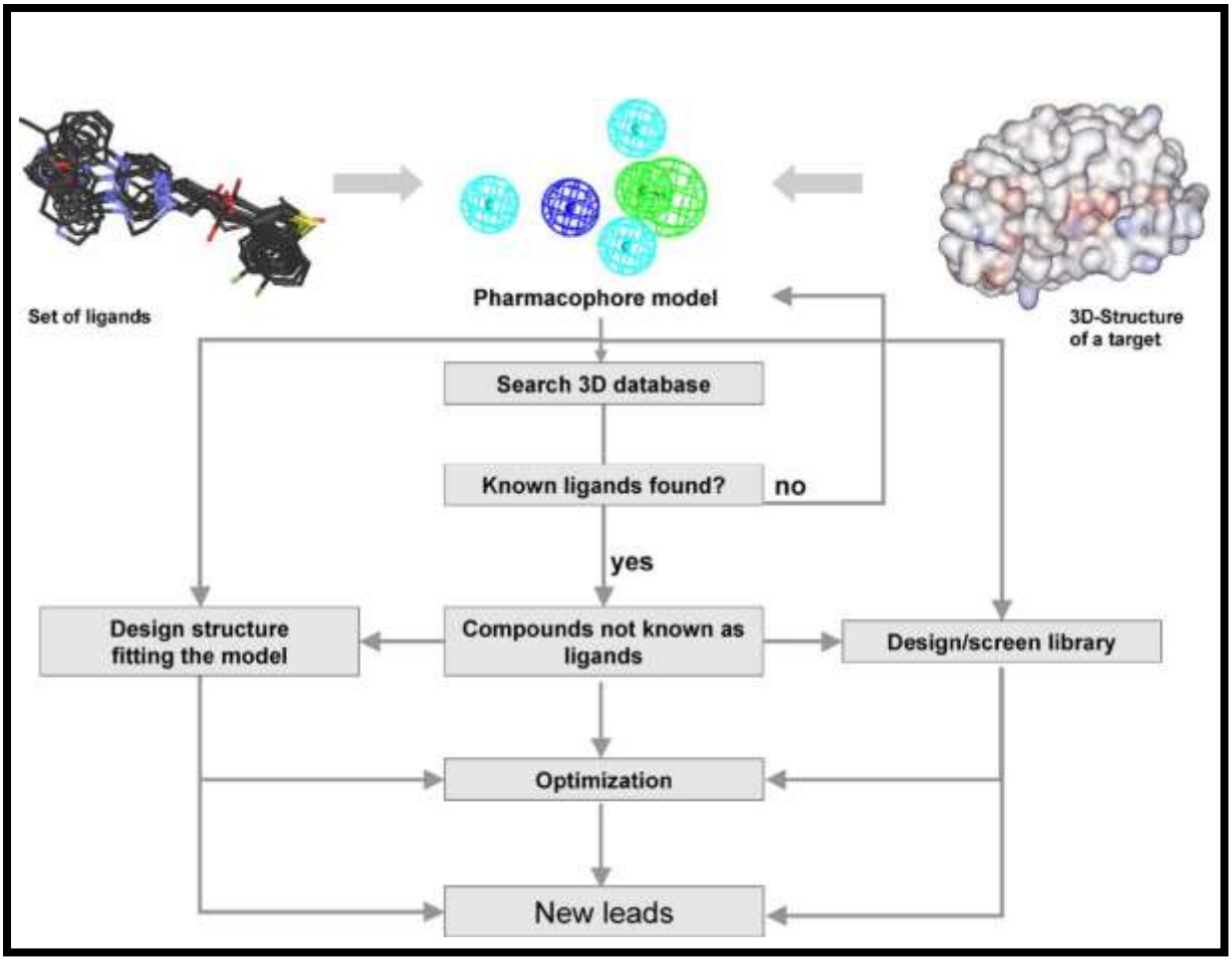

Figure 2.38: Pharmacophore-based virtual screening workflow (Langer & Wolber, 2004; Wolber & Langer, 2005).

Another method, often used during virtual screening, is the use of molecular docking. In the field of molecular modelling, docking is a method which predicts the preferred orientation of one molecule to a second when bound to each other to form a stable complex. Knowledge of the preferred orientation in turn may be used to predict the strength of association or binding affinity between two molecules using, for example, scoring functions (Langer & Wolber, 2004; Wolber & Langer, 2005).

Other methods, such as the use of bio-isosteres, used during selection of compounds in this study will be discussed in greater detail in Chapter 3.

2.7 SUMMARY

In this chapter PD was discussed as a chronic neurodegenerative disorder with a largely unknown pathogenesis. Decreased levels of dopamine, particularly in the SNpc are known to be the main pathogenic feature of PD. Although PD is an

incurable disease, symptomatic treatments that are reasonably effective, particularly in the early stages of the disease, are available. The introduction of L-dopa as symptomatic treatment was a therapeutic breakthrough, making it the most efficacious and best-tolerated drug for the treatment of PD. However, its long-term use is associated with debilitating side effects. Both the COMT and MAO enzymes are important drug targets since they are responsible for the metabolism of dopamine and its precursors. As such, the identification of inhibitors of these enzymes may be of value. One approach is to use virtual screening for the identification of potential COMT inhibitors. In addition to the therapeutic value of COMT inhibition, the 3D structure of COMT, the catalytic cycle of COMT and known inhibitors were explored in this chapter. This provides the necessary background information for the discovery of compounds that can be investigated as COMT inhibitors in the next chapters. Quercetin, a flavonoid, can be classified as a first-generation COMT-inhibitor which also possesses MAO-inhibitory activity, indicating that structurally related flavonoids should be explored with regards to these activities.

CHAPTER 3

VIRTUAL SCREENING:

3.1. INTRODUCTION

As mentioned earlier, computer-aided molecular design methods, which include pharmacophore design and 3D database searches, are aimed at decreasing the overall cost associated with the discovery and development of new drugs by identifying the most promising candidates to focus the experimental efforts on (Kirchmair *et al.*, 2008; Langer & Wolber, 2004; Seidel *et al.*, 2010; Wolber & Langer, 2005).

Pharmacophores help in the understanding of key interactions between a target and a ligand. A pharmacophore is an ensemble of steric and electrostatic features of different compounds which are necessary to ensure optimal supra-molecular interactions with a specific biological target structure and to trigger/block its biological response (Langer & Wolber, 2004; Wolber & Langer, 2005).

Due to their abstract nature and simplicity, 3D pharmacophore models are efficient filters for the screening of large drug databases. By reducing the complexity of the hit identification process, lower overall search times can be achieved. The pharmacophore-based queries can be used to identify drug candidates with scaffolds and functional groups that differ from the original ligands used in the pharmacophore design. This can lead to the development of compounds with better pharmacokinetic and toxicological properties, but it has to be remembered that the pharmacophoric representations are greatly simplified and therefore cannot explain the complete biophysical nature of drug interactions (Kirchmair *et al.*, 2008; Seidel *et al.*, 2010).

Firstly, a pharmacophore model is created that specifies the type and geometrical constraints of the chemical features that need to be matched by the screened molecules. Methods may include the *structure-based* or *ligand-based* approaches. In this study a *structure-based* method was used where the chemical features are determined by using the complementary interactions between a ligand and its binding site. This method requires the structural information of the macromolecule and the active conformation of the bound ligand since it incorporates the binding site

interactions, often resulting in a highly restrictive model with orientation constrained features (Seidel *et al.*, 2010).

During structure-based pharmacophore generation (**Figure 3.1**) interaction sites are determined, clustering of the vectors for H-bonding and of the hydrophobic regions is done and, the transformation of the obtained clusters into a feature-based pharmacophore hypothesis occur (Langer & Wolber, 2004; Wolber & Langer, 2005).

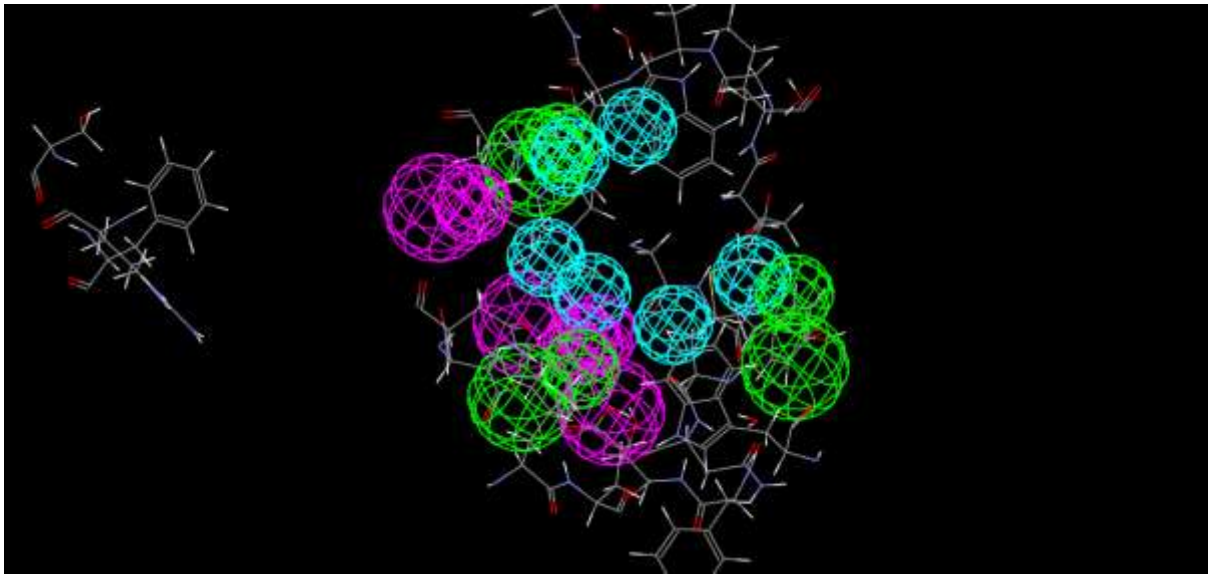

Figure 3.1: A *structure-based* pharmacophore model. The green spheres represent hydrogen bond acceptor features, the purple spheres represent hydrogen bond donor features and the blue spheres represent hydrophobic features. Figure drawn using Discovery Studio® 3.1 modelling software.

Pharmacophore models contain features which may represent atoms, H-bond acceptors, H-bond donors, ionisable groups, hydrophobic groups and aromatic rings (Langer & Wolber, 2004; Wolber & Langer, 2005). Together with these features, geometrical constraints may be applied. These constraints may include distances and angles. Features will only map if they are solvent accessible (Kirchmair *et al.*, 2008; Langer & Wolber, 2004; Wolber & Langer, 2005).

After features have been added, it is important to add location constraints. Location constraints define the relative location of the features. A shape constraint may also be used to constrain a pharmacophore or refine a hit-list. This may consist of two groups which include shape-only and mixed queries. With shape-only constraints the

shape is aligned to the ligand and with mixed queries the shape is aligned to the ligand and the location constraints. Once a shape constraint is added, the ligand will match all features of the pharmacophore if a matching atom is found in the right location of the features and if the overall shape of the molecule (after being aligned) is similar to the shape. Additionally an exclusion constraint may be added, which specifies one or more spherical spaces in a pharmacophore that must not contain any atoms or bonds (Langer & Wolber, 2004; Wolber & Langer, 2005).

After the pharmacophore has been generated, the next step requires the creation of the ligand database for screening, which has to allow different molecular conformations. This can be achieved by recording pre-computed conformations of all the molecules that will be screened. Furthermore, the database is searched for conformations that will bind to the macromolecule using a multistep filtering process. Firstly, a fast pre-filtering step is applied. This step involves the elimination of molecules that do not fit into the macromolecule based on their feature-types, feature-counts and quick distance checks. The molecules that might fit the query are closely examined to see whether their conformations are able to match the spatial arrangement of the query features using 3D matching algorithms. The latter process is slower, but more restrictive. The conformers that comply with the query are then put into a hit-list. This hit-list is constructed using Discovery Studio® 3.1 modelling software which calculates the root mean square deviation of the interaction and only selects interactions with a value below 1. It is required that the distance between each pair of features of the database molecule must be of such a value that it is possible to align them within the specific tolerances of the mapped query features. Furthermore, the hit-values are computed for the hit-list which can be used to score and rank the screening results (Seidel *et al.,* 2010).

The hit-list can then be analysed to evaluate the effectiveness of the pharmacophore models using the literature protocol as described by Kirchmair *et al.* (2008) and Seidel *et al.* (2010).

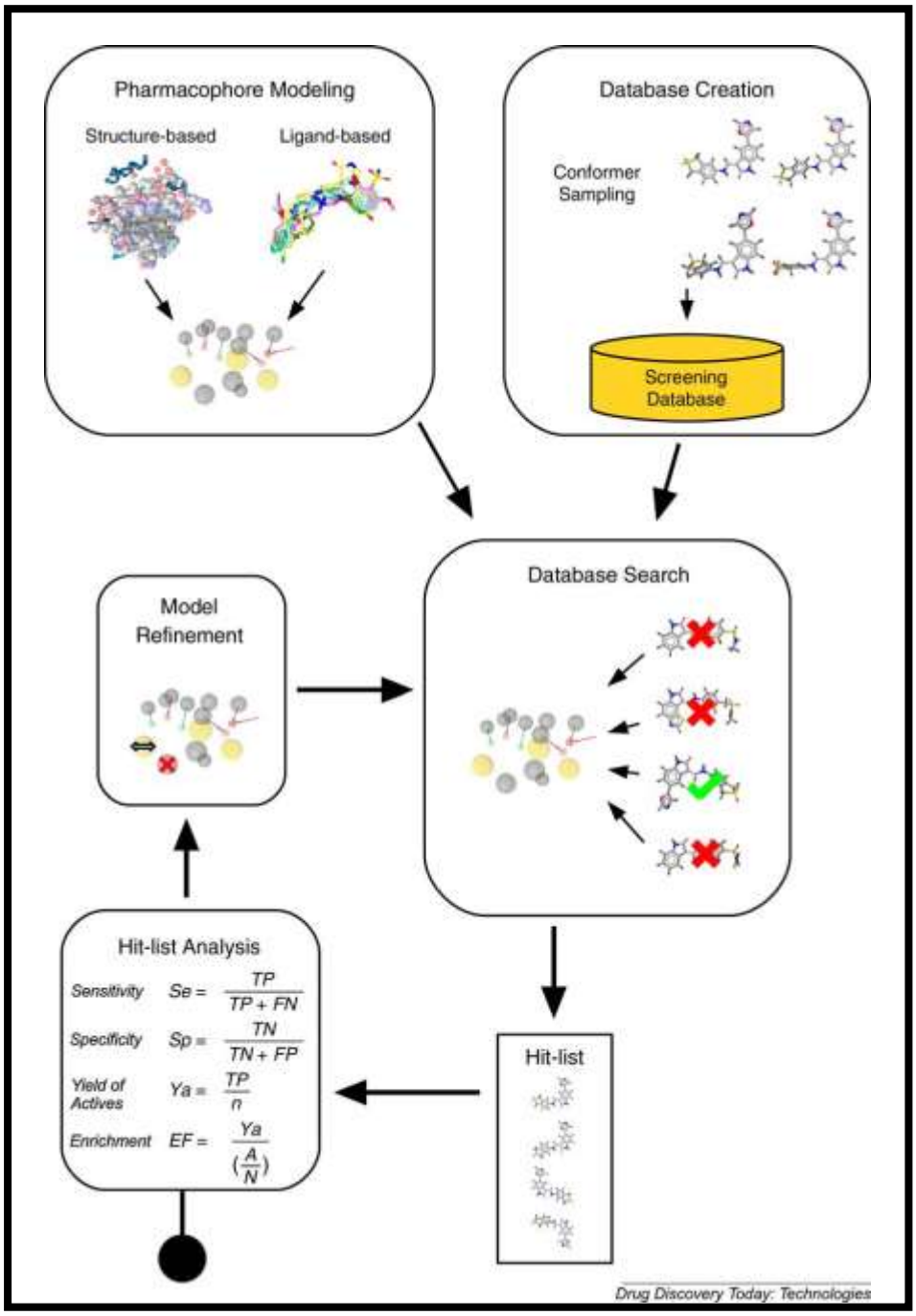

Figure 3.2: The 3D pharmacophore-based screening workflow (Seidel *et al.*, 2010).

Firstly, the pharmacophore model will select *n* molecules from a database with *N* entries. The selected hit-list will then consist of active compounds (true positive compounds) and decoys (false positive compounds). The active molecules that are not retrieved by the model are defined as false negative compounds and the true negative compounds are the database decoys that were not selected (Kirchmair *et al.,* 2008).

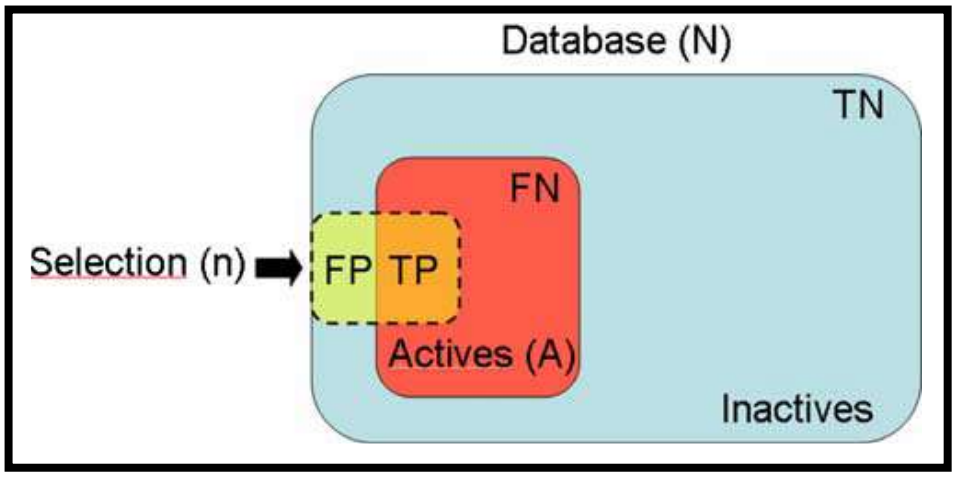

Figure 3.3: Selection of *n* molecules from a database containing *N* entries (Kirchmair *et al.*, 2008). Where FP represents the retrieved false positive compounds, TP represents the retrieved true positive compounds, FN represents the retrieved false negative compounds, TN represents the retrieved true negative compounds, (n) represents the selection of compounds and (A) represents the active compounds.

There are several useful calculation measures which can be used to determine the effectiveness of a pharmacophore model (Kirchmair *et al.*, 2008; Seidel *et al.*, 2010). Calculation measures may include sensitivity (Se), which is the ratio of the retrieved true positive compounds (TP) to all active compounds (A) in the database (the sum of the TP and false negative (FN) compounds (**Equation 3.1**). The values can range between 0 and 1. A value of 0 indicates that none of the active compounds were found whereas a value of 1 illustrates that the active compounds were all found.

$$Se = \frac{N \text{ selected actives}}{N \text{ total actives}} = \frac{TP}{TP+FN}$$

Equation 3.1: Equation to calculate the sensitivity (Se) (Kirchmair *et al.*, 2008).

Specificity (Sp) is the amount of rejected true negative compounds (TN) divided by the amount of TN compounds plus the amount of false positive (FP) compounds (**Equation 3.2**). The value ranges between 0-1 and it shows the percentage of truly

inactive compounds that were identified. A value of 0 illustrates none of the negative compounds were identified whereas a value of 1 indicates that all of the compounds were identified (Kirchmair *et al.*, 2008; Seidel *et al.*, 2010).

$$Sp = \frac{N \text{ discarded actives}}{N \text{ total inactives}} = \frac{TN}{TN+FP}$$

Equation 3.2: Equation to calculate the specificity (Sp) (Kirchmair *et al.*, 2008).

The yield of actives (Ya) measures the probability that one of the *n* selected compounds is active (**Equation 3.3**). Furthermore it represents the hit rate that would be achieved if all the molecules selected by the pharmacophore model were tested for activity. However it contains no information about the composition of the database (Kirchmair *et al.*, 2008; Seidel *et al.*, 2010).

$$Ya = \frac{TP}{n}$$

Equation 3.3: Equation to calculate the yield of actives (Ya) (Kirchmair *et al.*, 2008).

The accuracy (Acc) illustrates the percentage of molecules that are correctly identified by the model (Kirchmair *et al.*, 2008; Seidel *et al.*, 2010) (**Equation 3.4**).

$$Acc = \frac{TP+TN}{N} = \frac{A}{N}.Se + \left(1 - \frac{A}{N}\right).Sp$$

Equation 3.4: Equation to calculate the accuracy (Acc) (Kirchmair *et al.*, 2008).

The balanced labelling performance (Ibal) can be defined as a weighted accuracy descriptor (**Equation 3.5**). A value of 1 would indicate that all the active and inactive molecules are correctly identified by the model (Kirchmair *et al.*, 2008; Seidel *et al.*, 2010).

$$I_{bal} = \frac{1}{2}.Se + \frac{1}{2}.Sp$$

Equation 3.5: Equation to calculate the balanced labelling performance (Ibal) (Kirchmair *et al.*, 2008).

According to Kirchmair *et al.* (2008) and Seidel *et al.* (2010), the Receiver Operating Characteristics (ROC) curves are another method for the assessment of screening results. The ROC curves show the increase of false positives as true positives increases, thus describing Se for any possible change of *n* as a function of (1-Sp). The X-coordinate denotes the false positive value whereas the Y-coordinate denotes the true positive value. Most of the active molecules will have a higher score than the decoys if all the molecules scored by a pharmacophore model screening protocol with sufficient discriminatory power are ranked according to score – in other words from high to low. Since some of the actives will result in a lower score than some of the decoys an overlap between the distributions of active molecules may occur. This will lead to the prediction of false positives and negatives.

An ideal ROC curve representing distributions where no overlap between the scores of active molecules and decoys exist, would rise vertically along the Y-axis until the X-axis (Se) reaches 1, i.e. all the actives are retrieved where after it would continue

horizontally to the right until all the decoys are retrieved, which corresponds to Se = 1 and Sp = 0. The ROC curve for a set of actives and decoys with randomly distributed scores tends towards the Se = 1-Sp line asymptotically, with an increasing number of actives and decoys. The ROC curve normally lies between the ideal curve and the random graph due to an overlapping in the distribution of active molecules and decoys. The ROC curve of a random database is represented by the median. After the hit-list is analysed the pharmacophore model can be refined to deliver better results (Kirchmair *et al.,* 2008; Seidel *et al.,* 2010).

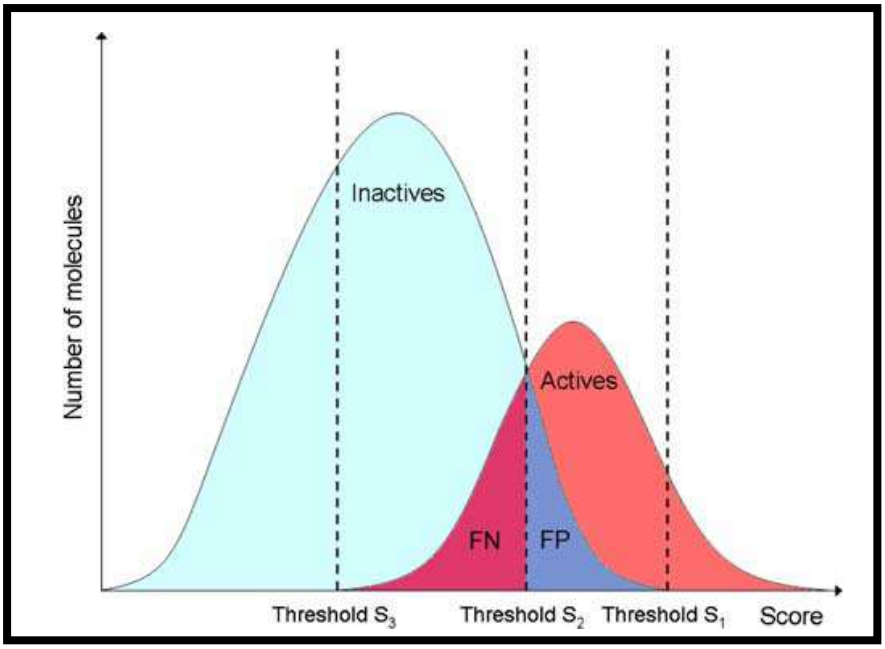

Figure 3.4: Theoretical distributions for active molecules and decoys according to their score. Due to distributions overlap, different ratios of false positives (FP) and false negatives (FN) are retrieved, depending on the selection threshold S (Kirchmair *et al.*, 2008).

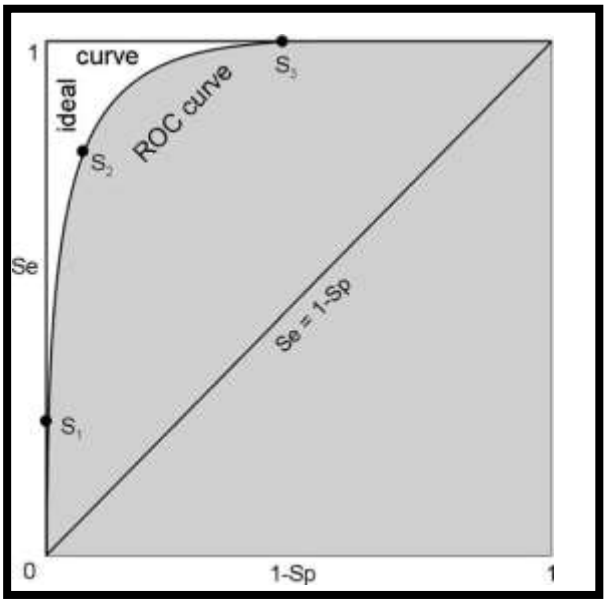

Figure 3.5: The ROC curves for ideal and overlapping distributions of actives and decoys. A random distribution causes a ROC curve which tends towards the Se = 1 - Sp line asymptotically with increasing number of actives and decoys (Kirchmair *et al.*, 2008).

In order to maximise the potential hits in this study, in addition to the pharmacophore approach, several other methods for identifying hits were also utilised. These included the use of ligand fingerprinting and molecular docking, as well as the identification of catechol bio-isosteres and compounds that are structurally related to known inhibitors.

According to Edwing *et al*. (2001) the computational study of molecular recognition is an important component of structure-based drug design. Thus, molecular docking can be described as a method of finding the low-energy binding modes of a small molecule, or ligand, within the active site of a macromolecule, or receptor, whose structure is known (Edwing *et al.*, 2001). This computational method requires an accurate representation of the molecular energetics as well as an efficient algorithm to search the potential binding modes (Edwing *et al.*, 2001). The original DOCK algorithm addressed rigid body docking using a geometric matching algorithm to superimpose the ligand onto a negative image of the binding pocket (Edwing *et al.*, 2001). The process of molecular docking, as described by Edwing and co-workers (2001), is summarised in **Figure 3.6**.

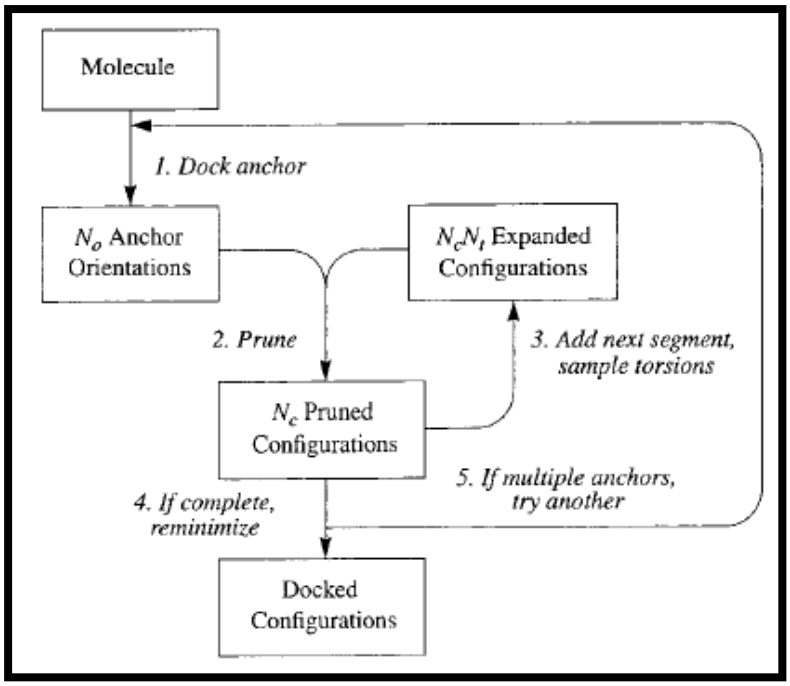

Figure 3.6: Flowchart of the anchor and grow docking algorithm (Edwing *et al.*, 2001).

A bio-isostere is a group that can be used to replace another group while retaining the desired biological activity (Meanwell, 2011; Patani & LaVoie, 1996). The combination of conformational restrictions and bio-isosteric replacements has become a valuable tool for the design of highly selective enzyme inhibitors, anti-metabolites and receptor ligands (Hübner *et al.*, 2000). This strategy led to the design of agonists and antagonists selectively recognizing dopamine (DA), norepinephrine (NA), serotonin (5-HT) and GABA receptors (Hübner *et al.*, 2000).

It is hypothesised that the multipronged approach discussed above will increase the chances of identifying hits, especially since cost and availability of ligands are also a consideration.

3.2 PHARMACOPHORE MODELS

3.2.1 CONSTRUCTION AND SCREENING OF THE PHARMACOPHORE MODELS

In this study *structure-based* models were generated using the X-ray crystal structure of the human COMT enzyme (PDB code: 3BWM). Since the enzyme crystallises as a dimer, the monomer where DNC is located was used for pharmacophore generation.

The following steps were followed using Discovery Studio® 3.1 modelling software:

(a) Protein Preparation:

- The crystal structure of the COMT enzyme was retrieved from the Brookhaven Protein Data Bank (www.rcsb.org/pdb).
- The correctness of the valences of the FAD cofactor and the co-crystallised ligands (DNC - 3,5-dinitrocatechol, SAM - S-adenosyl methionine and magnesium) were verified and the protein models were automatically typed with the Momany and Rone CHARMm force field.
- With the tools provided in Discovery Studio® 3.1 modelling software, the pH was set to 7.4 and hydrogen atoms were added to the FAD cofactor and the co-crystallised ligands.
- The pKa values and protonation states of the ionisable amino acids were calculated and hydrogen atoms were added at pH 7.4 to the protein model, including the water molecules.
- A fixed atom constraint was applied to the backbone of the enzyme and the model was energy minimised using the Smart Minimizer algorithm with the maximum steps set to 5000, a gradient of 0.1 and an energy charge of 0. For this procedure the implicit generalized Born solvation model with molecular volume was used with a nonbond list radius of 14, a nonbond higher cut-off of 12 and a nonbond lower cut-off of 10.
- The electrostatics was set to spherical cut-off.
- Finally, the minimised structure was saved.

(b) Determine hydrogen bond interactions:

- The structure of DNC was selected to show the hydrogen bond interactions with the residues of the active site.
- Hydrogen bonds between the hydroxyl groups of DNC and residues Lys 144 and Glu 199 were observed.

(c) Pharmacophore construction:

- All crystal waters, except those water molecules which undergo hydrogen bonding with the co-crystallised ligands (which includes waters 402, 411, 441 and 458) were deleted from the protein model,
- The binding site of the COMT enzyme was defined based on the location of DNC using a sphere with a radius of 9 Å surrounding the ligand.
- To determine important interactions between the co-crystallised ligand and amino acid residues, an interaction map between the ligands and amino acid residues was generated.
- Based on the interaction analysis, pharmacophore features were generated for the model. The acceptor, donor and hydrophobic features were clustered in turn. With this step a group of features that represent the same interaction is combined into a single feature.
- Location constraints were added to the features. These are spheres which are placed around the centre of the features and define the ideal location for the ligand atoms. The sphere represents the tolerance of the allowable deviation of the ligand atoms from the ideal position. In the last step, exclusion constraint features were placed around the model. While the software screens a virtual database for ligands that may map to the pharmacophore model, the algorithm attempts to find ligands that do not bind in the excluded zones. The binding of ligands is thus confined to the active site only, and the selection of ligands that would have unfavourable steric interactions with surrounding amino acids is decreased. A shape constraint was also added to the co-crystallised ligand.
- *Pharmacophore model 1* contained an acceptor orientated towards Lys 144, a donor orientated towards Asn 170, a donor orientated towards Glu 199, and a hydrophobic feature located on the oxygen atom of the hydroxyl group of

DNC. Exclusion constraints were added to Trp 38, Met 40, Trp 143, Lys 144, Asp 169, Asn 170, Leu 198 and Glu 199.

- *Pharmacophore model 2* contained an acceptor orientated towards Lys 144, a donor orientated towards Asp 169, a donor orientated towards Glu 199, and a hydrophobic feature located on the oxygen atom of the hydroxyl group of DNC. Exclusion constraints were added to Trp 38, Met 40, Gly 66, Trp 68, Trp 71, Trp 143, Asp 141, Lys 144, Asp 169, Asn 170, Leu 198 and Glu 199.
- *Pharmacophore model 3* contained an acceptor orientated towards Lys 144, a donor orientated towards Glu 199, and a hydrophobic feature located on the oxygen atom of the hydroxyl group of DNC. Two new acceptors were created and orientated towards Mg^{2+}. Exclusion constraints were added to Trp 38, Met 40, Gly 66, Trp 68, Trp 71, Trp 143, Asp 141, Lys 144, Asp 169, Asn 170, Leu 198 and Glu 199.

(d) Literature validation for computer generated pharmacophore models 1, 2 and 3:

The first effective bi-substrate inhibitor for COMT (IC_{50} = 2 µM) was developed by rational design using the interactions observed in the crystal structure of the quaternary complex between the enzyme, SAM, DNC and the magnesium ion (Lerner *et al.*, 2001). The proposed features of both pharmacophore models 1 and 2 were in agreement with these observed interactions. Furthermore, Lerner and co-workers (2001) have identified Asp 141, Lys 144, Asp 169, Asn 170 and Glu 199 as potential hydrogen bond donors in the quaternary complex, therefore the crystal waters undergoing hydrogen bonding with these residues and with SAM (waters 402, 411, 441 and 458) were not deleted. Pharmacophore model 1 has a donor orientated towards Asn 170 and pharmacophore model 2 has a donor orientated towards Asp 169. Both these pharmacophore models have an acceptor orientated towards Lys 144. These two pharmacophore models are thus very similar, only differing in the orientation of their hydrogen bond donors.

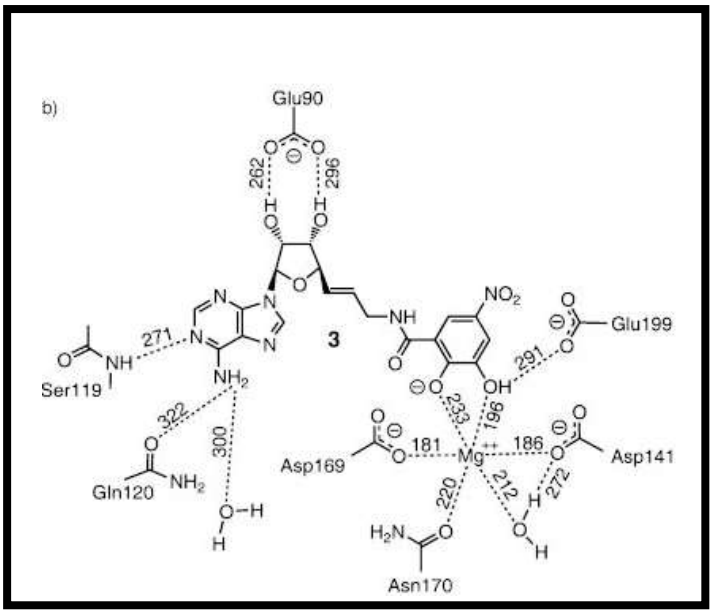

Figure 3.7: Schematic drawing of the interactions (dashed-lines) in the quaternary complex of the COMT inhibitor binding site, consisting of hydrogen bond interactions of the oxygens of the DNC with Asp 141, Asp 169, Asn 170 and Glu 199, respectively. Also illustrated are the hydrogen bond interactions of Gln 120 and Ser 119 with the nitrogen groups of SAM. Distances are given in pm (Lerner *et al.*, 2001).

According to Lerner *et al.* (2001) COMT is a magnesium dependent enzyme and the coordination between the ligand and the magnesium ion is therefore crucially important for the transfer of a methyl group from SAM to endogenous and exogenous catechols. The construction of pharmacophore model 3 was based on the above. Since the Mg^{2+} ion is coordinated with the OH-groups of DNC, we have added two acceptors orientated towards Mg^{2+}.

(e) Pharmacophore validation and library screening:

- After the pharmacophore models had been constructed, test sets were constructed. The test sets consisted of ligands which are known to inhibit COMT as listed by Kiss & Soares-da-Silva (2014). Conformations of the test set were generated (250 of each ligand) by using the BEST method with the minimum features set as 2 and the maximum features set as 4.
- The generated conformations were then queried by the pharmacophore model to determine which conformations fit the features best.
- The structures of the FDA approved drugs (DrugBank), which contains all of the drug molecules approved by the FDA of the United States, were

subsequently screened with the pharmacophore models (Screen Library protocol). None of the features were set as required features and the fitting method was set to rigid. Both 3- and 4-feature hits were considered for *in vitro* evaluation as inhibitors of human COMT.

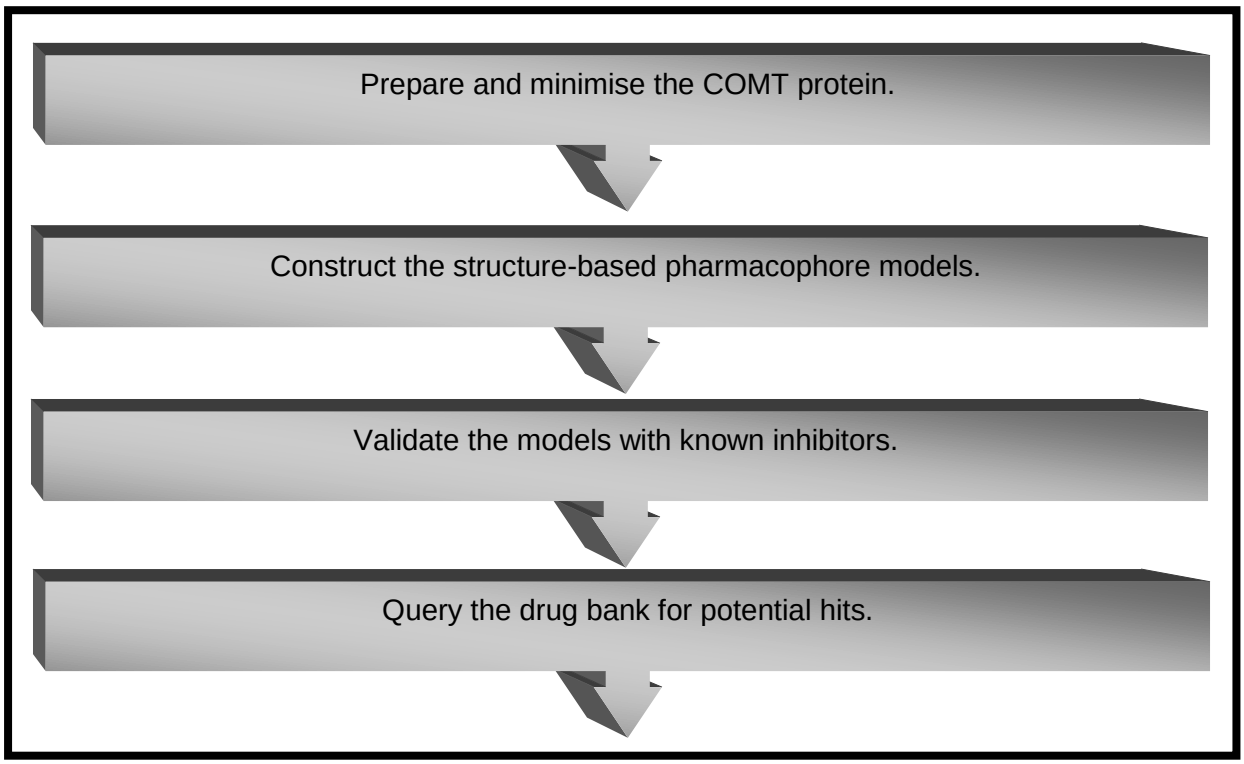

Figure 3.8: Workflow for the construction of a structure-based pharmacophore.

3.2.2 RESULTS

3.2.2.1 PHARMACOPHORE MODEL 1

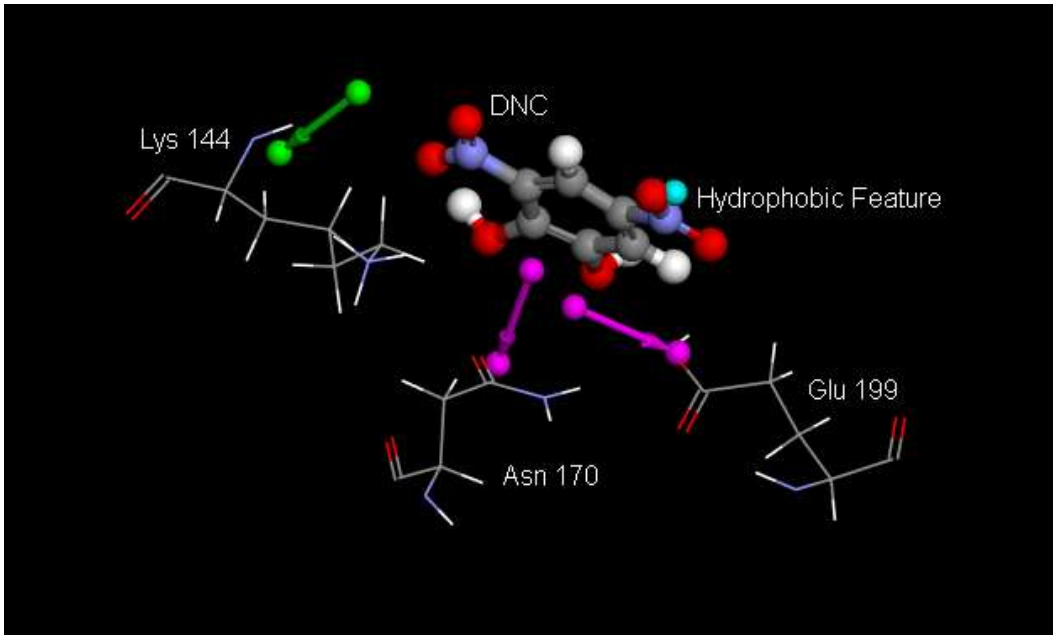

Figure 3.9: A 3D representation of *structure-based* pharmacophore model 1, which was constructed using the X-ray crystal structure of the COMT enzyme (PDB: 3BWM). The green arrows represent hydrogen bond acceptor features, the purple arrows represent hydrogen bond donor features and the blue spheres represent hydrophobic features. Exclusion spheres are not indicated for the purpose of clarity. Figure drawn using Discovery Studio® 3.1.

As shown in **Figure 3.9**, the acceptor, donor and hydrophobic features of pharmacophore model 1 correspond to interactions with the following residues:

1. Acceptor with Lys 144
2. Donor with Asn 170
3. Donor with Glu 199
4. Hydrophobic feature on an oxygen atom of DNC

Table 3.1: A list of the compounds in the Drug Bank which mapped to pharmacophore model 1 and which were derived from the structure of COMT using the *structure-based* approach. Also given are the fit-values and the molecular weight of the respective compounds.

Name and Structure of Compounds	Fit-Value	Molecular Weight (g/mol)
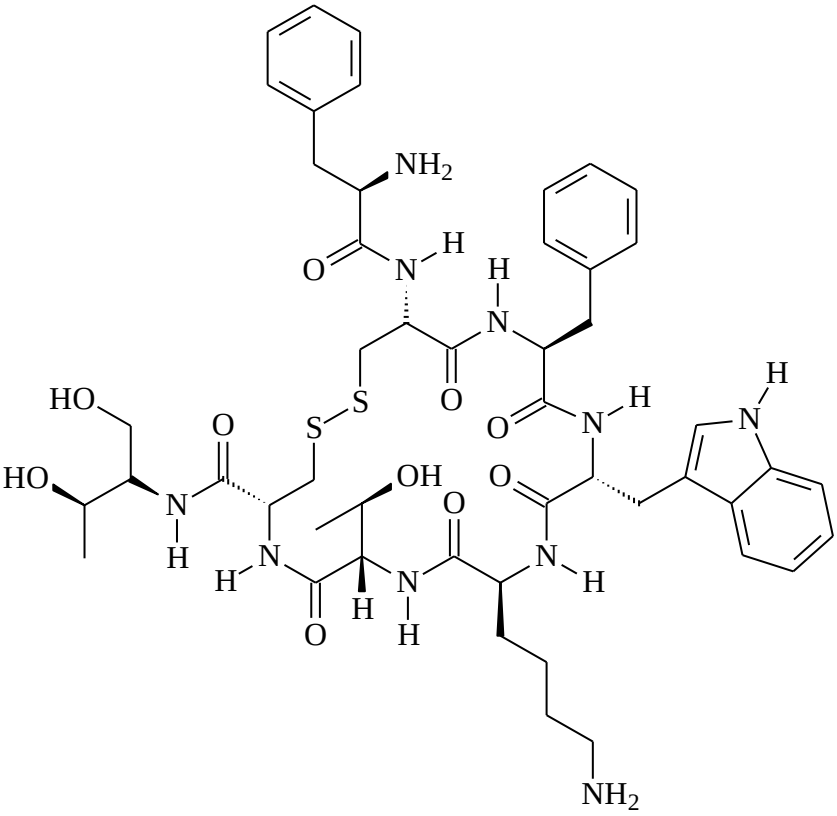 Octreotide	2.86698	1019.24
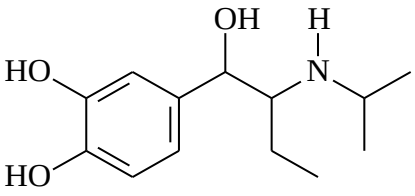 Isoetarine	2.8199	239.311

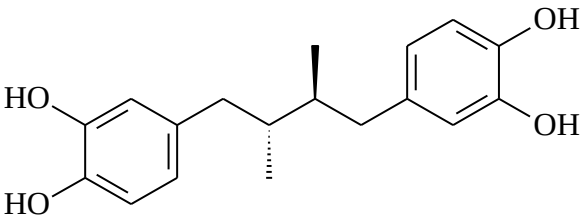 Masoprocol	2.78875	302.365
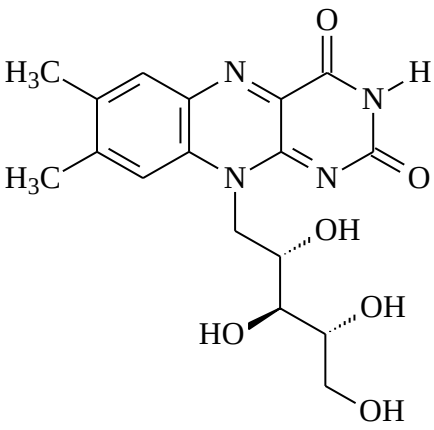 (-)-Riboflavin	2.73895	376.364
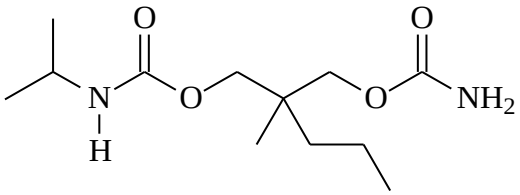 Carisoprodol	2.73534	260.33
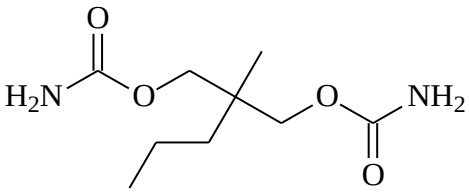 Meprobamate	2.7172	218.25

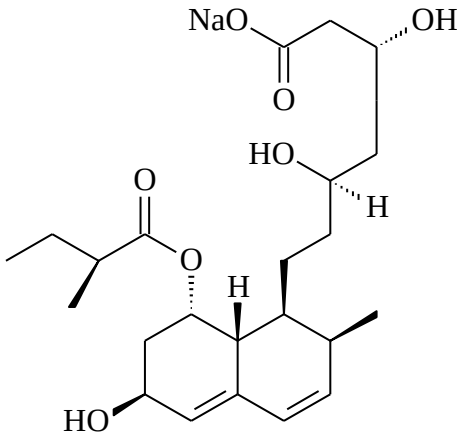 Pravastatin	2.70204	424.528
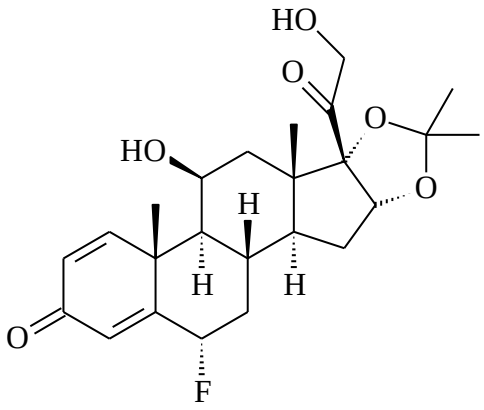 Flunisolide	2.65671	434.498
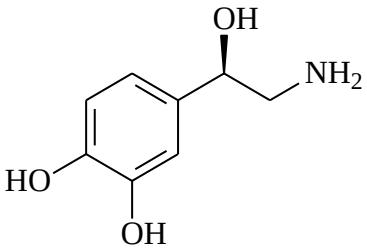 Norepinephrine	2.65504	169.178
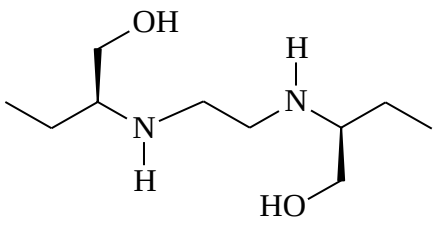 Ethambutol	2.60938	204.31

3.2.2.2 PHARMACOPHORE MODEL 2

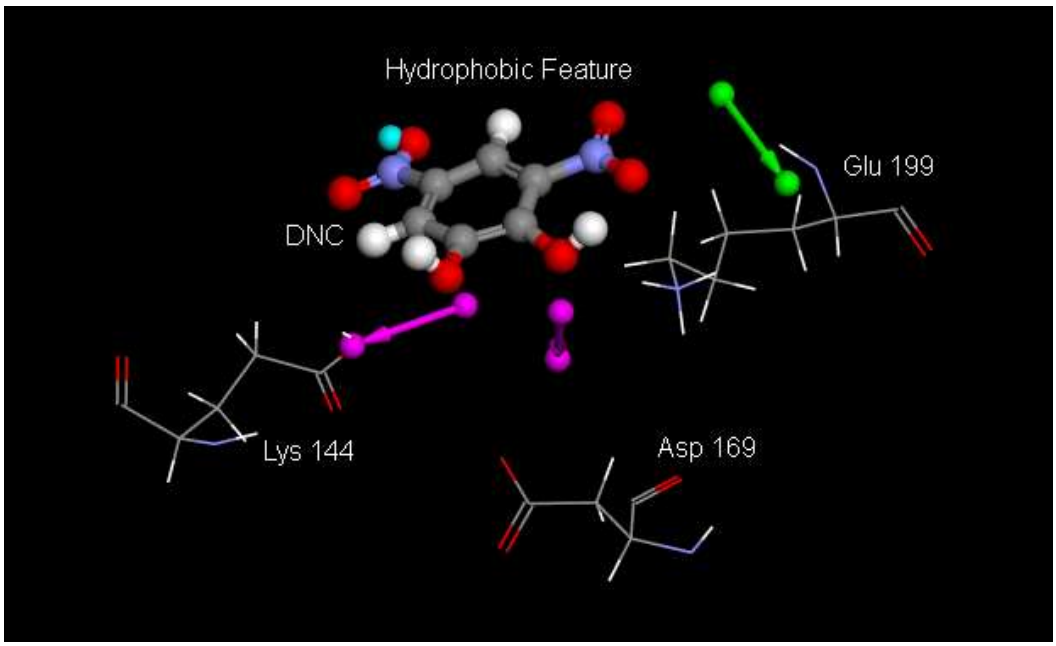

Figure 3.10: A 3D representation of *structure-based* pharmacophore model 2, which was constructed using the X-ray crystal structure of the COMT enzyme (PDB: 3BWM). The green arrows represent hydrogen bond acceptor features, the purple arrows represent hydrogen bond donor features and the blue spheres represent hydrophobic features. Exclusion spheres are not shown for the sake of clarity. Figure drawn using Discovery Studio® 3.1.

As shown in figure 3.10, the acceptor, donor and hydrophobic features of pharmacophore model 2 correspond to interactions with the following residues:

1. Acceptor with Lys 144
2. Donor with Asp 169
3. Donor with Glu 199
4. Hydrophobic feature on an oxygen atom of DNC

Table 3.2: A list of the compounds in the Drug Bank which mapped to pharmacophore model 2 and which were derived from the structure of COMT using the *structure-based* approach. Also given are the fit-values and the molecular weight of the respective compounds.

Name and Structure of Compounds	**Fit-Value**	**Molecular Weight (g/mol)**
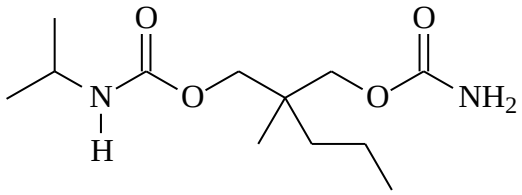 Carisoprodol	2.73534	260.33
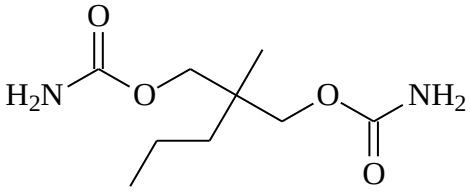 Meprobamate	2.7172	218.25
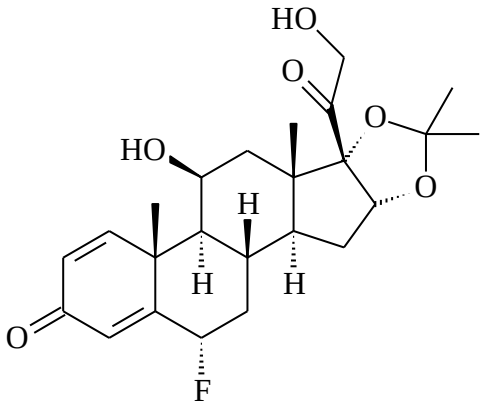 Flunisolide	2.65671	434.498

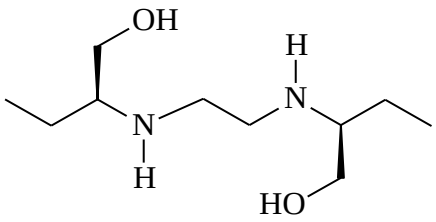 Ethambutol	2.60938	204.31
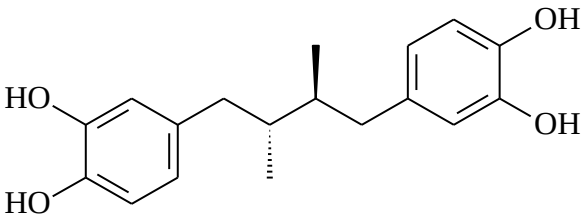 Masoprocol	2.5521	302.365
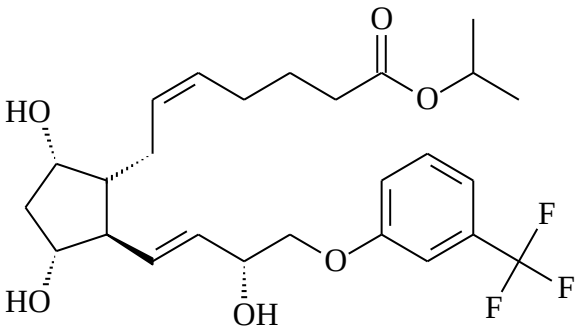 Travoprost	2.5504	500.548
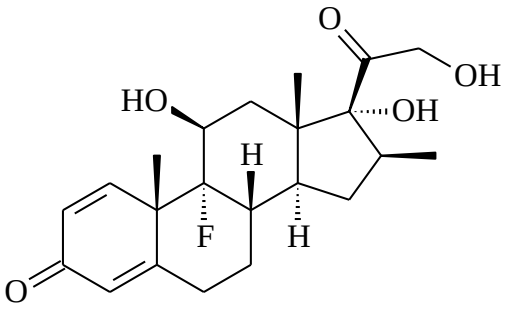 Betamethasone	2.4537	392.461

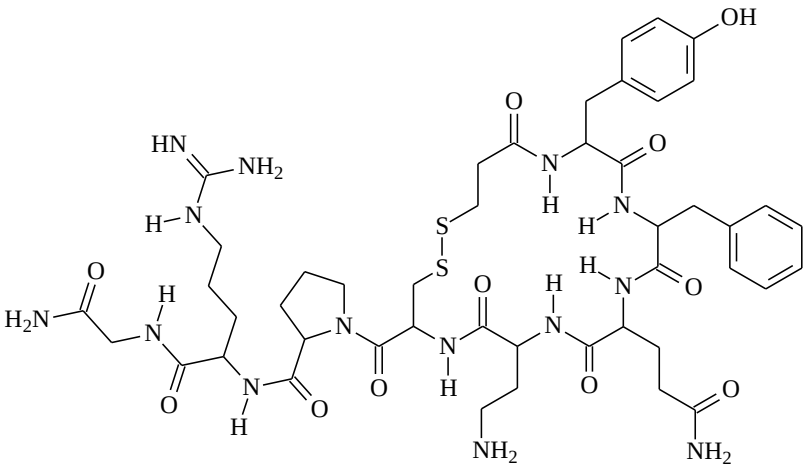 Desmopressin	2.43374	1069.22
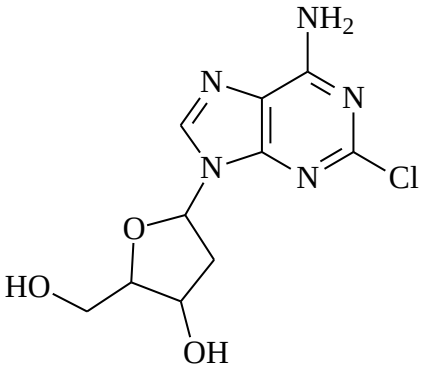 Cladribine	2.42515	285.687
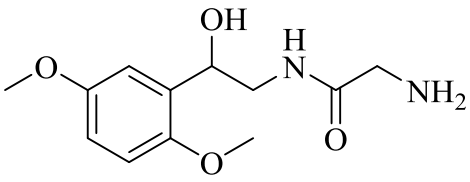 Midodrine	2.39458	254.282

3.2.2.3 PHARMACOPHORE MODEL 3

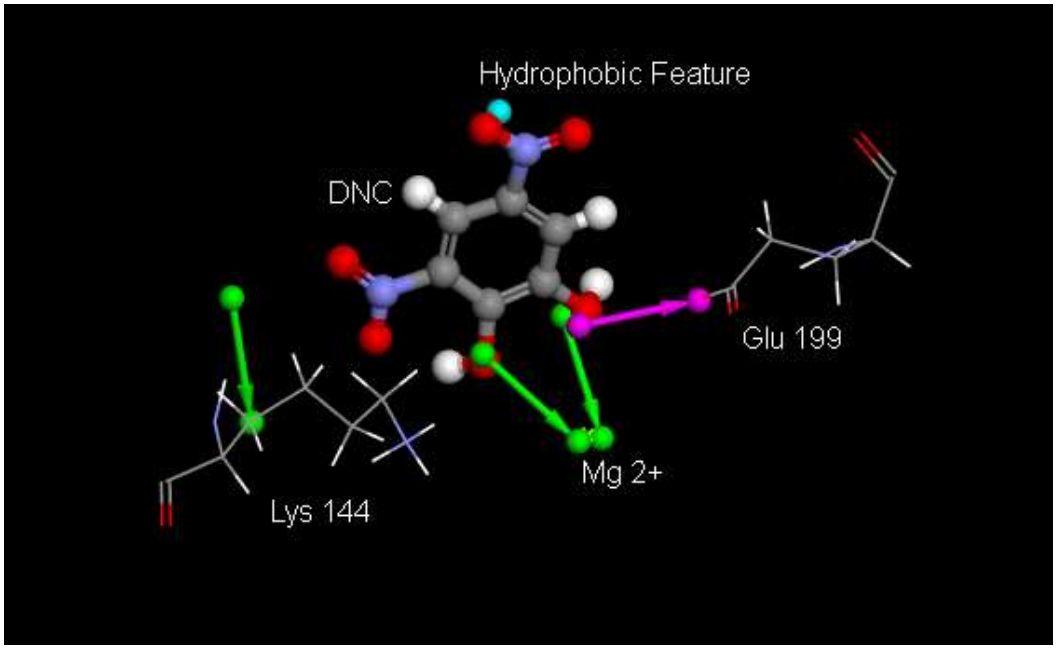

Figure 3.11: A 3D representation of *structure-based* pharmacophore model 3, which was constructed using the X-ray crystal structure of the COMT enzyme (PDB: 3BWM). The green arrows represent hydrogen bond acceptor features, the purple arrows represent hydrogen bond donor features and the blue spheres represent hydrophobic features. Figure drawn using Discovery Studio® 3.1.

As shown in figure 3.11, the acceptor, donor and hydrophobic features of pharmacophore model 3 correspond to interactions with the following residues:

1. Acceptor with Lys 144
2. Additionally, two acceptors with Mg^{2+}
3. Donor with Glu 199
4. Hydrophobic feature on an oxygen atom of DNC

Table 3.3: A list of the compounds in the Drug Bank which mapped to pharmacophore model 3 and which were derived from the structure of COMT using the *structure-based* approach. Also given are the fit-values and the molecular weight of the respective compounds.

Name and Structure	Fit-Value	Molecular Weight (g/mol)
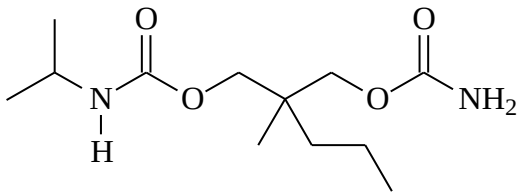 Carisoprodol	2.73534	260.33
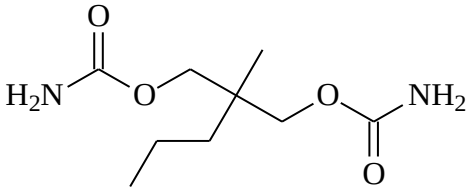 Meprobamate	2.7172	218.25
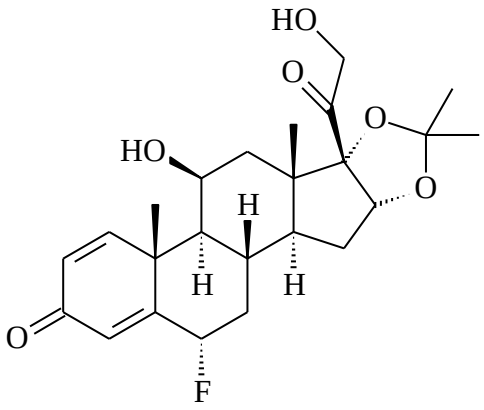 Flunisolide	2.65671	434.498

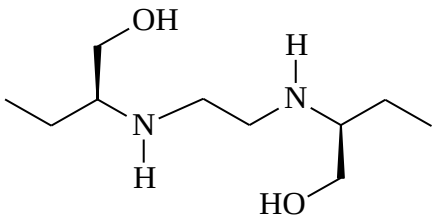 Ethambutol	2.60938	204.31
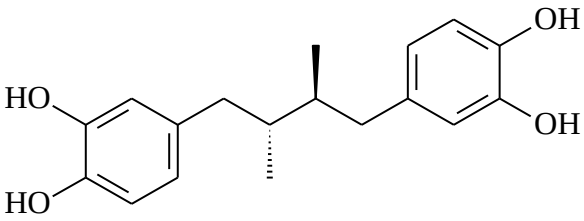 Masoprocol	2.5521	302.365
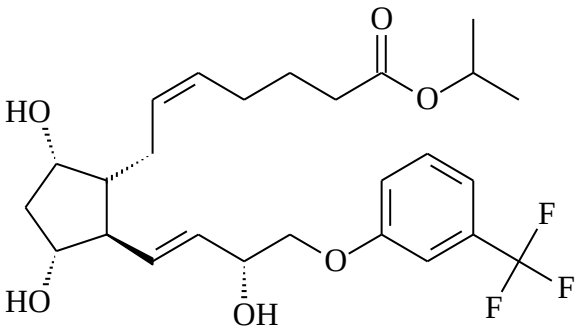 Travoprost	2.5504	500.548
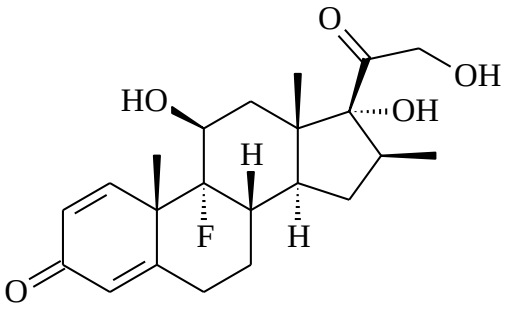 Betamethasone	2.4537	392.461

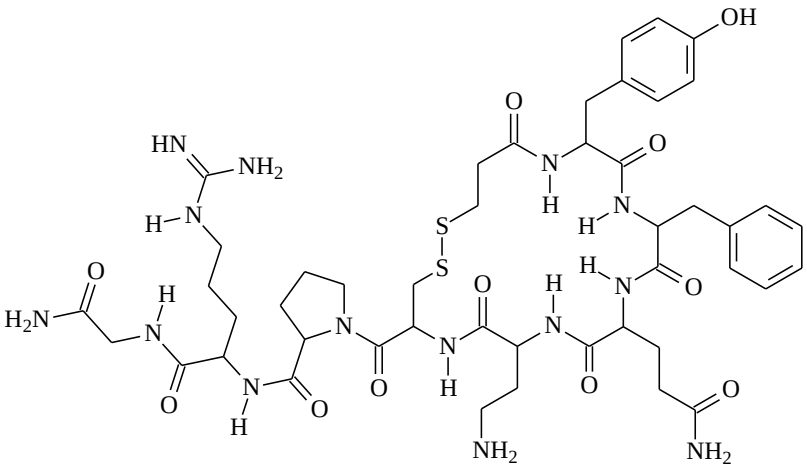 Desmopressin	2.43374	1069.22
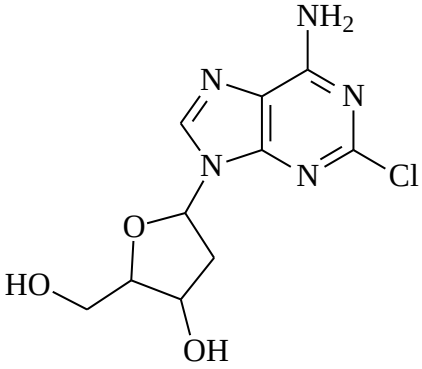 Cladribine	2.42515	285.687
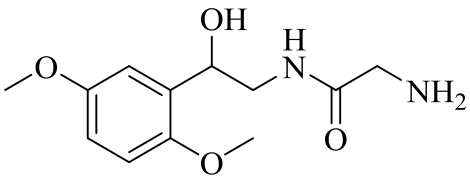 Midodrine	2.39458	254.282

3.2.2.4 COMPOUNDS ON THE HIT-LIST OF PHARMACOPHORE MODEL 1, 2 AND 3

As earlier mentioned, the top ten results of each pharmacophore model are listed in **Tables 3.1, 3.2** and **3.3**. Results obtained for the pharmacophore models were further analysed and not surprisingly, since these pharmacophore models are very similar, several drugs mapped to pharmacophore models 1, 2 and 3. These are

listed in **Table 3.4**. This list includes compounds under the top fifty hits of each pharmacophore model.

Table 3.4: A list of the compounds in the Drug Bank which mapped to pharmacophore models 1, 2 and 3 (all compounds in the top fifty included). Also given are the molecular weights of the respective compounds.

Name and Structure of Compounds	**Molecular Weight (g/mol)**
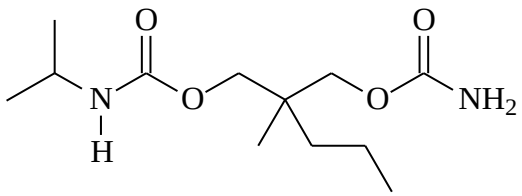 Carisoprodol	260.33
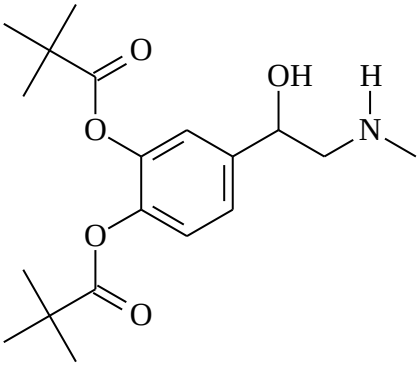 Dipivefrine	351.437

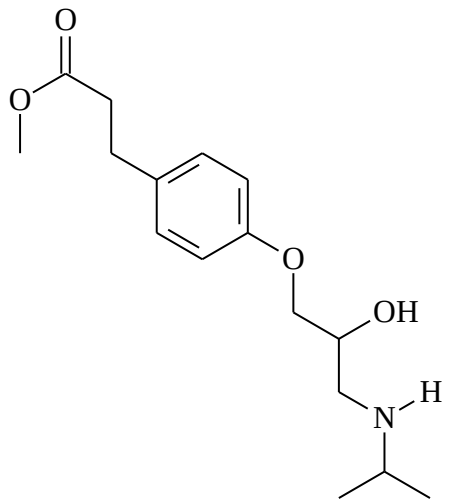 Esmolol	295.374
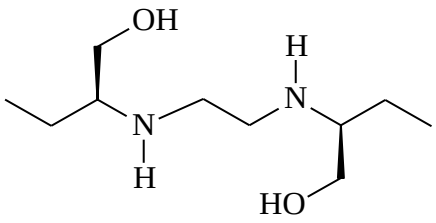 Ethambutol	204.31
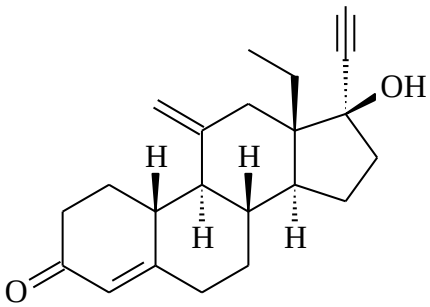 Etonogestrel	324.457

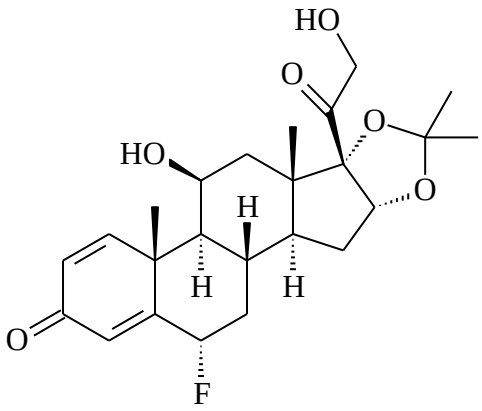 Flunisolide	434.498
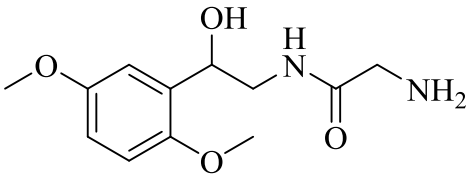 Midodrine	254.282
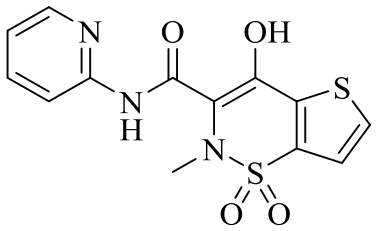 Tenoxicam	337.376
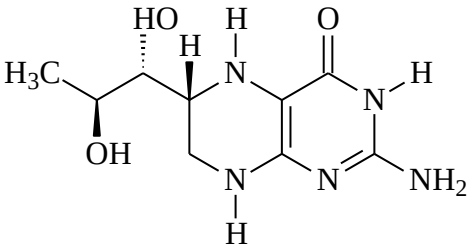 (6*R*)-5,6,7,8-Tetrahydrobiopterin	314.17

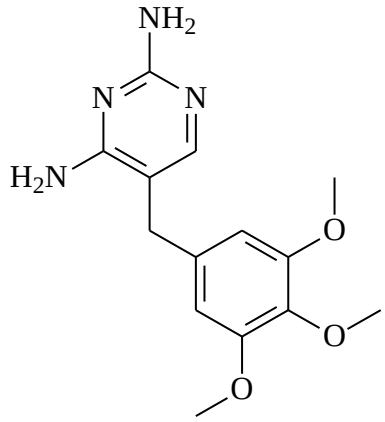 Trimethoprim	290.32

3.2.3 ANALYSIS OF RESULTS

The hit-list of each pharmacophore was then analysed to evaluate its effectiveness using the literature protocol as described by Kirchmair *et al.* (2008) and Seidel *et al.* (2010).

PHARMACOPHORE MODEL 1:

Table 3.5: The evaluation of pharmacophore model 1. This table contains the five equations used to analyse and evaluate the pharmacophore model as well as a conclusion.

	Equation	***Conclusion***
Sensitivity:	$Se = \frac{TP}{TP+FN} = \frac{7}{7+0} = 1$	The Se value of 1 shows that the model has an excellent sensitivity for compounds that have the ability to inhibit COMT. The Se value is equal to 1, which demonstrates that the model retrieved all the active COMT inhibitors.

Specificity:	$Se = \frac{TN}{TN+FN} = \frac{4}{4+2} = 0.6667$	The Sp value of 0.6667 indicates that more than half of the decoys were discarded. Therefore the model may also retrieve decoys in addition to truly active COMT inhibitors. The model therefore has a moderate ability to distinguish between inhibitors and non-inhibitors.
Yield of actives:	$Ya = \frac{TP}{n} = \frac{7}{10} = 0.7$	The Ya value is calculated as 0.7. Therefore 70.00% of the hits are truly active.
Accuracy:	$Acc = \frac{TP+TN}{N} = \frac{7+4}{15} = 0.7333$	This result shows that the model is 73.33% accurate.
Balanced labelling performance:	$I_{bal} = \frac{1}{2}.Se + \frac{1}{2}.Sp$ $= \frac{1}{2}(1) + \frac{1}{2}(0.6667) = 0.83335$	The value of 0.83335 indicates a good balanced labelling performance.

Pharmacophore model 1 constructed for COMT was sensitive to the known inhibitors of COMT in the test set and moderately specific with regards to identifying compounds that do not bind to COMT. This model has a good accuracy and balanced labelling performance and it was concluded that it could be a useful tool in the identification of compounds in a virtual database with the potential to inhibit COMT.

PHARMACOPHORE MODEL 2:

Table 3.6: The evaluation of pharmacophore model 2. This table contains the five equations used to analyse and evaluate the pharmacophore model as well as a conclusion.

	Equation	***Conclusion***
Sensitivity:	$Se = \frac{TP}{TP+FN} = \frac{7}{7+0} = 1$	The Se value of 1 shows that the model has an excellent sensitivity for compounds that have the ability to inhibit COMT. The Se value is equal to 1, which demonstrates that the model retrieved all the active COMT inhibitors.
Specificity:	$Se = \frac{TN}{TN+FN} = \frac{4}{4+2} = 0.6667$	The Sp value of 0.6667 indicates that more than half of the decoys were discarded. Therefore the model may also retrieve decoys in addition to truly active COMT inhibitors. The model therefore has a moderate ability to distinguish between inhibitors and non-inhibitors.
Yield of actives:	$Ya = \frac{TP}{n} = \frac{7}{10} = 0.7$	The Ya value is calculated as 0.7. Therefore 70.00% of the hits are truly active.
Accuracy:	$Acc = \frac{TP+TN}{N} = \frac{7+4}{15} = 0.7333$	This result shows that the model is 73.33% accurate.
Balanced labelling performance:	$I_{bal} = \frac{1}{2}.Se + \frac{1}{2}.Sp$ $= \frac{1}{2}(1) + \frac{1}{2}(0.6667) = 0.83335$	The value of 0.83335 indicates a good balanced labelling performance.

Pharmacophore model 2 constructed for COMT was sensitive to the known inhibitors of COMT in the test set and moderately specific with regards to identifying compounds that do not bind to COMT. This model has a good accuracy and balanced labelling performance and therefore it was identified as a useful tool to identify compounds in a virtual database that can act as COMT inhibitors.

PHARMACOPHORE MODEL 3:

Table 3.7: The evaluation of pharmacophore model 3. This table contains the five equations used to analyse and evaluate the pharmacophore model as well as a conclusion.

	Equation	***Conclusion***
Sensitivity:	$Se = \frac{TP}{TP+FN} = \frac{6}{6+0} = 1$	The Se value of 1 shows that the model has an excellent sensitivity for compounds that have the ability to inhibit COMT. The Se value is equal to 1, which demonstrates that the model retrieved all the active COMT inhibitors.
Specificity:	$Se = \frac{TN}{TN+FP} = \frac{4}{4+3} = 0.5714$	The Sp value of 0.5714 indicates that more than half of the decoys were discarded. Therefore the model may also retrieve decoys in addition to truly active COMT inhibitors. The model therefore has a moderate ability to distinguish between inhibitors and non-inhibitors.
Yield of actives:	$Ya = \frac{TP}{n} = \frac{6}{10} = 0.6$	The Ya value is calculated as 0.6. Therefore 60.00% of the hits are truly active.

Accuracy:	$Acc = \frac{TP+TN}{N} = \frac{6+4}{15} = 0.6667$	This result shows that the model is 66.67% accurate.
Balanced labelling performance:	$I_{bal} = \frac{1}{2}.Se + \frac{1}{2}.Sp$ $= \frac{1}{2}(1) + \frac{1}{2}(0.5714) = 0.7857$	The value of 0.7857 indicates a good balanced labelling performance.

Pharmacophore model 3 constructed for COMT was sensitive to the known inhibitors of COMT in the test set, and moderately specific with regards to identifying compounds that do not bind to COMT. This model has a good accuracy and balanced labelling performance and therefore it was regarded as a useful tool to identify compounds in a virtual database that can act as COMT inhibitors.

Based on this analysis, while phamacophore models 1 and 2 are very similar, pharmacophore 3 model appears to be the weakest of the three. This might be due to the addition of two added acceptors orientated towards the Mg^{2+} ion to pharmacophore model 3.

3.3 SCREENING A LIBRARY BY FINGERPRINT

3.3.1 METHOD

The following steps were followed using Discovery Studio® 3.1 modelling software:

(a) Preparation of the library to be screened:

- The database of FDA approved drugs was downloaded from www.drugbank.ca.
- The database was opened with Discovery Studio® 3.1 modelling software.
- The ligands were prepared with the Prepare Ligands module using the following settings: change ionisation, generate tautomers and generate isomers were set to false. Fix bad valences was set to true.

(b) Preparation of the reference ligand:

- The reference ligand, DNC, was drawn in Discovery Studio.
- Hydrogen bonds were added to DNC and the structure was briefly optimised briefly with “clean geometry”.
- The ligand was prepared using the Prepare Ligands module employing the same settings as those for preparation of the test library.

(c) Finding similar molecules by fingerprint:

- The compounds from the library to be screened and the reference ligand were subjected to the “Find similar molecules by fingerprint” module in Discovery Studio.

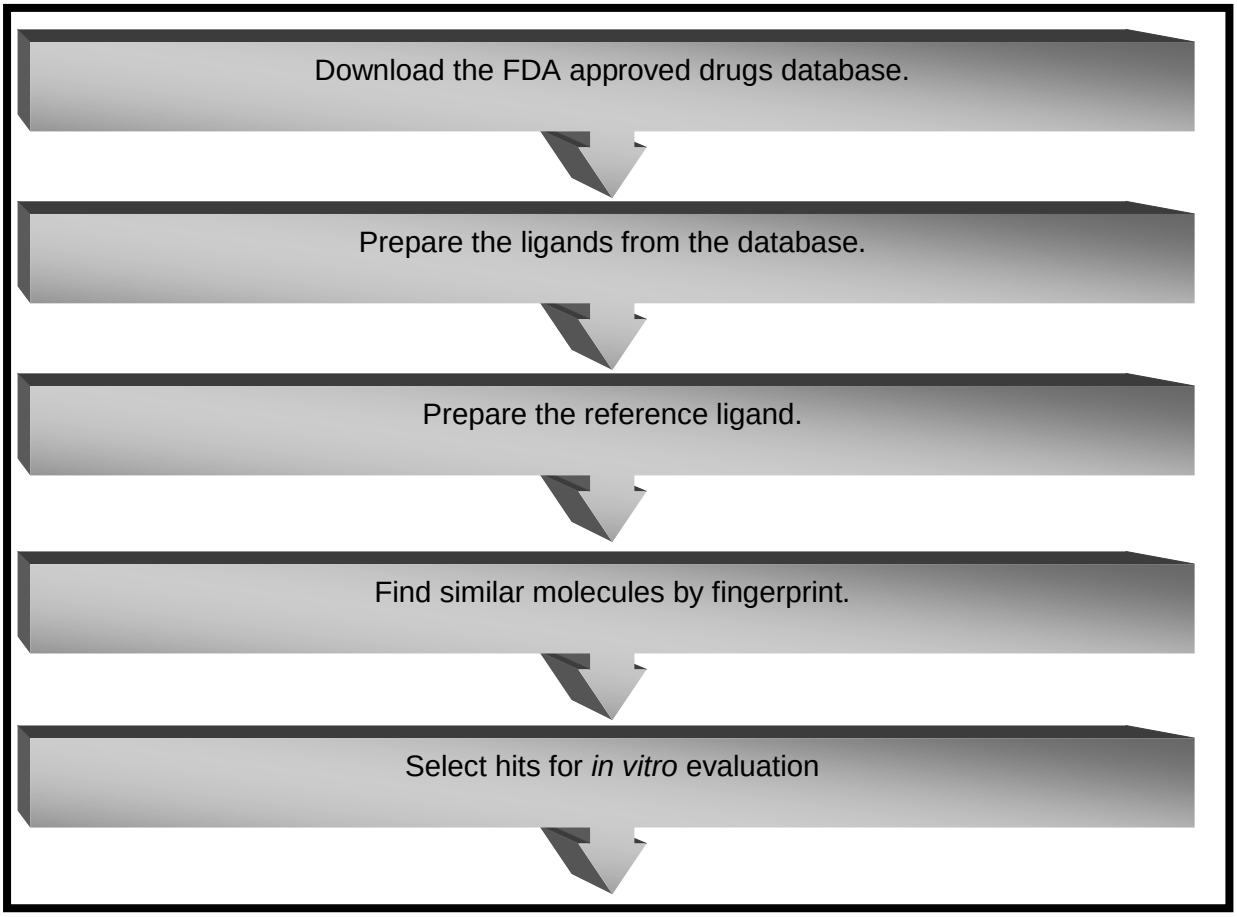

Figure 3.12: Workflow for screening a library by fingerprint.

3.3.2 RESULTS

Table 3.8: A list of the twenty five compounds identified by screening a library by the fingerprint method using DNC as reference ligand. Also given are the molecular weights of the respective compounds.

Name and Structure of Compounds	Molecular Weight (g/mol)
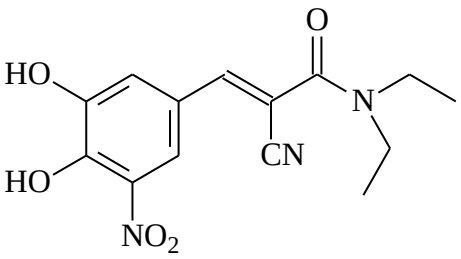 Entacapone	305.286
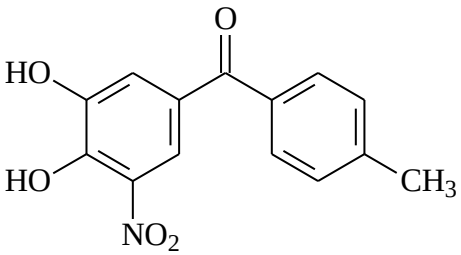 Tolcapone	273.241
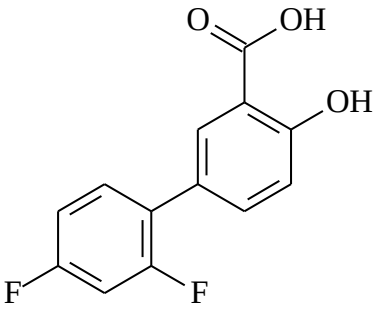 Diflunisal	250.198

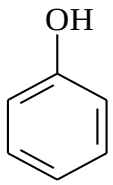 Phenol	94.1112
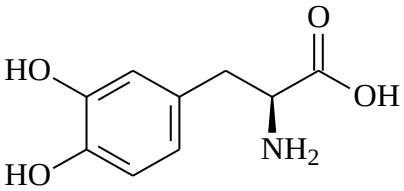 Levodopa	197.188
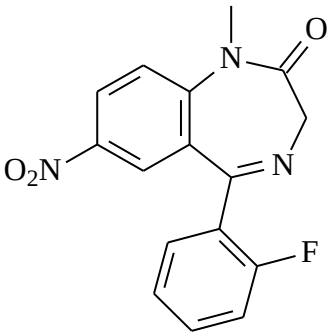 Flunitrazepam	313.283
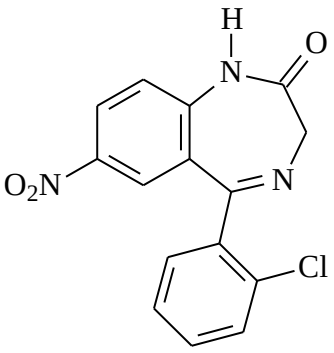 Clonazepam	315.711
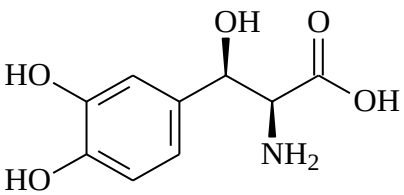	213.187

Droxidopa	
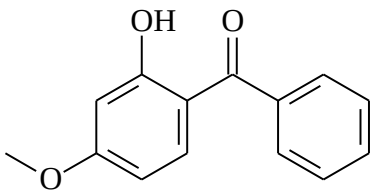 Oxybenzone	228.243
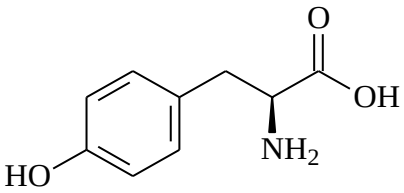 L-tyrosine	181.189
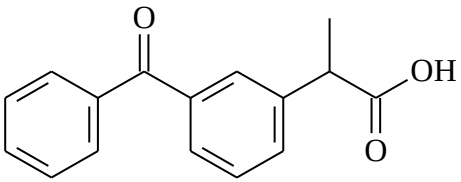 Ketoprofen	254.281
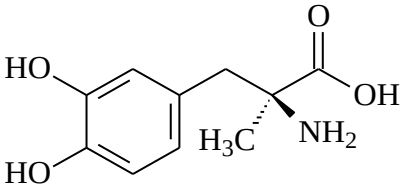 Methyldopa	211.215
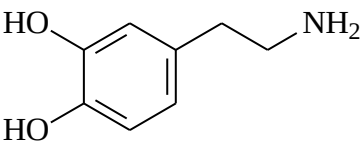 Dopamine	153.178

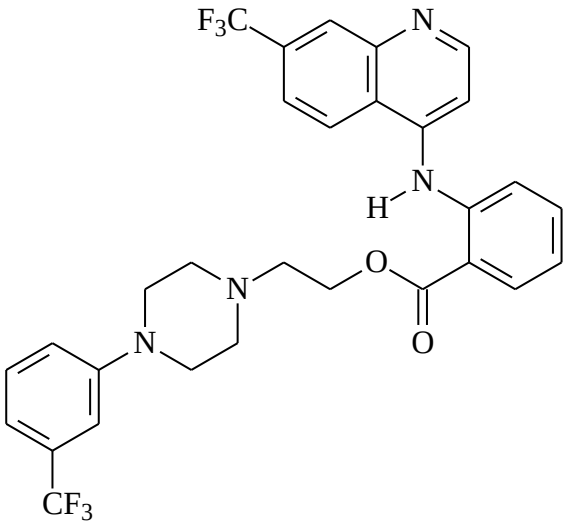 Antrafenine	588.543
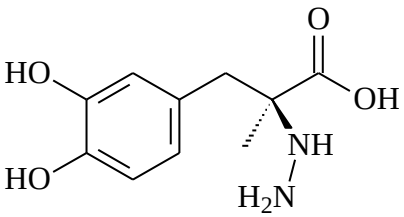 Carbidopa	226.229
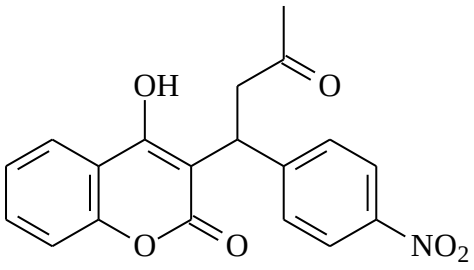 Acenocoumarol	353.325
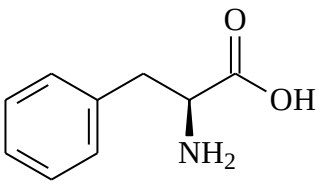 L-phenylalanine	165.189

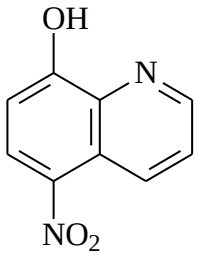 Nitroxoline	190.156
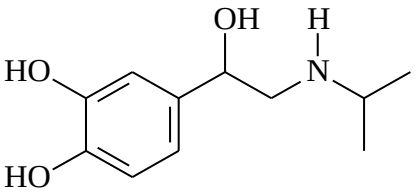 Isoprenaline	211.258
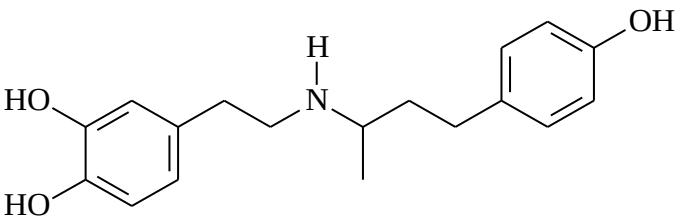 Dobutamine	301.38
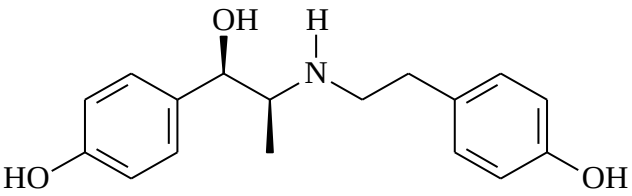 Ritodrine	287.354
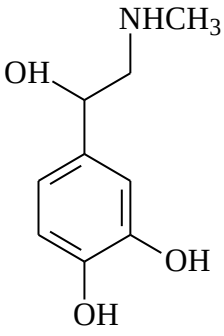	183.204

Epinefrine	
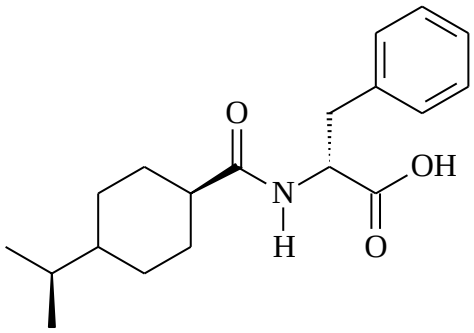 Nateglinide	317.423
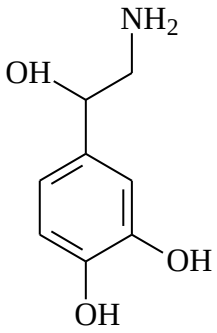 Norepinephrine	169.178
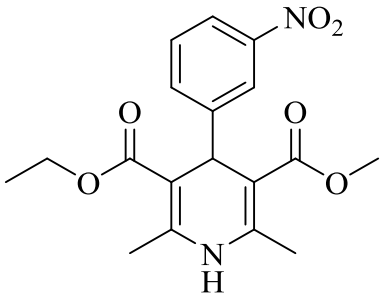 Nitrendipine	360.361

3.4 MOLECULAR DOCKING

3.4.1 METHOD

As mentioned earlier the crystal structure of the COMT enzyme was retrieved from the Brookhaven Protein Data Bank. The X-ray crystal structure of human COMT (PDB code: 3BWM) was used to carry out these studies.

The following steps were followed using Discovery Studio® 3.1 modelling software:

(a) Protein Preparation:

- The protein was prepared using the method previously described in paragraph 3.2.1 (Construction and screening of the pharmacophore models, protein preparation).

(b) Docking:

- The ligands and the backbone constraint were removed from the model and the binding site was set to a radius of 10 Å from the ligand, DNC.
- Structures of the top ten hits from the three pharmacophore models, the hit-list of the fingerprinting approach, DNC and tolcapone were drawn in Discovery Studio® 3.1, and hydrogen atoms were added according to the appropriate protonation states at pH 7.4. The geometries of the ligands were briefly optimised using a fast Dreiding-like force field (1000 interactions) and the atom potential types and partial charges were assigned with the Momany and Rone CHARMm force field.
- Docking of the ligands was carried out with the CDOCKER algorithm with the generation of 10 random ligand conformations and a heating target temperature of 700 K in full potential mode.
- The docking solutions were refined using the Smart Minimizer algorithm. Ten possible binding solutions were computed for each docked ligand and the best-ranked binding conformation of each ligand was determined according to the CDOCKER and CDOCKER interaction energy values.

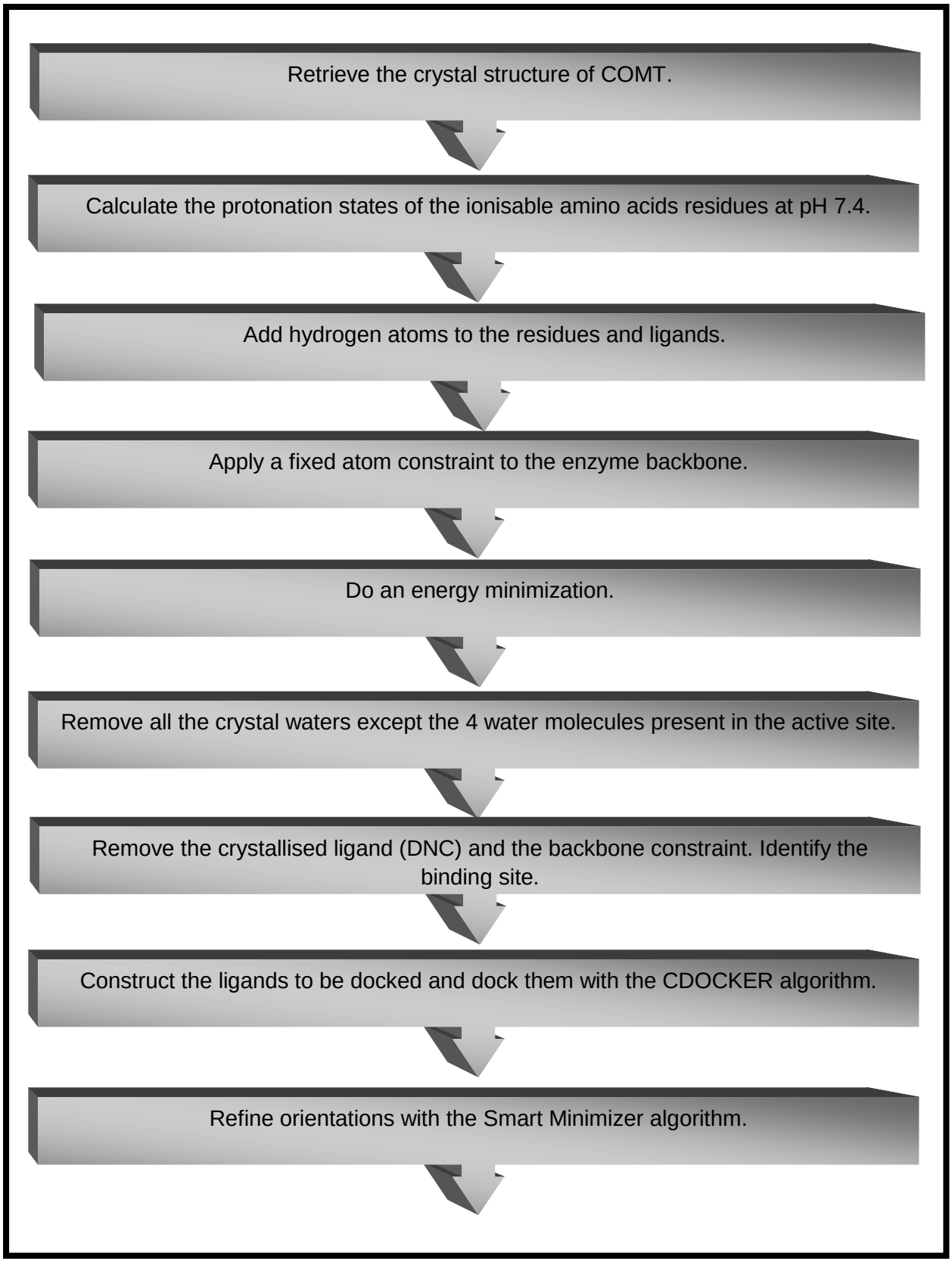

Figure 3.13: Workflow for docking ligands into the active site of the COMT enzyme.

3.4.2 RESULTS

Of the eighteen compounds selected from the top fifty hit-lists of pharmacophore models 1, 2 and 3 and also selected from the hit-list of the fingerprinting approach, only eight compounds were successfully docked into the active site of the COMT enzyme. These include carisoprodol, diflunisal, ethambutol, ketoprofen, midodrine, oxybenzone, (6*R*)-5,6,7,8-tetrahydrobiopterin and trimethoprim. The CDOCKER energies and CDOCKER interaction energies of these compounds are given in **Table 3.9** respectively.

Table 3.9: This table contains the results of the CDOCKER energies and the CDOCKER interaction energies of the test drugs. Also given are the CDOCKER results of DNC and tolcapone as reference.

Name of Compound		-CDOCKER Interaction Energy (kcal/mol)	-CDOCKER Energy (kcal/mol)
DNC		30.397	19.8086
1	Tolcapone	36.3414	25.8482
2	Midodrine	34.8534	26.0261
3	Ethambutol	34.5762	26.941
4	Diflunisal	33.8059	22.7632
5	Trimethoprim	29.951	22.8252
6	(6*R*)-5,6,7,8-Tetrahydrobiopterin	29.6893	17.9281
7	Carisoprodol	28.7419	35.0299
8	Oxybenzone	25.5181	-2.54751
9	Ketoprofen	16.2604	-22.856

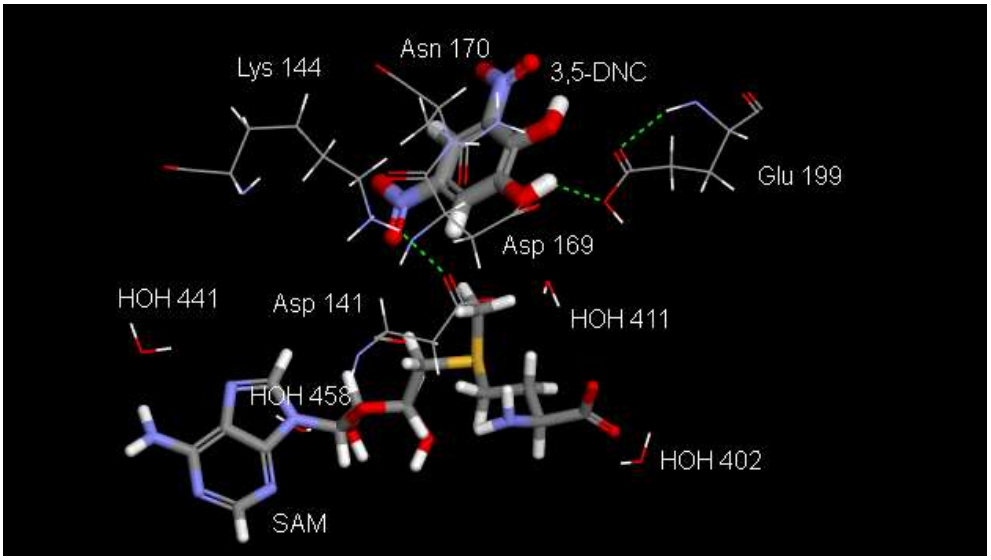

Figure 3.14: Schematic illustration of the interactions between DNC and the amino acid residues of COMT. Also illustrated are the hydrogen bond interactions.

As shown in **Figure 3.14**, hydrogen bond interactions are observed between DNC and certain amino acid residues (as indicated by the dash-lines) in the active site. For example, there is an interaction between DNC and Glu 199, where an oxygen atom of DNC acts as a hydrogen bond acceptor.

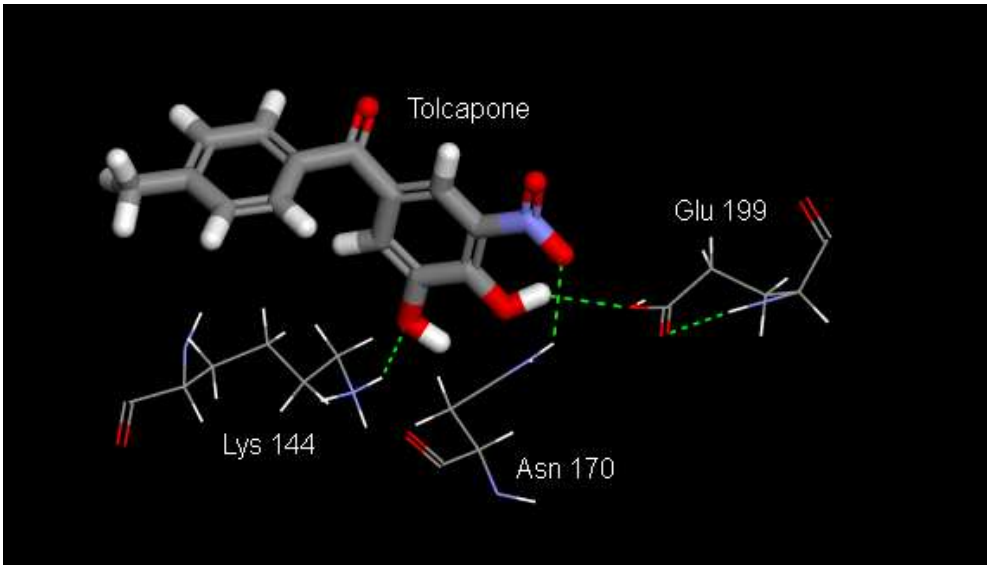

Figure 3.15: Schematic illustration of the hydrogen bond interactions (dash-lines) between tolcapone and Lys 144, Asn 170 and Glu 199 in the COMT active site.

As illustrated in **Figure 3.15**, tolcapone has hydrogen bond interactions with Lys 144, Asn 170 and Glu 199. Tolcapone is a potent inhibitor of COMT with a CDOCKER interaction energy value of -36.3414 kcal/mol.

Furthermore, ethambutol and diflunisal also have good CDOCKER interaction values of -34.5762 kcal/mol and -33.8059 kcal/mol, respectively (**Table 3.9**). Both ethambutol (**Figure 3.16 B**) and diflunisal (**Figure 3.16 C**) have hydrogen bond interactions with amino acid residue Glu 199.

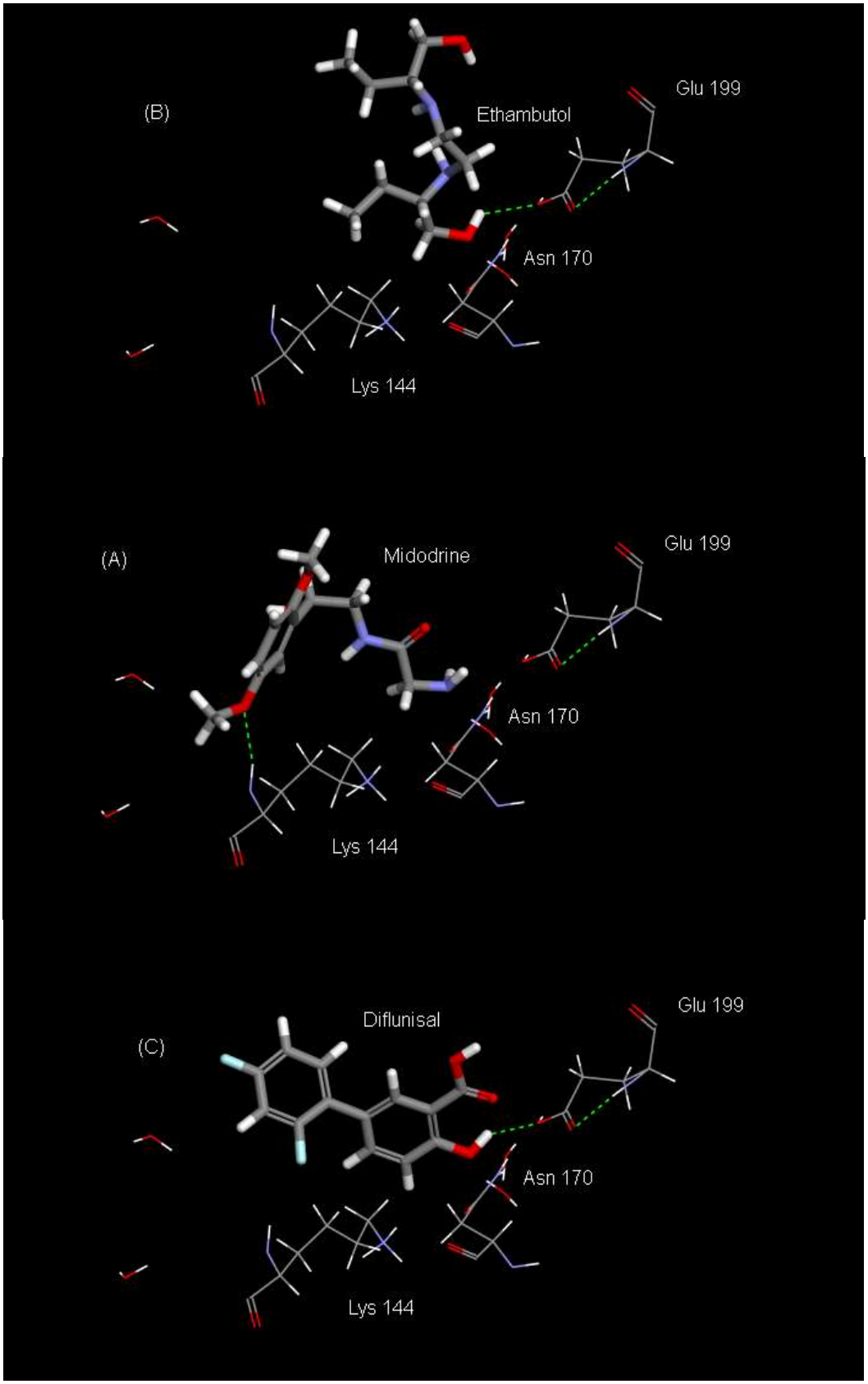

Figure 3.16: Schematic illustration of the hydrogen bond interactions (dash-lines) between the test drugs and the amino acid residues.

The fact that only eight of the eighteen hits docked successfully, could indicate that the pharmacophore models may require refining. On the other hand, the successful docking of several compounds indicates the potential of these compounds to fit into the active site, and these were considered as especially promising candidates. Interactions similar to those observed for DNC and tolcapone were further observed for some of these compounds, which were also encouraging.

3.5. BIO-ISOSTERES

3.5.1 INTRODUCTION

The concept of isosterism between relatively simple chemical entities was originally contemplated by James Moir in 1909 (Meanwell, 2011). The concept was further refined by H. G. Grimm's hydride displacement law and captured more effectively in the ideas advanced by Irving Langmir based on experimental observations (Langmir, 1919; Meanwell, 2011).

According to Meanwell (2011), bio-isosteres can be recognized as chemical substituents with similar physical or chemical properties which, produce broadly similar biological properties to another chemical compound. The purpose of exchanging one bio-isostere for another is to enhance the desired biological or physical properties of a compound without making significant changes in chemical structure (Meanwell, 2011).

Classical bio-isosteres represent the results of an early appreciation of the concept and encompass structurally simple, mono-, di-, and trivalent atoms or groups and ring equivalents (Meanwell, 2011; Patani & LaVoie, 1996). In contrast, nonclassical bio-isosteres extend the concept to structural elements that offer a more subtle and sophisticated form of biochemical mimicry, relying upon functionality that can differ quite substantially in electronic, physicochemical, steric, and topological representation from that being emulated (Meanwell, 2011; Patani & LaVoie, 1996).

3.5.2 METHOD

A literature survey was performed to identify bio-isosteres of phenol and catechol (indicated in **Table 3.10**). After identification of these bio-isosteres (Meanwell, 2011; Patani & LaVoie, 1996), the Sigma-Aldrich database was searched and molecules containing these moieties. It was hypothesised that, while these compounds would probably only be weak inhibitors of COMT, they could serve as synthetic starting points for the development of non-catechol inhibitors.

3.5.3 RESULTS

Table 3.10: A list of compounds that contain bio-isosteres of catechol and phenol.

	Structure of the bio-isosteres
1	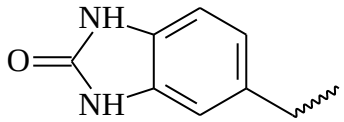
2	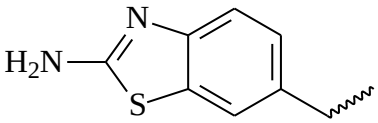
3	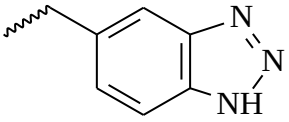
4	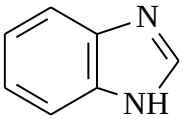
5	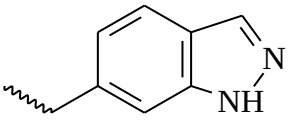

6	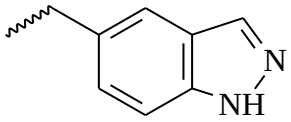
7	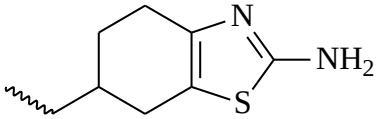

3.6 SELECTION OF COMPOUNDS

A group of results were obtained from each pharmacophore model (**Table 3.1, 3.2, 3.3, 3.4**) and out of this group only compounds with a molecular weight smaller than 500 g/mol were considered for *in vitro* evaluation. The docking results for these compounds were also kept in mind. The cost and availability of these compounds were further also taken into consideration. Secondly, the hit-list of the ligand fingerprint approach (**Table 3.8**) was used in the selection process.

Furthermore, since catechols are the natural substrates of the COMT enzyme and the most effective inhibitors of COMT also contain this moiety, several bio-isosteres of catechol and phenol (**Table 3.10**) were identified and compounds containing these moieties that were commercially available and affordable, were obtained and selected for *in vitro* screening. Lastly, since it was known that quercetin was a known COMT inhibitor, the structurally related kaempferol was also selected for screening.

Table 3.11: This table contains a list of compounds selected for *in vitro* screening. Also given is the molecular weight of the compounds and the reason for selection of each compound.

Name and Structure of Compounds		Molecular Weight (g/mol)
On the top ten hit-list of Pharmacophore model 1.		
1	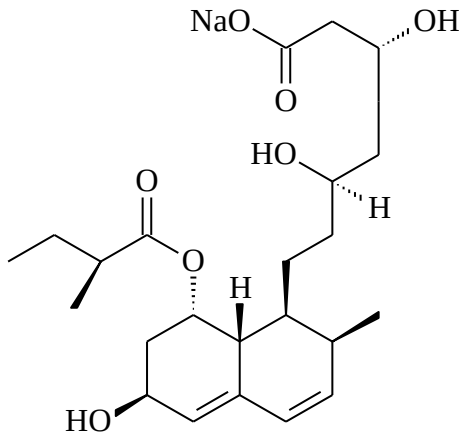 Pravastatin	424.528
2	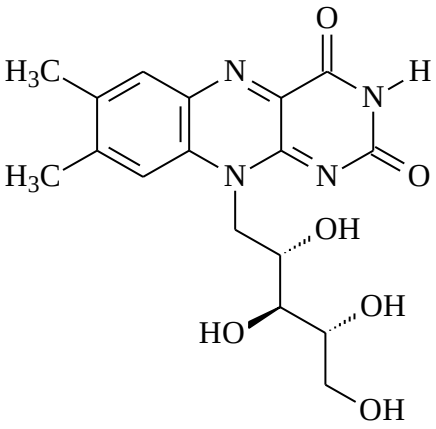 (-)-Riboflavin	376.37
On the top ten hit-list of Pharmacophore model 2.		

3	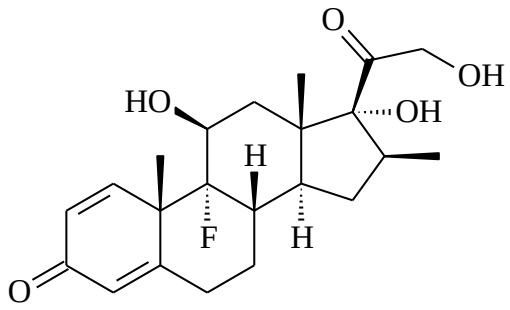 Betamethasone	392.461
On the top fifty hit-list of Pharmacophore models 1, 2 and 3.		
4	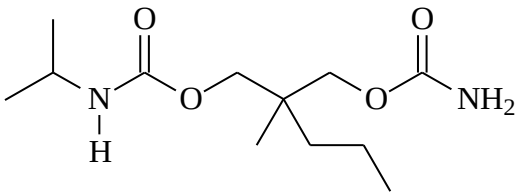 Carisoprodol	260.33
5	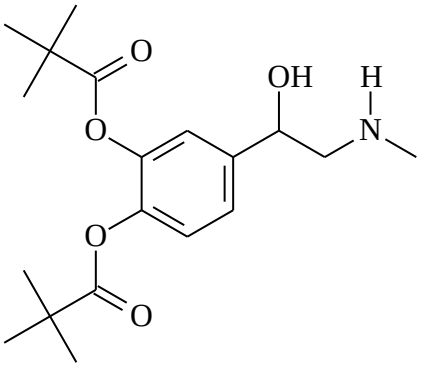 Dipivefrine	351.437

6	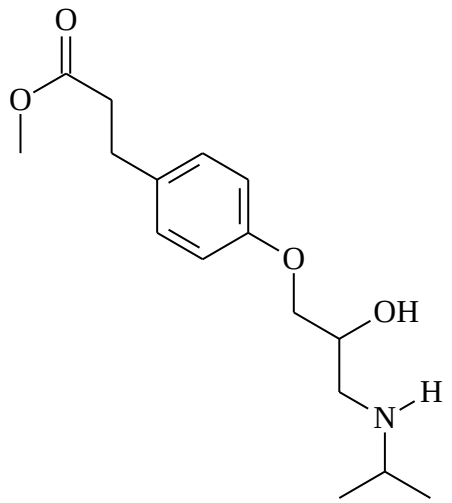 Esmolol	295.374
7	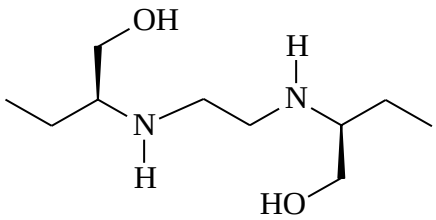 Ethambutol	204.31
8	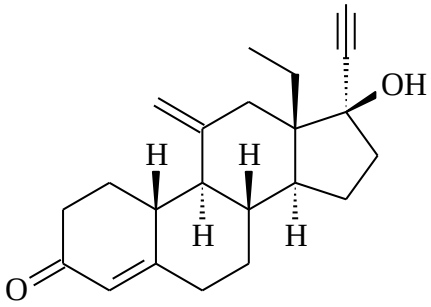 Etonogestrel	324.457

9	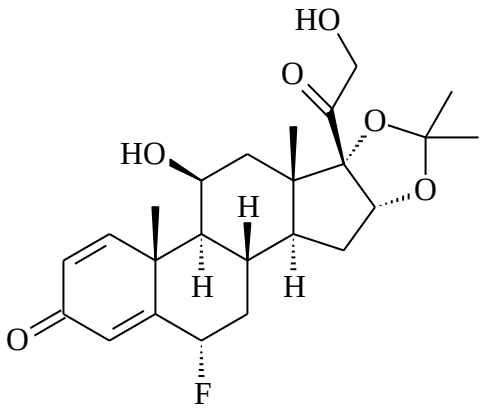 Flunisolide	434.498
10	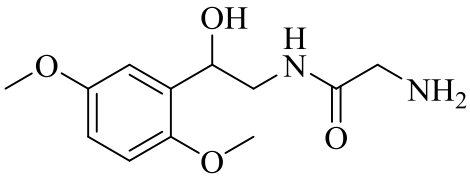 Midodrine	254.282
11	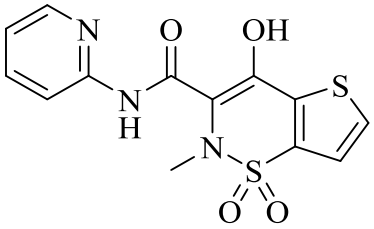 Tenoxicam	337.376
12	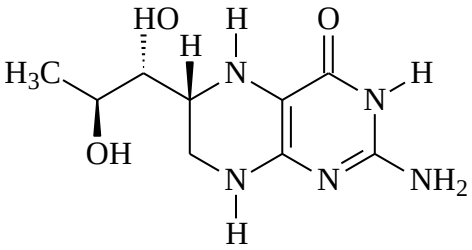 (6*R*)-5,6,7,8-Tetrahydrobiopterin	314.17

13	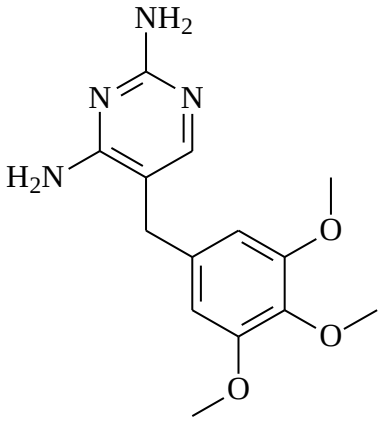 Trimethoprim	290.32
On the hit-list of the library screened by fingerprinting.		
14	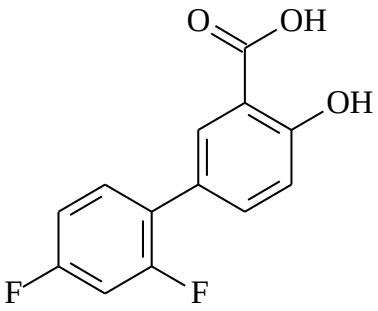 Diflunisal	250.198
15	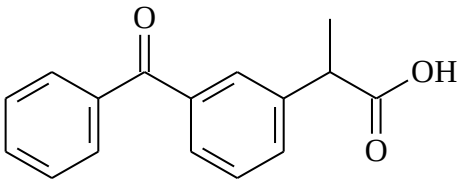 Ketoprofen	254.281
16	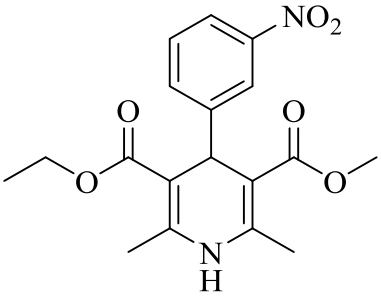	360.361

	Nitrendipine	
17	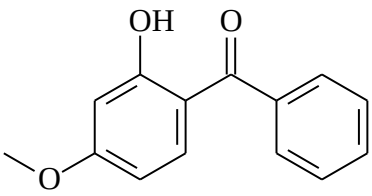 Oxybenzone	228.25
Contains a bio-isostere of catechol/phenol.		
18	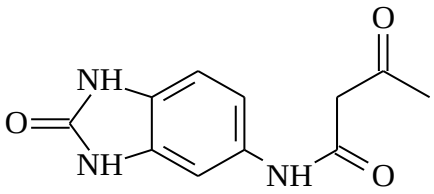 5-Acetoacetylamino benzimidazolone	233.22
19	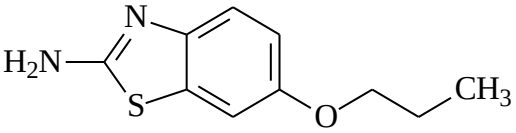 2-Amino-6-propoxybenzothiazole	208.28
20	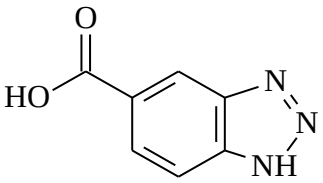 Benzotriazol-5-carboboxylic acid	163.13
21	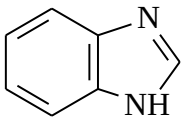 Benzimidazole	118.14

22	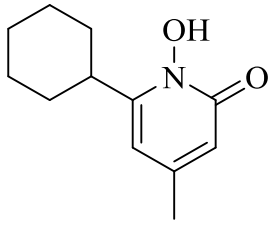 Ciclopirox	268.35
23	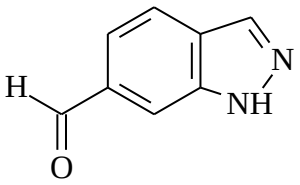 Indazole-6-carboxaldehyde	146.15
24	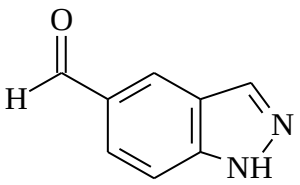 Indazole-5-carboxaldehyde	146.15
25	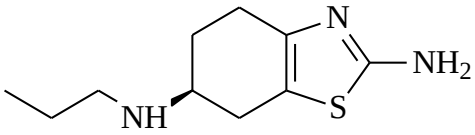 Pramipexole	211.324
Structurally similar to quercetin.		
26	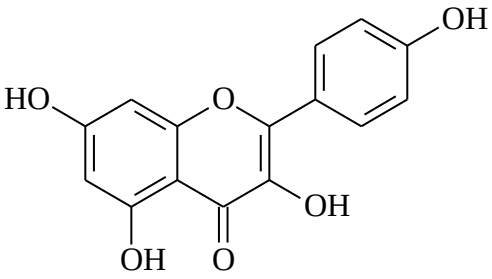 Kaempferol	286.23

3.7 SUMMARY

In this chapter pharmacophore models of COMT inhibitors were constructed according to the given protocol. These models were used for the virtual screening of the FDA approved drugs as potential COMT inhibitors. Descriptions of the pharmacophore models were given and residues involved in the key interactions of the active site of COMT were identified. The hit-lists were analysed to evaluate the effectiveness of the pharmacophore models using the literature protocol as described by Kirchmair *et al.* (2008) and Seidel *et al.* (2010). Compounds obtained from these models, as well as hits obtained from screening the library by fingerprinting, were docked into the COMT enzyme's active site. **Table 3.11** in this chapter provides a list of drugs, which were selected based on results from the pharmacophore mapping, screening of a library by fingerprinting, molecular docking, the bio-isostere approach, chemical similarity, cost, availability and molecular weight. These drugs and compounds were selected for *in vitro* evaluation.

CHAPTER 4

ENZYMOLOGY:

4.1 GENERAL BACKGROUND

4.1.1 INTRODUCTION

According to Rodwell (1993) enzyme kinetics can be defined as the study of the rate at which an enzyme catalyses the conversion of a substrate to the product and is used to determine the potency of the interaction between an inhibitor and a specific enzyme (Murray *et al*., 2003; Rodwell, 1993).

Enzymes are protein catalysts that accelerate the rate of a chemical reaction by binding to a substrate and lowering the activation energy needed to convert it to a product. There are several factors that can influence the rate at which an enzyme works, for example:

• The concentration of a substrate [S]

• Temperature

• pH

• The presence of inhibitors

• Activation energies

In an enzyme catalysed transformation of a substrate (S) to a product (P), the rate limiting step is the breakdown of the Enzyme-Substrate complex (ES) (**Equation 4.1**).

$$E + S \underset{k-1}{\overset{k+1}{\rightleftharpoons}} ES \underset{k-2}{\overset{k+2}{\rightleftharpoons}} E + P$$

Equation 4.1: Enzyme catalysed transformation (Murray *et al*., 2003; Rodwell, 1993).

Seeing that the ES concentration cannot easily be measured experimentally, equations such as the Michaelis-Menten equation are used as alternative expressions for the determination of the rate of enzymatic reactions (Murray *et al*., 2003; Rodwell, 1993).

4.1.2 THE MICHAELIS-MENTEN EQUATION

The relationship between initial reaction velocity (V_i) and substrate concentration [S] can be illustrated in mathematical terms by the Michaelis-Menten equation (**Equation 4.2**):

$$\mathbf{V_i = \frac{V_{max}[S]}{K_m + [S]}}$$

Equation 4.2: The Michaelis-Menten equation (Murray *et al*., 2003; Rodwell, 1993).

Where V_{max} is the maximum value of V_i and K_m the Michaelis-Menten constant, which can be defined as the substrate concentration where V_i equals half of V_{max} (**Figure 4.1**).

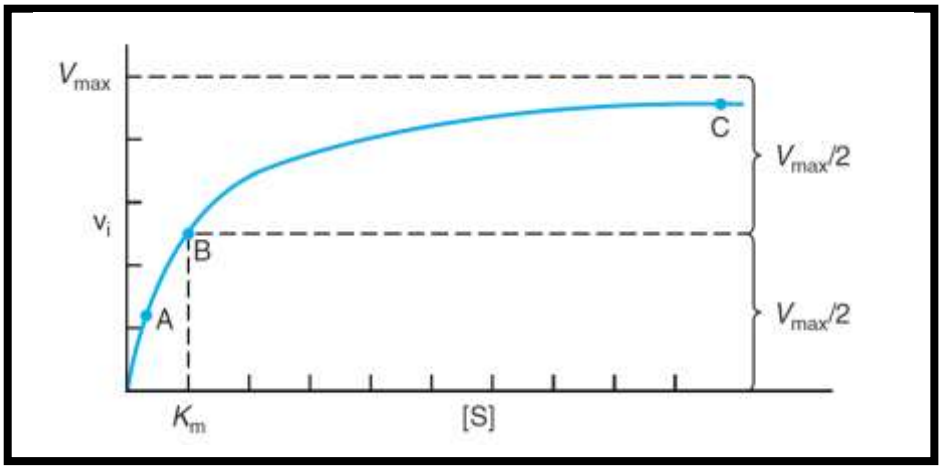

Figure 4.1: Relationship between substrate concentration and the initial velocity of an enzyme-catalysed reaction (Murray *et al.*, 2003).

V_i will almost always be directly proportional to the enzyme concentration (V_i α [E]) since enzyme activity assays are usually done with an excess substrate over the enzyme. Thus when the [S] is increased, V_i will follow with increased values until V_{max} is reached. The enzyme is saturated when V_i does not further increase with the increase in [S] (Murray *et al*., 2003).

Under certain circumstances, the Michaelis-Menten equation can be reduced to three different forms. Firstly, if the value of K_m is much higher than [S], the expression K_m + [S] can be replaced by K_m (**Equation 4.3**):

$$V_i = \frac{V_{max}[S]}{K_m}$$

Equation 4.3: When [S] is less than K_m (Murray *et al*., 2003; Rodwell, 1993).

Secondly, if the value of K_m is much lower than that of [S], the term K_m + [S] can be replaced by [S], thus giving **Equation 4.4**:

$$V_i = V_{max}$$

Equation 4.4: When [S] is greater than K_m (Murray *et al*., 2003; Rodwell, 1993).

Lastly, the Michaelis-Menten equation can also be reduced if the values of K_m and [S] are equal. Then V_i can be set equal to half the maximal rate (V_{max} /2) resulting in **Equation 4.5**:

$$V_i = \frac{V_{max}}{2}$$

Equation 4.5: When [S] = K_m (Murray *et al*., 2003; Rodwell, 1993).

Since impractically high concentrations of the substrate are needed to determine V_{max} and K_m, it is not always possible to determine these values with the Michaelis-

Menten equation. However, by inverting the Michaelis-Menten equation, the so-called Lineweaver-Burk equation is obtained which can be used to determine V_{max} and K_m accurately at very low substrate concentrations (Murray *et al*., 2003; Rodwell, 1993).

4.1.3 THE LINEWEAVER-BURK EQUATION

$$\frac{1}{V_i} = \left[\frac{K_m}{V_{max}}\right]\frac{1}{[S]} + \frac{1}{V_{max}}$$

Equation 4.6: The Lineweaver-Burk equation (Murray *et al*., 2003; Rodwell, 1993).

A straight line is obtained when the inverse of both the initial velocity ($1/V_i$) as well as the substrate concentration (1/[S]) are plotted. This straight line is termed the double reciprocal or Lineweaver-Burk plot (**Figure 4.2**).

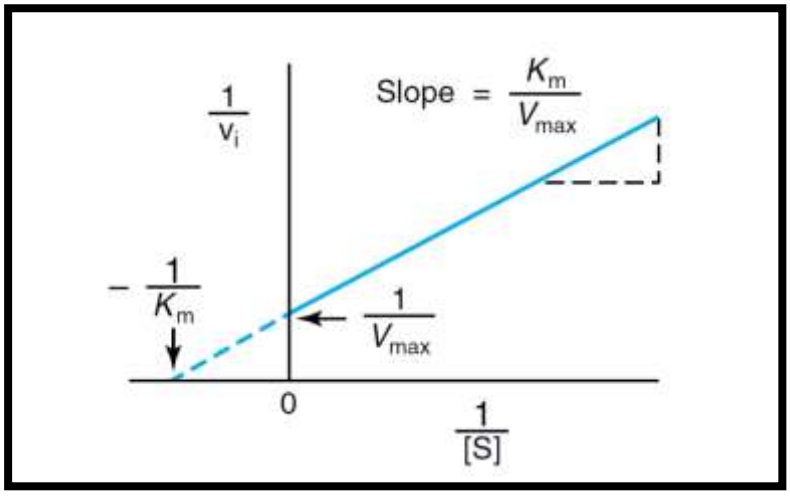

Figure 4.2: Lineweaver-Burk plot (Murray *et al*., 2003; Rodwell, 1993).

When examining this plot, it can be seen that the y-axis intercept is equal to $1/V_{max}$, the slope is K_m/V_{max} and the x-axis intercept is equal to $-1/K_m$. Thus, the K_m value may be determined by setting y equal to zero and solving x (Murray *et al*., 2003).

Lineweaver-Burk plots can also be used to determine whether a compound is a competitive or non-competitive inhibitor. Competitive inhibitors bind to the active site of the enzyme and prevent binding of the substrate (and *vice versa*), while non-competitive inhibitors bind to a site other than the active site of the enzyme. This binding by a non-competitive inhibitor then reduces the catalytic activity of the enzyme (Murray *et al*., 2003).

When examining the Lineweaver-Burk plot of a competitive inhibitor, two straight lines (one depicting a situation where no inhibitor is present, and the other where an inhibitor is present) with the same y-intercept will be observed. In this scenario, the V_{max} values remain unchanged, while the K_m values will vary (**Figure 4.3**) (Murray *et al*., 2003; Rodwell, 1993).

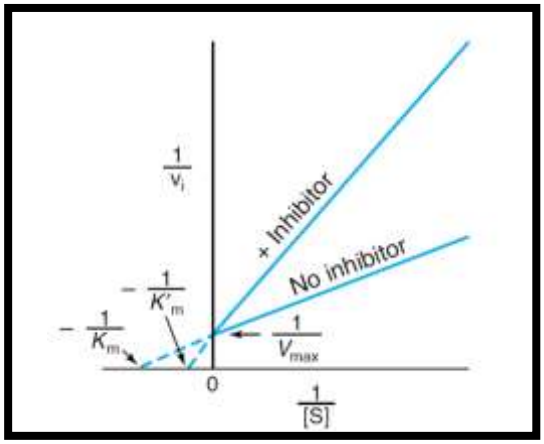

Figure 4.3: Lineweaver-Burk plot indicating competitive inhibition (Murray *et al*., 2003).

After the determination of K_m in the absence of an inhibitor, the K_i can be calculated from the following equation (**Equation 4.7**):

$$\frac{1}{K_m} = \frac{1}{K_m' + \frac{[I]}{K_i}}$$

Equation 4.7: The Michaelis-Menten equation for a competitive system (Murray *et al*., 2003; Rodwell, 1993).

K_i can be used to determine the affinity of an inhibitor for the enzyme, since low K_i values are indicative of good potency while higher K_i values signify weaker potency.

With non-competitive inhibition (under the same conditions) the Lineweaver-Burk plot will also show two straight lines but with different y-intercepts and the same x-intercept. The V_{max} values will thus vary while the K_m values will remain the same (**Figure 4.4**) (Murray *et al*., 2003; Rodwell, 1993).

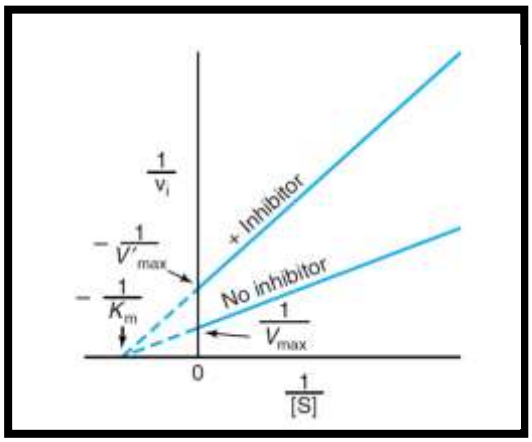

Figure 4.4: Lineweaver-Burk plot indicating non-competitive inhibition (Murray *et al*., 2003).

4.1.4 IC_{50} VALUE DETERMINATION

IC_{50} values are another way to measure the effectiveness of an inhibitor. The IC_{50} is defined as the concentration of the inhibitor that produces a 50% inhibition of the enzyme rate. **Equation 4.8** illustrates the relationship between the IC_{50} value and K_i (Cheng & Prusoff, 1973).

$$K_i = \frac{IC_{50}}{\left(1+\frac{[S]}{K_m}\right)}$$

Equation 4.8: The relationship between IC_{50} and K_i (Cheng & Prusoff, 1973).

4.2 COMT BIOASSAYS

4.2.1 INTRODUCTION

In this section the evaluation of selected drugs as *in vitro* inhibitors of the COMT enzyme will be discussed. The selection of the compounds to be screened was based on the results obtained from pharmacophore mapping, finding similar molecules by fingerprint, molecular docking, a bio-isostere search, chemical similarity, cost, availability and molecular weight, as previously discussed. The *in vitro* screening of these potential inhibitors was based on the literature protocol as described by Aoyama and co-workers (2005). In total, twenty-six test drugs were selected for *in vitro* analysis.

In this assay, norepinephrine is used as substrate and its conversion to the product (*DL*-normetanephrine) is monitored by HPLC. The principle of the assay is based on the fact that the test inhibitors would decrease the formation of normetanephrine from norepinephrine (**Figure 4.5**).

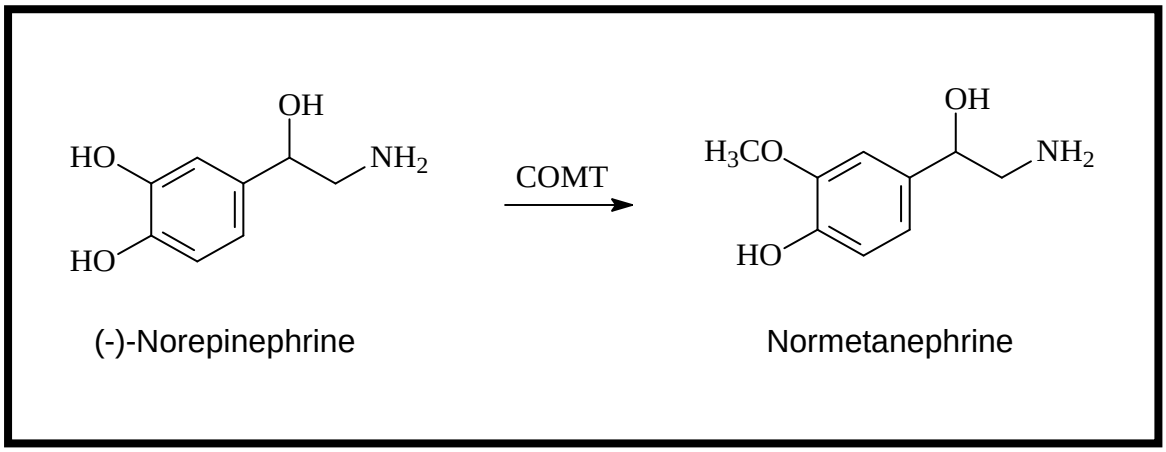

Figure 4.5: *O*-Methylation of the substrate (-)-norepinephrine catalysed by COMT (Aoyama *et al.*, 2005).

4.2.2 CHEMICALS AND MATERIALS

Table 4.1: This table contains the suppliers of reagents and materials used for this assay as well as the abbreviations of each reagent.

Materials	Abbreviations	Supplier
(-)-Norepinephrine	NE	Sigma-Aldrich
DL-normetanephrine hydrochloride	NMN	Sigma-Aldrich
Catechol-*O*-methyltransferase purified from porcine liver	COMT	Sigma-Aldrich
3,5-Dinitrocatechol	DNC	Sigma-Aldrich
S-adenosyl-*L*-methionine chloride salt	SAM/AdoMet	Sigma-Aldrich
Magnesium chloride	$MgCl_2$	Sigma-Aldrich
Dimethyl sulphoxide	DMSO	Merck
Sodium phosphate dibasic	$Na_2HPO_4.2H_2O$	Sigma-Aldrich
Sodium dihydrogen orthophosphate dihydrate	$NaH_2PO_4.2H_2O$	Merck
Boric acid	BA	Sigma-Aldrich
Sodium-1-hexanesulfonate monohydrate		Sigma-Aldrich
Acetonitrile, HPLC grade		Merck
Perchloric acid	$HClO_4$	Sigma-Aldrich
Test drugs		Sigma-Aldrich

4.2.3 INSTRUMENTATION AND HPLC REQUIREMENTS

The following instruments and settings were used in this study:

- HPLC analyses were performed with an Aligent 1100 HPLC system equipped with Shimadzu RF-551 fluorescence detector and a USP L1 Luna C18 column (250 x 4.6 mm, 5 µm).
- A mixture of an aqueous phase and an organic phase was used to prepare the mobile phase. The aqueous phase consisted of 10 mM sodium phosphate buffer (pH 7.0) containing 80 mM boric acid and 4 mM sodium-1-hexanesulfonate. The organic phase consisted of acetonitrile, and the aqueous and organic phases were mixed in a ratio of 85:15.
- The HPLC system was set to a flow rate of 1 ml/min with a sample injection volume of 20 µl. A retention time of ± 4.7 min was recorded for normetanephrine and the stop time of each run was thus set to 7.0 min.
- Fluorescence detection was recorded at an excitation wavelength of 283 nm and an emission wavelength of 315 nm (response time 0.5; range x 1; low sensitivity).
- The Graphpad Prism® 5 software package was used to construct sigmoidal dose-response curves and to determine the IC_{50} values.

4.2.4 METHODS

4.2.4.1 CALIBRATION CURVE

The residual rates of NMN formation were determined by constructing a linear calibration curve (**Figure 4.6**) from solutions of NMN (0, 1, 2, 5, 10 and 30 µM) dissolved in a 25 mM sodium phosphate buffer (pH 7.8). Perchloric acid (1 M; 12.5 µl) was added to each calibration standard with a final volume of 137.5 µl. This calibration curve was used to quantify the normethanephrine produced from (-)-norepinephrine in the enzyme reactions catalysed by COMT.

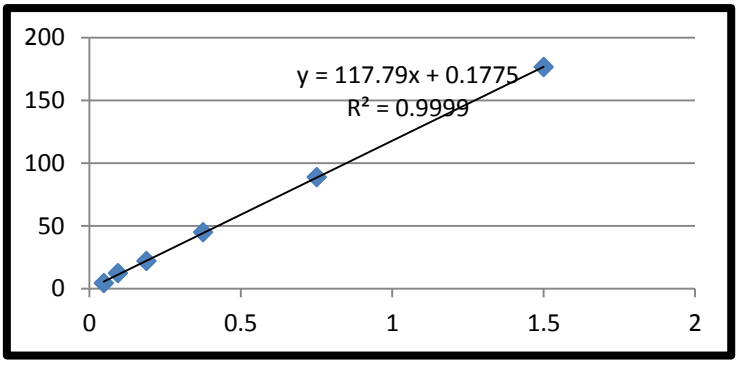

Figure 4.6: Example of a calibration curve routinely obtained.

4.2.4.2 DETERMINATION OF IC_{50} VALUES

To determine the potencies of the test drugs as inhibitors of COMT, the concentration (IC_{50}) that produces 50% inhibition (compared to the activity recorded in the absence of inhibitor) was determined.

4.2.4.3 EXPERIMENTAL METHOD

- COMT purified from porcine liver was obtained from Sigma-Aldrich and stored at -86 ºC. The purified COMT (750 units/5 ml) was dissolved in 20 ml sodium phosphate buffer (25 M, pH 7.8) containing 0.5 mM dithiothreitol.
- Different concentrations of the test inhibitor were prepared in DMSO and added to the enzyme reactions to yield the following concentration range: 0, 0.1, 0.3, 1, 3, 10, 30 and 100 µM (**Table 4.2**).
- As reference inhibitors the known COMT inhibitors, tolcapone and entacapone, were also evaluated. Tolcapone and entacapone were also prepared in DMSO and added to the enzyme reactions to yield the following concentration range: 0, 0.0003, 0.001, 0.003, 0.01, 0.1 and 1 µM. The lower concentration range was used, since tolcapone and entacapone are potent COMT inhibitors.
- The incubations contained the following for the purpose of the IC_{50} value determinations:

Table 4.2: This table contains the composition of each enzyme reaction to a final volume of 137.5 µl.

Reagents and final concentrations in the incubations	Volume (per 137.5 µl)	Storage conditions
2 mM $MgCl_2$	10 µl	Room temperature
250 µM Substrate (NE)	35 µl	–20 °C
200 µM SAMe	25 µl	–20 °C
Test inhibitor (dissolved in DMSO)	5 µl	Room temperature
COMT solution	50 µl	–86 °C
1 M $HClO_4$	12.5 µl	2–8 °C

- To prepare the enzyme reactions 10 µl $MgCl_2$ was firstly added, followed by 35 µl of the substrate (NE), 25 µl SAMe and lastly 5 µl of the test inhibitor.
- The enzyme reactions were preincubated at 37 °C for 10 minutes. Afterwards 50 µl aliquot of enzyme stock solution was added to yield concentrations of 0.1 mg/ml.
- The enzyme reactions were then incubated at 37 °C for 60 minutes and were subsequently terminated by adding 12.5 µl of 1 M perchloric acid.
- The samples were centrifuged at 16000 x g for 10 min at 25 ºC and the supernatants were analysed by the HPLC method. Norepinephrine (NE) and *DL*-normetanephrine (NMN) were analysed at an excitation wavelength of 283 nm and an emission wavelength of 315 nm. The peak areas of normetanephrine were recorded and the corresponding concentrations of normetanephrine formed were calculated using the calibration curve.
- In the presence of an inhibitor the conversion of NE to NMN was inhibited. Using the Prism 5 (GraphPad) software package, the data were fitted to the equation for one-site competition to yield a sigmoidal curve of concentration of normetanephrine formed versus inhibitor concentration. From this fit, the IC_{50} value was estimated. For each test inhibitor the IC_{50} values was determined in triplicate and expressed as mean ± standard deviation (SD) (Aoyama *et al.*, 2005).

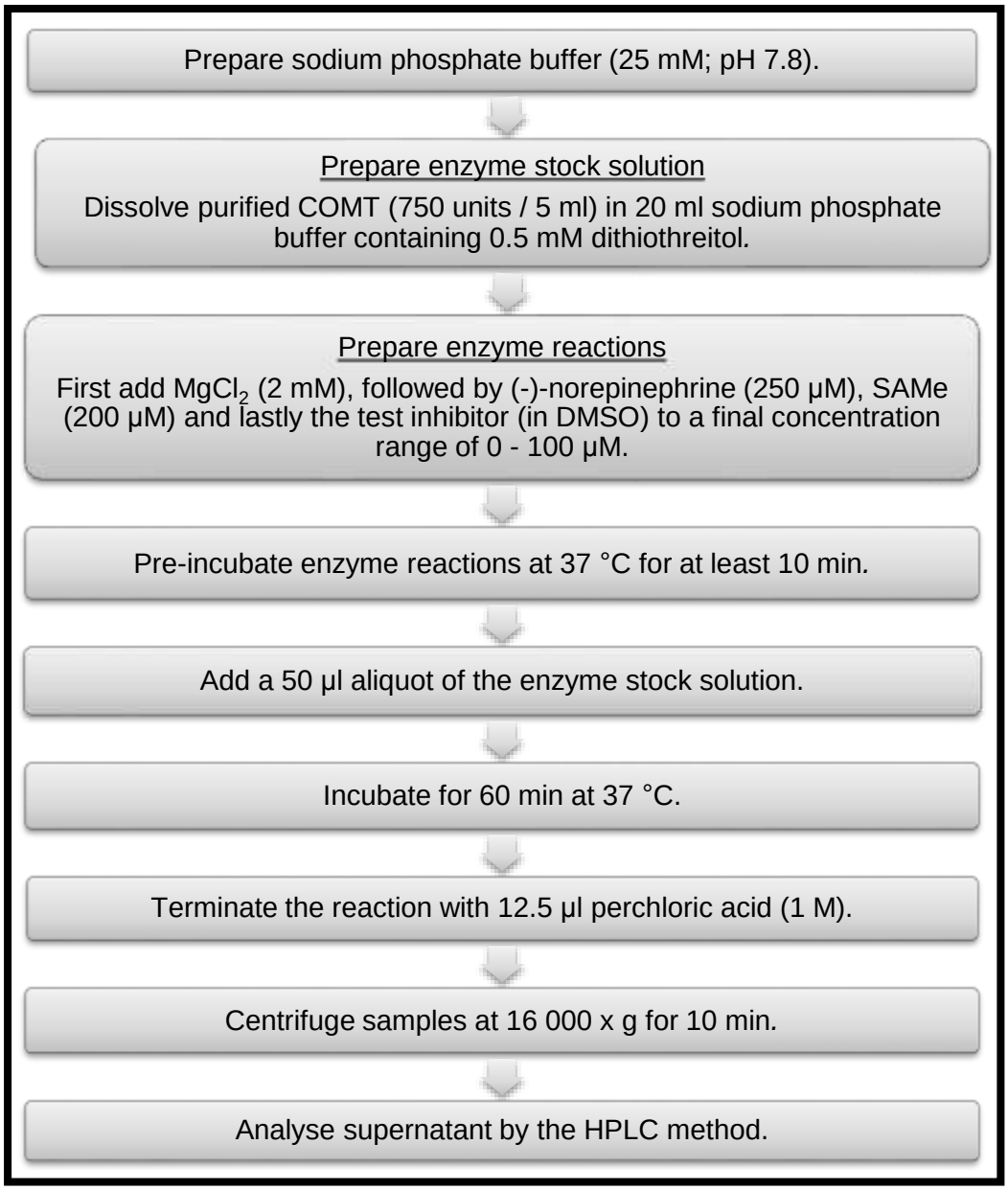

Figure 4.7: Diagrammatic representation of the method followed to determine the IC_{50} values.

4.2.5 RESULTS

The IC_{50} values of the test inhibitors and the IC_{50} values of the reference inhibitors, entacapone and tolcapone, are provided in **Table 4.3**. The sigmoidal curve (**Figure 4.8**) constructed for the inhibition of COMT by kaempferol is also given below.

Table 4.3: The IC_{50} values for the inhibition of COMT by the test inhibitors and the reference inhibitors, entacapone and tolcapone.

Test drug	**COMT IC_{50} (µM)** **Mean ± SD***
Betamethasone	No inhibition
Carisoprodol	No inhibition
Diflunisal	No inhibition
Flunisolide	No inhibition
Kaempferol	2.799 ± 0.588
Ketoprofen	No inhibition
Midodrine	No inhibition
Nitrendipine	No inhibition
(-)-Riboflavin	No inhibition
Tenoxicam	No inhibition
Trimethoprim	No inhibition
Entacapone	0.00047 ± 0.00007
Tolcapone	0.0068 ± 0.0027

**All values are expressed as the mean ± SD of triplicate determinations.*

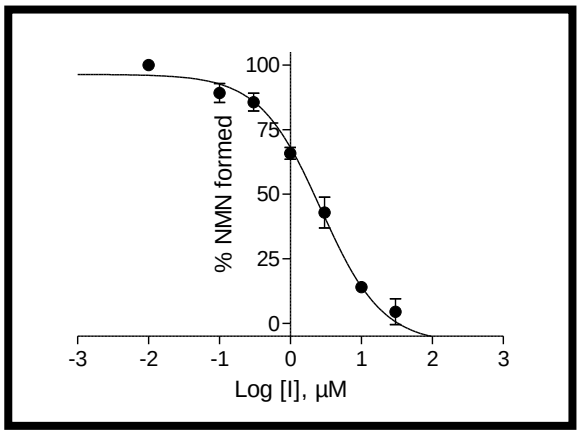

Figure 4.8: The sigmoidal dose-response curves for the inhibition of COMT by kaempferol. This curve was used to determine the IC_{50} value for COMT inhibition.

4.2.6 DISCUSSION

From the IC_{50} values obtained for each of the test drug (**Table 4.3**), the following can be concluded:

- As mentioned earlier, twenty-six test compounds were selected based on the results obtained from the pharmacophore mapping, finding similar molecules by fingerprint, molecular docking, a bio-isostere search, chemical similarity, cost availability and molecular weight.
- However, only eleven of the test compounds were evaluated as *in vitro* inhibitors of COMT due to complications arising from the import of the COMT enzyme to South-Africa. The department of Fishery and Forestry placed a moratorium on the import of all porcine products, which meant that the porcine enzyme could no longer be obtained. Due to financial constraints, it was also not feasible to use the human enzyme instead.
- Firstly, the reference inhibitors, entacapone (IC_{50} = 0.00047 µM) and tolcapone (IC_{50} = 0.0068 µM), proved to be highly potent COMT inhibitors. The measured IC_{50} values are similar to those reported in literature of 0.00016 µM and 0.000036 µM for entacapone and tolcapone, respectively (Bonifati & Meco, 1999).

- Of the eleven test compounds that were evaluated, ten had little or no COMT inhibitory activity at the maximum tested concentration of 100 µM. These compounds may have the required features to map to the pharmacophore models, but they are not inhibitors *in vitro.*
- This suggests that the pharmacophore models and screening would have to be modified. For example, shape constraints could be used instead of exclusion constraints. The COMT enzyme is a difficult target as the form of the enzyme continuously changes as cofactors, the magnesium and substrates bind. The active site is also quite shallow and close to the enzyme surface, which complicates pharmacophore modelling (Kiss & Soares-da-Silva, 2014). Since the enzyme was no longer available, there was unfortunately no reason to refine the pharmacophore models during this study.
- Another possibility might be to rather select more compounds from the fingerprint and chemical similarity hit-lists as the only active compound identified was kaempferol.
- This is most likely due to the fact that kaempferol is structurally similar to quercetin (**Figure 4.9**) and therefore has similar biological activities, such as the inhibition of COMT.

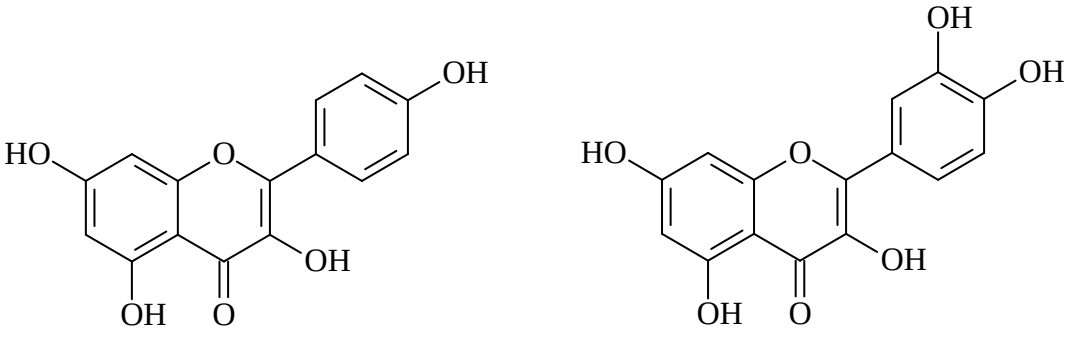

Kaempferol (A) **Quercetin (B)**

Figure 4.9: The structures of the members of the flavonol subclass of flavonoids.

- Since none of the compounds from the bio-isostere approach was screened in the end, it is impossible to determine how effective this approach would have been.

4.2.7 CONCLUSION

In this section it was shown that the initial pharmacophore models generated in this study had to be optimised as results obtained from biological screening were disappointing. This could unfortunately not be done as the enzyme was no longer available for biological screening. Identification of a ligand by fingerprint also proved to be ineffective and only kaempferol was identified as an *in vitro* inhibitor of COMT. Based on the IC_{50} values obtained, kaempferol is not as potent as the reference inhibitors, entacapone and tolcapone, but may serve as a lead for the design of more potent non-nitrocatechol COMT inhibitors for the treatment of PD. Since none of the compounds containing catechol bio-isosteres were screened as COMT inhibitors, it is not possible to come to any conclusions about the feasibility of this approach.

4.3 MAO-A AND MAO-B BIOASSAYS

4.3.1 INTRODUCTION

Due to complications experienced with the availability of the COMT enzyme, eighteen compounds, obtained from screening the pharmacophore models of COMT and screening by ligand fingerprinting were evaluated as *in vitro* inhibitors of the MAO enzymes. For this purpose the fluorometric method described by Strydom *et al.* (2011) was employed (Novaroli *et al.*, 2005). The assay is based on the measurement of the extent by which an inhibitor reduces the MAO-catalysed oxidation of kynuramine to the fluorescent product, 4-hydroxyquinoline (**Figure 4.10**). The kynuramine assay has the advantage that the fluorescence of the 4-hydroxyquinoline product, formed during the oxidation by MAO, can be directly measured, resulting in increased sensitivity.

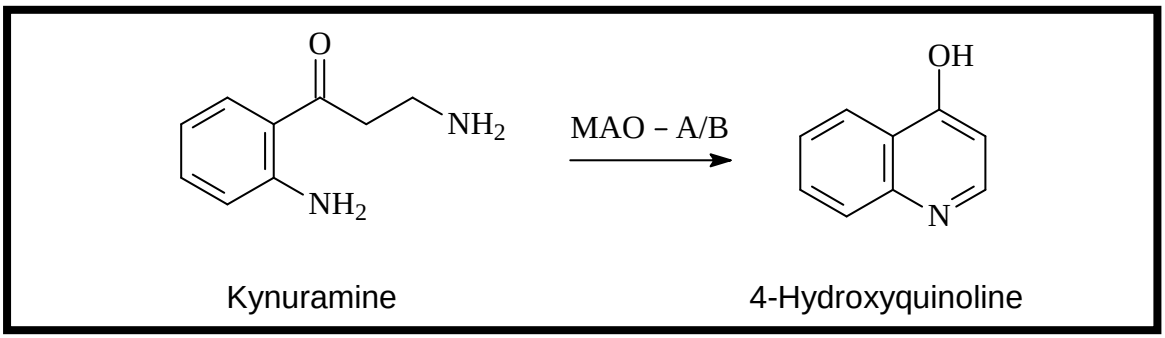

Figure 4.10: The oxidation of kynuramine to 4-hydroxyquinoline (Novaroli *et al.*, 2005).

4.3.2 OVERVIEW OF THIS SECTION

The following in vitro bioassays will be described in this section:

- Determination of the IC_{50} values for the inhibition of MAO-A and MAO-B. For this purpose sigmoidal concentration-inhibition curves will be constructed. These experiments will be conducted for all test compounds.
- The reversibility of the inhibition of MAO by selected inhibitors will be examined. For this purpose the recovery of enzyme activity after dialysis of the enzyme-inhibitor complexes will be evaluated. To determine if the active inhibitors are competitive inhibitors, Lineweaver-Burk plots will be constructed. These studies will be conducted for a selected test compound.

4.3.3 CHEMICALS AND INSTRUMENTATION

Table 4.4: This table contains the suppliers of reagents and materials used for this assay as well as the abbreviations of each reagent.

Materials	Abbreviations	Supplier
Recombinant human monoamine oxidase A, expressed in insect microsomes	MAO-A	Sigma-Aldrich
Recombinant human	MAO-B	Sigma-Aldrich

monoamine oxidase B, expressed in insect microsomes		
Kynuramine		Sigma-Aldrich
4-Hydroxyquinoline		Sigma-Aldrich
Sodium hydroxide	NaOH	Sigma-Aldrich
Monopotassium phosphate	KH_2PO_4	Merck
Dipotassium phosphate	K_2HPO_4	Merck
Potassium Chloride	KCl	Merck
Dimethyl sulphoxide	DMSO	Merck
Test Compounds		Sigma-Aldrich
(*R*)-Deprenyl		Sigma-Aldrich
Pargyline		Sigma-Aldrich

4.3.4 INSTRUMENTATION AND SETTINGS

The following instruments and settings were used in this study:

- A Varian Cary Eclipse fluorescence spectrophotometer was used for the fluorometric measurements. The concentrations of 4-hydroxyquinoline were measured fluorometrically at an excitation wavelength of 310 nm and an emission wavelength of 400 nm. The PMT voltage of the spectrofluorometer was set to medium with excitation and an emission slit widths of 5 mm and 10 mm for MAO-A and MAO-B, respectively.
- The Graphpad Prism® 5 software package was used to construct sigmoidal dose-response curves and to determine the IC_{50} values.

4.3.5 CALIBRATION CURVE

Quantitative estimations of 4-hydroxyquinoline were done by constructing a linear calibration curve with solutions of 4-hydroxyquinoline (0.0469, 0.09375, 0.1875, 0.375, 0.75 and 1.5 µM) dissolved in 200 µl potassium phosphate buffer (100 mM, pH 7.4, made isotonic with KCl 20.2 mM). A volume of 80 µl NaOH (2 N) was added to each calibration standard to yield a final volume of 280 µl. Control samples were added to confirm that the test inhibitors do not fluorescence or reduce the fluorescence of 4-hydroxyquinoline under the conditions used in the assay. The fluorescence values obtained in the inhibition studies should fall within the range obtained for the calibration curve, which should display a high degree of linearity.

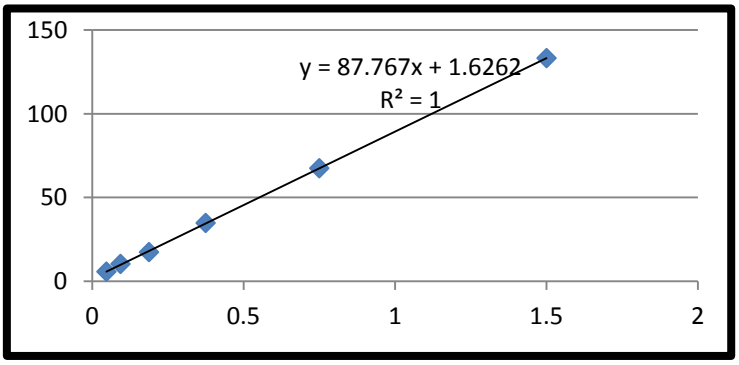

Figure 4.11: Example of a calibration curve routinely obtained.

4.3.6 THE IC50 VALUES DETERMINATION FOR THE TEST INHIBITORS

4.3.6.1 EXPERIMENTAL METHOD

- Recombinant human MAO-A and MAO-B (5 mg/ml) were obtained from Sigma-Aldrich and stored at -86 ºC. MAO-A and MAO-B was diluted in potassium phosphate buffer (100 mM, pH 7.4, made isotonic with KCl, 20.2 mM) to yield concentration of 0.03 and 0.06 mg/ml, respectively
- Different concentrations of the test inhibitor were prepared in DMSO and added to the enzyme reactions to yield the following concentration range: 0, 0.003, 0.01, 0.1, 1, 10, and 100 µM (**Table 4.5**).

- The incubations contained the following for the purpose of the IC_{50} value determinations:

Table 4.5: This table contains the composition of each enzyme reaction to a final volume of 280 µl.

Reagents and final concentrations in the incubations	Volume (per 280 µl)	Storage conditions
200 µM Substrate (Kynuramine)	50 µl	-20 ºC
100 mM Potassium phosphate buffer	92 µl	4 ºC
Test inhibitor (dissolved in DMSO)	8 µl	Room temperature
MAO-A or MAO-B solution	50 µl	–86 °C

- To prepare the enzyme reactions, 50 µl of the substrate (kynuramine) was firstly added (to yield a concentration of 50 µM in the 200 µl reaction) followed by 92 µl potassium phosphate buffer, and lastly 8 µl of the test inhibitor.
- The enzyme reactions were preincubated at 37 °C for 15 minutes. Afterwards a 50 µl aliquot of the enzyme stock solution was added to yield concentrations of MAO-A and MAO-B of 0.0075 mg/ml and 0.015 mg/ml, respectively.
- The enzyme reactions were then incubated at 37 °C for 20 minutes and subsequently terminated by adding 80 µl of sodium hydroxide (2 N).
- The concentration of 4-hydroxyquinoline in each incubation was determined spectrofluorometrically by measuring the fluorescence of the supernatant at an excitation wavelength of 310 nm and an emission wavelength of 400 nm. The PMT voltage of the spectrofluorometer was set to medium with excitation and an emission slit widths of 5 mm and 10 mm for MAO-A and -B.
- In order to determine an IC_{50} value, the initial rate of MAO catalysis was graphically plotted against the logarithm of the inhibitor concentration in order to obtain a sigmoidal dose-response curve. Each sigmoidal curve consisted of at least 6 different inhibitor concentrations spanning 3 orders of magnitude. GraphPad Prism® 5 was used to fit the inhibition date to the one site competition model. The IC_{50} values were determined in triplicate and expressed as mean ± standard deviation (SD).

- A linear calibration curve was constructed using authentic 4-hydroxyquinoline (0.047–1.56 µM). This curve was used to quantify the 4-hydroxyquinoline formed in the enzyme reactions. The enzyme catalytic rates were expressed as nmol 4-hydroxyquinoline formed/ min.mg protein.

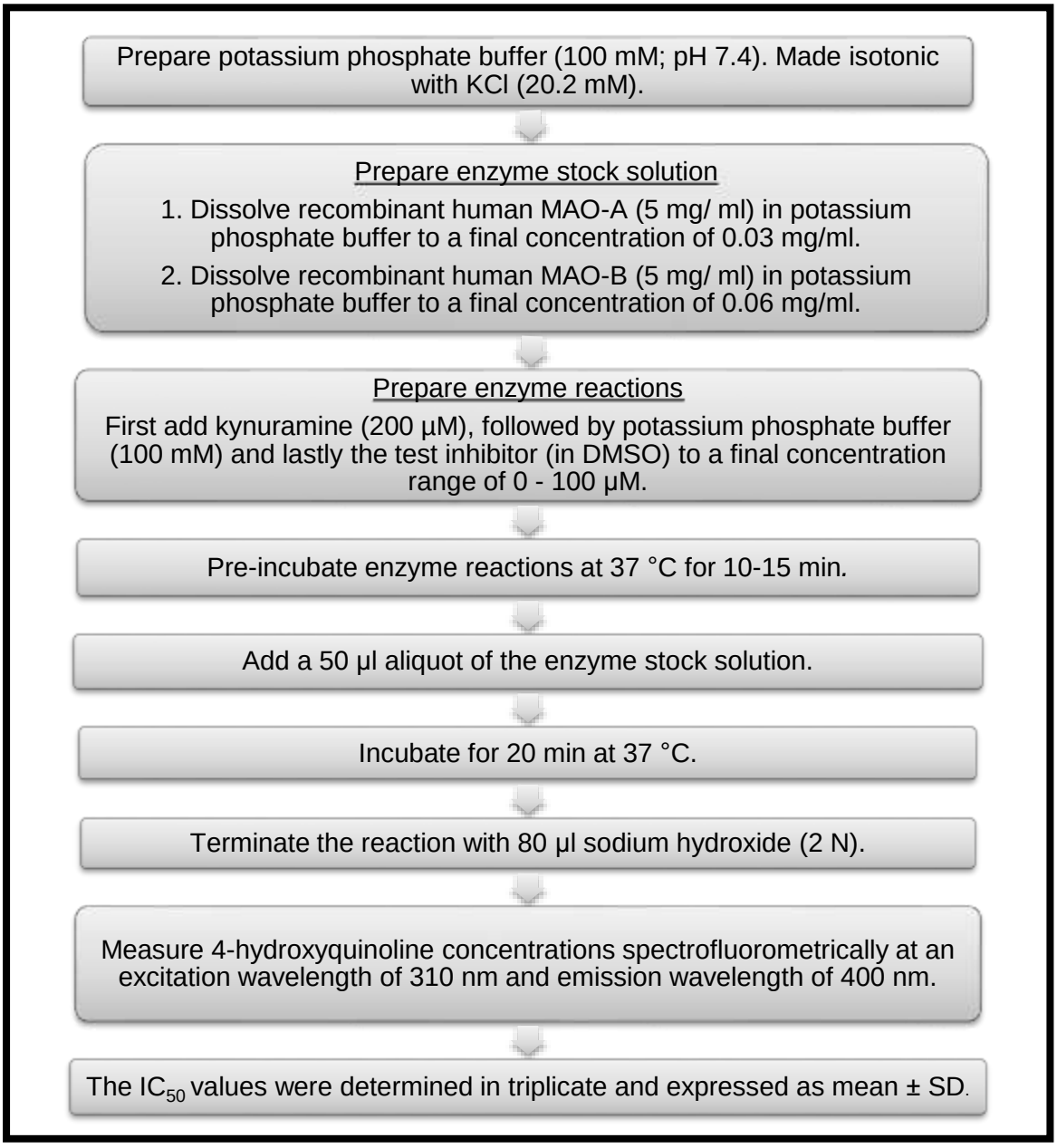

Figure 4.12: Diagrammatic representation of the method followed to determine the IC_{50} values for MAO inhibition.

4.3.6.2 RESULTS

The IC_{50} values of the test compounds are given in **Table 4.6**. The lower the IC_{50} value, the higher the binding affinity of the inhibitor to the enzyme. Examples of the sigmoidal curves constructed for the inhibition of MAO-A and MAO-B by the test compounds are shown in **Figures 4.13** and **4.14**.

Table 4.6: The IC_{50} values for the inhibition of MAO-A and MAO-B by the test compounds.

Test compound	**MAO-A (μM)** **Mean ± SD***	**MAO-B (μM)** **Mean ± SD***
Betamethasone	No inhibition	146.050 ± 53.952
Carisoprodol	No inhibition	No inhibition
Diflunisal	No inhibition	No inhibition
Dipivefrine	No inhibition	No inhibition
Ethambutol	No inhibition	No inhibition
Esmolol	No inhibition	No inhibition
Flunisolide	No inhibition	No inhibition
Etonogestrel	No inhibition	No inhibition
Kaempferol	0.589 ± 0.019	37.147 ± 3.694
Ketoprofen	No inhibition	No inhibition
Midodrine	No inhibition	No inhibition
Nitrendipine	No inhibition	16.353 ± 1.534
Oxybenzone	24.967 ± 0.737	2.872 ± 0.697
Pravastatin	No inhibition	No inhibition
(-)-Riboflavin	111.033 ± 9.573	13.119 ± 3.586

Tenoxicam	144.667 ± 3.006	94.055 ± 0.799
(6R)-5,6,7,8-Tetrahydrobiopterin	No inhibition	No inhibition
Trimethoprim	No inhibition	No inhibition

**All values are expressed as the mean ± SD of triplicate determinations.*

MAO-A

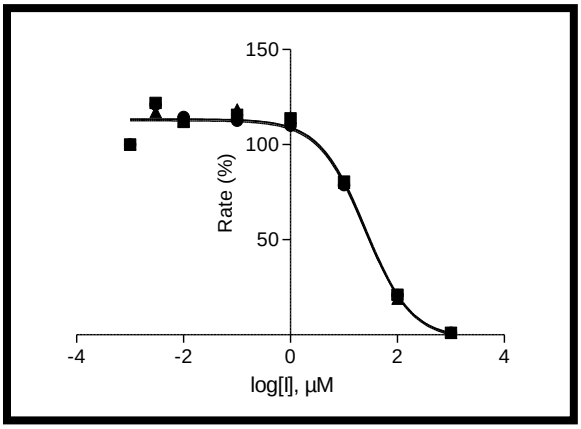

MAO-B

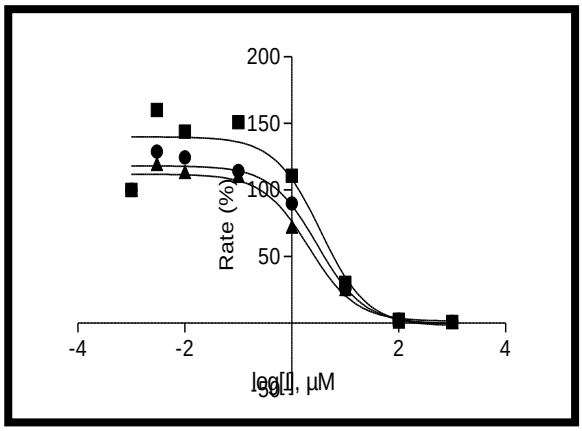

Figure 4.13: The sigmoidal dose-response curves for the inhibition of MAO-A and MAO-B by oxybenzone. These curves were used to determine IC_{50} values for both MAO-A and MAO-B inhibition.

Nitrendipine

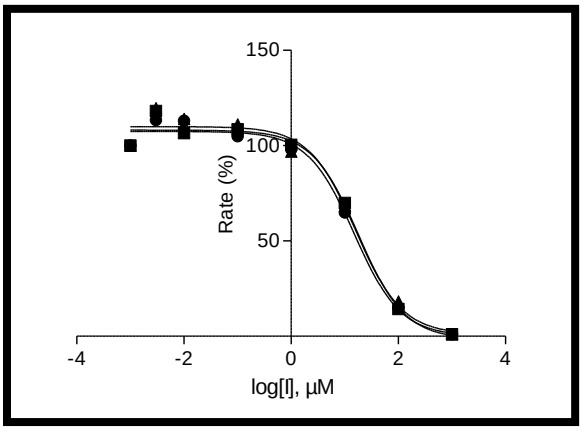

(-)-Riboflavin

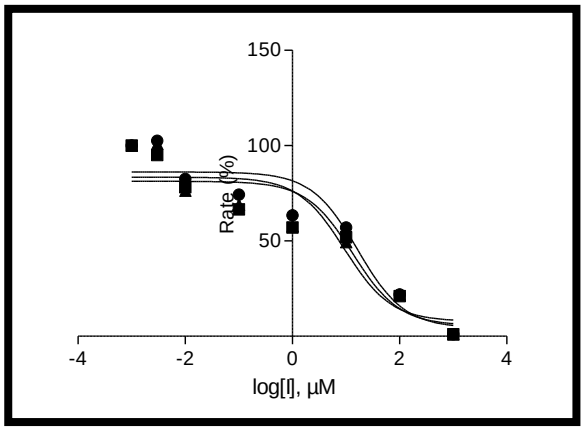

Figure 4.14: The sigmoidal dose-response curves for the inhibition of MAO-B by nitrendipine and (-)-riboflavin. These curves were used to determine IC_{50} values for MAO-B inhibition.

4.3.6.3 DISCUSSION

From the IC_{50} values obtained for each of the test compounds (**Table 4.6**), the following can be concluded:

- Only two of the test compounds exhibited MAO-A inhibitory activity with IC_{50} values <25 µM. These drugs include kaempferol (0.589 µM) and oxybenzone (24.967 µM).
- Three of the test drugs exhibit MAO-B inhibitory activity with IC_{50} values <20 µM. These include oxybenzone (2.872 µM), (-)-riboflavin (13.119 µM) and nitrendipine (16.353 µM).
- An explanation for the inhibition of the MAOs by the above mentioned compounds are not clear at this stage. Molecular docking studies will be conducted to determine important interactions between the ligand and the active sites of the MAOs and to determine possible binding modes of these compounds.

4.3.7 MOLECULAR MODELLING

4.3.7.1 INTRODUCTION

Molecular modelling can be used for the design of novel compounds for a specific receptor or enzyme target. Molecular modelling may also be used to determine important interactions between the ligand and active site and to determine possible binding modes of inhibitors to an active site.

4.3.7.2 METHOD

- Molecular docking studies were carried out using Discovery Studio® 3.1 modelling software. The CDOCKER module was used for molecular docking.
- The following structures, which were obtained from the Protein Data Bank, were used for these studies:
  - Human MAO-A co-crystallised with harmine (pdb: 2ZX5).
  - Human MAO-B co-crystallised with safinamide (pdb: 2V5Z).
- The correctness of the valences of the FAD cofactor and the co-crystallised ligands were verified and the protein models were typed with the Momany and Rone CHARMm force field.
- Within the Discovery Studio® environment, the pH was set to 7.4 and hydrogen atoms were added to the FAD cofactor, and the co-crystallised ligands.
- The pKa values and protonation states of the ionisable amino acids were calculated and hydrogen atoms were added at pH 7.4 to the protein models, including the waters.
- A fixed atom constraint was applied to the backbone of the enzymes and the models were energy minimised using the Smart Minimizer algorithm with the maximum steps set to 50 000. For this procedure the implicit generalized Born solvation model with molecular volume was used.
- Structures of the ligands to be docked were constructed within Discovery Studio 3.1®, and their hydrogen atoms were added according to the appropriate protonation states at pH 7.4. The geometries of the ligands were briefly optimised using a fast Dreiding-like force field (1000 interactions) and

the atom potential types and partial charges were assigned with the Momany and Rone CHARMm force field.

- Docking of the ligands was carried out with the CDOCKER algorithm with the generation of 10 random ligand conformations and a heating target temperature of 700 K in full potential mode.
- The docking solutions were refined using the Smart Minimizer algorithm. Ten possible binding solutions were computed for each docked ligand and the best-ranked binding conformation of each ligand was determined according to the CDOCKER interaction energies.

4.3.7.3 RESULTS AND DISCUSSION

MAO-A

Eleven of the eighteen test compounds were successfully docked into the crystal structure model of human MAO-A using the Discovery Studio® 3.1 modelling software. The CDOCKER interaction energies were also determined (**Table 4.7**).

Table 4.7: The results of the docking experiments and the IC_{50} values of the selected test compounds for the inhibition of human MAO-A.

Name	Prominent interactions	-CDOCKER Interaction Energy (kcal/mol)	MAO-A IC_{50} (μM)
Test compounds which docked into the active site of hMAO-A			
Carisoprodol	Hydrogen bond interaction with Phe 208.	38.492	-
Diflunisal	Hydrogen bond interactions with FAD 600 and Cys 323.	37.4552	-
Esmolol	Hydrogen bond interaction with Cys 323.	53.9663	-

Ethambutol	Hydrogen bond interaction with Phe 208 and Gln 215.	44.2916	-
Kaempferol	Hydrogen bond interactions with water 739, Asn 181, Cys 323 and Tyr 444.	46.6841	0.589
Ketoprofen	No interactions with surrounding residues.	30.4237	-
Midodrine	Hydrogen bond interactions with FAD 600 and water 710.	43.0974	-
Oxybenzone	Hydrogen bond interaction with Cys 323.	41.6255	24.967
Tenoxicam	Hydrogen bond interactions with water 739 and Tyr 407.	35.1382	144.667
(6*R*)-5,6,7,8-Tetrahydrobiopterin	Hydrogen bond interaction with Asn 181, Cys 323 and Thr 336.	41.9783	-
Trimethoprim	No interactions with surrounding residues.	41.9104	-
Test compounds which did not docked into the active site of hMAO-A			
Betamethasone	-	-	-
Dipivefrine	-	-	-
Etonogestrel	-	-	-
Flunisolide	-	-	-
Nitrendipine	-	-	-
Pravastatin	-	-	-
(-)-Riboflavin	-	-	111.033

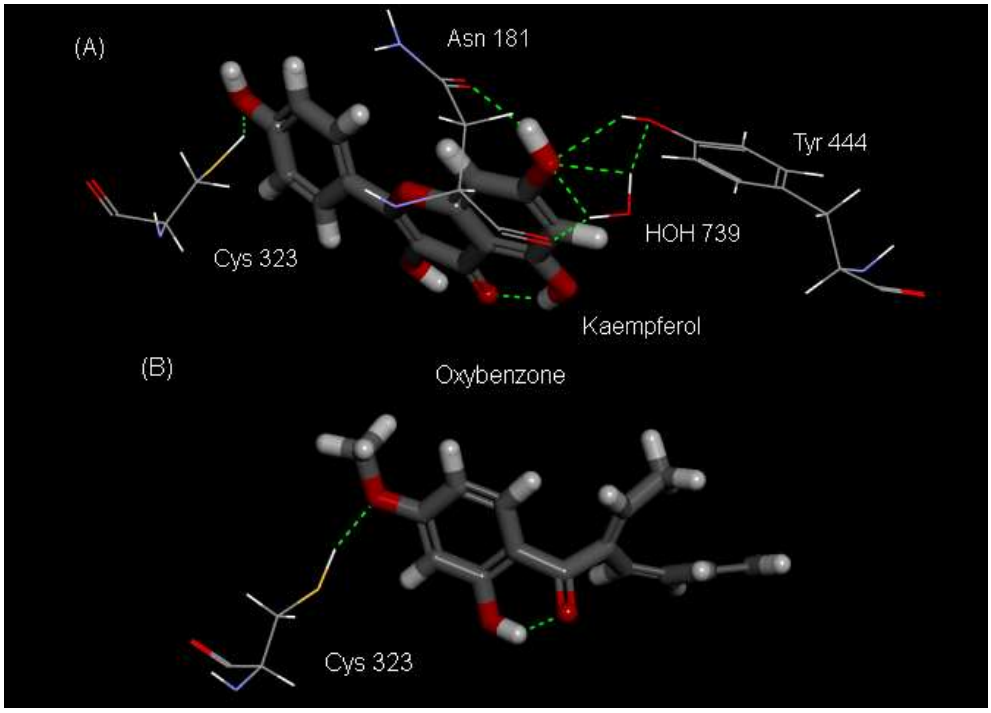

Figure 4.15: The figure illustrates selected compounds, **(A)** kaempferol and **(B)** oxybenzone, docked into the crystal structure of human MAO-A. The figure only illustrates the residues with whom the ligands interacted. The FAD and ligands are displayed in stick, while the interacting residues are displayed in wire frame.

The docking results of selected test compounds, kaempferol and oxybenzone, are illustrated in **Figure 4.15**. Since these test drugs had the best IC_{50} values, their docking results will be discussed in detail. The docking results may provide some insight into the MAO inhibitory activities of these compounds.

- The docking result of oxybenzone illustrates hydrogen bond interactions between the heterocyclic ring of oxybenzone and Cys 323. This compound had a CDOCKER interaction energy of -41.6255 kcal/mol and an IC_{50} value of 24.967 µM.
- The most potent hMAO-A inhibitor of the series, kaempferol, docked into the hMAO-A active site with a CDOCKER interaction energy of -46.6841 kcal/mol and displayed an IC_{50} value of 0.589 µM. The docking result illustrates hydrogen bond interactions between the phenol ring of kaempferol and Cys 323. Hydrogen bond interactions are further present between the heterocyclic ring of kaempferol, and water 739, Asn 181 and Tyr 444.

- The docking results of both kaempferol and oxybenzone illustrate a hydrogen bond interaction with Cys 323. Since the side chain of Cys 323 is also in van der Waals contact with the aromatic ring of the known hMAO-A inhibitor, clorgyline (De Colibus *et al.,* 2005), it may be concluded that a hydrogen bond interaction with Cys 323 may be an important feature for human MAO-A inhibitory activity.

MAO-B

Twelve of the eighteen test compounds were successfully docked into the active site of the human MAO-B (**Table 4.8)** using the Discovery Studio® 3.1 modelling software.

From the docking results the following observation were made:

- The active site of the human MAO-B consists of substrate and entrance cavities, which are separated by the gating switch, residues Ile 199 and Tyr 326. Key residues in the substrate cavity are Tyr 435 Tyr 398 and Gln 206. **Figure 4.16** illustrates that ethambutol, kaempferol, midodrine, (-)-riboflavin and (6*R*)-5,6,7,8-tetrahydrobiopterin are examples of test compounds which docked into the substrate and/or the entrance cavities of MAO-B.
- The CDOCKER interaction energies were determined by Discovery Studio® 3.1 modelling software. In this case, the CDOCKER interaction energy did not correlate with the IC_{50} values recorded (**Table 4.8**).

Table 4.8: The results of the docking experiments and the IC_{50} values of the selected test compounds for the inhibition of human MAO-B.

Name	**Interactions**	**-CDOCKER Interaction Energy (kcal/mol)**	**MAO-B IC_{50} (μM)**
Test compounds which docked into the active site of hMAO-B			
Carisoprodol	Hydrogen bond interaction with Leu 164.	45.9694	-

Diflunisal	Hydrogen bond interaction with water 1351.	35.164	-
Esmolol	Hydrogen bond interaction with water 1170.	57.0747	-
Ethambutol	Hydrogen bond interactions with Pro 102 and Ile 198.	40.3679	-
Kaempferol	Hydrogen bond interactions with water 1155, Cys 172 and Tyr 435.	43.1624	37.147
Ketoprofen	No interactions with surrounding residues.	38.4328	-
Midodrine	Hydrogen bond interactions with FAD, Ser, 59, Tyr 60, Gln 206, Tyr 398.	46.2736	-
Oxybenzone	No interactions with surrounding residues.	38.3058	2.872
(-)-Riboflavin	Hydrogen bond interactions with Cys 172, Thr 201, Gln 206 and Tyr 326.	26.6023	13.119
Tenoxicam	No interactions with surrounding residues.	34.9326	94.055
(6*R*)-5,6,7,8-Tetrahydrobiopterin	Hydrogen bond interactions with Pro 102 and Gln 206.	37.8255	-
Trimethoprim	No interactions with surrounding residues.	44.5123	-
Test compounds which did not docked into the active site of hMAO-B			
Betamethasone	-	-	146.050
Dipivefrine	-	-	-
Etonogestrel	-	-	-

Flunisolide	-	-	-
Nitrendipine	-	-	16.353
Pravastatin	-	-	-

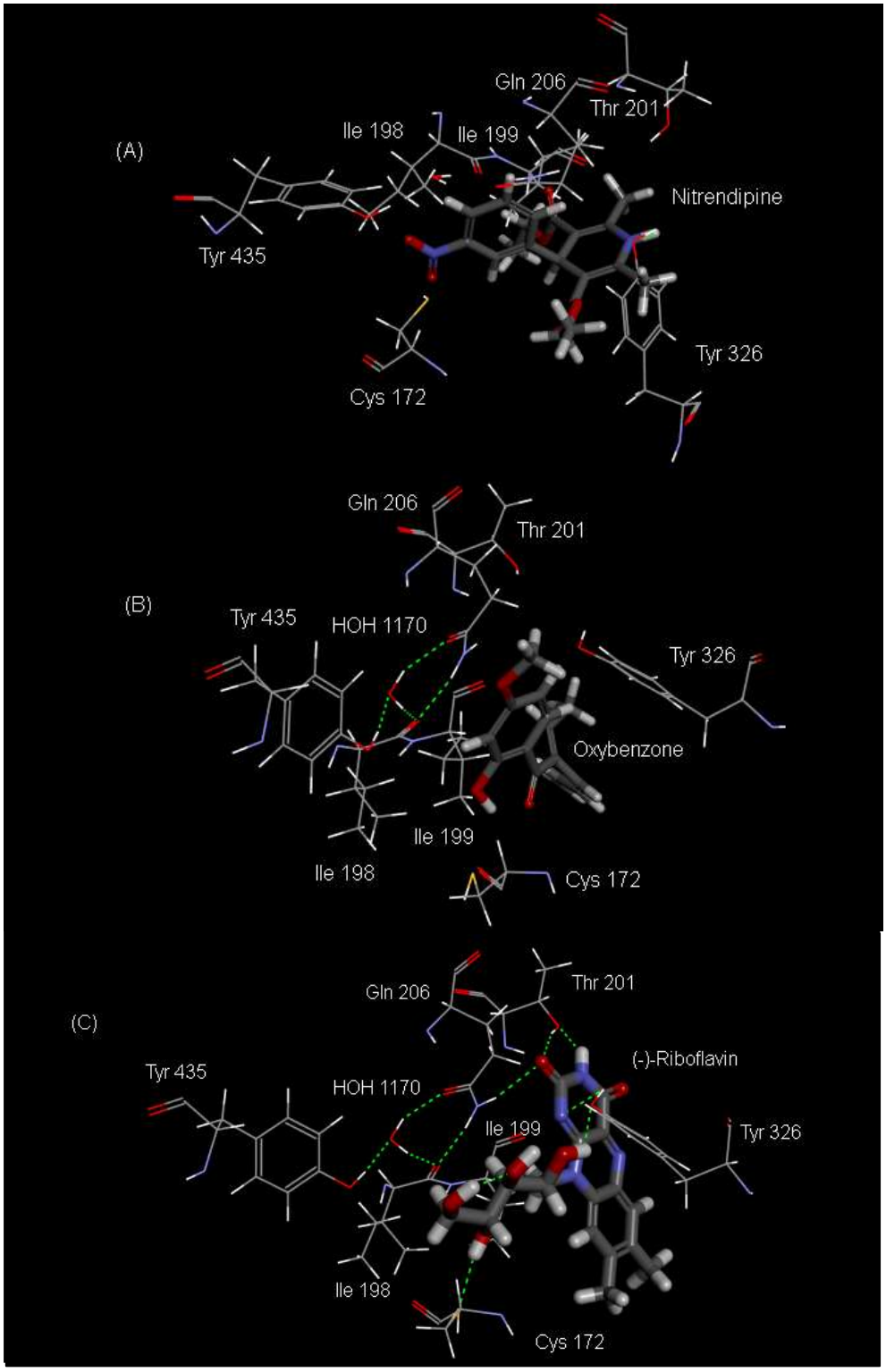

Figure 4.16: The figure illustrates the docking results of selected compounds, **(A)** nitrendipine, **(B)** oxybenzone and **(C)** (-)-riboflavin, into the crystal structure of human MAO-B. The figure only illustrates the residues with whom the ligands interacted. The FAD and ligands are displayed in stick, while the interacting residues are displayed in wire frame.

The docking results of selected compounds, nitrendipine, oxybenzone and (-)-riboflavin, are illustrated in **Figure 4.16**. Since the reversibility of MAO inhibition by these test compounds was evaluated, their docking results will be discussed in detail. The docking results may provide some insight into the human MAO-B inhibitory activities of these compounds. Oxybenzone was the most potent MAO-B inhibitor of the series.

- Although nitrendipine exhibited an IC_{50} value of 16.353 µM, the docking results indicated that nitrendipine did not fit within the active site of human MAO-B. Studies conducted by De Monte and co-workers (2014) investigated the binding of crocin, a compound isolated from *Crocus Sativus*, to MAO-B and it was found that crocin also does not fit within the active site of hMAO-B. A blind-docking simulation was carried out, which suggested that crocin binds to the protein surface, to an allosteric site, and may thus inhibit the oxidation of amine substrates (De Monte *et al.*, 2014). We hypothesise that nitrendipine may bind to this potential allosteric site situated in the area near the gate of the entrance tunnel to the binding pocket (De Monte *et al.*, 2014).
- The docking results of (-)-riboflavin, in contrast, illustrates hydrogen bond interactions between the heterocyclic ring of (-)-riboflavin and Thr 201, Gln 206 and Tyr 326. A hydrogen bond interaction is further present between the the hydrogen atom of (-)-riboflavin and Cys 172. This compound had a binding energy of -26.6023 kcal/mol and an IC_{50} value of 13.119 µM.
- The most potent hMAO-B inhibitor of the series, oxybenzone, docked into the hMAO-B active site with a CDOCKER interaction energy of -38.3058 kcal/mol and an IC_{50} value of 2.872 µM. Although oxybenzone has the most potent MAO-B inhibitory activity, it does not have the lowest binding energy of the series. Furthermore, the results with oxybenzone illustrated that there are no hydrogen bond interactions with nearby amino acid residues of the MAO-B enzyme. Thus, it is postulated that the inhibitory activity of oxybenzone may be due to van der Waals interactions between oxybenzone and the amino acid residues. However, more in depth studies have to be conducted to confirm this theory.
- In a study by Chimenti *et al.* (2009), the MAO inhibitory potential of both natural and synthetic chalcones has been illustrated. In 2009, Chimenti and

co-workers synthesised a series of chalcones and examined these compounds as MAO inhibitors using human MAO-A and MAO-B. All the compounds in this series were selective for the MAO-B isoform with IC_{50} values in the micro- and nanomolar range. The most active compound (**Figure 4.17 A**), inhibited MAO-B with an IC_{50} of 0.0044 µM. This compound was 11364-fold more selective for the MAO-B than the MAO-A isoform. Interestingly, there are structural similarities between compound **8** and oxybenzone **(Figure 4.17)**, such as a hydroxyl group on the heterocyclic ring and a carbonyl group ortho to the hydroxyl group. Binding of these compounds to the active site is therefore postulated to be similar.

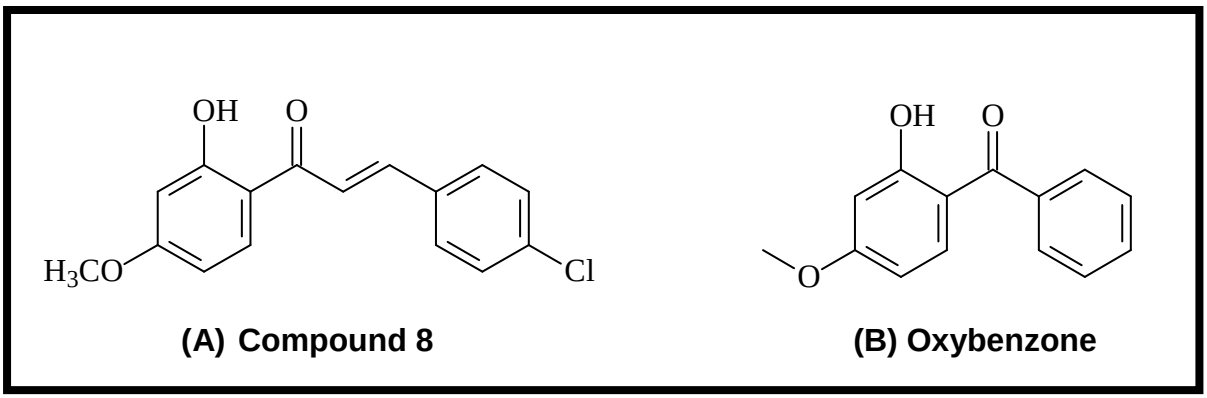

Figure 4.17: (A) Compound **8** from the series of synthesised chalcones (Chimenti *et al.,* 2009) and **(B)** oxybenzone.

In conclusion, although the docking studies yielded some insights, it is unlikely that molecular docking may be used to predict the human MAO inhibitory potencies of these test drug inhibitors.

4.3.8 THE REVERSIBILITY OF MAO INHIBITION

4.3.8.1 INTRODUCTION

In this section the reversibility of MAO-B inhibition by the most potent MAO-B inhibitor, oxybenzone (**Figure 4.18**), was examined.

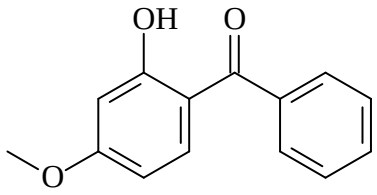

Oxybenzone

Figure 4.18: The structure of oxybenzone.

To determine the reversibility of MAO-B inhibition, the recovery of enzymatic activity after dialysis of the enzyme-inhibitor complex was examined. Oxybenzone (at a concentration of 4 × IC_{50}) was firstly preincubated with MAO-B for 15 min and then dialysed for 24 h. These incubations were carried out in triplicate and following dialysis were diluted twofold with the addition of kynuramine. These reactions were subsequently incubated for 20 min at 37 °C, and the formation of 4-hydroxyquinoline by MAO-B was measured at the endpoint of the enzyme reaction. Similar dialysis experiments were carried out in the absence of inhibitor (negative control) and presence of the irreversible MAO-B inhibitor, (R)-deprenyl (positive control). The enzyme activity of the negative control represents 100% residual activity. As third control, the residual MAO-B activity of undialysed mixtures of MAO-B and oxymebzone was also recorded. For reversible inhibition, enzyme activity is expected to recover to 100% following dialysis, while enzyme activity is not expected to recover with irreversible inhibition.

4.3.8.2 CHEMICALS AND INSTRUMENTATION

Materials and instrumentation were the same as described in section 4.3.3 and 4.3.4.

4.3.8.3 METHOD

- To examine the reversibility of MAO-B inhibition by the test compound, the recovery of the enzymatic activity after dialysis of the enzyme-inhibitor mixtures were evaluated.
- Recombinant human MAO-B (0.03 mg protein/ml) and oxybenzone (at 4 × IC_{50}) were combined in 0.8 ml of potassium phosphate buffer (100 mM, pH 7.4) containing 5% sucrose. DMSO (4%) served as co-solvent.
- The mixture was preincubated for 15 min at 37 °C.
- The mixtures were subsequently dialysed at 4 °C, employing the potassium phosphate buffer as dialysis buffer. Slide-A-Lyzer dialysis cassettes with a molecular weight cut-off of 10 000 and a sample volume capacity of 0.5–3 mL were used (Thermo Scientific, Waltham, MA, USA) for the dialysis.
- The dialysis buffer was replaced with fresh buffer at 3 h and 7 h after the start of dialysis.
- After 24 h of dialysis, the reactions were diluted twofold with the addition of kynuramine to give a final substrate concentration of 50 µM and a final oxybenzone concentration of 2 × IC_{50}.
- These reactions (500 µl) were incubated for 20 min at 37 ºC, and were subsequently terminated with the addition of NaOH (400 µl of 2 N) and 1000 µl water.
- The fluorescence emission of 4-hydroxyquinoline in these reactions was measured as at excitation and emission wavelengths of 310 and 440 nm, respectively. For this purpose a 3.5 ml quartz cuvette (pathlength 10 × 10 mm) was used.
- A linear calibration curve was constructed using authentic 4-hydroxyquinoline (0.047–1.56 µM). This curve was used to quantify the 4-hydroxyquinoline formed in the enzyme reactions. The enzyme catalytic rates were expressed as nmol 4-hydroxyquinoline formed/ min.mg protein.
- As negative control, MAO-B was preincubated and dialysed in the absence of inhibitor. As positive control, MAO-B was preincubated and dialysed in the presence of a concentration equal to 4 × IC_{50} of the irreversible inhibitor, (R)-deprenyl (IC_{50} = 0.079 µM) (Petzer *et al*., 2012). Also included in the study

were undialysed mixtures of MAO-B and oxybenzone, which were maintained at 4 °C for 24 h and diluted and assayed as above.

4.3.8.4 RESULTS

As mentioned earlier, oxybenzone is a potent inhibitor of MAO-B. The reversibility of the binding to MAO- B was thus determined. As illustrated in **Figure 4.19**, dialysis of mixtures containing MAO-B and oxybenzone resulted in the recovery of MAO-B activity to a level of 114 of the negative control value. This behaviour is consistent with a reversible interaction of oxybenzone with MAO-B. In contrast, after similar treatment of MAO-B with the irreversible inhibitor (R)-deprenyl (positive control), the MAO-B activity is not recovered since the enzyme activity after dialysis of the enzyme-inhibitor complex was only 2% of the negative control value. In undialysed mixtures of MAO-B and oxybenzone, inhibition persists and the activity is recorded at 27%. Since dialysis restores enzyme activity after incubation of MAO-B with oxybenzone, it may be concluded that oxybenzone is a reversible MAO-B inhibitor.

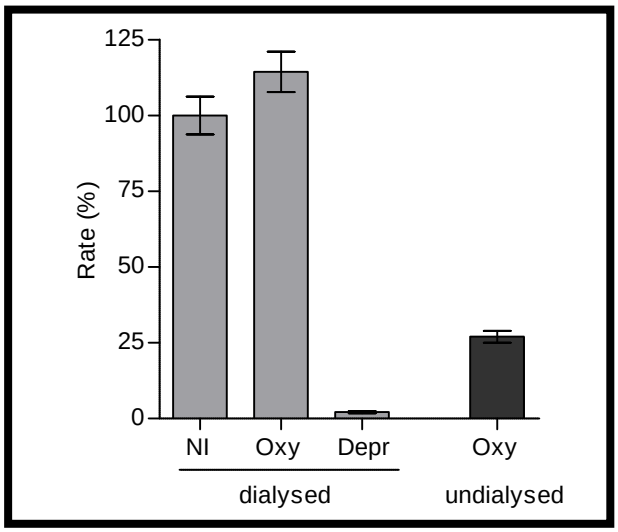

Figure 4.19: Reversibility of inhibition of MAO-B by oxybenzone. MAO-B and oxybenzone (at 4 × IC_{50}) was preincubated for 15 min, dialysed for 24 h and the residual enzyme activity was measured (Oxy–dialysed). Similar incubation and dialysis of MAO-B in the absence inhibitor (NI dialysed) and presence of the irreversible inhibitor, (R)-deprenyl (Depr dialysed), were also carried out. The residual activity of undialysed mixtures of MAO-B with oxybenzone was also recorded (Oxy–undialysed).

4.3.9 MODE OF MAO INHIBITION

4.3.9.1 INTRODUCTION

In the previous sections, it was shown that oxybenzone acts as a reversible inhibitor of MAO-B. To determine whether oxybenzone exhibits a competitive or non-competitive mode of inhibition (for this study a competitive mode of binding is preferred), Lineweaver-Burk plots for the inhibition of MAO-B by oxybenzone was constructed. For a competitive inhibitor the lines of the Lineweaver-Burk plots should intersect on the y-axis. If the lines intersect on the x-axis, the test inhibitor would have a non-competitive mode of binding.

4.3.9.2 CHEMICALS AND INSTRUMENTATION

Materials and instrumentation were the same as described in section 4.3.3 and 4.3.4.

4.3.9.3 EXPERIMENTAL METHOD FOR CONSTRUCTION OF LINEWEAVER-BURK PLOTS

- Lineweaver–Burk plots were constructed for the inhibition of MAO-B by oxybenzone.
- The initial rates of kynuramine oxidation were measured at eight different kynuramine concentrations (15–250 µM) in the absence and presence of five different test inhibitor concentrations. In this respect, the first plot was constructed in the absence of inhibitor, while the remaining five plots were constructed in the presence of the following inhibitor concentrations: ¼ × IC_{50}, ½ × IC_{50}, ¾ × IC_{50}, 1 × IC_{50} and 1¼ × IC_{50}. The concentrations of the test inhibitors that were selected for the study were: 0 µM, 0.718 µM, 1.435 µM, 2.153 µM, 2.872 µM and 3.59 µM.. The enzyme concentration in these incubations was 0.015 mg protein/ml.
- The rates of formation of the MAO generated 4-hydroxyquinoline were measured by fluorescence spectrophotometry as described above.
- The Prism® version 5.0 software package was used to perform the linear and non-linear regression analyses (Petzer *et al.,* 2012, Strydom *et al.,* 2011).

- The K_i value was estimated by global (shared) fitting of the inhibition data to the Michaelis-Menten equation using the Prism 5 software package. The K_i value was also estimated from a plot of the slopes of the Lineweaver-Burk plots versus inhibitor concentration (x-axis intercept equals $-K_i$).

4.3.9.4 RESULTS

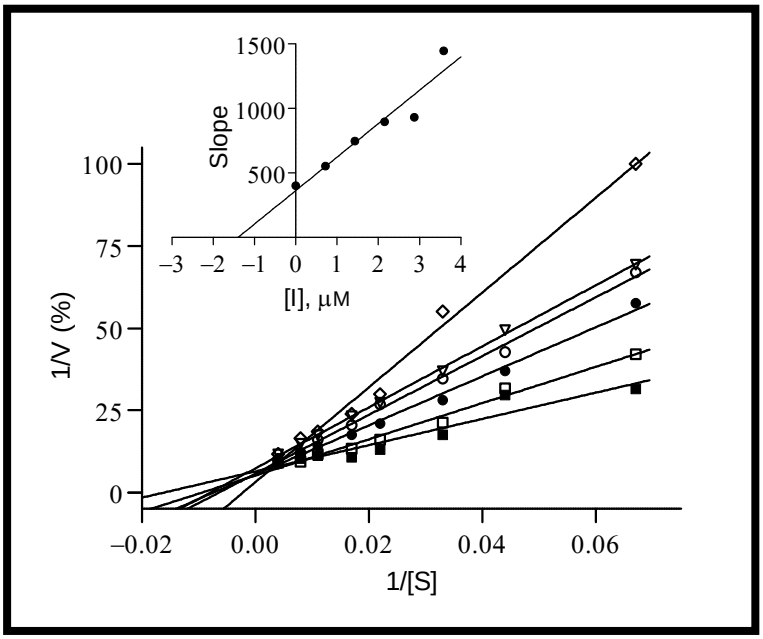

Figure 4.20: A graph illustrating the Lineweaver-Burk plots for the inhibition of MAO-B by oxybenzone. The Lineweaver-Burk plots are constructed in the absence (filled squares) and presence of various concentrations of oxybenzone. The following inhibitor concentrations were used: 0 µM, 0.718 µM, 1.435 µM, 2.153 µM, 2.872 µM and 3.59 µM. The inset is a graph of the slopes of the Lineweaver-Burk plots versus inhibitor concentration.

Figure 4.20 illustrates the Lineweaver-Burk plots for the inhibition of MAO-B, which were constructed in the absence and presence of various concentrations of oxybenzone. The lines intersected on the y-axis, illustrating that the test inhibitor (oxybenzone) exhibited a competitive mode of binding to MAO-B. Global (shared) fitting of the inhibition data directly to the Michaelis-Menten equation yields a K_i value of 1.44 ± 0.16 µM (R^2 = 0.97). From a plot of the slopes of the Lineweaver-Burk plots

versus inhibitor concentration a similar value (1.40 μM) is obtained (x-axis intercept equals $-K_i$).

4.4 SUMMARY

In this chapter the *in vitro* biological evaluation of selected test compounds were discussed. The COMT inhibitory activities of the test compounds were determined using the protocol described by Aoyama and co-workers (2005). Due to the unavailability of the COMT enzyme, only eleven of the twenty-six selected test compounds were evaluated *in vitro* for COMT inhibitory activity. The MAO inhibitory activities of eighteen test compounds were determined with a fluorometric assay using kynuramine as substrate. These test compounds were docked into crystal structure models of human MAO-A and MAO-B using the Discovery Studio 3.1® modelling software. Reversibility of binding to MAO-B was determined for oxybenzone. To determine the mode of binding, kinetic analysis for the inhibition of MAO-B by oxybenzone was carried out.

CHAPTER 5

CONCLUSION:

PD is an age-related neurodegenerative disorder characterised pathologically by the loss of neurons in the SNpc. This loss in turn, leads to a striatal dopamine deficiency, which is responsible for the major symptoms of the disease. PD has a high prevalence in the aging population, and due to an increase in life expectancy, PD is likely to become a larger problem in the future. The current treatment strategies are only symptomatic and there is a great need for the development of new drugs. Therefore, the main aim of this study was to identify through virtual screening, compounds that could inhibit COMT.

Virtual screening: Discovery Studio® 3.1 modelling software was used to construct structure-based pharmacophore models of COMT using a crystal structure of human COMT. *In silico* screening of a library of FDA approved drugs was then performed to identify possible inhibitors. Secondly, the FDA approved drug library was also docked into the active site of COMT. This approach provided information regarding possible binding orientations and establishes if the inhibitor fits within the active site cavity. The FDA approved drug library was also screened using a ligand fingerprint approach where the structures of known inhibitors served as reference library in order to identify chemically similar species. A literature survey was performed to identify bio-isosteres of both phenol and catechol. After the identification of these bio-isosteres, the Sigma-Aldrich database was searched and molecules containing these moieties were identified. A final selection of twenty-five compounds was made, also taking molecular weight, cost and availability into consideration. Lastly, kaempferol was added to the list of test compounds to be purchased due to its structural similarities to quercetin. In total twenty-six test compounds have been selected for *in vitro* evaluation.

IC_{50} determinations for inhibition of the COMT enzyme: The *in vitro* screening of the potential inhibitors was based on the literature protocol as described by Aoyama and co-workers (2005). The IC_{50} values of the test compounds were determined spectrofluorometrically using porcine COMT as enzyme source and norepinephrine (NE) as the substrate. In the presence of a test inhibitor the conversion of NE to *DL*-

normetanephrine (NMN) was inhibited. NMN was analysed at an excitation wavelength of 283 nm and an emission wavelength of 315 nm.

Due to the moratorium placed on the import of the porcine COMT enzyme to South-Africa, only eleven of the twenty-six test compounds were evaluated *in vitro.* The results showed that only kaempferol exhibited COMT inhibitory activity with an IC_{50} value of 2.799 µM. This is most likely due to the fact that kaempferol is structurally similar to quercetin (**Figure 5.1**) and may thus have similar interactions with the active sites of enzymes, resulting in similar biological activities, such as the inhibition of COMT and MAO.

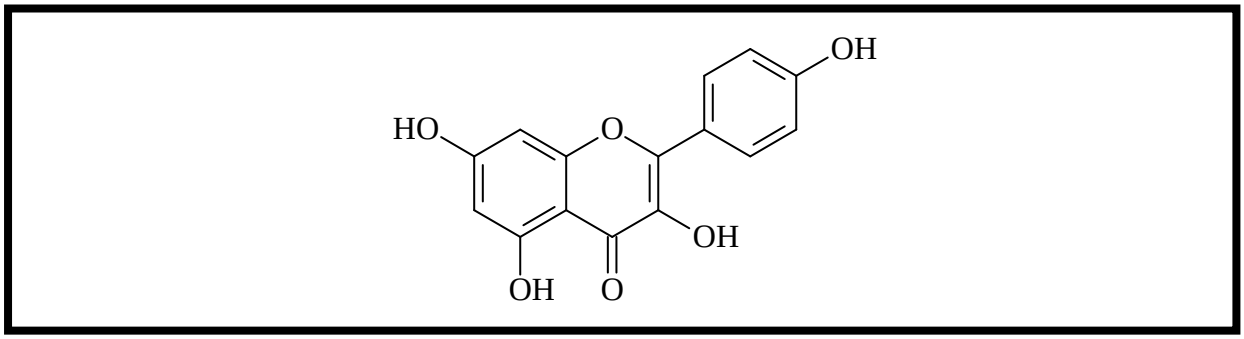

Figure 5.1: The structure of kaempferol.

IC_{50} determinations for the inhibition of the MAO enzyme: The IC_{50} values of the test compounds were determined spectrofluorometrically using recombinant human MAO-A and MAO-B enzymes, and kynuramine which is a mixed MAO-A/B substrate. The MAO-catalysed oxidation of kynuramine yields 4-hydroxyquinoline as product, which may be measured by fluorescence spectrophotometry at an excitation wavelength of 310 nm, and an emission wavelength of 400 nm.

The results showed six of the eighteen test drugs were inhibitors of the MAO-B isoform with IC_{50} values ranging from 2.872-146.050 µM. Three of these test drugs exhibited IC_{50} values smaller than 20 µM, which indicates that these test drugs are relatively potent MAO-B inhibitors. The most potent MAO-B inhibitor, oxybenzone, exhibited an IC_{50} value of 2.872 µM. The activity of this compound is particularly interesting and requires further investigation. In a previous study, MAO-B inhibitory activities were illustrated for a series of chalcones (Chimenti *et al.*, 2009). The most active compound of this series was compound **8** (**Figure 5.2 A**), which inhibited

MAO-B with an IC_{50} of 0.0044 µM. **Figure 5.2** illustrates structural similarities between compound **8** and oxybenzone.

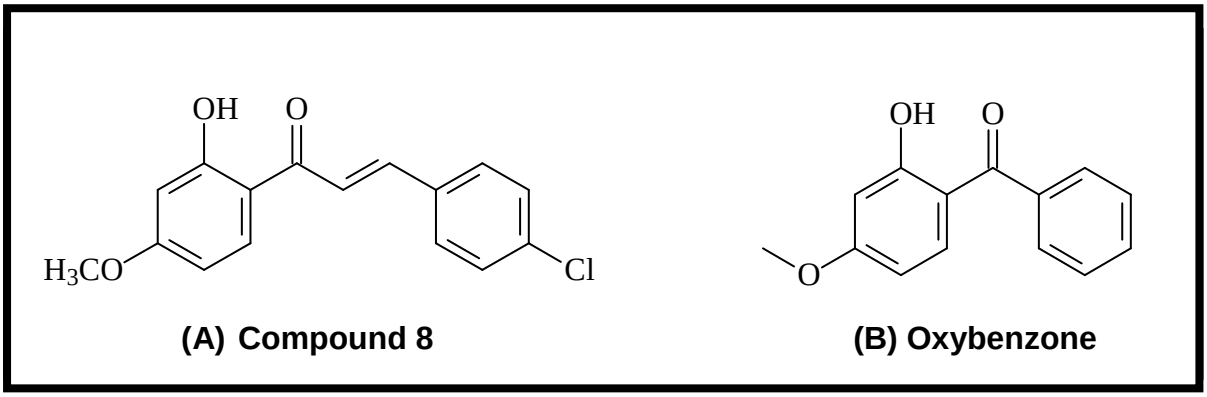

Figure 5.2: (A) Compound **8** from the series of synthesised chalcones (Chimenti *et al.,* 2009) and **(B)** oxybenzone.

The most potent MAO-A inhibitor, kaempferol, exhibited an IC_{50} value of 0.589 µM.

Molecular modelling of the MAO enzyme: Discovery Studio® 3.1 modelling software was used for the molecular docking studies. The crystal structure of MAO-A co-crystallised with harmine (PDB code: 2ZX5) and MAO-B co-crystallised with safinamide (PDB code: 2V5Z) was obtained from the Protein Data Bank. Molecular docking was carried out with the CDOCKER module in the Discovery Studio® 3.1 modelling software. Eleven of the eighteen test compounds were successfully docked into the active site of MAO-A, whereas twelve of these test drugs fitted within the active site of MAO-B.

MAO-A: The docking result of oxybenzone illustrated a hydrogen bond interaction between the heterocyclic ring of oxybenzone and Cys 323. Furthermore, the most potent hMAO-A inhibitor of the series, kaempferol, also possesses a hydrogen bond interaction between the phenol ring of kaempferol and Cys 323. According to De Colibus and co-workers (2005) a van der Waals interaction with Cys 323 can also observed for the known hMAO-A inhibitor, clorgyline. Thus, it may be concluded that a hydrogen bond interaction with Cys 323 may be an important feature for hMAO-A inhibitory activity.

MAO-B: Most compounds interacted with Tyr 326 or Tyr 398, while interactions with Cys 172, Gln 206, Ile 199 and Tyr 435 were also observed. Interestingly, for the most potent MAO-B inhibitor of the series, oxybenzone, no hydrogen bond interactions with the nearby amino acid residues of the human MAO-B enzyme were observed. Furthermore, it is postulated that the inhibitory activity of oxybenzone may be due to van der Waals interactions between oxybenzone and the amino acid residues. This is similar to interactions of known MAO-B inhibitors such as safinamide with the MAO-B enzyme.

Reversibility of binding: To determine whether binding of a selected test drug to the MAO enzymes is reversible, the recovery of enzymatic activity after dialysis of the enzyme-inhibitor complexes was determined. Oxybenzone, the most potent MAO-B inhibitor, was selected for the MAO-A and MAO-B reversibility studies, respectively. The irreversible inhibitors pargyline and (*R*)-deprenyl were also included, for MAO-A and MAO-B, respectively, as positive controls.

The results of these studies indicated that oxybenzone (**Figure 5.2 B**) possesses a reversible mode of binding to both the human MAO-B isoform, since enzyme activity was recovered after dialysis of mixtures containing the enzyme and inhibitor.

Kinetic studies: Since reversibility of binding was illustrated for oxybenzone for the inhibition of MAO-B, this compound was selected for further kinetic studies. Lineweaver–Burk plots were constructed for the inhibition of MAO-B by oxybenzone. For this purpose, the initial rates of kynuramine oxidation were measured at different kynuramine concentrations in the absence and presence of different test inhibitor concentrations. The lines of the Lineweaver-Burk plots intersected on the y-axis, which is indicative of a competitive mode of binding. It may thus be concluded that oxybenzone binds competitively to the MAO-B isoform.

In conclusion, despite some challenges, the aims and objectives of identifying a COMT inhibitor by virtual screening, as set out in Chapter 1 have been achieved. Screening of the pharmacophore models and a library by fingerprinting were not very effective methods for identifying new COMT inhibitors, and unfortunately the pharmacophore models could not be refined as the enzyme was no longer available. In addition, the effectiveness of the bio-isostere approach could also not be assessed. A dual COMT and MAO-B inhibitor, namely kaempferol has however been

identified. Furthermore, another three compounds also inhibited the MAO enzymes and may serve as lead compounds in future studies.

BIBLIOGRAPHY

Alcaraz, L.E., Blanco, S.E., Puig, O.N., Tomas, F. & Ferretti, F.H. 2000. Antibacterial activity of flavonoids against methicillin-resistant *Staphylococcus aureus* strains. *Journal of Theoretical Biology,* 205: 231-240.

Aminoff, M.J. 2009. Pharmacologic management of parkinsonism and other movement disorders. (In Katzung, B.G., Masters, S.B. & Trevor, A.J. Basic and Clinical Pharmacology. 11th ed. McGraw-Hill Lange: New York. 469-486).

Aoyama, N., Makoto T. & Kazuhiro, I. 2005. Improved assay for catechol-*O*-methyltransferase activity utilizing norepinephrine as an enzymatic substrate and reversed-phase high-performance liquid chromatography with fluorescence detection. *Journal of Chromatography A*, 1074: 47–51.

Aristieta, A., Azkona, G., Sagarduy, A., Miguelez, C., Ruiz-Ortega, J.A., Sanchez-Parnaute, R. & Ugedo, L. 2012. The role of the subthalamic nucleus in l-dopa induced dyskinesia in 6-hydroxydopamine lesioned rats. *PLOS One*, 7: 1-14.

Axelrod, J. & Tomchick, R., 1958. Enzymatic *O*-methylation of epinephrine and other catechols. *Journal of Biological Chemistry,* 233: 702-705.

Belluzzi, E., Bisaglia, M., Lazzarini, E., Tabares, L.C., Beltramini, M. & Bubacco, L. 2012. Human SOD2 modification by dopamine quinones affects enzymatic activity by promoting its aggregation: possible implications for Parkinson's disease. *PLOS One,* 7: 1–9.

Betarbet, R., Sherer, T.B., Di Monte, D.A. & Greenmyre, J.T. 2002. Mechanistic approaches to Parkinson's disease. *Brain Pathology*, 12: 499-510.

Binda, C., Newton-Vinson, P., Hubálek, F., Edmondson, D.E. & Mattevi, A. 2002. Structure of human monoamine oxidase B, a drug target for the treatment of neurological disorders. *Nature Structural & Molecular Biology*, 9: 22-26.

Bonifati, V. & Meco, G. 1999. New, selective catechol-*O*-methyltransferase inhibitors as therapeutics agents in Parkinson's disease. *Pharmacology & Therapeutics,* 81: 1-36.

Bonnet, U. 2003. Moclobemide: Therapeutic use and clinical studies. *CNS Drug Reviews*, 9: 97140.

Boyer, E.W. & Shannon, M. 2005. The serotonin syndrome. *New England Journal of Medicine*, 352: 1112-1120.

Boyle, A. & Ondo, W. 2015. Role of apomorphine in the treatment of Parkinson ’s disease. *CNS Drugs,* 29: 83–89.

Brown, J.H., Laiken, N. 2011. Muscarinic receptor agonists and antagonists. (In Brunton, L. L., Chabner, B.A., Knollmann, B.C. 12th ed. Goodman & Gilman's The Pharmacological Basis of Therapeutics. McGraw-Hill:New York. Available: http://accessmedicine.mhmedical.com/book.aspx?bookid=374. Date of access: 26 February, 2015.)

Brunton, L.L., Chabner, B.A., Knollmann, B.C. 2011.Treatment of central nervous system degenerative disorders. (In Standaert D.G., Roberson, E. D. 12th ed. Goodman & Gilman's The Pharmacological Basis of Therapeutics. McGraw-Hill: New York. Available: http://accessmedicine.mhmedical.com/book.aspx?bookid=374. Date of access: 26 February, 2015.)

Chen, J.J. & Swope, D.M. 2005. Clinical pharmacology of rasagiline: a novel, second-generation propargylamine for the treatment of Parkinson disease. *The Journal of Clinical Pharmacology*, 45: 878-894.

Cheng, Y. & Prusoff, W.H. 1973. Relationship between the inhibition constant and the concentration of inhibitor which causes 50 percent inhibition of an enzymatic reaction. *Biochemical Pharmacology,* 22: 3099-3108.

Chimenti, F., Fioravanti, R., Bolasco, A., Chimenti, P., Secci, D., Rossi, F., Yánez, M., Orallo, F., Ortuso, F. & Alcaro, S. 2009. Chalcones: A valid scaffold for monoamine oxidase inhibitors. *Journal of Medicinal Chemistry,* 52: 2818-2824.

Churchyard, A., Mathias, C.J., Boonkongchuen, P. & Lees, A.J. 1997. Autonomic effects of selegiline: possible cardiovascular toxicity in Parkinson’s disease. *Journal of Neurology, Neurosurgery & Psychiatry*, 63: 228-234.

Cohen, G. & Spina, M.B. 1989. Deprenyl suppresses the oxidant stress associated with increased dopamine turnover. *Annals of Neurology*, 26: 689-690.

Cools, R. 2006. Dopaminergic modulation of cognitive function-implications for L-dopa treatment in Parkinson's disease. *Neuroscience & Biobehavioral Reviews,* 30: 1–23.

Dauer, W. & Przedborski, S. 2003. Parkinson's disease: mechanisms and models. *Neuron*, 39: 889–909.

De Clercq, E. 2000. Current lead natural products for the chemotherapy of human immunodeficiency virus (HIV). *Medicinal Research Reviews,* 20: 323-349.

De Colibus, L., Li, M., Binda, C., Lustig, A., Edmondson, D.E. & Mattevi, A. 2005. Three-dimensional structure of human monoamine oxidase A (MAO A): Relation to the structures of rat MAO A and MAO B. *Proceedings of the National Academy of Sciences of the United States of America*, 102: 12684-12689.

De Monte, C., Carradori, S., Chimenti, P., Secci, D., Mannina, L., Alcaro, F., Petzer, A., N'Da, C.I., Gidaro, M.C., Costa, G., Alcaro, S. & Petzer, J.P. 2014. New insights into the biological properties of *Crocus Sativus L.*: chemical modifications, human monoamine oxidases inhibition and molecular modelling studies. *European Journal of Medicinal Chemistry,* 82: 164-171.

Doble, A. 1999. The role of excitotoxicity in neurodegenerative disease: implications for therapy. *Pharmacology Therapeutics,* 81:163–221.

Dorsey, E.R., Constantinescu, R., Thompson, J.P., Biglan, K.M., Holloway, R.G., Kieburtz, K., Marshall, F.J., Ravina, B.M., Schifitto, G., Siderowf, A. & Tanner, C.M. 2007. Projected number of people with Parkinson disease in the most populous nations, 2005 through 2030. *Neurology*, 68: 384–386.

Edmondson, D.E., Mattevi, A., Binda, C., Li, M. & Hubalek, F. 2004. Structure and mechanism of monoamine oxidase. *Current medicinal chemistry*, 11: 1983-1993.

Edmondson, D.E., Binda, C. & Mattevi, A. 2007. Structural insights into the mechanism of amine oxidation by monoamine oxidases A and B. *Archives of biochemistry and biophysics*, 464: 269-276.

Edwing, T.J.A., Makino, S., Skillman, A.G. & Kuntz, I.D. 2001. Dock 4.0: Search strategies for automated molecular docking of flexible molecule databases. *Journal of Computer-Aided Molecular Design,* 15: 411-428.

Eidelberg, D. & Pourfar, M. 2011. Movement and cerebellar disorders. (In Porter, R.S. & Kaplan, J.L. The merck manual of diagnosis and therapy. *19th ed*. Merck Sharpe & Dohme corp: New Jersey. 1765-1770).

Eslamboli, A., Georgievska, B., Ridley, R.M., Baker, H.F., Muzyczka, N., Burger, C., Mandel, R.J., Annett, L. & Kirik, D. 2005. Continuous low-level glial cell line-derived neurotrophic factor delivery using recombinant adeno-associated viral vectors provides neuroprotection and induces behavioral recovery in a primate model of Parkinson's disease. *The Journal of Neuroscience*, 25: 769–777.

Fernandez, H. H. & Chen, J. J. 2007 Monoamine oxidase-B inhibition in the treatment of Parkinson's disease. *Pharmacotherapy*, 27: 174s-185s.

Filomeni, G., Graziani, I., De Zio, D., Dini, L., Centonze, D., Rotilio, G. & Ciriolo, M.R. 2010. Neuroprotection of kaempferol by autophagy in models of rotenone-mediated acute toxicity: possible implications for Parkinson's disease. *Neurobiol*ogy of *Aging,* 33: 767-785.

Gershanik, O.S. 2015. Improving L-dopa therapy: the development of enzyme inhibitors. *Movement Disorders,* 30: 103–113.

Gill, S.S., Patel, N.K., Hotton, G.R., O'Sullivan, K., McCarter, R., Bunnage, M., Brooks, D.J., Svendsen, C.N. & Heywood, P. 2003. Direct brain infusion of glial cell line-derived neurotrophic factor in Parkinson's disease. *Nature Medicine,* 9: 589-595.

Guldberg, H.C. & Marsden, C.A. 1975. Catechol-*O*-methyltransferase: pharmacological aspects and physiological role. *Pharmacology Reviews,* 27: 135-206.

Hampton, M.B. & Orrenius, S. 1997. Dual regulation of caspase activity by hydrogen peroxide: implications for apoptosis. *Federation of European Biochemical Societies Letters*, 414: 552–556.

Havsteen, B. 1983. Flavonoids: A class of natural products of high pharmacological potency. *Biochemical Pharmacology,* 32: 1141-1148.

Healy, D.G., Abou-Sleiman, P.M. & Wood, N.W. 2004. Genetic causes of Parkinson's disease: UCHL-1. *Cell & Tissue Research,* 318: 189–194.

Heo, H.J., Kim, D.O., Choi, S.J., Shin, D.H. & Lee, C.Y. 2004. Apple phenolics protect *in vitro* oxidative stress-induced neuronal cell death. *Journal of Food Science,* 69: S357-360.

Hirsch, E.C., Vyas, S. & Hunot, S. 2012. Neuroinflammation in Parkinson's disease. *Parkinsonism & Related Disorders,* 1: 210–212.

Hsieh, W. & Chiang, B. 2014. A well-refined *in vitro* model derived from human embryonic stem cell for screening phytochemicals with midbrain dopaminergic differentiation-boosting potential for improving Parkinson's disease. *Journal of Agriculture & Food Chemistry*, 62: 6326-6336.

Hunn, B.H.M., Cragg, S.J., Bolam, J.P., Spillantini, M.G. & Wade-Martins, R. 2014. Impaired intracellular trafficking defines early Parkinson's disease. *Trends in Neuroscience,* 38: 178-188.

Hübner, H., Haubmann, C., Utz, W. & Gmeiner, P. 2000. Conjugated enynes as nonaromatic catechol bioisosteres: Synthesis, binding experiments, and computational studies of novel dopamine receptor agonists recognizing preferentially the D_3 subtype. *Journal of Medicinal Chemistry,* 43: 756-762.

Hwang, O. 2013. Role of oxidative stress in Parkinson's disease. *Experimental Neurobiology,* 22: 11-17.

Hynd, M.R., Scott, H.L. & Dodd, P.R. 2004. Glutamate-mediated excitotoxicity and neurodegeneration in Alzheimer's disease. *Neurochemistry International,* 45: 583-595.

Ishige, K., Schubert, D. & Sagara, Y. 2001. Flavonoids protect neuronal cells from oxidative stress by three distinct mechanisms. *Free Radical Biology & Medicine,* 30: 433-446.

Ito, H., Kobayashi, E., Takamatsu, Y., Li, S.H., Hatano, T., Sakagami, H., Kusama, K., Satoh, K., Sugita, D., Shimura, S., Itoh, Y. & Yoshida, T. 2000. Polyphenols from *Eriobotrya japonica* and their cytotoxicity against human oral tumor cell lines. *Chemical & Pharmaceutical Bulletin,* 48: 687-693.

Jatana, N., Sharma, A. & Latha, N. 2013. Pharmacophore modelling and virtual screening studies to design potential COMT inhibitors as new leads. *Journal of Molecular Graphics Modelling,* 39: 145–164.

Kaakkola, S. 2000. Clinical pharmacology, therapeutic use and potential of COMT inhibitors in Parkinson's disease. *Drugs,* 59: 1233-1250.

Kakkar, A.K. & Dahiya, N. 2015. Management of Parkinson's disease: current and future pharmacotherapy. *European Journal of Pharmacology,* 750: 74–81.

Kirchmair, J., Markt, P., Distinto, S., Wolber, G. & Langer, T. 2008. Evaluation of the performance of 3D virtual screening protocols: RMSD comparisons, enrichment assessments, and decoy selection - What can we learn from earlier mistakes? *Journal of Computer-Aided Molecular Design,* 22: 213–228.

Kiss, L.E. & Soares-da-Silva, P. 2014. Medicinal chemistry of catechol *O*-methyltransferase (COMT) inhibitors and their therapeutic utility. *Journal of Medicinal Chemistry,* 57: 8693-8717.

Koppenhöfer, D., Kettenbaum, F., Susloparova, A., Law, J.K.Y., Vu, X.T., Schwab, T., Schäfer, K.H. & Ingebrandt, S. 2014. Neurodegeneration through oxidative stress: monitoring hydrogen peroxide induced apoptosis in primary cells from the subventricular zone of BALB/c mice using field-effect transistors. *Biosensors & Bioelectronics,* 67: 490–496.

Korlipara, L.V.P., Cooper, J.M. & Schapira, A.H. V. 2004. Differences in toxicity of the catechol-*O*-methyl transferase inhibitors, tolcapone and entacapone to cultured human neuroblastoma cells. *Neuropharmacology*, 46: 562–569.

Kumagai, T., Kosaka, R., Ido, T., Araki, T., Imai, Y., Mizugaki, M & Itoyama, Y. 1999. III. 2. Neuroprotective effects of monoamine oxidase inhibitor and glutamate receptor inhibitor on MPTP-induced dopamine and DOPAC depletion in mice. *CYRIC annual report.* p5.

Kupsch, A., Sautter, J., Götz, M.E., Breithaupt, W., Schwarz, J., Youdim, M.B.H., Riederer, P., Gerlach, M. & Oertel, W.H. 2001. Monoamine oxidase-inhibition and MPTP-induced neurotoxicity in the non-human primate: comparison of rasagiline (TVP 1012) with selegiline. *Journal of Neural Transmission*, 108: 985-1009.

La Casa, C., Villegas, I., Alarcón de la Lastra, C., Motilva, V. & Martín Calero, M.J. 2000. Evidence for protective and antioxidant properties of rutin, a natural flavone, against ethanol induced gastric lesions. *Journal of Ethnopharmacology,* 71: 45-53.

Lakhanpal, P. & Rai, D.K. 2007. Quercetin: a versatile flavonoid. *Internet Journal of Medical Update,* 2: 22-37.

Lang, U.E., Hellweg, R., Seifert, F., Schubert, F. & Gallinat, J. 2007. Correlation between serum brain-derived neurotrophic factor level and an *in vivo* marker of cortical integrity. *Biological Psychiary,* 62: 530-535.

Lang, A.E. & Lozano, A.M. 1998. Medical progress: Parkinson's disease. *The New England Journal of Medicine,* 339: 1044-1053.

Langer, T. & Wolber, G. 2004. Pharmacophore definition and 3D searches. *Drug Discovery Today: Technologies,* 1: 203-207.

Langmir, I. 1919. Isomorphism, isosterism and covalence. *Journal of the Americam Chemical Society*, 41: 1543-1559.

Lee, M.H., Lin, R.D., Shen, L.Y., Yang, L.L., Yen, K.Y. & Hou, W.C. 2001. Monoamine oxidase B and free radical scavenging activities of natural flavonoids in *Melastoma candidum D.* Don. *Journal of Agricultural & Food Chemistry,* 49: 5551-5555.

Lee, J.Y., Baek, S. & Kim, Y. 2007. Receptor-oriented pharmacophore-based in silico screening of human catechol *O*-methyltransferase for the design of antiparkinsonian drug. *Bulletin- Korean Chemical Society,* 28: 379–385.

Lees, A.J., Hardy, J. & Revesz, T. 2009. Parkinson's disease. *The Lancet Neurology*, 373: 2055–2066.

Leonard, J. V & Schapira, A.H. V. 2000. Mitochondrial respiratory chain disorders II : neurodegenerative disorders and nuclear gene defects. *The Lancet Neurology*, 355: 389–394.

Lerner, C., Ruf, A., Gramlich, V., Masjost, B., Zürcher, Jakob-Roetne, R., Borroni, E. & Diederich, F. 2001. X-ray crystal structure of a bisubstrate inhibitor bound to the enzyme catechol-*O*-methyltransferase: A dramatic effect of inhibitor preorganization on binding affinity. *Angewadte Chemie,* 40: 4040-4042.

Li, L., Klebe, D., Doycheva, D., McBride, D.W., Krafft, P.R., Flores, J., Zhou, C., Zhang, J.H. & Tang, J. 2015. G-CSF ameliorates neuronal apoptosis through GSK-3β inhibition in neonatal hypoxia–ischemia in rats. *Experimental Neurology,* 263: 141–149.

Li, S. & Pu, X.P. 2011. Neuroprotective effect of kaempferol against a 1-methyl-4-phenyl-1,2,3,6-tetrahydropyridine-induced mouse model of Parkinson's disease. *Biological & Pharmaceutical Bulletin,* 34: 1291-1296.

Lipski, J., Nistico, R., Berretta, N., Guatteo, E., Bernardi, G. & Mercuri, N.B. 2011. *L*-DOPA: a scapegoat for accelerated neurodegeneration in Parkinson's disease? *Progress in Neurobiology,* 94: 389-407.

Lundström, K., Tenhunen, K., Tilgmann, J., Karhunen, T., Panula, P. & Ulmanen, I. 1995. Cloning, expression and structure of catechol-*O*-methyltransferase. *Biochimica et Biophysica Acta (BBA) - Protein Structure & Molecular Enzymology,* 1251: 1-10.

Ma, Z., Liu, H. & Wu, B. 2013. Structure-based drug design of catechol-*O*-methyltransferase inhibitors for CNS disorders. *British Journal of Clinical Pharmacology,* 77: 410–420.

Mandel, S., Weinreb, O., Amit, T. & Youdim, M.B.H. 2005. Mechanism of neuroprotective action of the anti-parkinson drug rasagiline and its derivatives. *Brain Research Reviews*, 48: 379387.

Männistö, P.T. & Kaakkola, S. 1990. Rationale for selective COMT inhibitors as adjuncts in the drug treatment of Parkinson's disease. *Pharmacology & Toxicology,* 66: 317–323.

Männistö, P.T. & Kaakkola, S. 1999. Catechol-*O*-methyltransferase (COMT): biochemistry, molecular biology, pharmacology, and clinical efficacy of the new selective COMT inhibitors. *Pharmacological Reviews,* 51: 593–628.

McEwen, C.M., Sasaki, G. & Jones, D.C. 1969. Human liver mitochondrial monoamine oxidase. II. Determinants of substrate and inhibitor specificities. *Biochemistry*, 8: 3952-3962.

Meanwell, N.A. 2011. Synopsis of some recent tactical application of bioisosteres in drug design. *Journal of Medicinal Chemistry,* 54: 2529-2591.

Middleton, E.J. 1998. Effect of plant flavonoids on immune and inflammatory cell functions. *Advances in Experimental Medicine & Biology,* 439: 175-182.

Miller, J.R. & Edmondson, D.E. 1999. Structure-activity relationships in the oxidation of parasubstituted benzylamine analogues by recombinant human liver monoamine oxidase A. *Biochemistry*, 38: 13670-13683.

Mogi, M., Harada, M., Kondo, T., Riederer, P., Inagaki, H., Minami, M. & Nagatsu, T. 1994a. Interleukin-1β, interleukin-6, epidermal growth factor and transforming growth factor-α are elevated in the brain from parkinsonian patients. *Neuroscience Letters,* 180: 147-150.

Mogi, M., Harada, M., Riederer, P., Narabayashi, H., Fujita, K. & Nagatsu, T. 1994b. Tumor necrosis factor-α (TNF-α) increases both in the brain and in the cerebrospinal fluid from parkinsonian patients. *Neuroscience Letters,* 165: 208-210.

Montastruc, J.L., Chaumerliac, C., Desboeuf, K., Manika, M., Bagheri, H., Rascol, O. & LapeyreMestre, M. 2000. Adverse drug reactions to selegiline: *A review of the French Pharmacovigilance Database. Clinical Neuropharmacology*, 23: 271-275.

Moskuag, J.O, Carlson, H., Myhrstad, M. & Blomhoff, R. 2004. Molecular imaging of the biological effects of quercetin and quercetin-rich foods. *Mechanism of Ageing & Development*, 125: 315-24.

Müller, T. 2015. Catechol-*O*-methyltransferase inhibitors in Parkinson's disease. *Drugs*, 75: 157–174.

Murray, R., Granner, D., Mayes, P., Rodwell, V. 2003. Enzyme kinetics. (In Murray, R., Granner, D., Mayes, P., Rodwell, V. *eds.* Harper's Illustrated Biochemistry. 26th ed, McGraw-Hill: New-York. 62-73.)

Murphy, K.J., Chronopoulos, A.K., Singh, I., Francis, M.A., Moriarty, H., Pike, M.J., Turner, A.H., Mann, N.J. & Sinclair, A.J. 2003. Dietary flavanols and procyanidin oligomers from cocoa (Theobroma cacao) inhibit platelet function. *American Journal of Clinical Nutrition,* 77: 1466-1473.

Mytilineou, C., Radcliffe, P., Leonardi, E.K., Werner, P. & Olanow, C.W. 1997. L-Deprenyl protects mesencephalic dopamine neurons from glutamate receptor-mediated toxicity in vitro. *Journal of Neurochemistry*, 68: 33-39.

Narayana, K.R., Reddy, M.S., Chaluvadi, M.R. & Krishna, D.R. 2001. Bioflavonoids classification, pharmacological, biochemical effects and therapeutic potential. *Indian Journal of pharmacology,* 33: 2-16.

Naidu, P.S. & Kulkarni, S.K. 2004. Quercetin, a bioflavonoid, reverses haloperidol induced catalepsy. *Methods & Findings in Experimental & Clinical Pharmacology,* 26: 323-236.

Nicotra, A. & Parvez, S.H. 1999. Methods for assaying monoamine oxidase A and B activities: recent developments. *Biogenic Amines*, 15: 307-320.

Nirmala, P., & Ramanathan, M. 2011. Effect of kaempferol on lipid peroxidation and antioxidant status in 1, 2-dimethyl hydrazine induced colorectal carcinoma in rats. *European Journal of Pharmacology,* 654: 75-79.

Novaroli, L., Reist, M., Favre, E., Carotti, A., Catto, M. & Carrupt, P.A. 2005. Human recombinant monoamine oxidase B as a reliable and efficient enzyme source for inhibitor screening. *Bioorganic & Medicinal Chemistry,* 13: 6212-6217.

Olanow, C.W., Hauser, R.A., Gauguster, L., Malapira, T., Koller, W., Hubble, J., Bushenbark, K., Lilienfeld, D. & Esterlitz, J. 1995. The effect of deprenyl and levodopa on the progression of Parkinson's disease. *Annals of Neurology*, 38: 771-777.

Pålhagen, S., Heinonen, E., Hägglund, J., Kaugesaar, T., Mäki-Ikola, O., Palm, R. & The Swedish Parkinson Study, G. 2006. Selegiline slows the progression of the symptoms of Parkinson disease. *Neurology*, 66: 1200-1206.

Paisán-Ruíz, C., Jain, S., Evans, E.W., Gilks, W.P., Simón, J., Van Der Brug, M., De Munain, A.L., Aparicio, S., Gil, A. M., Khan, N., Johnson, J., Martinez, J.R., Nicholl, D., Carrera, I.M., Peňa, A.S., De Silva, R., Lees, A., Martí-Massó, J.F., Pérez-Tur, J., Wood, N.W. & Singleton, A.B. 2004. Cloning of the gene containing mutations that cause PARK8-linked Parkinson's disease. *Neuron*, 44: 595-600.

Patani, G.A. & LaVoie, E.J. 1996. Bioisosterism: A rational approach in drug design. *Chemical Reviews,* 96: 3147-3176.

Petzer, A.L., Harvey, B.H., Wegener, G. & Petzer, J.P. 2012. Azure B, a metabolite of methylene blue, is a high-potency, reversible inhibitor of monoamine oxidase. *Toxicology & Applied Pharmacology*, 258: 403-409.

Polymeropoulos, M.H., Lavedan, C., Leroy, E., Ide, S.E., Dehejia, A., Dutra, A., Pike, B., Root, H., Rubenstein, J., Boyer, R., Stenroos, E.S., Chandrasekharappa, S., Athanassiadou, A., Johnson, W.G., Lazzarini, A.M., Duvoisin, R.C., Iorio, G.D., Golbe, L.I., Nussbaum, R.L., Reports, E., Lavedant, C., Leroyt, E., Papapetropoulos, T., Di, G. & Golbe, L. 1997. Mutation in the α-synuclein gene identified in families with Parkinson's disease. *Science,* 276: 2045–2048.

Rafi, M.M., Rosen, R.T., Vassil, A., Ho, C.T., Zhang, H., Ghai, G., Lambert, G. & DiPaola, R.S. 2000. Modulation of bcl-2 and cytotoxicity by licochalcone-A, a novel estrogenic flavonoid. *Anticancer Research,* 20: 2653-2658.

Ramsay, R.R. 2013. Inhibitor design for monoamine oxidases. *Current Pharmaceutical Design*, 19: 2529-2539.

Rodwell, V. W. 1993. Enzymes: Kinetics. (In Murray, R.K., Granner, D.K., Mayes, P.A., Rodwell, V.W. ed. Harper's biochemistry. 23rd edition. New Jersey: Appleton & Lange. 60-70).

Sagi, Y., Driguès, N. & Youdim, M.B.H. 2005. The neurochemical and behavioral effects of the novel cholinesterase–monoamine oxidase inhibitor, ladostigil, in

response to L-dopa and L-tryptophan, in rats. *British Journal of Pharmacology*, 146: 553-560.

Schroeter, H., Williams, R.J., Matin, R., Iversen, L. & Rice-Evans, C.A. 2000. Phenolic antioxidants attenuate neuronal cell death following uptake of oxidized low-density lipoprotein. *Free Radical Biology & Medicine,* 29: 1222-1233.

Schroeter, H., Spencer, J.P., Rice-Evans, C.A. & Williams, R.J. 2001. Flavonoids protect neurons from oxidized low-density-lipoprotein-induced apoptosis involving c-Jun N-terminal kinase (JNK), c-Jun and caspase-3. *Biochemistry Journal,* 358: 547-557.

Segura-Aguilar, T., Ibis, G., Bendix, F. & Wolber, G. 2010. 3D pharmacophore elucidation and virtual screening. *Drug Discovery Today: Technology,* 7: e221-e228.

Seidel, T., Ibis, G., Bendix, F. & Wolber, G. 2010. Strategies for 3D pharmacophore-based virtual screening. *Drug Discovery Today: Technologies,* 7: 221-228.

Sherer, T.B., Betarbet, R. & Greenamyre, J.T. 2002. Environment, mitochondria and Parkinson's disease. *The Neuroscientist,* 8: 192-197.

Singer, T.P. & Ramsay, R.R. 1995. Flavoprotein structure and mechanism 2. Monoamine oxidases: old friends hold many surprises. *The Journal of the Federation of American Societies for Experimental Biology*, 9: 605-610.

Singer, T.P., Salach, J.I., Castagnoli, N.J.R., & Trevor, A. 1986. Interactions of the neurotoxic amine 1-methyl-4-phenyl-1,2,3,6-tetrahydropyridine with monoamine oxidases. *The Biochemical Journal*, 235: 785-789.

Singh, A., Naidu, P.S. & Kulkarni, S.K. 2003. Reversal of aging and chronic ethanol –induced cognitive dysfunction by quercetin.a bioflavonoid. *Free Radical Research,* 37: 1245-1252.

Singh, A. & Pattipati, S. 2003. Quercetin potentiates L-Dopa reversal of drug induced catalepsy in rats: possible COMT/MAO inhibition. *Pharmacology,* 68: 81-88.

Son, S.-Y., Ma, J., Kondou, Y., Yoshimura, M., Yamashita, E. & Tsukihara, T. 2008. Structure of human monoamine oxidase A at 2.2-Å resolution: The control of opening

the entry for substrates/inhibitors. *Proceedings of the National Academy of Sciences of the United States of America,* 105: 5739-5744.

Srivatsal, S., Cholerton, B., Leverenz, J.B., Wszolek, Z.K., Uitti, R.J., Dickson, D.W., Weintraub, D., Trojanowski, J.Q., Van Deerlin, V.M., Quinn, J.F., Chung, K. A., Peterson, A.L., Factor, S. A., Wood-Siverio, C., Goldman, J.G., Stebbins, G.T., Bernard, B., Ritz, B., Rausch, R., Espay, A.J., Revilla, F.J., Devoto, J., Rosenthal, L.S., Dawson, T.M., Albert, M.S., Mata, I.F., Hu, S.-C., Montine, K.S., Johnson, C., Montine, T.J., Edwards, K.L., Zhang, J. & Zabetian, C.P. 2015. Cognitive profile of LRRK2 -related Parkinson's disease. *Movement Disorders,* 00: 1-5.

Stocchi, F., Borgohain, R., Onofrj, M., Schapira, A.H.V., Bhatt, M., Lucini, V., Giuliani, R. & Anand, R. 2012. A randomized, double-blind, placebo-controlled trial of safinamide as add-on therapy in early Parkinson's disease patients. *Movement Disorders*, 27: 106-112.

Strydom, B., Bergh, J.J. & Petzer, J.P. 2011. 8-Aryl- and alkyloxycaffeine analogues as inhibitors of monoamine oxidase. *European Journal of Medicinal Chemistry,* 46: 3474-3485.

Symes, A.L., Lal, S. & Sourkes, T.L. 1975. Effect of catechol-*O*-methyltransferase inhibitors on brain apomorphine concentrations and stereotyped behaviour in the rat. *Journal of Pharmacy and Pharmacology*, 27: 947-948

Tzeng, S.H., Ko, W.C., Ko, F.N. & Teng, C.M. 1991. Inhibition of platelet aggregation by some flavonoids. *Thrombosis Research,* 64: 91-100.

Van Laar, V.S., Roy, N., Liu, A., Rajprohat, S., Arnold, B., Dukes, A. A., Holbein, C.D. & Berman, S.B. 2015. Glutamate excitotoxicity in neurons triggers mitochondrial and endoplasmic reticulum accumulation of Parkin, and, in the presence of N-acetyl cysteine, mitophagy. *Neurobiology of Disease,* 74: 180–193.

Vigren, J., Tilgmann, C., Lundström, K. & Liljas, A. 1991. Crystallisation and preliminary X-ray investigation of a recombinant form of rat catechol-*O*-methyltransferase. *Proteins*, 11: 233-236.

Williams, H.J., Owen, M.J. & O'Donovan, M.C. 2007. Is COMT a susceptibility gene for schizophrenia? *Schizophrenia Bulletin,* 33: 635–641.

Winogrodzka, A., Bergmans, P., Booij, J., van Royen, E. A., Janssen, A. G. & Wolters, E.C. 2001. [^{123}I]FP-CIT SPECT is a useful method to monitor the rate of dopaminergic degeneration in early-stage Parkinson's disease. *Journal of Neural Transmission,* 108: 1011–1019.

Wolber, G. & Langer, T. 2005. LigandScout: 3-D pharmacophores derived from protein-bound ligands and their use as virtual screening filters. *Journal of Chemistry Information & Modelling,* 45: 160–169.

Woodard, R.W., Tsai, M.D., Floss, H.G., Crooks, P.A. & Coward, J.K. 1980. Stereochemical course of the transmethylation catalysed by catechol-*0*-methyltransferase. *Journal of Biological Chemistry,* 255: 9124-9127.

Yacoubian, T.A. & Standaert, D.G. 2009. Targets for neuroprotection in Parkinson's disease. *Biochimica et Biophysica Acta*, 1792: 676–687.

Yamada, M. & Yasuharaz, H. 2004. Clinical Pharmacology of MAO Inhibitors: Safety and Future. *NeuroToxicology*, 25: 215–221.

Youdim, M.B.H. & Bakhle, Y.S. 2006. Monoamine oxidase: isoforms and inhibitors in Parkinson's disease and depressive illness. *British Journal of Pharmacology*, 147(suppl.): S287–S296.

Youdim, M.B.H. & Buccafusco, J.J. 2005. Multi-functional drugs for various CNS targets in the treatment of neurodegenerative disorders. *Trends in Pharmacological Sciences*, 26: 2735.

Youdim, M.B., Edmondson, D. & Tipton, K.F. 2006. The therapeutic potential of monoamine oxidase inhibitors. *Nature reviews neuroscience*, 7: 295-309.

Youdim, M.B.H., Wadia, J.S. & Tatton, N.A. 1999. Neuroprotective properties of the antiparkinson drug rasagiline and its optical S-isomer. *Neuroscience Letters, Supplement,* 54:45.

Youdim, M.B.H. & Weinstock, M. 2004. Therapeutic applications of selective and non-selective inhibitors of monoamine oxidase A and B that do not cause significant tyramine potentiation. *Neurotoxicology*, 25: 243-250.

Yu, X., Yao, J.Y., He, J. & Tian, J.W. 2015. Protection of MPTP-induced neuroinflammation and neurodegeneration by rotigotine-loaded microspheres. *Life Science,* 62: 379–388.

Zecca, L., Youdim, M.B.H., Riederer, P., Connor, J.R. & Crichton, R.R. 2004. Iron, brain ageing and neurodegenerative disorders. Nature Reviews *Neuroscience*, 5: 863-873.

Zuk, M., Kulma, A., Dymin´ska, L., Szoltysek, K., Prescha, A., Hanuza, J. & Szopa, J. 2011. Flavonoid engineering of flax potentiate its biotechnological application. *BMC Biotechnology,* 11: 1-19.

ADDENDUM

LIST OF COMPOUNDS USED FOR THE TEST SETS

The test sets were constructed using Discovery Studio® 3.1 modelling software consisting of ligands which are known to inhibit COMT (Kiss & Soares-da-Silva, 2014).

Structure of Ligands	
1	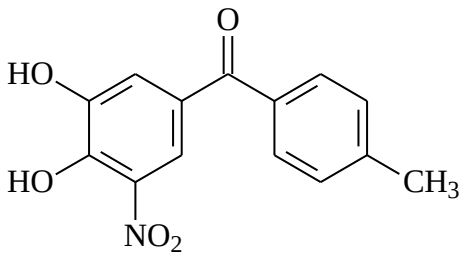
2	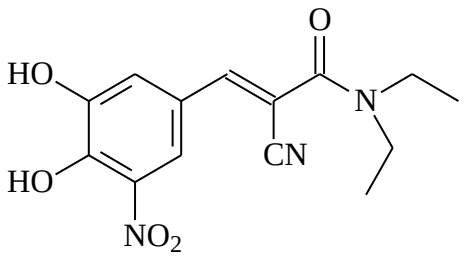
3	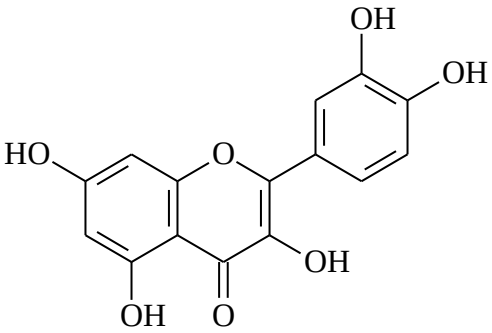
4	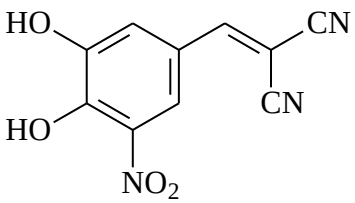

5	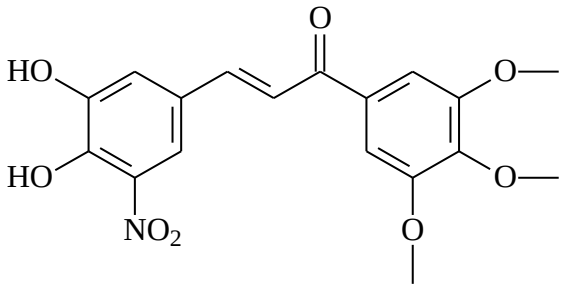
6	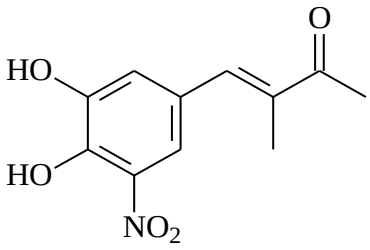
7	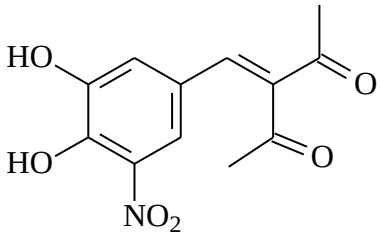
8	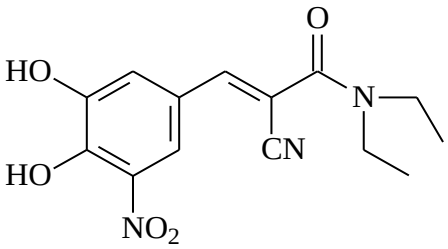
9	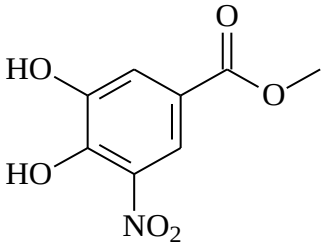

10	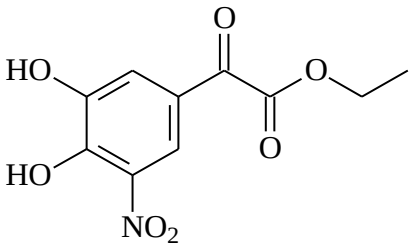
11	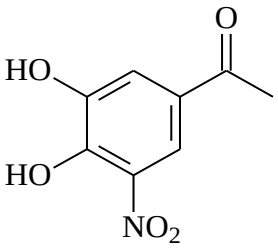
12	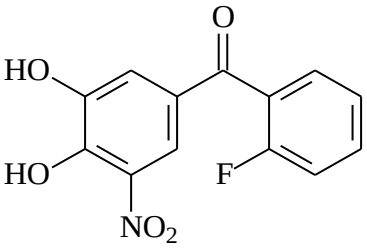
13	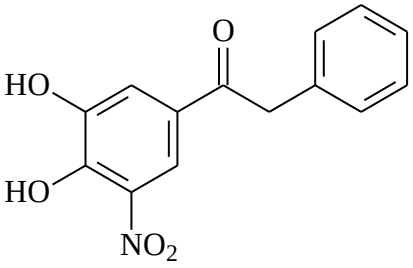
14	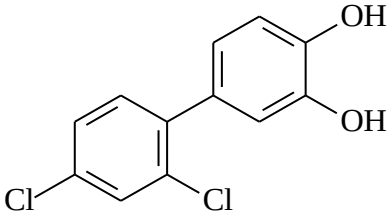
15	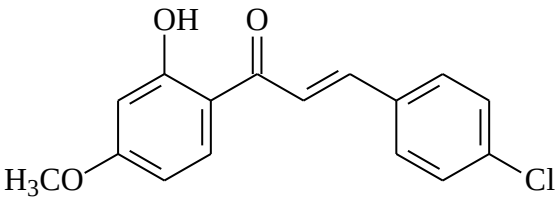

16	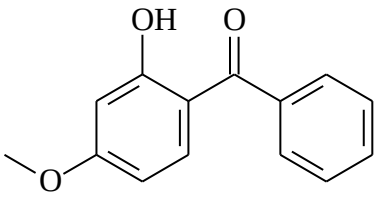
17	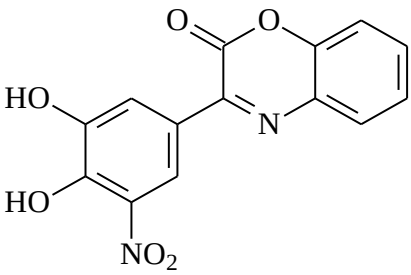
18	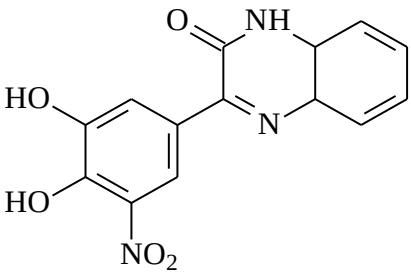
19	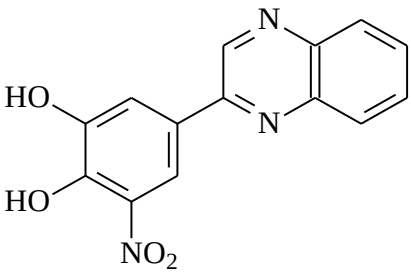
20	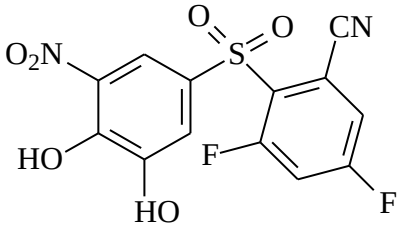
21	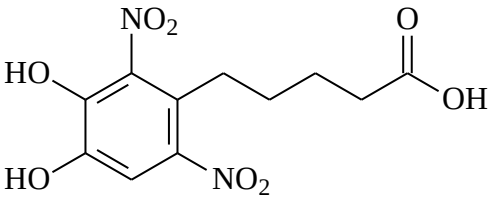

22	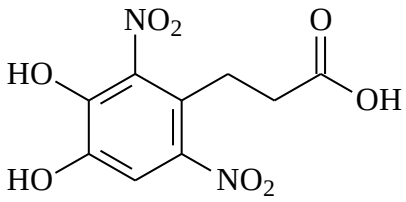
23	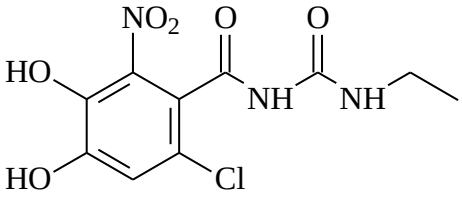
24	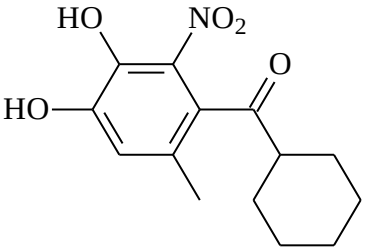
25	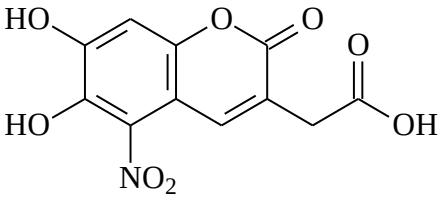
26	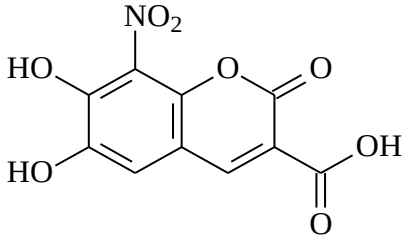
27	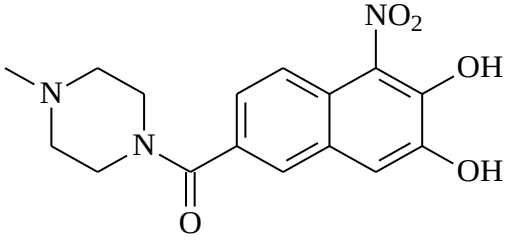

28	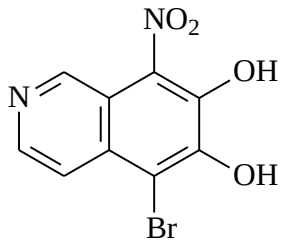
29	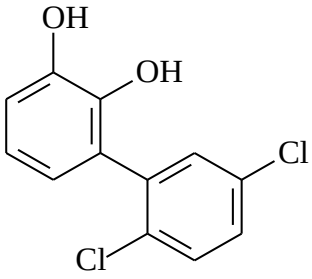
30	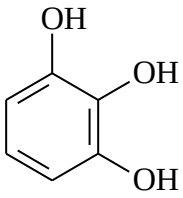
31	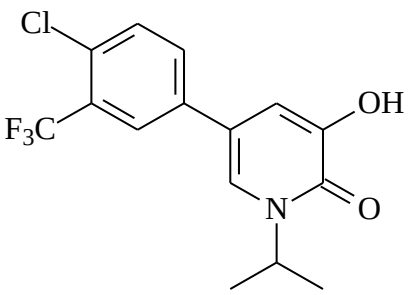
32	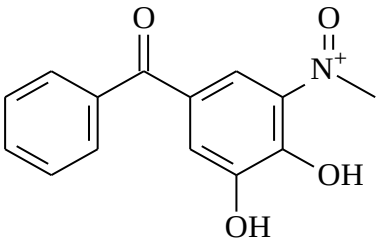
33	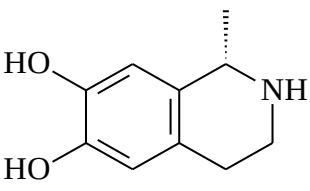

MOLECULAR DOCKING RESULTS OF COMT

Carisoprodol:

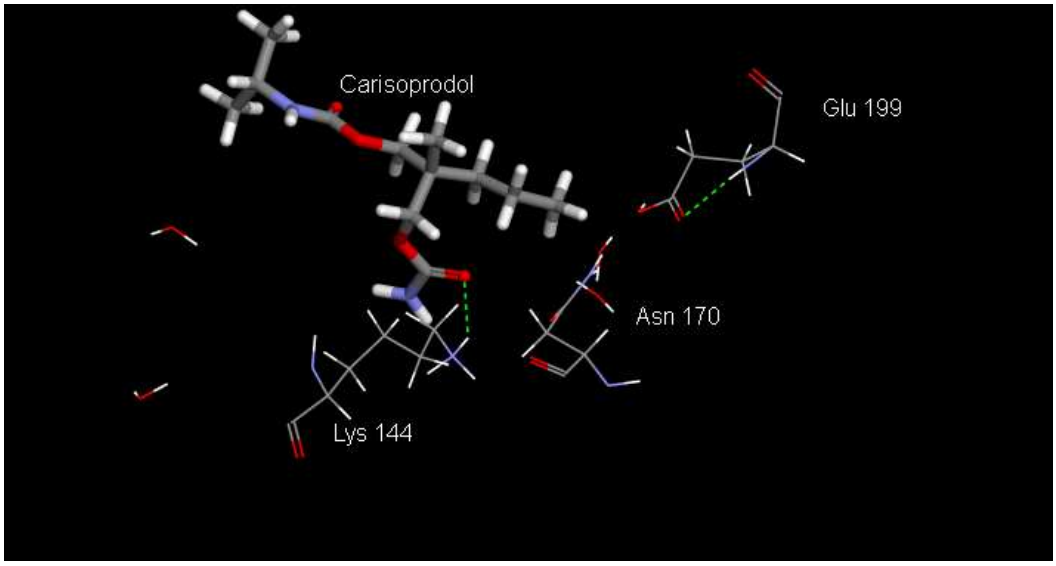

Ketoprofen:

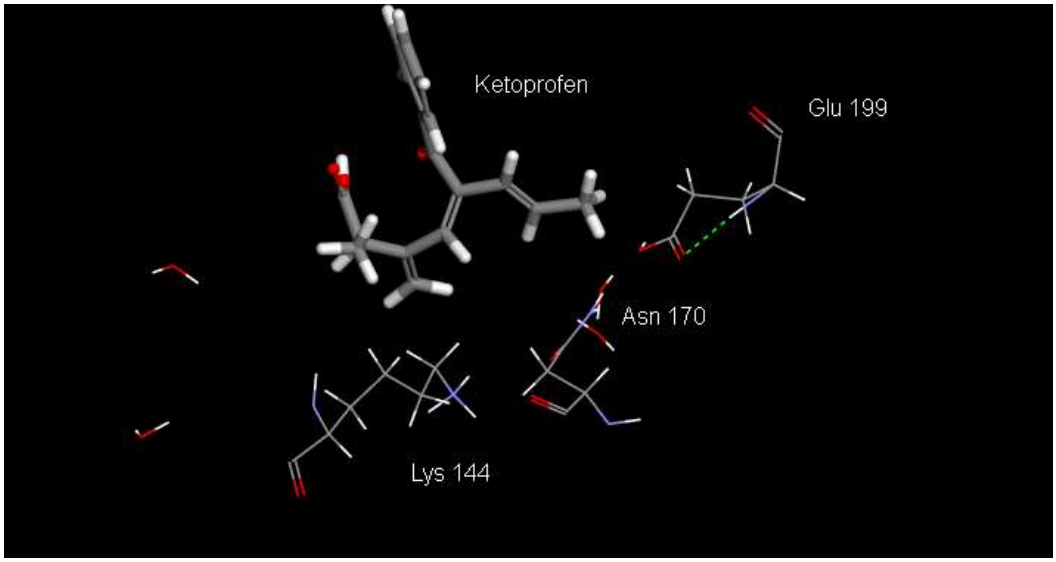

Oxybenzone:

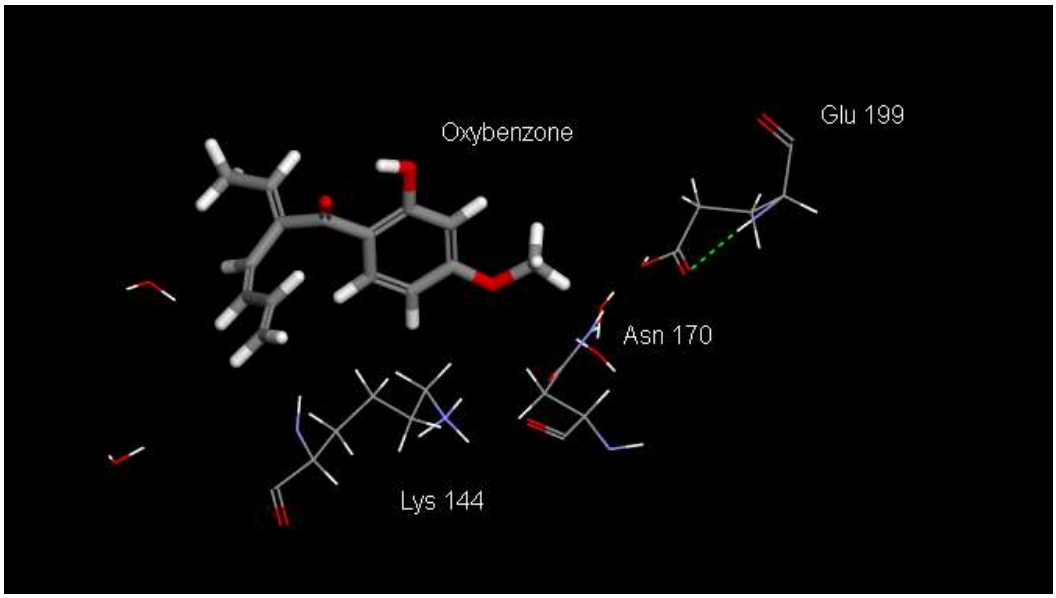

(6*R*)-5,6,7,8-Tetrahydrobiopterin:

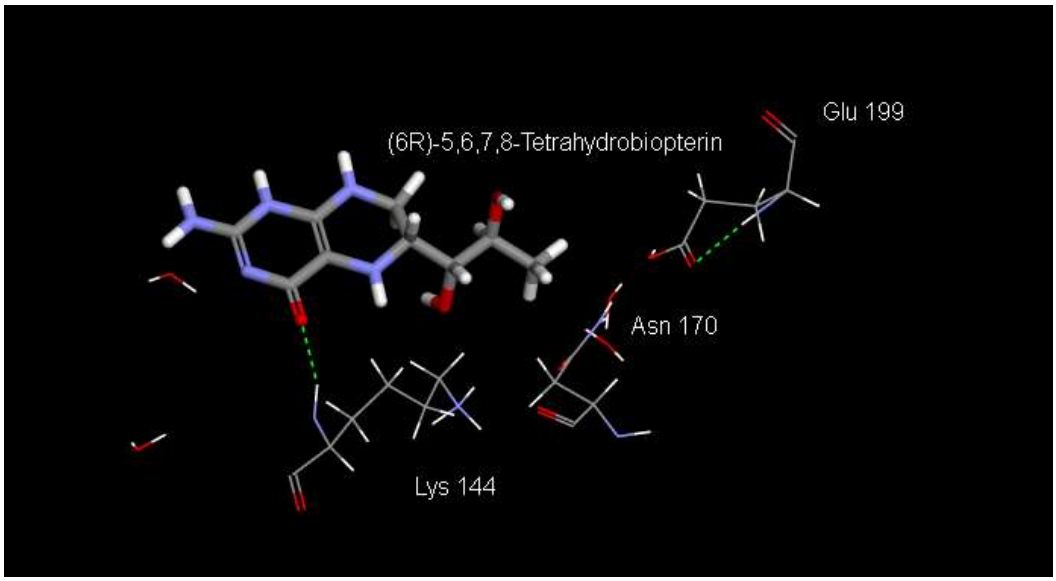

Trimethoprim:

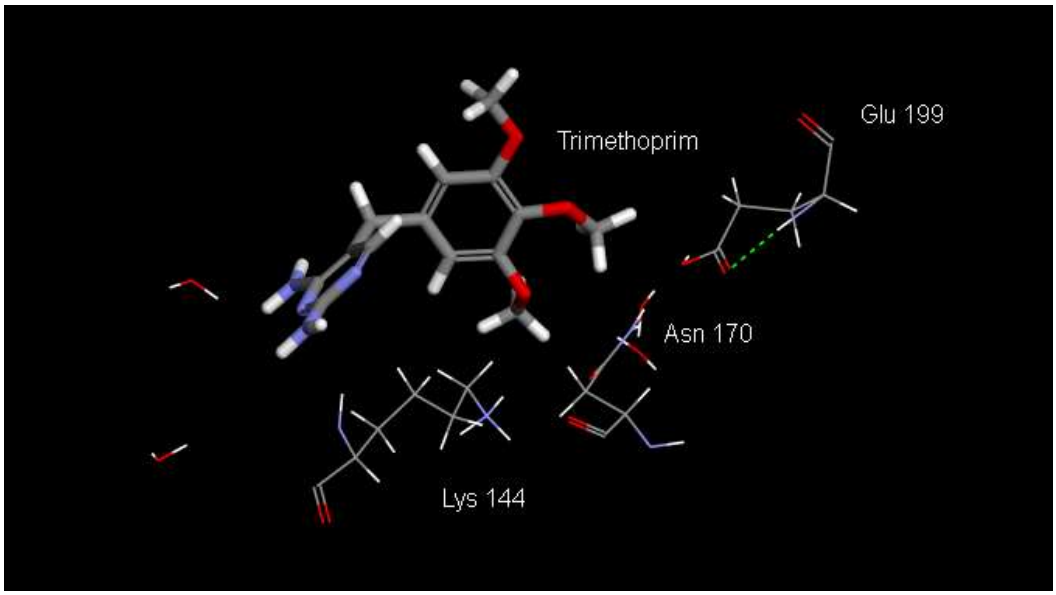

SIGMOIDAL PLOTS FOR THE INHIBITION OF MAO BY THE TEST INHIBITORS

MAO-A:

Kaempferol:

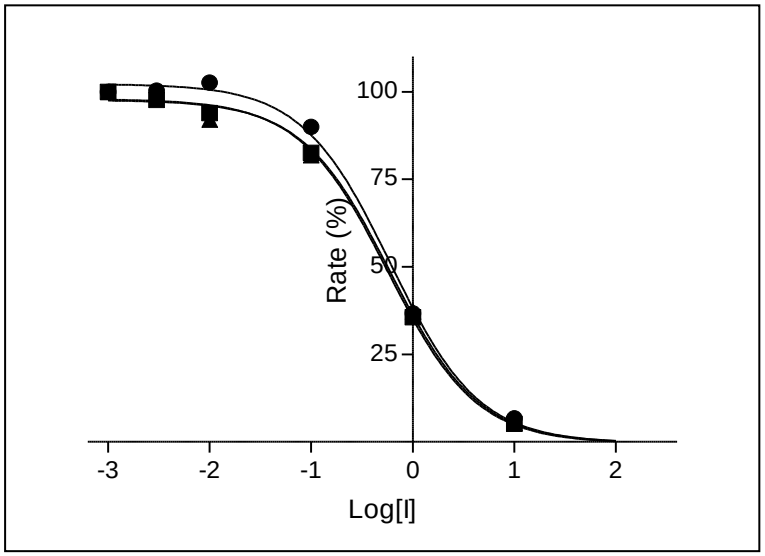

(-)-Riboflavin:

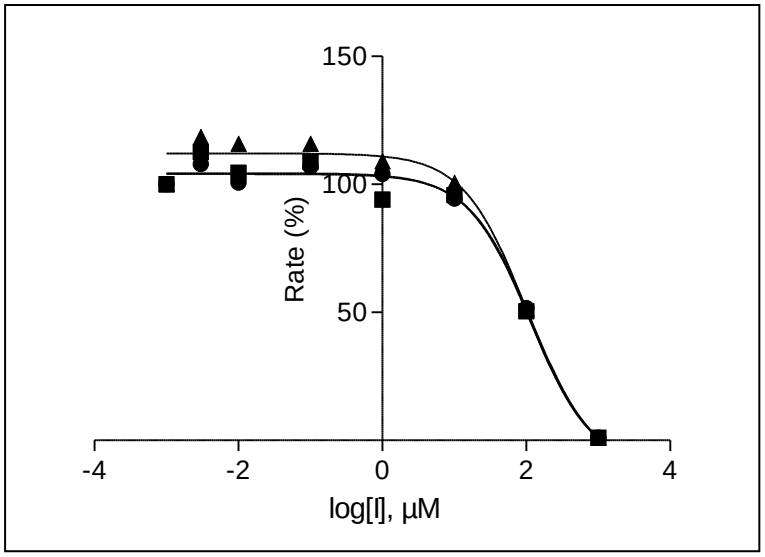

Tenoxicam:

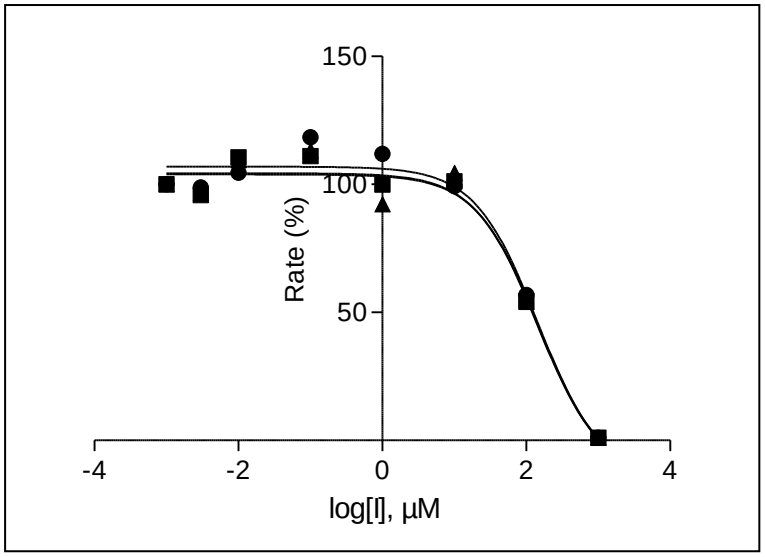

MAO-B:

Betamethasone:

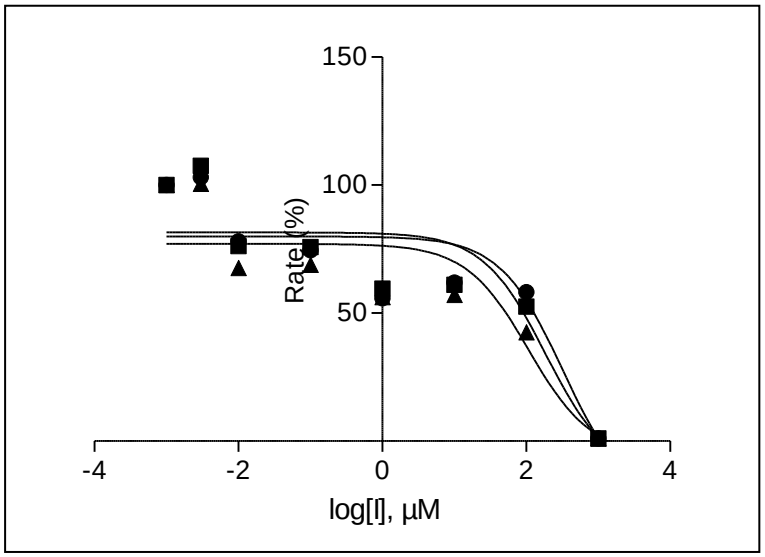

Kaempferol:

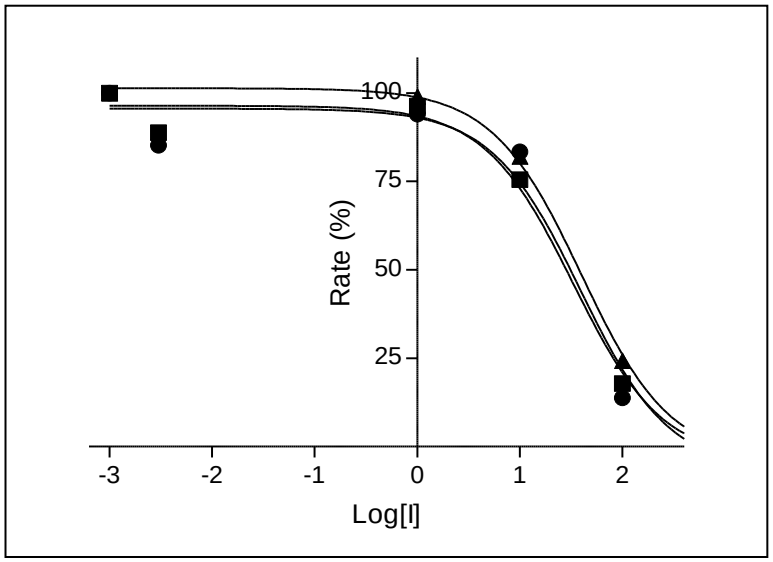

Tenoxicam:

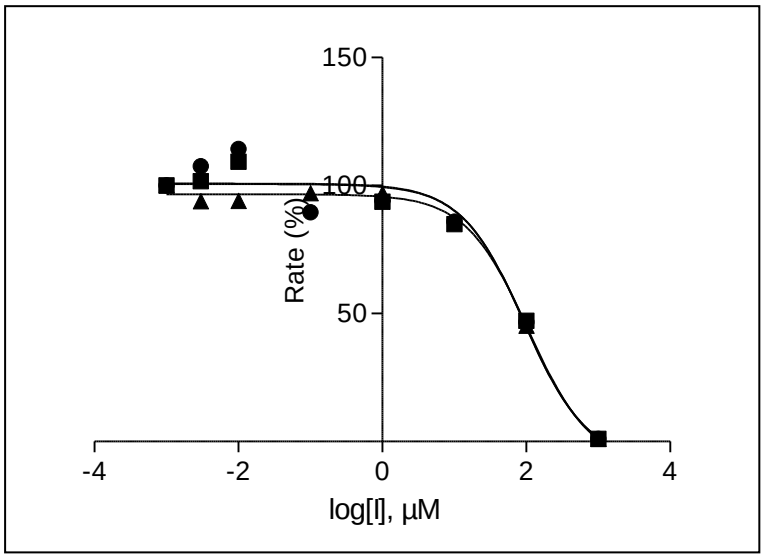

LIST OF MOLECULAR DOCKING RESULTS OF MAO

MAO-A:

Carisoprodol:

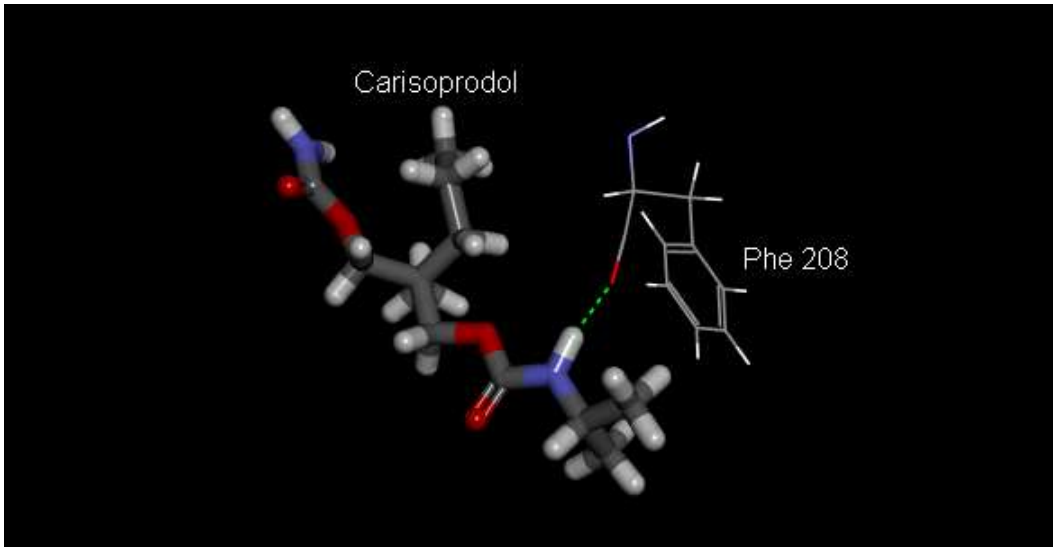

Diflunisal:

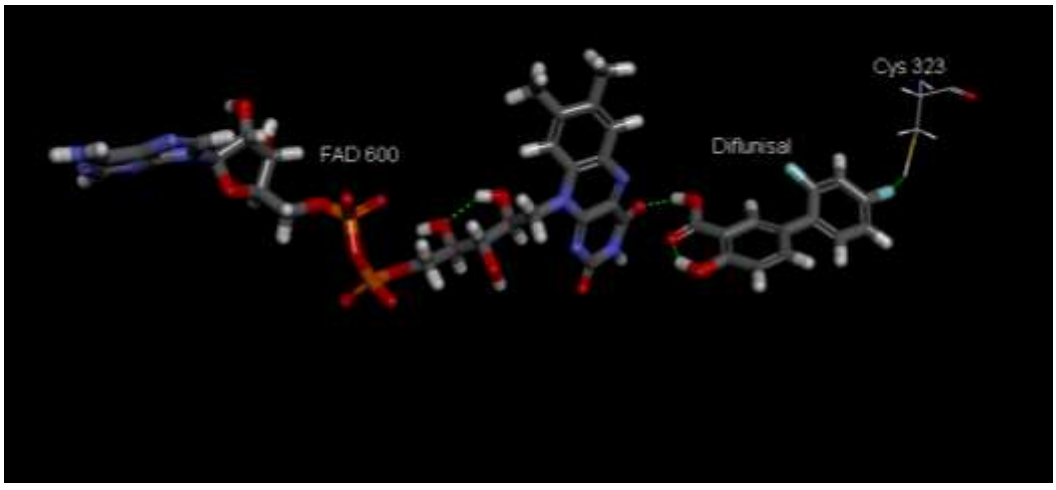

Esmolol:

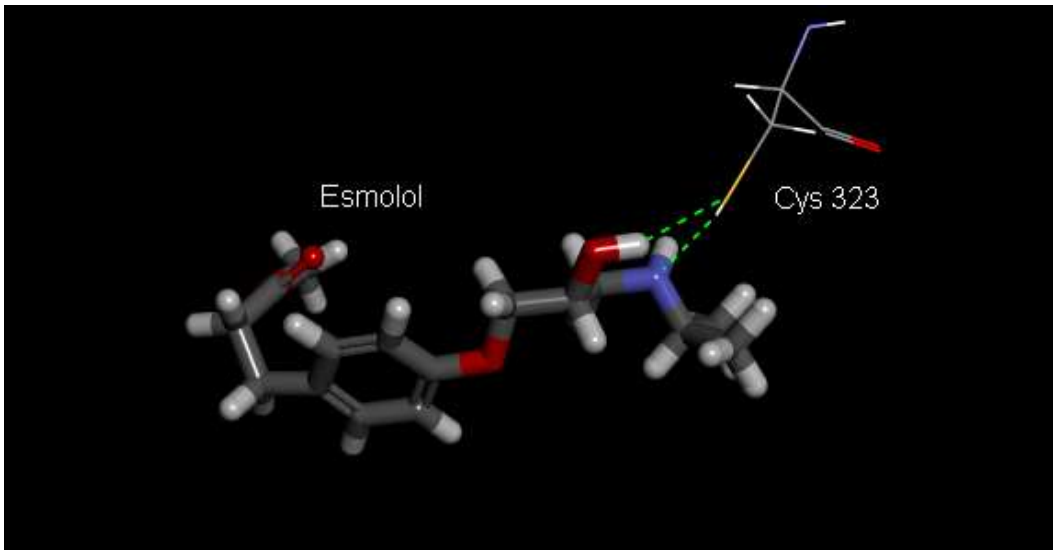

Ethambutol:

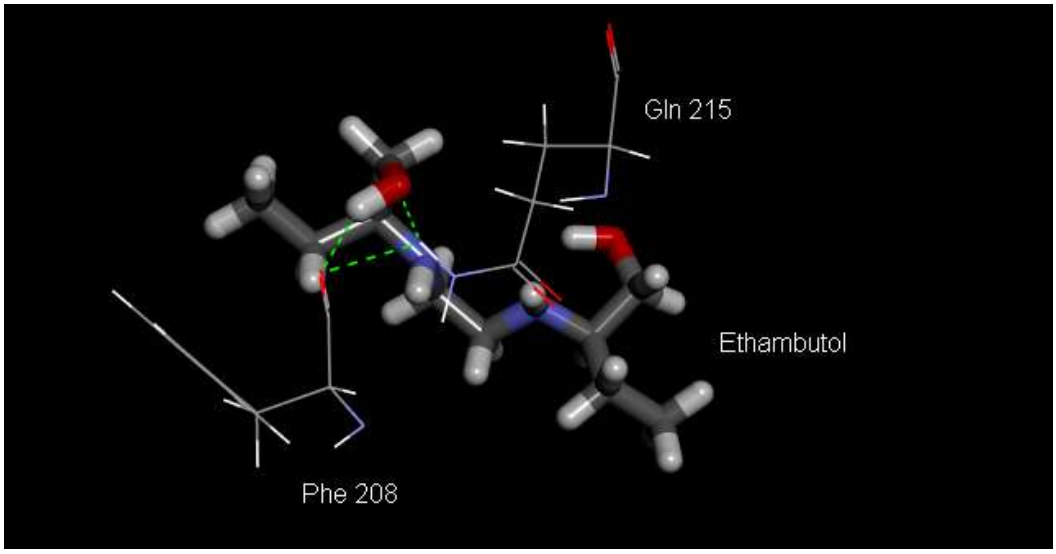

Kaempferol:

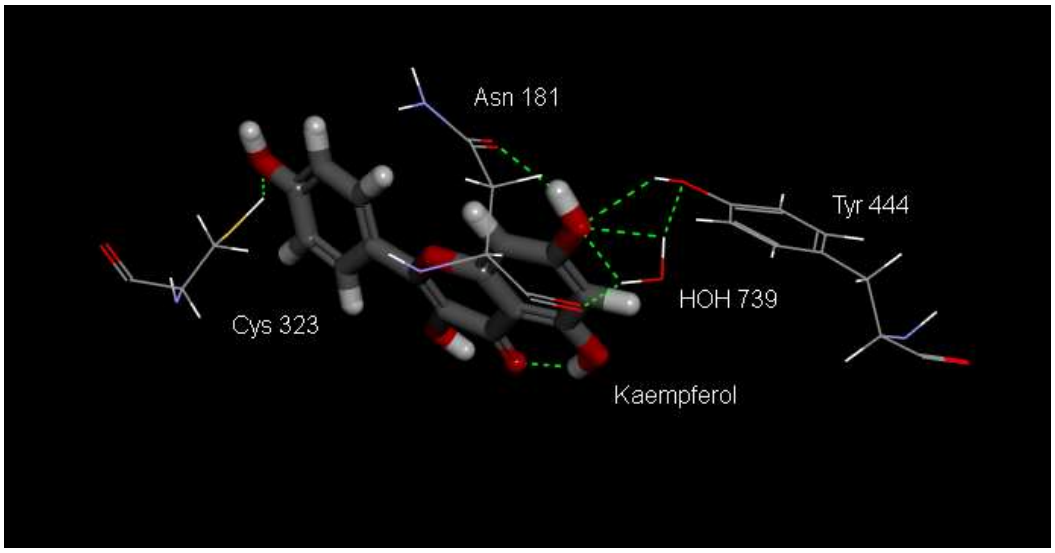

Ketoprofen:

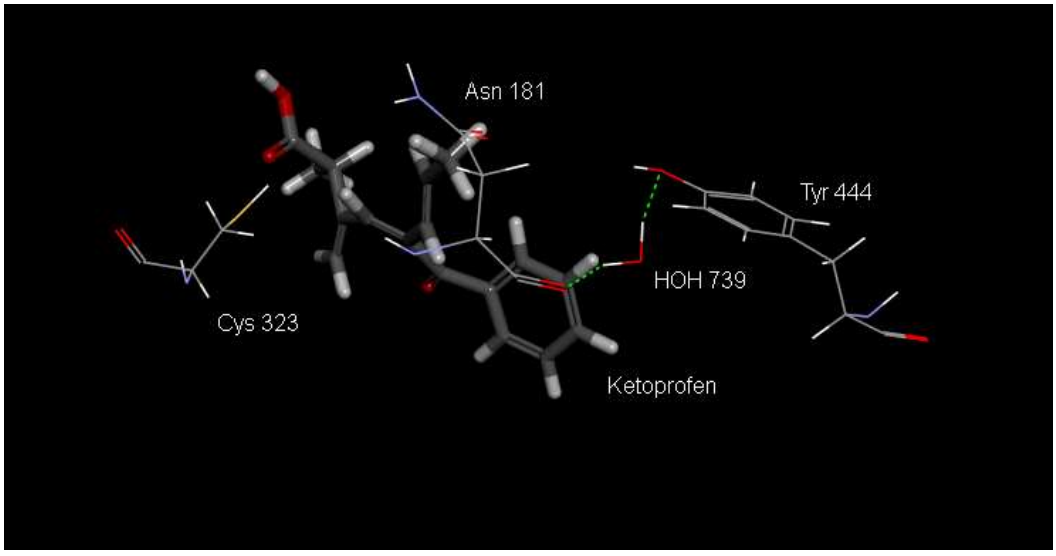

Midodrine:

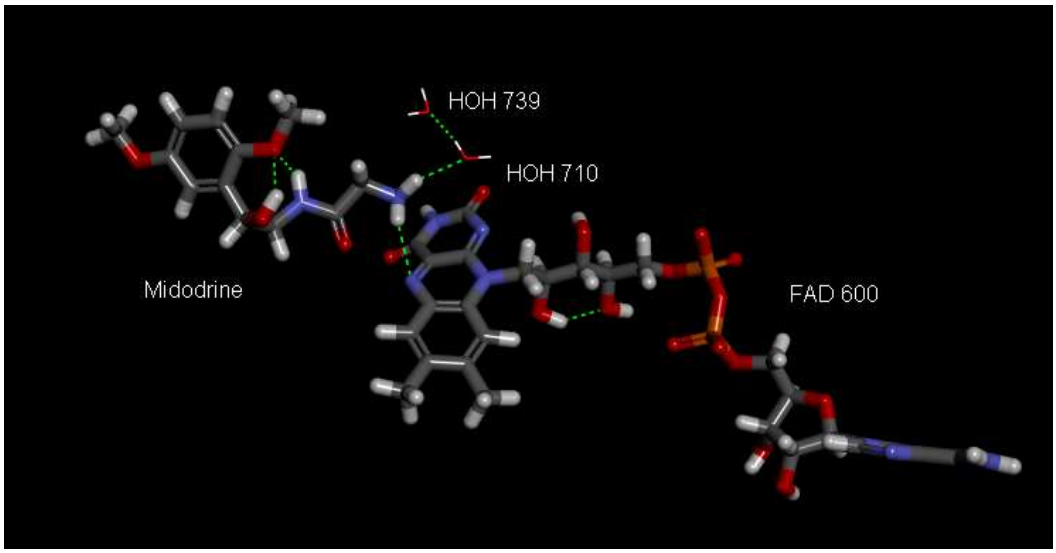

Oxybenzone:

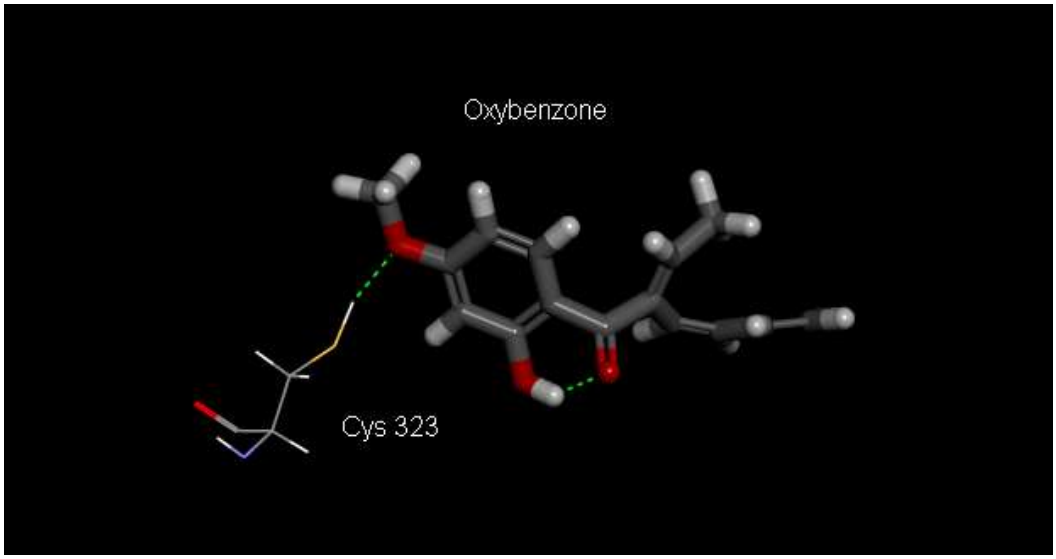

Tenoxicam:

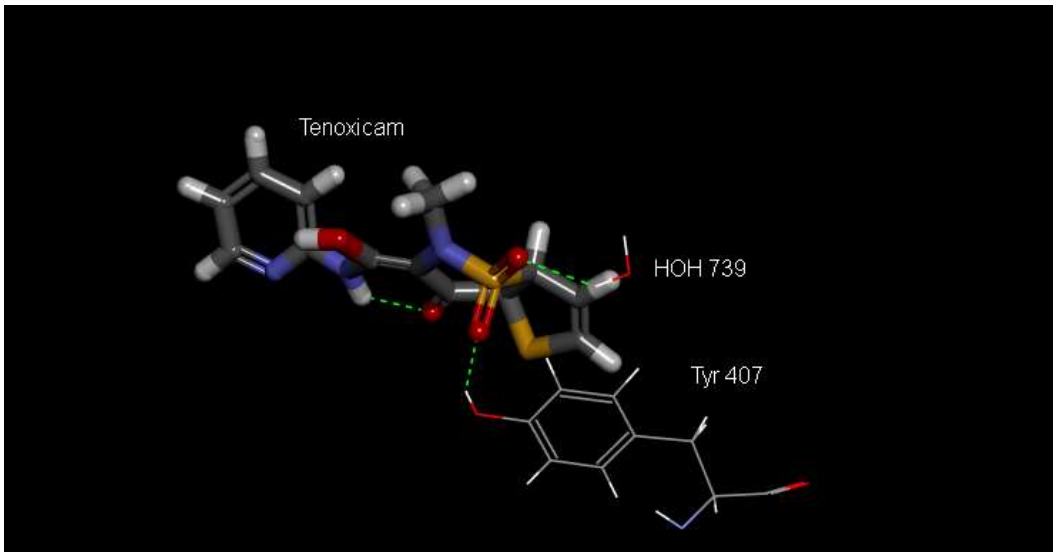

(6*R*)-5,6,7,8-Tetrahydrobiopterin:

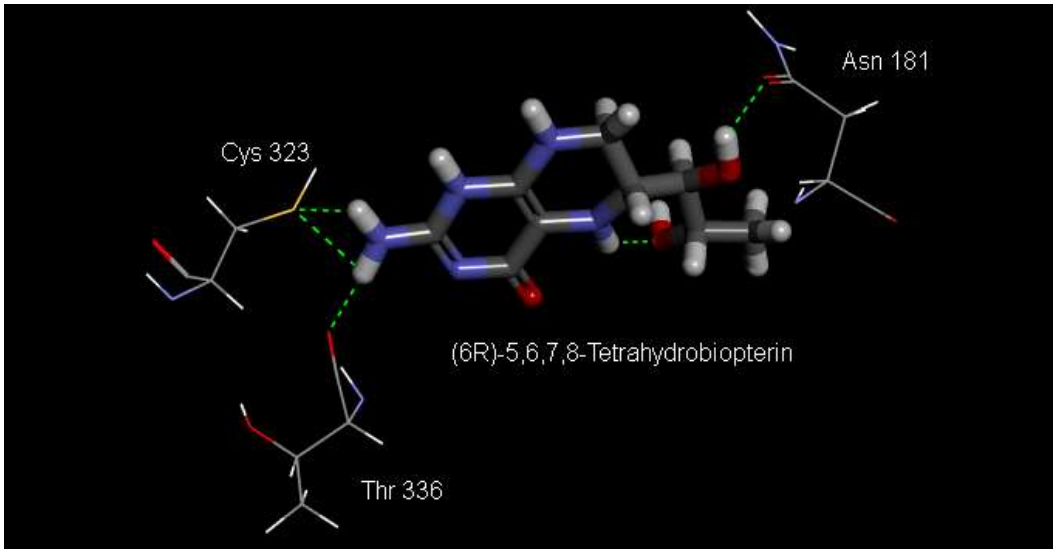

Trimethoprim:

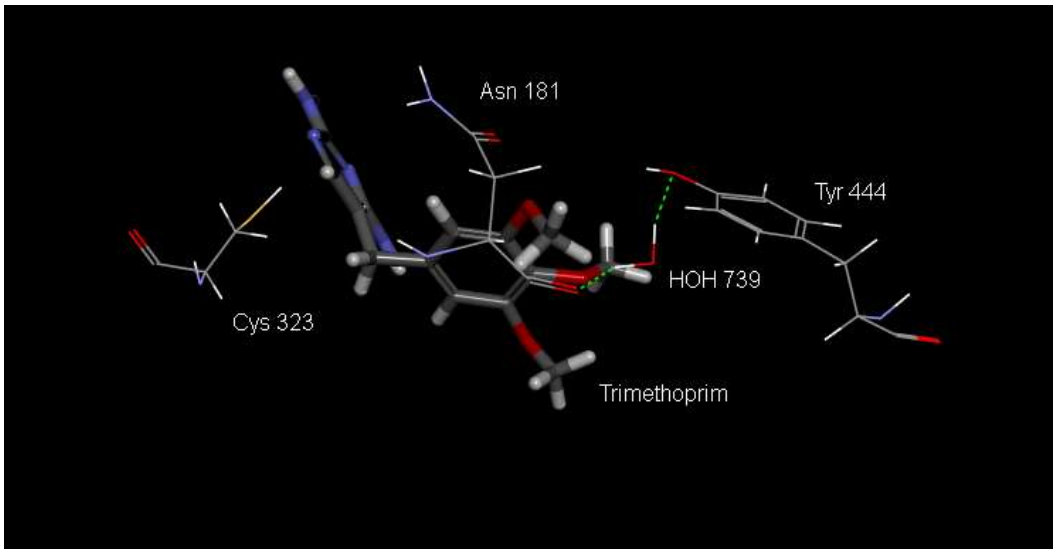

MAO-B:

Carisoprodol:

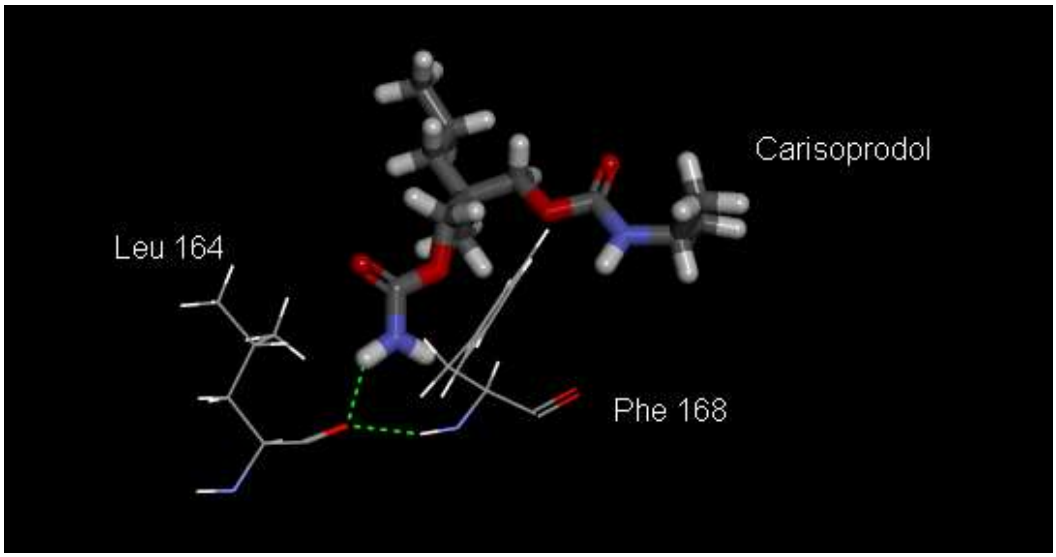

Diflunisal:

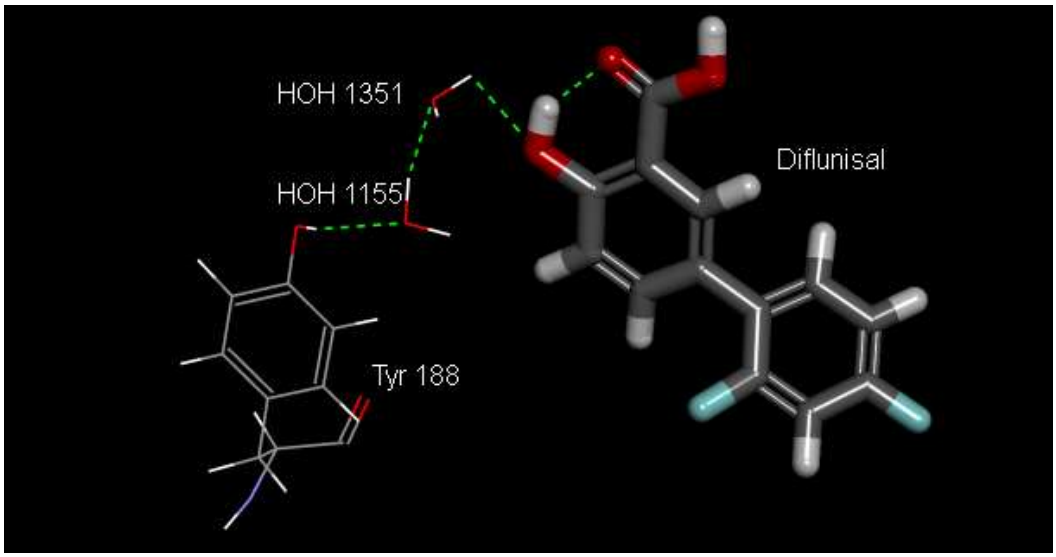

Esmolol:

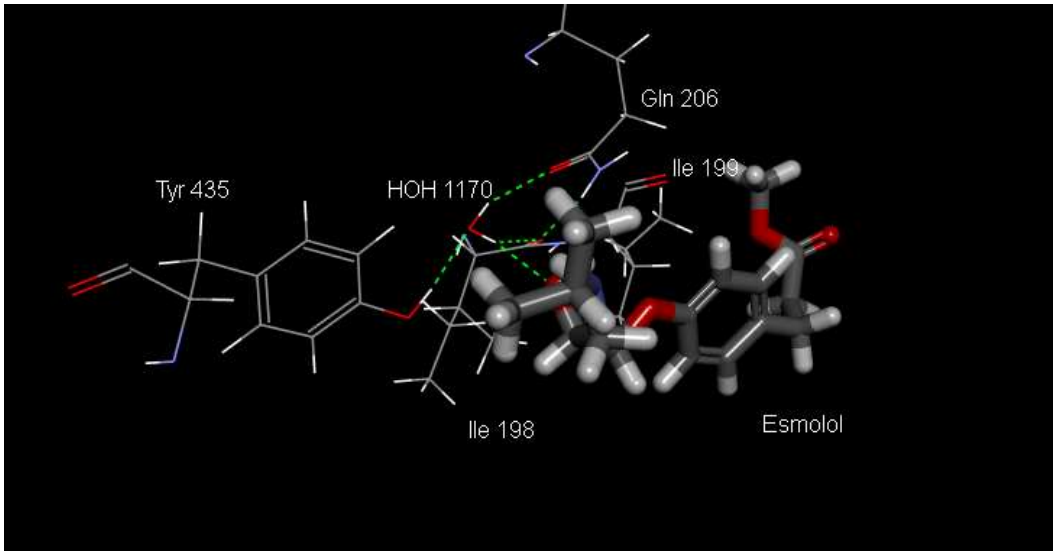

Ethambutol:

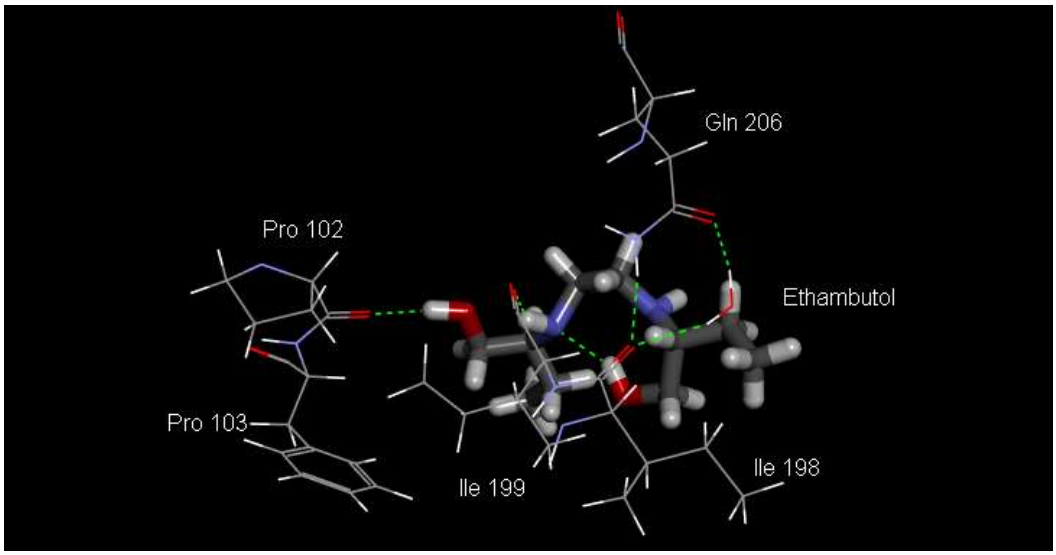

Kaempferol:

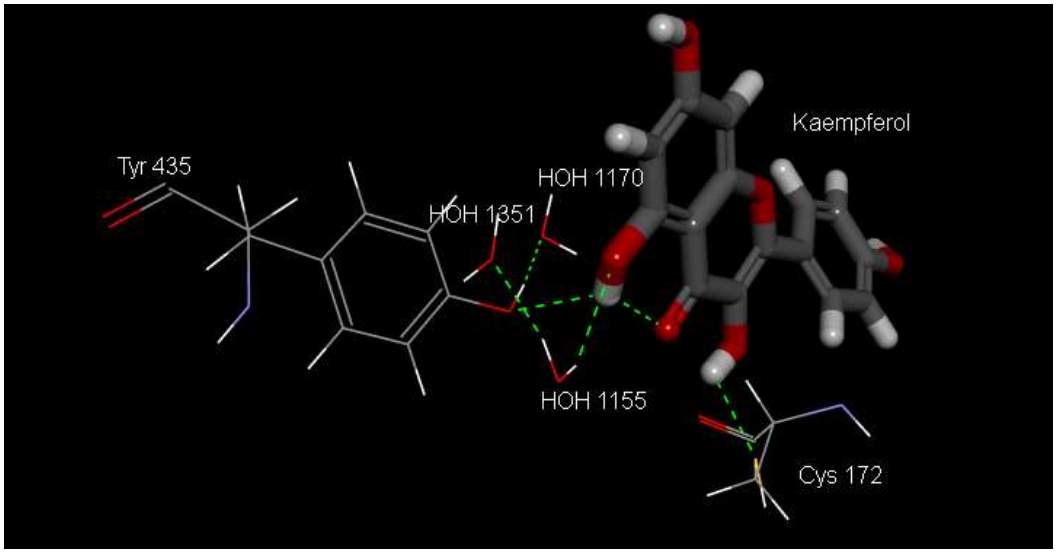

Ketoprofen:

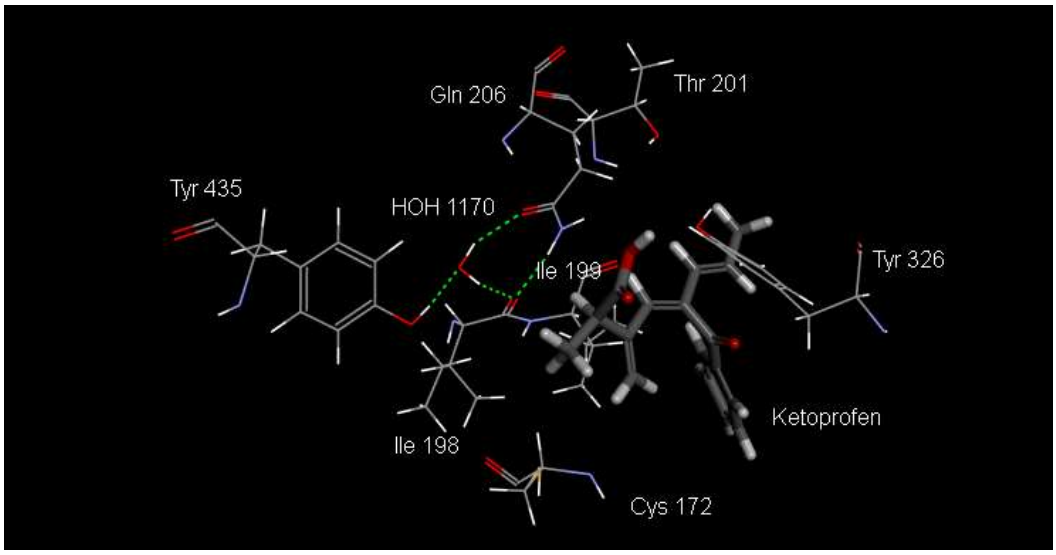

Midodrine:

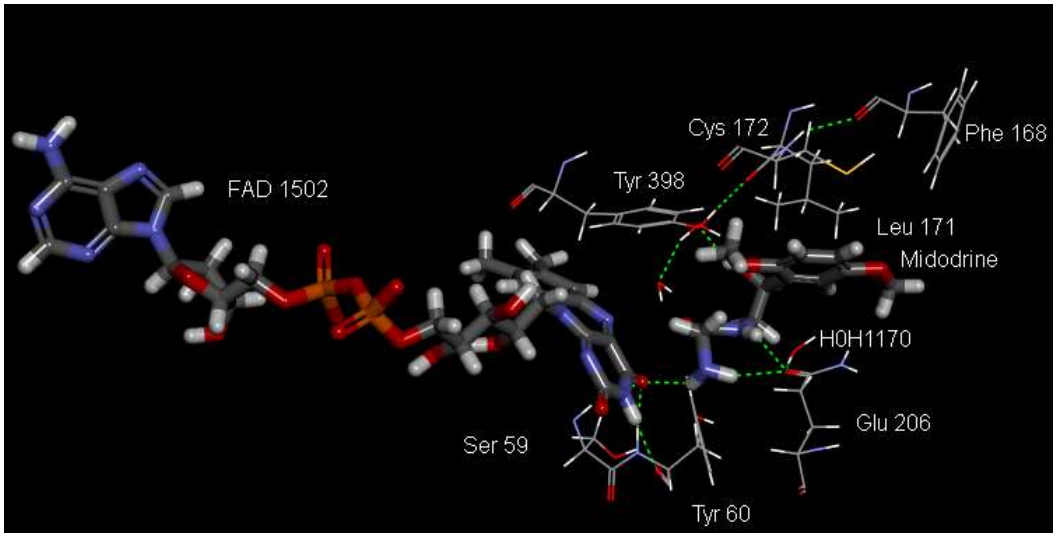

Tenoxicam:

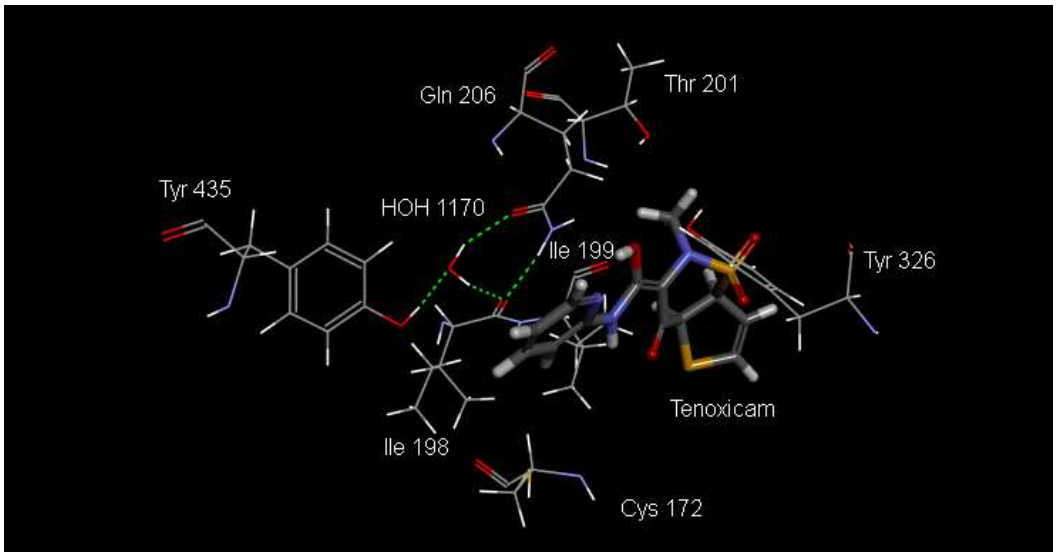

(6*R*)-5,6,7,8-Tetrahydrobiopterin:

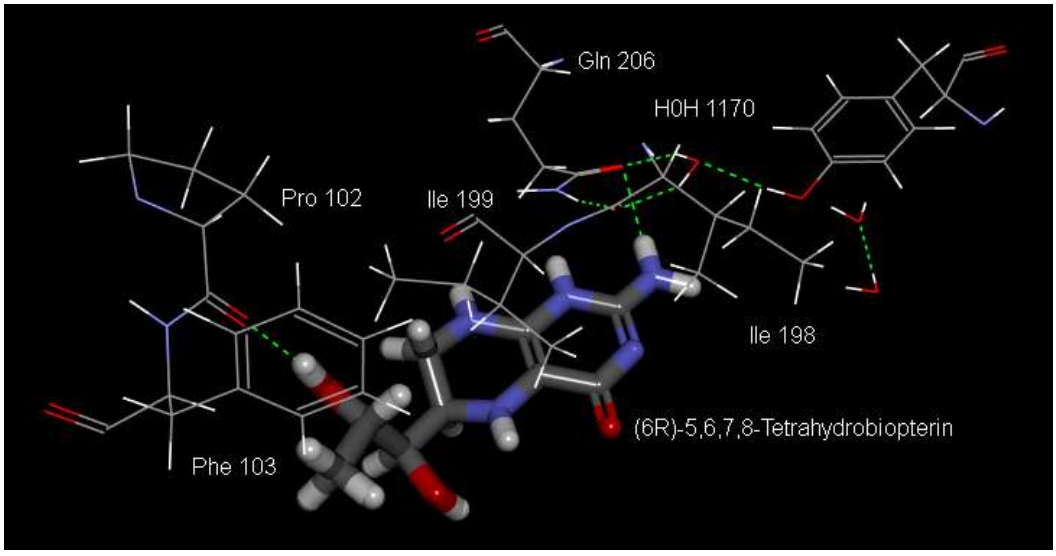

Trimethoprim:

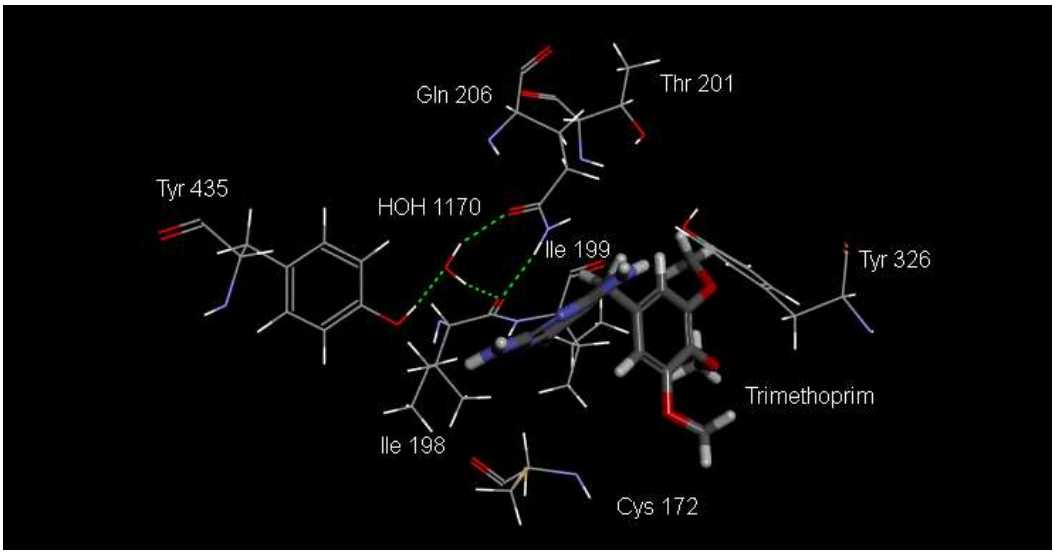

ACKNOWLEDGEMENTS

I would like to thank the following people for guiding and assisting me with my master's degree:

- My supervisor, Dr. A.C.U. Lourens
- My co-supervisors Prof. J.P. Petzer and Prof. A. Petzer
- Prof. J. Du Preez
- Miss. M. Geldenhuys
- Miss J. De Beer
- NRF for funding
- NWU for funding and facilities provided.
- My loving parents, Mrs L. Smit and Dr. J. Smit, for all their love and support.
- And lastly our Heavenly Father for giving me the strength, perseverance and opportunities to achieve my goals.